Spectral and Energy Efficiency in Cellular Mobile Radio Access Networks

Abdelrahman Arbi

Department of Electronic and Electrical Engineering

University of Sheffield

A thesis submitted for the degree of

Doctor of Philosophy

June 2017

Dedicated to:

To the soul of my father Salama, may Allah have a mercy on him.

To my mother Hailma.

To my small wonderful family, my wife Darin and my kids Jomana and Tammam.

To my brothers and sisters.

Abstract

Driven by the widespread use of smartphones and the release of a wide range of online packet data services, an unprecedented growth in the mobile data usage has been observed over the last decade. Network operators recently realised that the traditional approach of deploying more macro cells could not cope with this continuous growth in mobile data traffic and if no actions are taken, the energy demand to run the networks, which are able to support such traffic volumes risks to become unmanageable.

In this context, comprehensive investigations of different cellular network deployments, and various algorithms have been evaluated and compared against each other in this thesis, to determine the best deployment options which are able to deliver the required capacity at a minimum level of energy consumption. A new scalable base station power consumption model was proposed and a joint evaluation framework for the relative improvements in throughput, energy consumption and energy efficiency is adopted to avoid the inherent ambiguity of using only the bit/J energy efficiency metric.

This framework was applied to many cellular network cases studies including macro only, small cell only and heterogeneous networks to show that pure small cell deployments outperform the macro and heterogeneous networks in terms of the energy consumption even if the backhaul power consumption is included in the analysis. Interestingly, picocell only deployments can attain up to 3 times increase in the throughput and 2.27 times reduction in the energy consumed when compared with macro only RANs at high target capacities, while it offers 2 times more throughput and reduces the energy consumption by 12% when compared with the macro/pico HetNet deployments. Further investigations have focused on improving the macrocell RAN by adding more sectors and more antennas. Importantly, the results have shown that adding small cells to the macrocell RAN is more energy efficient than adding more sectors even if adaptive sectorisation techniques are employed. While dimensioning the network by using MIMO base stations results in less consumed energy than using SISO base stations.

The impact of traffic offloading to small cell, sleep mode, and inter-cell interference coordination techniques on the throughput and energy consumption in dense heterogeneous network deployments have been investigated. Significant improvements in the throughput and energy efficiency in bit/J were observed. However, a decrease in the energy consumption is obtained only in heterogeneous networks with small cells deployed to service clusters of users.

Finally, the same framework is used to evaluate the throughput and energy consumption of massive MIMO deployments to show the superiority of massive MIMOs versus macrocell

RANs, small cell deployments and heterogeneous networks in terms of achieving the target capacity with a minimum level of energy consumption. 1.6 times reduction in the energy consumption is achieved by massive MIMOs when compared with picocell only RAN at the same target capacity and when the backhaul power consumption is included in the analysis.

Acknowledgment

It is with immense gratitude that I thank my first supervisor Professor Timothy O'Farrell for his tremendous support during my Ph.D. study, his encouragement and endless enlightening ideas were very helpful to the completion of this work.

My thanks go also to my second supervisor Dr. Mohammed Benaissa and to many of my colleagues in the wireless communication group especially my friends Dr. Salim Abukhrais and Dr. Ravinder Singh for their support during the writing up stage.

Special thanks to Dr. Loutfi Nuaymi and Dr. Charith Abhayaratne for accepting to be my PhD examiners and for their time to review my thesis and their very helpful comments.

Also, I deeply appreciate the great patience of my wife and the members of my family in Libya. None of this would have been possible without the prayers of my mother in Libya and the support of my wife here.

1. Table of Contents

List of Figures

List of Tables

List of Abbreviations

3GPP	The 3rd Generation Partnership Project
ABS	Almost Blank Subframe
APC	Area Power Consumption
BB	Baseband
BTS	Base Station
CLSM	Close Loop Spatial Multiplexing
CDF	Cumulative Density Function
CRE	Cell Range Expansion
CAS	Coarse Adaptive Sectorisation
CRS	Cell Reference Signal
CoMP	Coordinated Multipoint
CSI	Channel State Information
CSIT	Channel State Information Transmitter
CSIR	Channel State Information Receiver
DAS	Distributed Antenna System
dB	Decibel
dBm	Decibel with reference to 1 milliwatt
DTX	Discontinuous Transmission
EDGE	Enhanced Data rates for GSM Evolution
eICIC	Enhanced Inter-Cell Interference Coordination
ECG	Energy Consumption Gain
ECR	Energy Consumption Ratio

EE	Energy Efficiency
ETG	Energy throughput gain
ERG	Energy Reduction Gain
FDD	Frequency Division Duplex
FAS	Fine Adaptive Sectorisation
FTP	File Transfer Protocol
FeICIC	Further Enhanced inter Dell Interference Coordination
GSM	Global System for Mobile Communications
GPRS	General Packet Radio Service
HetNet	Heterogeneous Network
HSDPA	High-Speed Downlink Packet Access
HSUPA	High-Speed Uplink Packet Access
ICT	Information Communication Technology
LNA	Low Noise Amplifier
LTE	Long Term Evolution
LTE-A	Long Term Evolution Advanced
MBSFN	Multicast and Broadcast Single Frequency Network
MIMO	Multiple Input Multiple Output
MISO	Multiple Input Single Output
MRC	Maximum Ratio Combining
MRT	Maximum Ratio Transmission
MU-MIMO	Multi-User MIMO
MVCE	Mobile Virtual Centre of Excellence
OFDM	Orthogonal Frequency Division Multiplexing
OFDMA	Orthogonal Frequency Division Multiple Access

OPEX	Operational Expenditure
PA	Power Amplifier
PAPR	Peak to Average Power Ratio
PF	Proportional Fair
QoS	Quality of Service
RAN	Radio Access Network
RF	Radio Frequency
SISO	Single Input Single Output
SIMO	Single Input Multi Output
SINR	Signal to Interference plus Noise Ratio
SIR	Signal to Interference Ratio
SNR	Signal to Noise Ratio
SC- OFDMA	Single carrier Orthogonal Frequency Division Multiple Access
SON	Self-organising Network
TDD	Time Domain Duplex
TRX	Transceiver
TTI	Transmission Time Interval
TPG	Throughput Gain
UMTS	Universal Mobile Telecommunication Service
UE	User Equipment
WCDMA	Wide Code Division Multiple Access
ZF	Zero Forcing

Chapter 1

Introduction

1.1 Overview

Mobile communication systems have significantly evolved over the last decade, the evolution process has passed through a number of important phases of development. The number of mobile subscribers astronomically increased to reach 4 billion in 2008, which represents a worldwide penetration level of 60% [1]. The mobile quickly became the preferred method of voice communications, and after the launch of 3G systems, the volume of mobile data traffic exceeded that of voice traffic for the first time in 2010 [2].

Driven by the widespread use of smartphones, and the release of a wide range of online packet-data-based services, a massive growth in the mobile data usage was observed in the years leading to 2010. As a result, the 2G and 3G networks became congested and unable to meet the growth in demand. For this reason, the work on the standardisation of 3GPP long-term evolution (LTE) started in 2004, and the first version of LTE standard (release 8) was published in 2008. The first commercial deployment of LTE network took place in Sweden in December 2009 and became rapidly adopted worldwide with more than one billion active LTE subscriptions by 2016 [3].

The growth in the demand for mobile data services is expected to continue for the foreseeable future, predictions of 1000 times increase in the area capacity demand by 2020 compared to the 2010 levels are often cited in the open literature [4]. Network operators have started deploying multiple solutions to improve the capacity of existing networks. These solutions include upgrading the existing networks by the deployment of more advanced techniques and deploying more sites. With the continuous growth in mobile traffic, network operators have realised that an economically sustainable capacity growth strategy is needed to meet such rapidly growing demand [5], and if no action is taken, the amount of required energy consumption to operate such networks could increase to unprecedented levels, and hence risks to become unmanageable.

1.2 Research aim

As indicated previously, an economically sustainable capacity growth strategy is needed when evolving the existing networks to meet the continuous rapid growing demand for data traffic. In this context, a clear understanding of the various capacity improvement enabling techniques and their impact on the network energy consumption is required. A comprehensive study of different cellular network deployments and various algorithms will be evaluated and compared

against each other through system level simulations in this thesis. The aim is to determine the best deployment options which are able to deliver the required capacity at the lowest possible level of energy consumption. Although the evolution of any cellular network is often very case-specific, the author of this thesis aims to provide a set of general guidelines and recommendations on what is the most energy efficient evolution path to be followed by network operators to support the rapid growth in mobile data traffic over the next years.

1.3 Motivation

Improving network coverage, capacity, deployment cost and reliability were regarded as the key main objectives to achieve by mobile network operators when deploying new networks, or upgrading an existing one. The energy was considered critical only in mobile user's equipment because the limited storage capacity of batteries imposes strict limits on their power consumption. Recently, the energy efficiency in the radio access network (RAN) has become a major concern for network operators, not only because of the rise in the cost of energy needed to operate the network, but also to reduce their carbon footprint. The information and communication technology (ICT) sector was responsible for about 2% of the global CO2 emissions in 2009 and predicted to grow to about 2.8% in 2020 [6]. Therefore, a paradigm shift in the process of the design and operation of cellular networks is needed to have the network energy consumption as an important key performance indicator to consider during any planning or deployment process.

In this regard, a unified evaluation framework for the spectral and energy efficiency of radio access networks (RAN) is needed. The existence of well-defined and accurate energy efficiency metrics represent the first step in the development of such a framework Energy efficiency metrics for any system are often defined according to the purpose of that system. For example, as the coverage was the key performance indicator in the early generations of mobile networks, the area power consumption has been adopted as an energy efficiency metric with the goal to minimise the consumed power per one kilometre square of the coverage area. More recently, the objective of energy efficient designs became the maximisation of the number of bits transmitted per energy unit and measured by the bit/J metric termed (EE) in this thesis, or its reciprocal which termed as energy consumption rate (ECR) and measured in J/bit.

The bit/J and ECR metrics exhibit inherent ambiguity when used to compare the energy consumption of two networks, as it not clear whether the energy efficiency improvement indicated is attributable to a true energy saving or to increases in the data throughput. This can result in misleading claims when comparing the energy efficiency of two networks if the throughput or data volume is not predefined.

A simulation of a simple scenario of macrocell densification is briefly presented here to illustrate this issue of ambiguity when the bit/J metric is adopted as energy efficiency metric. A two-tier hexagonal macro cell deployment is simulated at a bandwidth of 20 MHz, and at various cell radii values (cell radius is decreased gradually from 1 km to 200 metres), each cell has a base station equipped with an omnidirectional antenna. The transmit power of the base station is set to 40 watts when the cell radius is 1 km and scaled down at other cell radii to obtain always the same received power at the cell edge (71 dBm). Users are uniformly deployed in the target area, and their signal to noise and interference values are estimated through a simple system-level simulation, where only the distance-dependent path loss is implemented. The data rate of each user is calculated by using Shannon formula when an equal distribution of bandwidth among all of the users is assumed. The area average throughput is estimated as the sum data rates of all the users divided by the coverage area. The area average throughput results are plotted in Figure 1-1 versus the cell radius with cell average traffic load α_t as a parameter (see section 3.5 for more details about the cell average load meaning in this thesis). A significant increase in the area average throughput is observed when the cell radius is decreasing, while it also decreases when the cell average traffic load decreases.

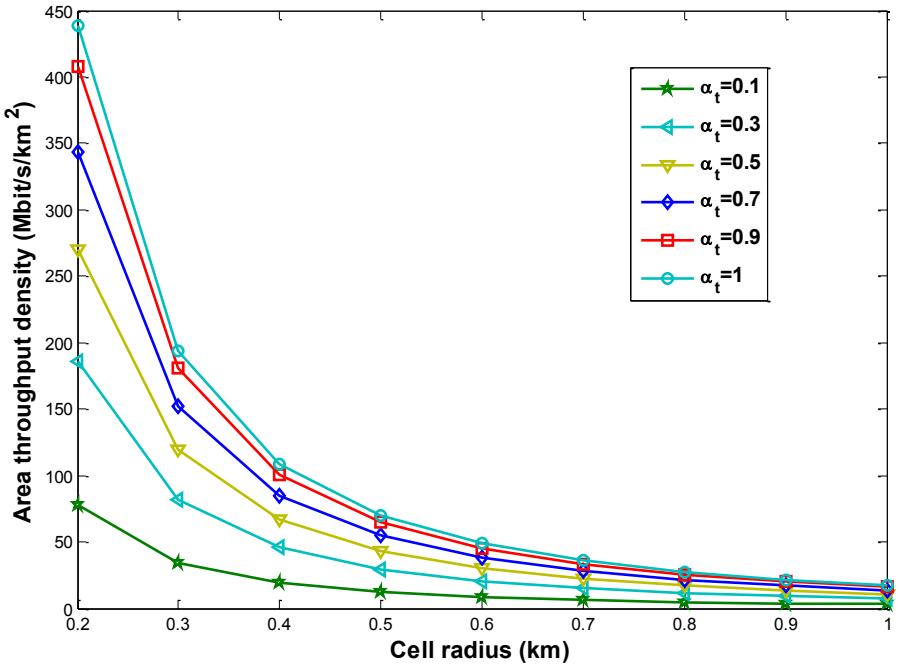

Figure 1-1: The area average throughput versus the cell radius with cell average load as a parameter

Evaluating the network power consumption by only considering the RF transmitted power can result in a misleading conclusion that decreasing the radius of the macro cells results in a reduction in the network power consumption as shown in Figure 1-2 which is not realistic as completely different results are obtained when including the base station circuit power consumption in the analysis.

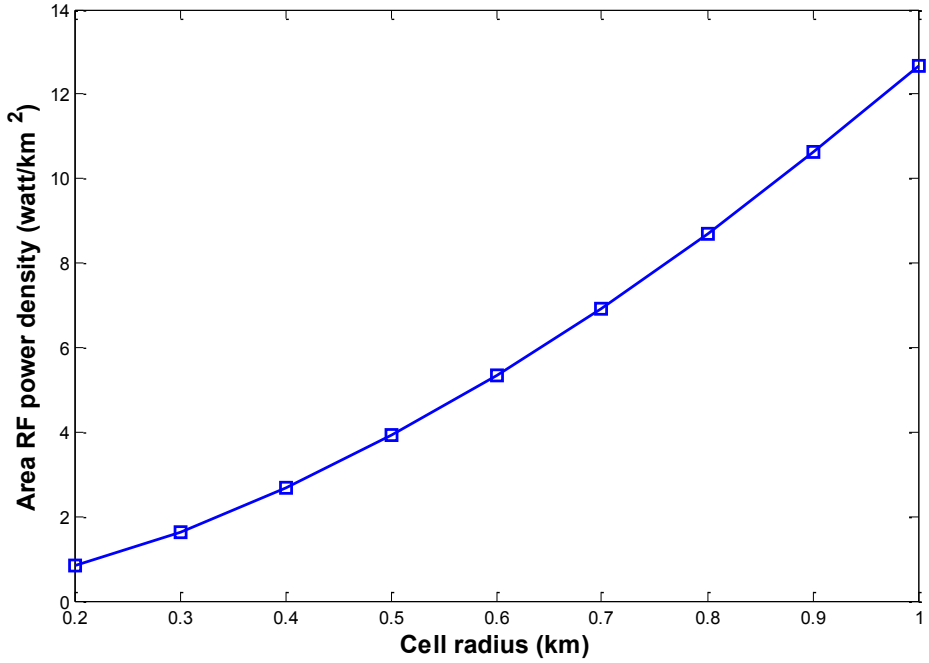

Figure 1-2: The area RF power density versus the cell radius

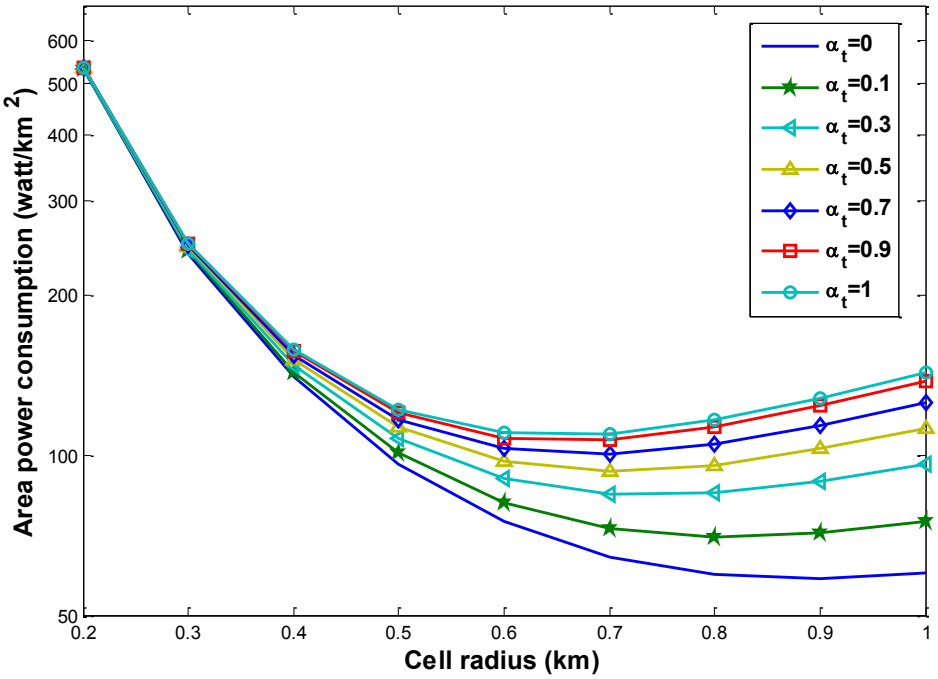

Figure 1-3: The area power consumption versus cell radius and average traffic load

Figure 1-3 shows the existence of an optimum cell radius which minimises the area power consumption of the network. This value changes according to the variation of the cell average traffic load. For example, at an average load of unity, the optimum cell radius is around 600 m, while when there is no traffic in the network, the optimum cell radius extends to 1 km which demonstrates the benefit of implementing the sleep mode and cell zooming techniques to

reconfigure the cell radius and switching off some base station according to the traffic load in the network as we will see in more details in chapter 6.

In contrast, when using the EE metric (bit/J), the results show that densifying the macrocell RAN by reducing the cell radius is always more energy efficient than deploying large macro cells as shown in Figure 1-4. This observation leads to a different conclusion than what has been observed based on the area power consumption metric. Substantial improvements in the bit/J metric are observed at high levels of average traffic load and at small cell sizes, but the disadvantage of relying only on this metric is the lack of any indication of whether or not this improvement was due to an actual reduction in the network power consumption or an increase in the traffic throughput.

Another issue highlighted here is the non-suitability of bit/J metric to be used for comparing between the energy consumption of two idle networks or at very low average traffic load, for example, when the average traffic load decreases from one to 0.15 at cell radius of 200 metres, the energy efficiency degrades by more than 80%, while the area power consumption shows very negligible reduction at the same conditions.

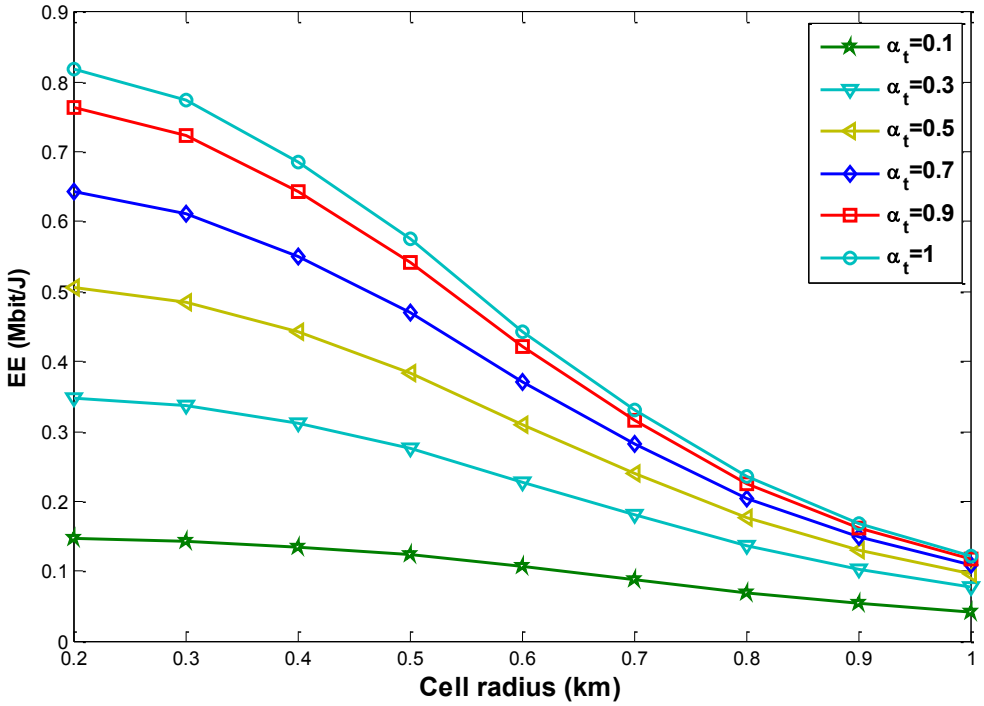

Figure 1-4: The energy efficiency versus cell radius and average traffic load

In addition, an accurate estimation of the base station power consumption is required because underestimating or overestimating the power consumption of the base station can result in quite different results about the network energy efficiency. For example, when only the RF transmitted power is considered, the densification of the macrocell RAN leads to a decrease in

the overall power consumption of the network. However, when the total consumed power is considered, different outcomes are obtained. Finally, the development a system level simulation tool is necessary to evaluate the performance of RAN deployments considered in this thesis for different configuration parameters, which is essential for quantifying the network energy consumption.

1.4 Objectives

To achieve the main research aim, the following objectives have been set:

1. Developing a scalable base station power consumption model to be used for estimating the power consumption of various types of base stations. The model should scale with the cell average load, the number of antennas and must be easy to integrate into a system level simulation.
2. The application of a unified evaluation framework for the throughput and energy consumption in cellular networks to assess the different network deployments considered in this thesis. As a part of the framework, three figures of merit are defined to quantify the relative throughput gain, relative energy consumption gain and the improvement in the energy efficiency of the evaluated network with respect to a reference network.
3. The development of Matlab simulation tools based on a static Monte-Carlo system level simulator, to be used for evaluating the downlink performance of the considered network deployments. Furthermore, comprehensive analysis of throughput and energy consumption in the traditional macrocell only deployments, small cell deployments and heterogeneous networks is to be carried out with and without the consideration of the impact of backhaul power consumption on the overall network energy consumption.
4. The analysis of the impact of high order sectorisation on the network throughput and energy consumption and compare it versus the deployment of small cells instead of adding more sectors in macrocell RAN. Also, implementing various adaptive sectorisation schemes to quantify how much energy is saved when sectors are switched off in low traffic conditions.
5. Carrying out a comparative analysis of the energy consumption in SISO and MIMO networks for so-called greenfield deployments as well as existing deployments. Moreover, the discontinuous transmission (DTX) feature is to be investigated to evaluate its potential to reduce the energy consumption in the SISO and MIMO networks.
6. In the context of heterogeneous networks, investigating the impact of traffic offloading to small cells, sleep mode and inter-cell interference coordination on the RAN

throughput and energy consumption. Two deployments are considered; sparse and dense HetNet deployments.

7. Investigation of the power consumption in massive MIMOs, and evaluating the throughput gain and energy consumption in massive MIMOs compared with the traditional macrocell RAN and the small cell and heterogeneous network deployments.

1.5 Thesis contribution

The thesis delivers important insights about throughput and energy consumption of different RAN deployments including macro, heterogeneous networks, small cells and massive MIMOs. Various techniques such as adaptive sectorisation, sleep mode, inter-cell interference are also evaluated in the context of their impact of the throughput and energy consumption of the considered deployments. As an outcome of the research, the following contributions are provided:

1. Developed new scalable base station power consumption model to be used throughout the research project, where the degradation of the power amplifier efficiency due to output back off is captured, and a different method for estimating the cooling unit power consumption is proposed (see chapter 3).

2. Applied the joint evaluation framework developed by O'Farrell [7] for analysing the throughput and energy consumption in the various RAN deployments considered in the thesis. It was extended to be applied on dense small cell deployments where the cell coverages may overlap and need to be characterised by their deployment density rather than their coverage areas. The advantage of using such a framework is avoiding the inherent ambiguity of the bit/J by clearly indicating whether the improvement in the energy efficiency was due to an actual reduction in the energy consumption or not (see chapter 3).

3. Quantifying the impact of increasing the sectorisation order on the RAN throughput and energy consumption and providing a new analysis of two adaptive sectorisation schemes on the macro RAN energy consumption. Furthermore, the question of whether increasing the sectorisation order from 3 to 6 in macrocell RAN is more energy efficient or not than deploying small cells on top of 3-sector macrocells is answered. The finding was contra to the prevailing mobile network operators practice which deploys more sectors before adding small cells (see chapter 4).

4. More insights on the energy consumption of MIMO was provided through the analysis of energy consumption in SISO and MIMO macro RANs in new and existing

deployments. Although MIMO base stations consume more energy than SISO ones, dimensioning the network using MIMO base stations is more energy efficient than using SISO base stations when the same requirement of coverage and capacity are assumed. Also upgrading SISO base station in an existing deployment to 2x2 MIMOs does not only improves the users' data rates but results in an actual reduction in the RAN energy consumption if the same level of offered traffic is assumed in case of SISO and MIMO. An important lesson from this finding is adaptive antenna muting should not be applied to reduce the number of antennas from 2 to one during the low traffic periods (see chapter 5).

5. In the context of heterogeneous networks, quantifying by simulation the gains in the users' data rates due to offloading traffic from macrocells to small cells, and the reduction in the energy consumption at various small cell densities, different cell range expansion values (CRE) and at two cases of user location distributions. Importantly, the thesis showed a joint improvement in the network throughput and a reduction in the energy consumption is possible only in case of deploying the small cells in the centre of users' clusters (see chapter 6).

6. Proposed implementing new distributed sleep mode scheme where more savings in the energy consumption is achieved by applying the sleep mode on the small cells and the backhaul links (see chapter 6).

7. Evaluated the potential of the inter-cell interference coordination (eICIC) not only on the throughput of the dense heterogeneous network but also on the RAN energy consumption to show that significant improvement in the RAN ECG is achievable when eICIC is combined with the distributed sleep mode (see chapter 6).

8. Modifying an existing power consumption model of massive MIMO base stations to include the losses in the power supply, cooling unit, and the losses due to the degradation in the power amplifier efficiency. Also, updating the way the model estimates the power consumption in the RF transceiver to become scalable with the bandwidth, and considering the case of using only uplink pilots to estimate the channel (see chapter 7).

9. By using the same framework of chapter 3, comparing the throughput and energy consumption of a massive MIMO case study versus the traditional macrocell RAN, small cell and heterogeneous network deployments. The objective is to identify which deployments consume the least amount of energy. This comparison constitutes the basis for providing more insights on the energy consumption of these deployments, and for providing a set of beneficial guidelines and recommendations to the mobile network operators when deciding which deployment should be considered to evolve their networks if reducing the network energy consumption is one of their goals (see chapter 7).

1.6 Thesis outline

The thesis is structured into eight chapters; a summary of each chapter is presented below:

1. The first chapter provides an introduction to the research topic and highlights the need for a sustainable evolution strategy to be adopted by the cellular network operators when evolving their networks to meet the continuous growth in mobile data. The aim and the motivation of the research are also presented, followed by summarising the planned objectives of the thesis, and the thesis contributions. The thesis layout and list of publications are presented at the end of the chapter.

2. Chapter 2 presents a background about the evolution of cellular networks and discusses the need for upgrading the existing network to meet the growth in demand for wireless access services in the next generation networks. The enabling techniques for improving the network capacity are also presented including the upgrade and improvement of existing sites and the need for further densification of the network by the deployment of more sites. The importance of energy consumption in cellular networks is covered in details by highlighting the need for a consistent set of metrics and figures of merit for the energy efficiency of the network. In addition, a review of the existing base station power consumption models is presented, followed by providing a detailed review of the various energy consumption reduction approaches in cellular networks with more focus on the network planning and deployment-related approaches.

3. In chapter 3, the motivation for proposing a different evaluation framework for the spectral and energy efficiency in cellular networks is highlighted. The process of modelling the power consumption of radio base stations has been described in detail, where a base station power consumption model is proposed followed by defining how the throughput and energy consumption will be evaluated in the thesis. The application of the evaluation framework is illustrated by a case study of various types of cellular

network deployments including macro cell RANs, small cell RANs and heterogeneous network deployments.

4. Chapter 4 addresses the issue of throughput and energy consumption in cellular networks, which arises when high order sectorisation and small cell densification are used to enhance the RAN capacity. The chapter investigates the energy consumption of a heterogeneous RAN comparing 3- and 6-sector macro/micro and macro/pico deployments. The aim was to ascertain if network operators can obtain greater energy savings by increasing the sectorisation order before densifying with a small cell overlay, or should an overlay of small cells be added without increasing the sectorisation order. The analysis was extended by considering various adaptive sectorisation schemes to quantify how much energy is saved when sectors are switched off in low traffic conditions.

5. A comparative analysis of the energy consumption of SISO and MIMO RANs is presented in chapter 5, when certain capacities are set as targets to achieve. The analysis is carried out in the case of new deployments where the operators have the choice to decide whether to deploy SISO or MIMO base stations, and in the case of existing networks, where the target was to evaluate whether upgrading the SISO base stations by adding more antennas leads to an increase in the network energy consumption or not. The discontinuous transmission (DTX) feature was also implemented to quantify the extra energy savings which can be achieved in SISO and MIMO RANs through system level simulation.

6. Chapter 6 concentrates on evaluating the throughput and energy consumption in heterogeneous networks: Two scenarios are considered, the first scenario investigates the impact of traffic offloading to small cells on the RAN average throughput, and the RAN energy consumption in heterogeneous deployments. The objective is to examine whether or not the amount of reduction in the energy consumption of macrocells due to traffic offloading to small cells is larger than the increase in energy consumption due to deploying more small cells. The analysis is extended by evaluating the extra energy savings due to enabling new distributed scheme of sleep mode in small cells. Two kinds of user deployments are considered; uniform and clustered user deployments. In the second scenario, the potential of deploying a dense layer of small cells to improve the RAN throughput, and reduce the energy consumption is evaluated. Also, the sleep mode and inter-cell interference coordination (eICIC) techniques were implemented to investigate their impact on the RAN performance and energy consumption.

7. Chapter 8 evaluates the potential of massive MIMOs as a promising candidate to improve the spectral and energy efficiency of next generations of cellular networks. The methodology to estimate the power consumption in massive MIMO base stations is described in details. The same evaluation framework presented in chapter 3 is adopted to evaluate the throughput gain, energy consumption gain, and energy throughput gain of massive MIMO networks with reference to a baseline deployment of a macro cell RAN when maximum ratio transmission (MRT) precoding is employed. Finally, the chapter compares the throughput and energy consumption gains of massive MIMO, small cells and heterogeneous networks in order to indicate which deployment is able to deliver the required capacity while consuming the smallest amount of energy.
8. Chapter 8 concludes the thesis by summarising the outcomes of the research and listing the concluding remarks. In addition, possible future work directions are given at the end of the chapter.

1.7 List of publications

1. A. Arbi and T. O'Farrell, "A comparative study of energy efficiency between MIMO and SISO based LTE RANs," *2015 IEEE International Conference on Communications (ICC)*, London, 2015, pp. 43-48. doi: 10.1109/ICC.2015.7248296. (See Chapter 5).

2. A. Arbi and T. O'Farrell, "Energy efficiency in 5G access networks: Small cell densification and high order sectorisation," *2015 IEEE International Conference on Communication Workshop (ICCW)*, London, 2015, pp. 2806-2811. doi: 10.1109/ICCW.2015.7247604. (See chapter 4).

3. Arbi, A., O'Farrell, T., Zheng, F., & Fletcher, S. C. (2017). Toward Green Evolution of Cellular Networks by High Order Sectorisation and Small Cell Densification. In C. Yang, & J. Li (Eds.), *Interference Mitigation and Energy Management in 5G Heterogeneous Cellular Networks* (pp. 1-28). Hershey, PA: IGI Global. doi:10.4018/978-1-5225-1712-2.ch001.(See Chapter 4).

Chapter 2

Background and Literature Review

2.1 Overview

Mobile communication has evolved from being a luxurious technology used by only a limited class of people to becoming ubiquitous; affordable to the majority of the global population. This process has seen a number of important phases of development over the last few decades. The number of mobile subscribers astronomically increased to reach 4 billion in 2008, which represents a worldwide penetration level of 60% [1]. The mobile quickly became the preferred method of voice communications, and after the launch of 3G systems, the volume of mobile data traffic grew considerably, this data volume exceeded that of voice traffic for the first time in 2010 [2].

As a backdrop to this thesis, a brief overview of the evolution of mobile networks will be presented in the following section.

2.1.1 Evolution from 1G to 3G

The first generation of Mobile telecommunication systems (1G) was released in Europe for the first time in the early 1980s. Each country had its own system and frequency allocation. Analogue communication techniques and large cell sizes were used in all 1G systems, which led to low system capacity compared with today's systems. The mobile handsets were bulky and expensive, which limited their adoption to business and government users. The launch of the second generation of mobile systems took place in Finland in 1991, with the deployment of the Global System for Mobile Communications (GSM), which became the most popular 2G system. IS-95, also known as cdmaOne, became the dominant 2G system in the USA [2].

Unlike the analog 1G systems, GSM was designed using digital technology, which enhanced the efficiency of the radio spectrum usage, and led to the introduction of smaller and less expensive mobile phones. GSM was originally designed for voice communications, but it was later enhanced to support instant messaging service (SMS) and circuit switched data services at up to 9.6 Kbits/s data rates. Packet switching data capabilities were added to GSM using general packet radio services (GPRS), known as 2.5G. The 2.5G systems had a maximum theoretical downlink rate of 171 Kbit/s which was further improved to reach 384 Kbit/s through enhanced data rates for GSM evolution (EDGE). As a result, the data usage increased, but the traffic volume in second generation networks remained dominated by voice traffic.

The need to support faster data rate services was the main reason behind the development of a new generation of cellular networks able to increase peak data rates. To achieve such a goal, the

Third-Generation Partnership Project (3GPP) was formed to develop the 3G WCDMA and TD-SCDMA technologies. The first release of WCDMA occurred in 1999, where packet switched data services were added. The Universal Mobile Telecommunication System (UMTS) was proposed as an evolution to GSM and quickly became the world's dominant 3G system. It had a downlink data rate of 384 Kbit/s, which was later enhanced to 14 Mbit/s with the 3.5G technologies of high-speed downlink packet access (HSDPA) and high-speed uplink packet access (HSUPA).

2.1.2 Long-term evolution LTE

A massive growth in data usage was recorded in the years leading to 2010 driven largely by the widespread use of smartphones, and the release of a wide range of online packet-data-based services such as social networking, video streaming, and gaming. As user expectations in terms of the achievable data rates and latency started to rise, the 2G and 3G networks became congested and unable to meet the continuous growth in demand. As a result, development of the fourth generation (4G) of mobile networks began by discussing the idea of developing a network based on packet switching technology with strict requirements of high data rates, low latency and high capacity. Work on the first 3GPP long-term evolution LTE standards started in 2004. The target performance in 3GPP LTE was defined relative to HSPA in Release 6, as summarised below [1]:

- Two to four times spectral efficiency compared with the HSPA Release 6.
- Peak rates of more than 100 Mbps downlink and 50 Mbps uplink.
- Less than 10 ms round trip times.
- Packet switched optimised.
- High level of mobility and security.
- Optimised terminal power efficiency.
- Flexibility in frequency allocation from below 1.5 MHz up to 20 MHz.

The first version of LTE standard (release 8) was released in 2008, where orthogonal frequency division multiple access (OFDMA) was used for downlink access and single carrier frequency division multiple access (SC-FDMA) for uplink access. The first commercial LTE network was deployed in Sweden in December 2009 and became rapidly adopted worldwide: the number of deployed LTE networks by the end of 2015 had reached 460 spread over 140 countries [8].

Since its first launch in 2009, LTE has witnessed a number of enhancements in subsequent releases. Release 13 is the last completed release while work on release 14 is still in progress and expected to be completed by June 2017. A summary of the main features of each release is presented below [8] [9].

1. Release 8: LTE, frozen in 2008.
    - High peak data rates: up to 300 Mbit/s in downlink and 75 Mbit/s in uplink when 20 MHz bandwidth and 4x4 MIMO are used.
    - Flexible bandwidth allocation from 1.4 MHz to 20 MHz.
    - All IP network.
    - Support of up to 4X4 MIMO techniques.
    - Support FDD and TDD duplex mode.
    - Simplified flat architecture.
    - Short round trip time (5ms).
2. Release 9: Enhancement to LTE, frozen in 2009.
    - The introduction of LTE femtocells.
    - Addition of the self-organising network feature (SON).
    - Evolution of multimedia broadcast multicast services (MBMS).
    - LTE positioning services.
    - Extension of MIMO beamforming functionality.
3. Release 10: LTE advanced, frozen in 2011.
    - Support for 8x8 MIMO in downlink and 4x4 in uplink.
    - Support of relay nodes.
    - Support of heterogeneous networks.
    - Carrier aggregation.
    - SON improvement.
    - Introduction of enhanced inter-cell interference coordination (eICIC).
4. Release 11: Enhancement to LTE-A, frozen in 2012.
    - Enhancement in carrier aggregation.
    - Coordinated multipoint transmission and reception (CoMP).
    - Introduction of new frequencies.
    - Introduction of advanced receivers to mitigate interference.
    - Introduction of further enhanced inter-cell interference coordination (FeICIC).
5. Release 12: Enhancement to LTE-A, frozen in 2014.
    - Dual connectivity in heterogeneous networks.
    - Carrier aggregation enhancements.
    - Machine type communications.
    - LTE in unlicensed spectrum.
    - Integration of LTE and Wi-Fi.
6. Release 13: Enhancements to LTE-A, frozen in 2015
    - Support for more carrier components.

- Enhancements in device-to-device and machine-type communications.
- Indoor positioning services.
- Three-dimensional (3D) beamforming.

2.1.3 Beyond 4G

The exponential growth in the demand for mobile data services which began in the years leading to 2010 is expected to continue for the foreseeable future. The 2015 Cisco visual networking index [10] reported that the global mobile data traffic grew by 69 percent in 2014, and predicted an approximately tenfold increase in traffic from 2.5 EB to 24.3 EB between 2014 and 2019. Other predictions suggest 1000 times increase in demand for wireless capacity by 2020 when compared to the levels of 2010 [4]. This projected growth is mainly due to the proliferation of the use of smart devices and the expansion of mobile services in developing societies. In response, operators must enhance the capacity of their networks. Therefore, after the deployment of 4G, the attention of the industry has turned to start the preparation process for the standardisation and release of a fifth generation (5G) of radio access networks.

5G is considered a common platform able to provide connectivity anywhere, anytime to anyone and anything on the globe. The main characteristics of 5G are the huge growth in the traffic volume, the growth in the number of connected devices and the ever-increasing range of diverse applications expected to use the 5G. As each application has its own requirements in terms of data rates, latency, and energy efficiency, a high degree of network flexibility is needed to accommodate them.

As mobile broadband will continue to represent an important portion of the 5G networks, the improvement in radio access network capacity and in users' data rates are considered crucial components in the evolution towards 5G. By looking into equations 2.1 and 2.2, we can easily understand that any improvement in the area capacity density requires an enhancement in one or more of the terms in the equations.

$$\textit{Area capacity density} = \textit{Bandwidth} \cdot \textit{Cell density} \cdot \textit{Cell spectral efficiency}\,. \qquad (2.1)$$

The term cell spectral efficiency refers to the sum of users' data rates in the cell divided by the overall bandwidth. When an orthogonal frequency allocation of bandwidth resources such as OFDMA is assumed, the cell spectral efficiency can be written as in (2.2).

$$\textit{Cell spectral efficiency} = \sum_i^n \frac{w_i}{Bandwidth}\, m_i \cdot log_2(1 + SINR_i)\,, \qquad (2.2)$$

Where n is the number of users in the cell, w_i is the bandwidth allocated to the user i, m_i refers to the MIMO spatial multiplexing gain achievable between the base station and user i, while $SINR_i$ is the signal to interference and noise ratio at the user's equipment. As can be clearly seen from equations (2.1) and (2.2), there exist three main technical approaches for operators to improve their radio access network (RAN) area capacity density. The first is to improve the cell spectral efficiency by enhancing the link spectral efficiency with more advanced signal processing techniques such as multiple-input multiple-output (MIMO) antennas, efficient modulation and coding schemes, and effective interference mitigation techniques. The second approach is the addition of a new radio spectrum, and the third is to increase the geographic spectrum reuse through cell densification of the RAN.

Historically, the reuse of the radio spectrum was the main reason for the growth of capacity in cellular mobile radio systems. According to Martin Cooper [11], a 1600-fold increase over the last 45 years has come from the reuse of spectrum, whereas a 625 fold increase has resulted from adding more spectrum and implementing more advanced signal processing techniques to enhance the link capacity. The wireless SISO channel link capacity is very close to its maximum Shannon limit, and more improvement in the cell spectral efficiency requires the implementation of more advanced antenna techniques such as single user MIMO, multi-user MIMOs, beamforming [12] and massive MIMOs [13]. Increasing the capacity with the addition of more spectrum is also required, but as the amount of non-exploited spectrum under 6 GHz bands is limited, technologies such as millimetre wave radio [14] and visible light communications are being considered [15].

Therefore, a combination of these techniques is required to meet the ongoing increase in demand. Given the potential of each technique, the deployment of more cells (i.e. base station densification) will continue to be the key enabling technique to achieve high target capacities in the next generation of cellular mobile networks. It should be noted that deploying these techniques will impact the network energy consumption, an issue which has become a major concern to network operators in recent years. Therefore, the reduction of energy consumption in cellular networks forms the basis of our research work. More details regarding the issue of energy efficiency of cellular networks are provided in section 2.3.

2.2 Approaches towards network capacity improvement

Current mobile networks consist mainly of macro base stations deployed in outdoor urban, suburban or rural areas, supported by Wi-Fi access points for indoor coverage. Small cells are deployed sparsely in hotspot zones to provide more capacity where needed, or to extend the macro cell coverage. The choice of method to increase the capacity of the network can vary from one operator to another; however, a common strategy of operators is observed when evolving their networks. This consists of first improving the existing macrocells by adding more

spectrum, more antennas, and more sectors before deploying new sites. These techniques have the advantage of improving the network capacity without adding more sites. When the capacity improvement resulting from these techniques is insufficient, operators densify their network by adding more macro sites or adding an overlay of indoor or outdoor small cells. These small cells include microcells, picocells and remote radio heads used for outdoor deployment; picocells, femtocells, and distributed antenna systems DAS used for indoor deployments. Each deployed technology has a different impact on the achieved capacity and on the RAN energy consumption. One of the aims of this research project is to investigate the effects of deploying these techniques on the RAN throughput and energy efficiency. The network evolution path followed in this thesis consists of the following approaches:

- RAN densification by macro base stations.
- RAN densification by high order sectorisation.
- Improvement of existing sites by adding advanced antenna techniques such as single user MIMO or massive MIMO.
- RAN densification by the deployment of outdoor heterogeneous networks.

To achieve this aim, a joint evaluation framework of the RAN throughput and RAN energy efficiency must be defined: the framework will include, in addition to the throughput and energy efficiency metrics, an updated base station power consumption model to estimate the RAN power consumption. A system-level simulator is developed for evaluating the throughput of various considered RAN architectures. Background information on the above-mentioned approaches is presented in the next section prior to an exploration of the issue of energy efficiency in cellular networks.

2.2.1 Macrocell densification

The term macrocell in mobile networks describes the area which is served by a single high power base station mounted on top of a tower. This area radius can vary from 500 metres in urban areas up to 5 km in rural areas. A regular hexagonal geometry is used to model the location of deployed macrocells. The simplest form of macro cell is when the base station consists of single sector equipped with an omnidirectional antenna. When more capacity is required, three sector base stations can be deployed, as shown in Figure 2-1. Deploying more macro sites has been the traditional method used to expand the coverage and capacity of existing networks. However, reducing the site-to-site distance between the macro sites cannot continue without limit due to the technical issues of inter-cell interference and, more importantly, due to the cost of macro base stations coupled with the difficulty of finding new sites, especially in urban and dense urban areas.

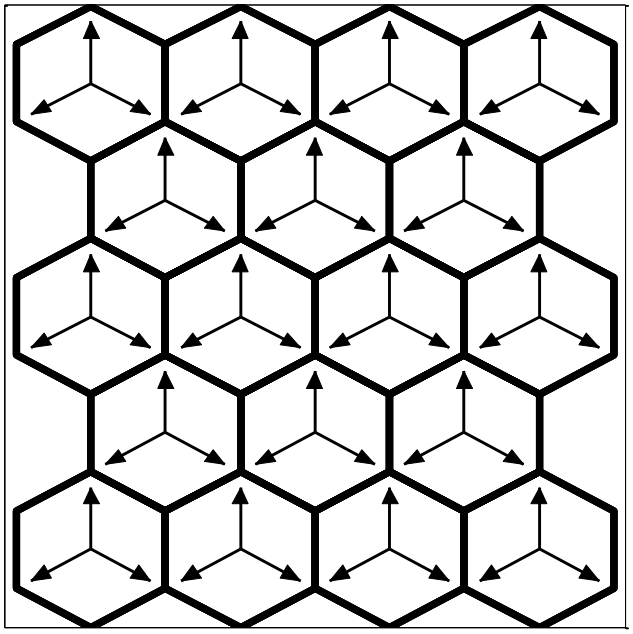

Figure 2-1: Three sector deployment

2.2.2 High order sectorisation

Present day cellular network deployments consist mainly of three sector macrocell base stations. When the traffic demand grows, operators need to evolve their cellular networks to provide the required capacity. Adding more sectors to the existing macro sites is considered to be the most cost-effective evolution path by the operators as it increases the network capacity without needing to add more base station sites to the network with backhaul capabilities. More than three sectors can be employed, as shown in Figure 2-2. Each sector has its own set of antennas, baseband, and RF modules. The disadvantage of adding more sectors is caused by the interference leakage between adjacent sectors meaning that the gain from adding more sectors does not scale up linearly with the number of sectors added to a site. However, the careful design of the antenna beamwidths can mitigate this effect to a large extent. Moreover, adding more sectors includes installing more antenna and hardware, which results in an increase in the cost and power consumption. Fortunately, the implementation of adaptive sectorisation can mitigate the increase in base station power consumption due to the addition of sectors. In adaptive sectorisation, the radio base station site is reconfigured to have fewer and larger beamwidth sectors to reduce the base station power consumption during periods of low traffic load.

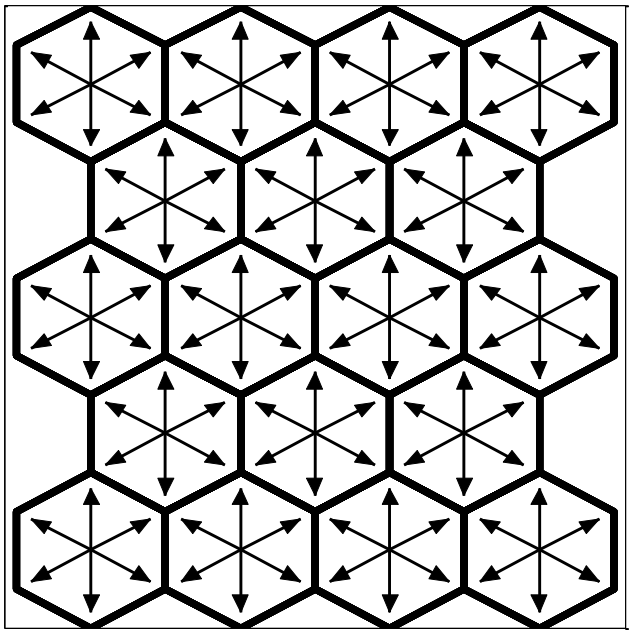

Figure 2-2: Six sector deployment

2.2.3 Deployment of MIMO techniques

Single-user MIMO wireless systems use multiple antennas at the transmitter and multiple antennae at the receiver equipment to either improve the system reliability and coverage via transceiver diversity and beamforming or to increase the transmission data rate via spatial multiplexing. When multiple antennae are used at the transmitter and a single antenna at the receiver, the system is known as multiple input single outputs (MISO), and transmit diversity gain is achieved. If the channel is known to the transmitter, an array gain can also be achieved; similarly, the single input multiple outputs (SIMO) scheme has a single antenna at the transmitter and multiple antennas at the receiver. This allows it to achieve both array and receive diversity gains. When the number of antennas at the transmitter is N_t and at the receiver N_r, a spatial multiplexing gain of $\min(N_t,N_r)$ is achievable in the transmitter-receiver link level capacity compared to the single input single output (SISO) channel capacity [16]. As we can see in equation (2.2), this gain translates into an improvement in the cell spectral efficiency which leads to a significant enhancement in the overall RAN capacity. The disadvantage of single-user MIMO schemes is that there is a minimum spacing distance required between the antennas to reduce the correlation between the different propagation paths in the MIMO channel, as correlation may lead to degradation of the channel diversity and the achievable capacity. Therefore, there is a physical limit on the maximum number of antennas that can be installed at the user equipment side, which in turn limits the number of simultaneous data streams that can be carried by the MIMO channel [17].

In multi-user MU-MIMO, one base station with multiple antennae communicates simultaneously with multiple users, each having one single or more antennas. Therefore, the multiuser MIMO channel can benefit from spatial multiplexing even with a single antenna at each user equipment. Another advantage of the MU MIMO systems is that users need only be a few meters apart to have different channel characteristics. In MU MIMO systems consisting of a base station with M antennas and K users, the transmitter must know the (K x M) channel matrix, H to be able to separate the received users' signals in the uplink and to achieve a spatial multiplexing gain of min (M,K) by directing each signal to its targeted receiver in the downlink.

Unlike single user (SU) MIMO systems, multiple data streams are transmitted to multiple users in MU MIMO, while SU MIMO increases the user data rate and MU MIMO systems increase the overall system capacity. An advantage of MU MIMO is that the advanced signalling processing is implemented in the transmitter, with the user's equipment only responsible for detecting its own destined data stream, which reduces the required level of complexity in the user's equipment compared with SU MIMO user equipment. To achieve optimal performance in MU MIMO systems, the inter-user interference must be completely suppressed by non-linear precoding schemes which require complex computations and accurate channel state information [18].

Recently, the idea of large-scale antennas systems also known as massive MIMO technology has been proposed in [19] and received wide interest as a potential technology to be deployed in the next generation mobile networks to meet the increasing demand for wireless services. This technology is an extended version of the MU MIMO systems whereby a large number of antennas at the base station serves multiple users' equipment simultaneously using the same time and frequency resources. The quasi-orthogonal properties of massive MIMO channel at very large numbers of antennae allows massive MIMO systems to offer high spatial multiplexing and large array gains through the use of linear low complex precoding techniques, which translates to a significant improvement in network energy efficiency and in the cell spectral efficiency. Values of up to 100 times improvement in spectral efficiency are often cited in literature when compared with single antenna systems [20]. However, as each antenna has its own RF transceiver, the circuit power consumption scales up linearly with the number of deployed antennas. A detailed evaluation of the RAN energy consumption when deploying massive MIMOs is provided in chapter 7.

2.2.4 Deployment of heterogeneous networks

The concept behind heterogeneous networks (HetNets) is to overlay an existing homogenous macro network with additional smaller low power base stations. These can be micro, pico or femto base stations, or a combination thereof. The advantage of network densification with

small cells is that it enhances the RAN capacity by increasing the spectrum re-use factor and reduces the distance between the user and the base station, thus improving the signal to interference and noise ratio, and decreasing the RF power transmitted by the small cells. This can result in an increase in the RAN capacity and a reduction in the consumed energy. Another advantage is that by offloading traffic from macro cells to the small cell layer, reduction in the users' contention for frequency resources is observed in the macro layer; hence, the per-user allocated bandwidth in macrocells increases, leading to higher data rates for macrocell users. Similarly, the users who are associated with small cells benefit from more per user allocated bandwidth and better SINR values, which also improves their achieved data rates.

2.3 Energy efficiency in cellular networks

As has already been highlighted, the continuous growth of demand for more capacity is expected to continue. According to the Cisco visual networking index for 2011-2015, mobile data traffic doubled between 2010-2011, and again between 2011-2012. If this exponential trend had continued, a 1000-times increase in mobile data traffic would occur by the end of 2020, as shown in Figure 2-3. However, a slowdown in this increase was observed in the period 2013-2015. The growth factor was 1.77 times in the period 2013-2014 and 1.63 between 2014-2015.

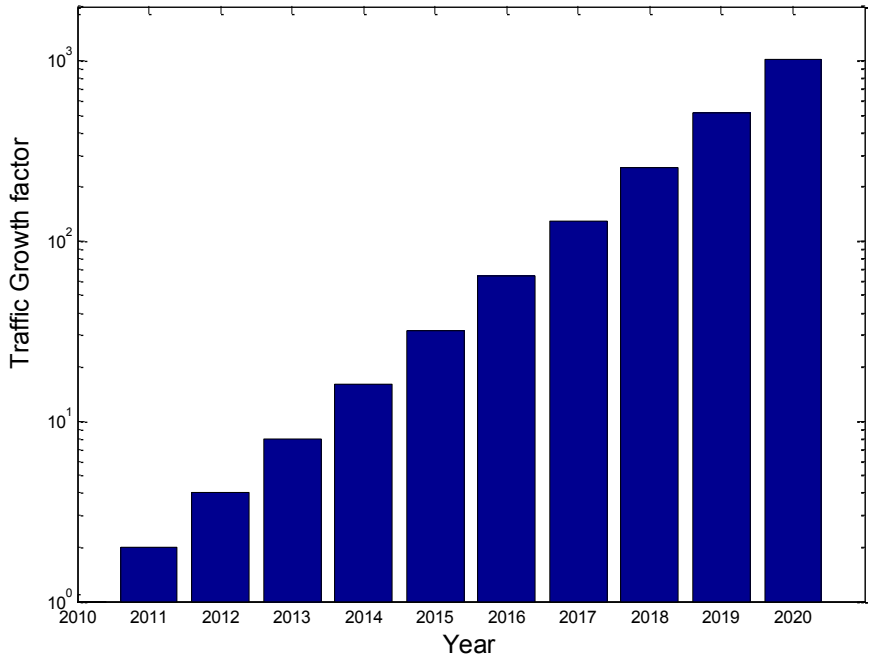

Figure 2-3: Projected traffic demand growth

Added to this is the fact that the number of mobile devices and connections is expected to grow to 11.6 billion by 2021 [21]. To meet such rapidly growing demand, operators have started to densify their networks by adding more sites and deploying multiple solutions and techniques to improve the capacity of existing network. This phase of network densification and upgrading

the existing network by the deployment of more advanced techniques is expected to intensify in 5G RANs. If no actions are taken, the energy demand for operation of a network able to deliver such massive data rates risks becoming unmanageable. Hence, a shift paradigm in the process of the design of cellular networks is needed. Unlike the previous generations of cellular networks where coverage and capacity were the two considered key performance indicators when designing the network, energy efficiency is now a major concern for network operators for the following reasons:

1. Economic reasons - reducing the network operating cost is an important target for the operators as the network energy consumption bill represents a significant cost of operation [22]. For example, the cost of energy represents 30% of the total operating expenses of the networks in the urban areas of India, and around 50% in rural areas [23].
2. Environmental reasons - the information and communication technology (ICT) sector was responsible for about 2% of the global CO2 emissions in 2009 and such emissions are predicted to grow to about 2.8% in 2020 [6].

Due to the above-mentioned reasons, a number of international research projects during the last ten years have addressed the issue of energy efficiency in cellular mobile networks. For example, the mobile VCE green radio project was initiated in 2009, a three-year collaboration between five UK universities and 12 international communication companies [24]. The project investigated a wide range of energy reduction techniques and focused on intermediate to long-term solutions to achieve more energy consumption savings in cellular networks. The FP7 EARTH project is another important project which has investigated the energy efficiency in mobile communication systems with the aim of the development of a new generation of energy efficient equipments, novel deployment strategies, and energy-aware network management solutions [25]. In 2010, The GreenTouch project was launched as a collaborative research consortium between more than 40 academic institutions and industrial companies with the aim of tackling the problem of energy efficiency in communication networks. At the end of the project in 2015, GreenTouch claimed that 98% of the energy consumed in an end-to-end network could be saved and 10 000 improvements in the EE (bit/j) in the mobile radio access network [26]. These values seem to be very optimistic and have been achieved according to GreenTouch by a combination of sleep mode techniques in small cells and adaptive antenna muting in massive MIMO deployments, large portion of the claimed energy savings are attributed to an expected significant reduction in the base station power consumption in 2020, for example, a massive MIMO base station with 200 antennas is assumed to consumed only around 25 watts in 2020 according to the IMEC used base station power consumption model [27] which seems to be very optimistic when compared with the proposed model in this thesis.

2.3.1 Performance and energy metrics

To evaluate any of the network key performance indicators, a well-defined and accurate metric is needed. A metric is defined as a system or standard of measurement, by which one or more characteristics of a system can be assessed. It must be a measurable quantity or calculated from other measurable quantities to provide quantified information about the evaluated system. Metrics are required when comparing the performance of two different systems and when setting an explicit target to achieve. They are also needed to quantify any gains or losses resulting from applying a certain configuration in the system [28]. When evaluating the performance of any system, defining a set of metrics as a performance baseline for the system can be very helpful to identify any problems leading to a degradation in the evaluated system performance.

An overview of the metrics used to measure the main key performance indicators in mobile networks is presented in the following section, followed by a discussion of the necessity of defining a consistent metric system to assess the energy efficiency in mobile networks.

2.3.1.1 The coverage and capacity metrics:

A. Coverage metrics

Quantifying the level of coverage in a cellular network is straightforward: the coverage probability is often used as a metric, and it is defined as the average area or average fraction of users who receive an SINR value above a certain threshold. In some cases, the term outage is used to refer to the coverage level, which refers to the average area or average fraction of users where the SINR is below a certain value. The network coverage can be also characterised by the cell edge coverage, which is defined by the 5^{th} percentile of the cumulative distribution function (CDF) of the users' SINRs.

B. Network capacity metrics

Multiple metrics are defined to quantify the capacity of cellular networks. The main metrics used in the ITU report titled "Requirement related to technical performance for IMT-advanced radio interfaces" [29] and in the ITU draft report "Minimum requirements related to technical performance for IMT-2020 radio interface" [30] are listed below:

- **Peak data rate**: is the maximum achievable data rate when all the bandwidth is assigned to a single user equipment where error-free transmission is assumed.
- **Peak spectral efficiency**: the peak data rate normalised by channel bandwidth and measured by (bit/s/Hz).

- **Cell average spectral efficiency**: is the sum throughput of all users divided by the channel bandwidth and measured in bit/s/Hz/cell. The channel bandwidth is defined as the operative bandwidth multiplied by the frequency reuse factor.
- **Area traffic capacity**: is the total sum throughput per area unit and measured in (Mbit/s/m^2).
- **The 5th percentile user spectral efficiency**: it refers to the cell edge user's spectral efficiency (the 5% point of the CDF of the normalised user throughput). Normalised user throughput equals the user throughput divided by the channel bandwidth, measured in bit/s/Hz.

2.3.1.2 Energy efficiency metrics

Energy efficiency metrics are often defined according to the purpose of the system: they can be classified into absolute metric and relative metrics. Absolute metrics can be expressed in two ways:

1) The ratio of the effective output of the system (useful performance) in the nominator to the input consumed energy in the denominator. An example of this type is the bits/joule metric.

2) The ratio of consumed energy or power in the nominator to the effective output of the system (useful performance) in the denominator. The area power consumption and the energy consumption ratio (ECR) are examples of this type [28].

When evaluating the energy efficiency of mobile network, the evaluations can be carried out on three levels: the component level, where the system effective output varies according to the evaluated component; the equipment level, where the base station is the main considered equipment in mobile RAN, and system effective output refers to either the base station coverage, capacity, or both; the network level, where the energy efficiency metric must access the overall effective output performance of the network, which can be the coverage, capacity, or both, while not ignoring the other features such as the actual consumed energy, load conditions, and QoS parameters.

Relative energy efficiency metrics are also used when comparing the energy consumption of one network with reference to a baseline reference network. An overview of the widely-used metrics of energy efficiency in mobile networks is presented for the three levels previously mentioned.

A. Component level

The choice of the component energy efficiency metric is relatively straightforward: the metrics used to assess the energy efficiency of the main common units or components in a typical radio base station are listed below:

The power amplifier and RF Transceiver: this unit consists of the power amplifier and downlink and uplink RF chains**.** The power amplifier represents the major consuming component in this unit, and its efficiency refers to how efficiently the input power to the power amplifier (DC+AC) is converted into output power. It is defined as the ratio of output power to the input power. Other components in the RF transceiver include the low noise amplifier, the mixer, oscillator, and the ADC and DAC converters. As their power consumption is relatively small when compared with the power amplifier, their energy efficiency metrics are out of the scope of this research project.

Baseband processing unit: the energy efficiency of the baseband processing unit is measured by the MFLOPS/watt metric where FLOPS measures the floating-point performance of the processor and refers to the number of Mega Flops performed for each watt of consumed power. A higher value of the metric means a higher energy efficiency of the unit.

Power supply unit: the main function of the power supply unit is the conversion of AC/DC, and DC/DC to provide the various DC values needed to operate the different components of the base station. Its energy efficiency is always measured as the ratio of the output power to the input power and refers to how much power is wasted during the conversion process.

Air conditioning system: The energy efficiency of a cooling unit is often measured by its energy efficiency rating (EER), which is defined by the amount of removed heat measured in British thermal units (BTU) for every watt of consumed electric power in the cooling unit.

B. Equipment level

The term equipment in this context refers to the radio base station (RBS). The standard body of telecommunication standards institute (ETSI) defines a number of methods and metrics to evaluate the energy efficiency of radio base stations [31]. Two types of radio base station architectures are considered: the integrated radio base station and distributed radio base station. In integrated radio base stations, the RF components are located in the same cabinet as the baseband processing unit, while in distributed radio base stations, remote radio heads are placed on top of the tower close to the antennas to reduce the feeder cable losses and connected to the baseband unit with fibre cable. For both of base stations, the ETSI document proposes averaging the three measurements of the power consumption of the radio base station site at three different load values (high, medium, low). The energy efficiency is defined as the

coverage with units of (Km^2/watt) and used as an energy efficiency metric for GSM equipment when deployed in rural areas, as in (2.3). The energy efficiency of GSM equipment when deployed in urban areas is usually measured with the capacity-related energy efficiency metric with units (subscribers/watt), as shown in (2.4).

$$EE_{coverage} = \frac{A_{coverage}}{P_{site}} . \tag{2.3}$$

$$EE_{capacity} = \frac{N_{busy\ hour}}{P_{site}} . \tag{2.4}$$

In 3G and 4G RBSs, the network capacity is the main performance indicator for the network. The ratio of the average daily data volume to the average daily consumed energy in the base station is proposed as an energy efficiency metric, as shown in (2.5), measured in bit/J [28].

$$EE_{equipment} = \frac{\overline{DV}}{\bar{E}} , \tag{2.5}$$

Where $\overline{DV}$ represents the total average daily data volume and $\bar{E}$, the total average energy consumption in the radio base station. An energy efficiency coverage indicator is also proposed in the same reference and defined as the ratio of the base station coverage over the consumed power, as in (2.6) with the units of $\frac{Km^2}{W}$.

$$EE_{coverage} = \frac{Area}{P_{equipment}} . \tag{2.6}$$

C. Network level

As a network consists of a number of deployed radio base stations, at the equipment, energy efficiency metrics can be used to evaluate the energy efficiency of the RAN. In this case, the only difference being that the RAN power consumption is calculated as the sum of power consumption of the individual base stations. The RAN aggregate throughput equals the sum of cells' throughputs, as in (2.7) and (2.8).

$$P_{RAN} = \sum_{i=1}^{k} P_i . \tag{2.7}$$

$$R_{RAN} = \sum_{i=1}^{k} R_i . \tag{2.8}$$

The area power consumption has been proposed in [32] as a network-level energy efficiency metric by dividing the average consumed power in the network by the network coverage, as in (2.9). It is the reciprocal of the metric (2.6) and is measured in watts per square kilometre.

$$Area\ power\ consumption = \frac{P_{RAN}}{A_{RAN}}, \tag{2.9}$$

Where A_{RAN} is the coverage area of the network. However, the authors of [33] argue that a single metric is not sufficient to provide a full picture of the status of the energy consumption in the network. Thus, they propose the use of both the area power consumption and the energy consumption reduction (ECR) measured in joules per bit metric to capture the full picture about the network energy consumption. Their justification for this is that the two metrics provide complementary information about the network energy efficiency. The area power consumption is more relevant in low traffic load cases, and as the area of the network to be evaluated is predefined, no confusion occurs when interpreting the metric. Any decrease in the area power consumption means a reduction in the consumed power. The second metric of ECR evaluates the network power consumption with respect to the network throughput, as shown in (2.10) and is more relevant in high traffic load cases.

$$ECR = \frac{P_{RAN}}{R_{RAN}}. \tag{2.10}$$

The drawback of this metric is that it can lead to misleading conclusions about the energy efficiency of the same network when evaluated at different traffic load values: it will show low efficiency when the traffic load is low and higher efficiency when the traffic load increases for the same network.

Two energy consumption relative metrics were also used in [34]: the energy consumption gain (ECG) and the energy reduction gain (ERG). These two metric are used to evaluate the energy consumption of the network under tests with a comparison to a baseline reference network. These have no units. ECG is expressed as (2.11).

$$ECG = \frac{Energy_{ref}}{Energy_{test}}. \tag{2.11}$$

ECG values greater than one, mean that the system under test is more energy efficient than the reference system. ERG is expressed by (2.12).

$$ERG = \frac{Energy_{ref} - Energy_{test}}{Energy_{ref}}\ X\ 100\ \%. \tag{2.12}$$

Its value is positive and lies between [0-100 %] if the tested network is consuming less energy than the reference network.

In summary, the proper evaluation of the energy efficiency of mobile networks is a serious issue, and the adoption of the right energy efficiency metrics is essential to assess the actual gains or losses in the network energy consumption. In general, no single metric can represent the whole state of energy consumption in the mobile network. However, choosing certain metrics rather than others may lead to contradictory or different results. Therefore, a set of well-defined energy efficiency metrics must be agreed upon to achieve valid and reliable results when assessing the energy efficiency of different networks or when evaluating the energy efficiency of the same network at different operating conditions.

2.4 Power consumption modelling in radio base stations

Radio base stations represent the main energy consuming element in a cellular network. According to [35], the radio access network of 3G network, which comprises the base stations, the base station controllers, and the radio network controller, comprise almost 80% of the overall power consumption of the cellular network, as shown in Figure 2-4.

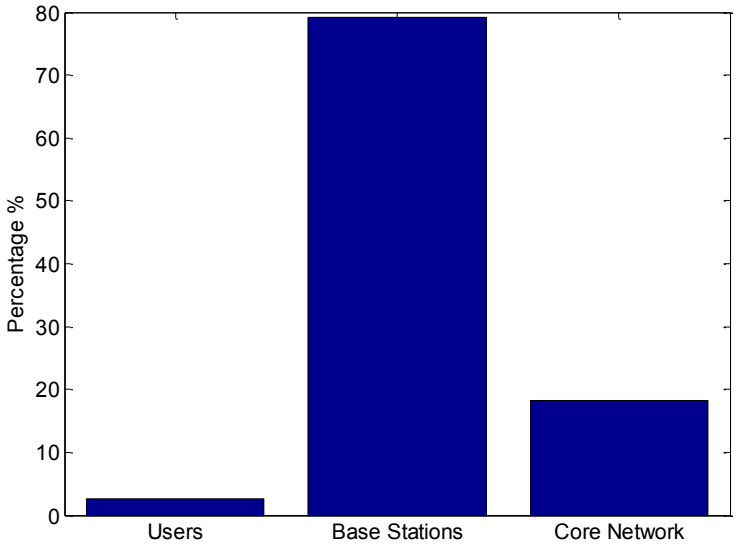

Figure 2-4: Power consumption distribution in 3G mobile networks

A differing figure is provided by Vodafone UK, who claimed that base stations account for around 60 % of the total cellular network energy consumption [36]. For this reason, knowing the RAN power consumption is essential for determining the network energy efficiency regardless of which metric is adopted to measure the network energy efficiency.

A number of radio base station RBS power consumption models are available in the open literature based on measurements taken from specific vendor's equipment. The models provide a

method of estimating the RBS total power consumption as a function of the peak transmitted radio frequency (RF) power and the average traffic load in the base station. These models have high levels of commonality because they are derived from similar RBS architectures.

Base station sites can vary in size and architecture depending on the equipment's manufacturer, the technology used, and the year of manufacturing; however, they consist of common key components: the antenna, RF transceiver, power amplifier, baseband processing unit, power supply unit, site cooling unit, and backhaul unit. The power consumption of macro and micro base station equipment in [32] is modelled as a linear function in the RF transmitted power, as in (2.13) and (2.14).

$$P_{ma} = a_{ma} * P_{tx} + b_{ma} \ , \tag{2.13}$$

$$P_{mi} = a_{mi} * P_{tx} + b_{mi} \ , \tag{2.14}$$

Where P_{ma} and P_{mi} denote the average consumed power for the macro and micro site, P_{tx} is the site radiated RF power, the parameters $a_{ma}$and a_{mi} account for the power consumption that scales with the radiated RF power, and $b_{ma}$and b_{mi} denote the overhead power consumption which is consumed independently of the average radiated power. The authors assume a full load case in their analysis and load scaling aspect is disregarded.

A more detailed power consumption model is presented in [37] to estimate the power consumption in GSM and UMTS macro base stations, as in (2.15):

$$P_{BS,Macro} = N_{sector}.N_{PApsec}.\left(\frac{P_t}{\mu_{PA}} + P_{SP}\right).(1 + C_c).(1 + C_{PSBB}) \ , \tag{2.15}$$

Where N_{sector} refers to the number of sectors, N_{PApsec} is the number of power amplifiers per sector, P_t is the RF transmitted power, μ_{PA} is the power amplifier efficiency, P_{SP} is the signal processing power overhead, C_c is the cooling power loss, and C_{PSBB} are the power losses in the power supply. This model does not provide any load scaling in the case of macro base stations. Unlike macro base stations, the authors modelled the power consumption of micro base stations as the sum of the static load independent part and dynamic load dependent part. The load is considered to vary only between the two states of no load at all and full load.

Similarly, the authors of [38] have developed a power consumption model for the macro and micro base station for the WiMAX, HSPA and LTE technologies. They modelled the macro base station as the sum of load independent parts, and load dependent parts, as in (2.16). They included the microwave backhaul power consumption in the model.

$$P_{macro} = P_{const} + P_{load} * F_i \ , \tag{2.16}$$

Where F_i is the load factor and ranges from 0 to 1.

$$P_{const} = n_s * P_{rect} + P_{link} + P_{airco} \ , \tag{2.17}$$

$$P_{load} = n_s * (n_{tx} * (P_{amp} + P_{trans}) + P_{proc}) \ , \tag{2.18}$$

Where n_s is the number of sectors, n_{tx} is the number of antennas, P_{rect} is the power consumption of the rectifier, P_{link} is the power consumption of the microwave link, P_{airco} is the power consumption of the cooling unit if needed, P_{trans} is the power consumption of the RF transceiver, P_{proc} is the power consumption of the baseband signal processing unit, and P_{amp} is the power consumption of the power amplifier and equals: $P_{amp} = \frac{P_{tx}}{\eta}$, where P_{tx} is the input power of antenna, and η is the efficiency of the power amplifier. The authors claimed that the same model can be used to calculate the power consumption of micro base stations by dropping off the backhaul power consumption, setting the number of sectors and antennas to one, and using a lower value for power consumption in the cooling unit.

Different methodologies for modelling the power consumption in various types of base stations has been presented in [39], where power consumption values of different base station components and subcomponents were provided at a reference configuration, followed by a method of how these values scale when changing the values of bandwidth, number of antennas, modulation and coding type, and duty cycle in time and frequency domain from those used in the reference configuration. The model assumes 10% losses in the cooling unit and relies on measured data to model the power consumption of the power amplifier.

The widely used Earth power consumption model published in [40] provides a comprehensive model to map the RF output power to the total consumed power in the various types of base stations. The model includes the losses in the power supply, cooling unit, power amplifier and feeder cable. The RF and baseband unit power consumptions are modelled as a function of the allocated bandwidth and number of RF transceivers. The power amplifier efficiency degradation due to transmitting at lower RF power was added to the model later in [41] without any details on how this extension was developed. The model is its final form is shown in (2.19).

$$P_{in} = N_{trx} \left(\frac{\frac{P_{out}}{\eta_{PA} * (1 - \sigma_{feed})} + P_{RF} + P_{BB}}{(1 - \sigma_{dc}).(1 - \sigma_{ms}).(1 - \sigma_{cool})} \right), \tag{2.19}$$

Where P_{in} is the consumed input power, N_{trx} is the number of sectors multiplied by number of antennas per sector, P_{RF} is the RF transceiver power consumption, P_{BB} is the power consumption in the baseband processing unit, η_{PA} is the power amplifier efficiency, σ_{dc} is the DC to DC converter efficiency, σ_{ms} is the main supply efficiency, σ_{cool} represents the cooling system power consumption in the base station, and P_{out} is the radiated RF power ranging from 0 to P_{max}. The full range of model parameters, reflecting the cutting edge of technology in 2010 and 2012 for each type of base station, are provided to simplify the model utilisation [42]. The model assumes that 10% of the overall power consumption of the macro base station is wasted in the cooling unit without any details on how this value has been obtained.

A similar power model was presented in [43] and was developed in Green Radio mobile VCE project [44]. The model incorporates the power amplifier and feeder cable efficiencies and is expressed as (2.20).

$$P_{in} = P_{cool} + P_{bh} + n_s.(P_{rect} + P_{bb}) + n_s.n_t.\alpha.\left(P_{trx} + \frac{P_{max}}{\eta_{pa}.\eta_{feed}}\right), \qquad (2.20)$$

Where P_{cool} is the cooling system power consumption, P_{bh} is the backhaul power consumption, P_{rect} is the power supply consumption, P_{bb} is the baseband signal processing power consumption, P_{trx} is the RF transceiver power consumption, P_{max} is the maximum RF radiated power, η_{pa} is the power amplifier efficiency, η_{feed} represents the efficiency of the feeder cable, and α refers to the cell average load. The model uses measured absolute values to represent the power consumption in the cooling unit and in the power supply, which prevents it from being scalable with the cell average traffic load and number of antennas.

Recently, the authors of [27] have presented a flexible future-proof power consumption model which estimates the power consumption of the various types of SISO and MIMO base station. It can also predict the power consumption of future generations of base stations. The model uses the concept of scaling the power consumption of the base station components and subcomponents (as previously presented in [39]) versus the bandwidth, number of antennas, modulation and coding types, and cell load. Measured data are used to model the power consumption of the power amplifier, and a fixed percentage of 10% is assumed for the losses in the cooling unit. The model is available only through a web interface which limits its use and makes its integration in system-level simulations complicated.

2.5 Approaches to energy efficiency improvement

A wide range of approaches have been proposed in the literature in order to reduce the energy consumption of cellular networks; these approaches can be classified into the following categories:

2.5.1 Hardware and base station architecture improvement

This category includes any hardware or base station architecture-related technique which may lead to a reduction in the power consumption in the base station. They include the following techniques:

2.5.1.1 Improvement of the power amplifier efficiency

The power amplifier represents the main power consuming component in macro and micro base stations, consuming around 60% of the total energy in LTE macro base stations [45]. Multicarrier signals, as found in OFDMA, exhibit high peak-to-average-power-ratios (PAPR), necessitating the PA being backed-off from its saturation power level in order to operate in the linear region of its input-output transfer function. Operating the PA below its saturation level results in reducing its efficiency. Several solutions have been proposed to improve the power amplifier efficiency at high PAPR values. For example, the Doherty power amplifier technique employs two power amplifiers; one is always active and a second one operates only during the signal peak periods, which makes it suitable for high PAPR signals. An efficiency range of 40% to 45% is achieved with such power amplifiers [46] [47].

Another technique is that of envelope tracking, which has the potential to achieve significant reductions in the power amplifier dissipated power by adjusting the DC supply power to track the variation in the amplitude of the input signal. An overall efficiency of 50 to 55 % is achieved when deploying this technique [48]. More techniques are proposed in the open literature to improve the efficiency of the power amplifier, such as class J amplifier architecture, which can maintain an efficiency of 45% over 10 dB of dynamic range, and switch mode power amplifiers, which can reach high-efficiency values: 70% to 90% values are often cited in literature [49, 50].

2.5.1.2 Base station architecture improvement

In distributed base station architectures, the baseband processing unit is located in the base station cabinet while the radio equipment and power amplifier are located at the top of the tower with a fiber cable connection to the indoor baseband processing unit. Such a design eliminates the -3 dB feeder cable losses and the need for cooling in distributed macro base stations, both of which provide high energy consumption savings when compared with traditional integrated base stations [51].

2.5.1.3 Baseband processing improvement

In parallel baseband processing architectures, all load dependent operations can be executed on a pool of processors. This design allows switching off some processors during periods of low traffic load, which leads to a reduction in the power consumed by the baseband unit [52]. A

novel mobile network architecture was first proposed in [53] as a potential solution to reduce the network deployment and operation costs. The baseband units of several base stations are moved into central remote location and connected to the radio head via high capacity fibre backhaul links. This architecture offers high processing capacity and saves energy by simplifying the process of turning off processors. An energy efficiency implementation of the idea was demonstrated in [54]. Significant reductions in the consumed power and improvement in the energy efficiency in bits per joule were obtained when compared with the case of traditional heterogeneous mobile RAN deployment. The authors of [55] evaluated the benefits of implementing a similar idea termed the RAN as service. They investigated the impact of implementing the RAN as service on the cloud in terms of the RAN energy efficiency and proposed a system-level power model to be used to estimate the power consumption of various cloud-based implementations of the RAN as a service concept. The model can serve as a reference for any future investigations of the energy efficiency if more advanced cloud-based functionalities are implemented.

2.5.2 Network planning and deployment techniques

One of the aims of this research project is to investigate the impact of various mobile network deployment strategies on the RAN spectral and energy efficiency. In this regard, a review of the related work is presented in the following sections with more concentration on the deployment strategies. In addition to the traditional homogeneous deployments of macro only cells and heterogeneous deployments, the impact of improving the capacity of existing sites by adding more sectors and deploying more advanced MIMO techniques is also covered. Most of the existing research in this area mainly focuses on improving the RAN coverage and capacity [56]. However, the RAN energy efficiency has become a vital issue for the operator in the recent years, and the issue has been extensively researched since 2009. As we will see from the review, considerable discrepancies in the obtained results are observed in the literature, the reason being the lack of a unified framework for the evaluation of the RAN energy efficiency which can result in conflicting results in many cases.

2.5.2.1 Homogenous network deployments

An example of work in the field is presented in [57], which used the *ECR* metric to demonstrate that a homogeneous small size macro cell deployment is theoretically always more energy efficient than a large size macro cell deployment in terms of the base station RF transmitted power. Similar conclusions were obtained by the authors in [58]; in practice, an optimum cell radius exists when the radio base station overhead power is taken into account [59]. The authors of [60] also showed that, for path exponent values > 2, small cells, including micro, pico and femtocells are more energy efficient than large macrocells if the overhead power is negligible. The authors of [32, 61, 62] used the area power consumption as a metric, which is defined as the

ratio of RBS power consumption to cell coverage area with units of $\mathrm{watt/m^2}$ as an energy efficiency metric. They determined the RBS transmit power according to the minimum required received power at the cell edge. This framework exhibited an optimum RBS coverage radius, which minimised the area power consumption value. The authors also applied their framework to a heterogeneous network topology to show the potential for reducing energy consumption by optimizing the inter-site distance (ISD) between macro cells for predetermined positions of small cells placed on the edges of the macrocells.

Similarly, the authors in [63] investigated cell densification using the $\mathrm{W/m^2}$ area power consumption metric and observed that smaller macro cell ranges are more energy efficient only when there is no overhead power at all. The same issue was investigated in [64]. The authors concluded that when realistic power models are used, it is more energy efficient to deploy the largest macro cell size which able to meet the capacity requirement. A similar conclusion was reached in [65] when using the area power consumption metric, and the same cell edge minimum received power condition. By using the cell edge capacity as a KPI, the authors in [65] showed that the energy efficiency was maximised for the largest feasible cell ranges when the overhead idle and backhaul power consumption were considered. The obtained results in [57, 58, 61, 62 63] are contradictory to each other due to the usage of different power consumption models and the lack of a unified methodology to evaluate the energy efficiency, when overhead circuit power consumption is ignored or underestimated, small cells seem to be more energy efficient, while when the overhead is considered, larger cells become the more energy efficient option to deploy. This observation demonstrates the necessity of the accurate modelling of the base station power consumption and the need for a unified evaluation framework to avoid such contradiction.

The framework presented in [59] investigated a joint metric based on a bit/J for the energy efficiency (EE) and $\mathrm{bit/\$}$ for the deployment efficiency (DE). The DE was obtained by calculating the ratio of the RAN data volume in bits to the RAN deployment cost in dollars. The RAN cost was taken from the summation of the Capital Expenditure (CapEx) and the Operational Expenditure (OpEx) over a predetermined period of time. The cell edge minimum received power was again used as a KPI with the inter-cell interference determined using a fluid model [66]. The results gave optimum EE and DE points as a function of the cell radius. However, the optimum radius for DE is significantly greater than that for EE, suggesting that both efficiencies cannot be simultaneously optimised. Further, the optimum points for both metrics were highly sensitive to the value of the path loss exponent, which was investigated over the range 3.5 to 4.5.

2.5.2.2 Deployment of high order sectorised sites

Adding more sectors to the existing macro sites is a more cost-effective evolution path than deploying more macrocells, as it increases the network capacity without needing to add more base station sites. However, the gain from adding more sectors does not scale up linearly with the number of sectors added to a site, while a linear increase in the power consumption of macro sites is observed when more sectors are deployed, which leads to a degradation in the network energy efficiency when measured by bits per joule metric.

Several publications have reported the impact of high order sectorisation on the RAN capacity. In [67], the authors evaluated the mean throughput per macro site against the antenna beamwidth for 3-, 6- and 12-sectors' circular antenna array deployments. Their results showed that when the optimum beamwidth is used, a 12-sector deployment is able to improve the site's mean throughput by a factor of 3.2 compared to a 3-sector deployment. It has been shown by simulation and field trials in [68] that high order sectorisation can offer potential capacity gains when utilised in HSPA+ cellular networks. Cooperation between the sectors of the same macro site was shown to mitigate the interference leakage between the sectors, leading to improvements in both the site throughput and the fairness between users [69].

A combination of horizontal and vertical sectorisation can also be used. For example, an antenna array of 10 vertical sectors and 16 horizontal sectors can offer up to 1.5 Gbit/s throughput when deployed inside a stadium environment [70]. The performance of horizontal and vertical high order sectorisation is evaluated in [71]. The authors concluded that both the horizontal and vertical sectorisation techniques give similar results in the case of small urban macro-cells whereas the horizontal sectorisation techniques outperform the vertical case in a large macro-cell scenario. In addition to the evaluation of the throughput gain when more sectors are deployed, the impact of using high order sectorisation techniques on the RAN energy consumption need to be evaluated, as adding more sectors involve adding more RF transceivers which will certainly lead to an increase in the site power consumption. Fortunately, this increase in the power consumption of sectorised macro sites can be reduced through the implementation of adaptive sectorisation techniques.

Adaptive sectorisation was originally proposed to address the limitations of designing the RAN to meet the peak traffic demand only. When the traffic intensity is low, the fixed sectorisation solution is no longer energy efficient as radio infrastructure unnecessarily remains switched on. In adaptive sectorisation, the radio base station site is reconfigured to have fewer and larger beamwidth sectors during periods of low traffic load. Results reported in the literature show a 30% power saving using adaptive sectorisation compared to a fixed tri-sectored site with only a 7.6% decrease in throughput [72]. The authors in [73] have proposed an energy-aware adaptive

sectorisation strategy to improve the energy efficiency of LTE networks, where each base station is capable of adapting to the temporal traffic variation by switching off one of its sectors and changing the beamwidth of the two remaining sectors to maintain the required coverage level. Their results show a 21% energy saving when one sector is switched off during a low traffic load period.

An electrically reconfigurable antenna concept has been proposed for adaptive sectorisation [74]. The concept allows the number of active sectors and the antenna beamwidth to be changed using a tuneable reflector. The authors have compared between the energy consumption of an always active 6-sector base station and a dynamic 6-sector base station which can dynamically switch off its sectors while adapting the antenna beamwidth. The work reports peak energy savings of 75% and mean energy savings of 38%. The authors in [75] proposed a traffic-sensitive dynamic sectorisation technique based on a low complexity heuristic algorithm. The proposed dynamic algorithm outperforms the semi-static sectorisation schemes and the base station on/off schemes. Adaptive sectorisation has also been proposed to enhance the network throughput in unbalanced traffic scenarios [76]. A dynamic sectorisation technique based on a genetic algorithm was used in an OFDMA network to adapt the antenna pattern when an unbalanced traffic distribution is encountered. An enhancement of up to 50 % was shown in the network throughput compared to a fixed sectorisation scenario.

2.5.2.3 Deployment of advanced MIMO techniques

Multiple-In-Multiple-Out (MIMO) techniques are used in RANs to enhance either cell capacity through spatial multiplexing or cell coverage through spatial diversity without increasing the channel bandwidth or the RF transmit power. However, the power consumption of a MIMO base station increases due to more signal processing and more RF chains when compared to a SISO base station. Many previous publications have investigated the issue of MIMO energy efficiency, with most of the cited results claiming that MIMO deployments can be more energy efficient than SISO deployments if only the RF transmitted power is taken into account. The authors of [77] have evaluated the MIMO energy efficiency in wireless sensor networks (WSNs) employing Alamouti diversity. Contrary to the widely-held view that MIMO systems would be more energy-efficient than SISO, the authors concluded the opposite when the overhead circuit energy consumption was taken into account. Their research demonstrated that in short-range applications, SISO WSNs can be more energy efficient than MIMO WSNs.

The energy consumption ratio (ECR) measured in J/bit has been evaluated for both SISO and MIMO 2x2 Alamouti schemes in [78] for both the Round Robin (RR) and Proportional Fair (PF) scheduling algorithms. When only the RF transmission power is considered, the authors concluded that the 2x2 MIMO transmission mode (i.e. the Alamouti space frequency block code)

is both more spectrally and energy efficient than SISO in both urban micro and urban macrocell deployment scenarios. Similarly, an evaluation of the SISO and different MIMO schemes has been presented in [79]. The studied MIMO schemes include the transmit diversity, open loop spatial multiplexing (OLSM), and the closed loop spatial multiplexing (CLSM) schemes. The energy consumption rating (ECR) is used as a metric for the energy efficiency, and the authors have shown that all the various MIMO schemes offer better energy efficiency than the SISO scheme when the overhead is not included in the evaluation. The authors of [80] investigated the MIMO energy efficiency for different cell types, and observed that a significant SINR improvement could be obtained with MIMO (e.g., 7.1 dB for a 2×2 configuration) independent of the cell type. However, an increase in base station power consumption was observed due to the increased complexity of the transceiver circuitry and the additional signal processing needed. The MIMO energy efficiency at the link level have been evaluated in [81] and obtained results have shown that MIMO does not provide any energy efficiency gain when more than two transmit antennas are used, and the circuit overhead power consumption is included in the analysis. The energy efficiency of the various MIMO schemes including the Alamouti scheme, transmit beamforming, receive diversity, spatial multiplexing, and transmit antenna selection between a single base station and single user were evaluated in [82] and compared against a SISO scheme using the energy per bit metric (ECR) and basic base station power consumption model. The results showed that all the MIMO schemes outperform SISO in terms of achieving the lowest ECR values when targeting the same spectral efficiency and outage probability. The 2x2 transmit antenna selection scheme is found to be the most energy efficient scheme among the evaluated schemes, the reason being that only a single RF chain is required in the selection scheme to achieve spatial diversity gain.

2.5.2.4 Heterogeneous network deployments

As mentioned previously, in heterogeneous networks (HetNets), existing homogenous macro networks are overlaid with additional smaller low power base stations, which leads to two advantages: improving the network capacity and the per users' data rates, and reducing the RAN power consumption when compared with macro cell deployments. Several published studies have shown that HetNet deployments improve the RAN throughput [83] by increasing the spectrum reuse factor while helping to alleviate the network energy consumption by deploying low power base stations where they are needed.

The impact of a HetNet deployment strategy on the power consumption of the mobile network has been evaluated by varying the number of microsites per macrocell as well as the macro cell size while aiming to achieve the same target RAN area spectral efficiency. It has been shown that the area power consumption can be decreased under full load conditions without affecting the target area throughput [32]. Similar analysis has been carried out in [61] by varying the

number of microsites per macro cell without defining any target RAN area spectral efficiency and comparing the results against macro only deployment. The obtained results have shown that there is an optimum macro inter-site distance which depends on the number of deployed micro cells per macro site. In addition, an improvement in the area spectral efficiency has been observed when increasing the number of microcells per macro site. However, this improvement starts to disappear gradually at large macro cell radii. In [84], it has been found that homogenous micro cell deployments offer higher RAN throughput values than that of macrocells only or heterogeneous RAN, but this high throughput is accompanied by an increase in the area power consumption when compared with macro only and macro-micro heterogeneous RANs.

The authors in [85] have also analysed the impact of different heterogeneous deployment strategies on the area power consumption for uniform and non-uniform user distributions. The results demonstrated that in WCDMA networks, the area power consumption can be decreased by up to 50% when small, low power base stations are deployed at the edges of the macrocells. In [86], an analytical and numerical evaluation of the energy efficiency of a network consisting of macrocell base stations overlaid by randomly distributed pico cells proved that an optimal pico cell to macrocell density ratio exists which maximises the energy efficiency of the network. The authors used a bit/s/m^2/joule metric for the energy efficiency and showed that this optimum ratio decreases when the macro density increases.

The impact of the deployment of an overlay of picocells on top of macrocells on the performance of LTE-A network has been analysed in [87]. The results show that when homogeneous traffic conditions are assumed, the network capacity is improved, but the energy efficiency (kbps/W) is only improved if the pico cell power consumption is very low. On the other hand, when simulating a real mobile network with non-homogeneous traffic assumption, the energy efficiency is improved by 30%. The reason for this is that the pico cells are deployed in hot spot zones and are able to offload more traffic from the macrocells.

The reduction in energy consumption obtained by offloading the traffic from macrocells to small cells was also investigated in [88] where the authors observed that deploying micro, pico, or femtocells over a macrocell layer led to a reduction in the RAN energy consumption by 23.6%, 28.8%, and 24.2%, respectively. The reduction in energy consumption depended on the area density of the deployed small cells: beyond a certain density, the overall energy consumption started to increase.

The authors of [89] studied a long-term energy-efficient strategy for the evolution of mobile networks. They evaluated the possible energy gains obtained when considering the upgrade of mobile network infrastructure over a period of 8 years. They compared the strategy of only

upgrading the macrocells with the strategy of joint macro/pico cell deployment. High, medium and low pico cell densities were considered. The results showed that deploying a high density of picocells consumes the least RAN energy while the carried traffic volume increased on average by 16%. The disadvantage of this is that a large number of backhaul links are needed for the pico sites. The authors also showed that the strategy of deploying a low density of picocells is cheaper than a macrocell only upgrade path: a reduction in the total energy consumption of 10.5 % is achieved through this. This energy saving can be increased by switching off the idle pico-cells during periods of low traffic volume.

More recently, the strategy of ultra-dense deployment of small-cells has gained significant attention and is regarded as one evolutionary path towards the achievement of the target capacities in 5G. However, deploying a large number of small-cells poses several concerns, chief amongst which is energy consumption. A reduction in the overall RAN RF transmit power is achieved when the density of small-cell base stations increases (i.e. the inter-site distance is reduced). This leads to a saving in RAN RF energy consumption which can be more enhanced if an efficient sleep mode capability is used [90]. However, this observation may not hold when the total power consumption of each small cell is taken into account, the reason being that the base station still consumes a non-negligible amount of energy even in sleep mode status. Another important issue that arises when the deployment density of small-cells increases is the energy consumed by the backhaul links, which can consume up to 50 % of the RAN total power consumption [91]. This limits the advantages of heterogeneous networks.

Another category of the heterogeneous networks is the macro-femto cells deployment, where femtocells are residential low power nodes usually deployed by the end users for indoor coverage. These use the consumer home internet connection as backhaul. The authors of [92] have investigated the femtocell deployments and pointed out that an effective interference management technique is needed to achieve a considerable energy saving amount in LTE-A. According to [93], the femtocell solution could improve the RAN overall energy efficiency measured in bits per joule, but this improvement is accompanied by a degradation in the throughput of macrocells when the density of the deployed femtocells increases. A joint deployment of macro and indoor femtocells has been investigated in [94] where the authors found that the energy efficiency of such deployment outperforms the traditional macro only deployments when measured by bit per joule metric. According to them, switching off or reducing the RF transmitted power of some base stations during low traffic periods leads to more energy saving. For instance, a reduction of 4 dB in the macro base stations transmitted power improves the energy saving by 36% while the throughput is degraded by only 10 %. The energy consumption of a joint deployment of macro-micro RAN and macro-femto RAN are compared in [95]. Interestingly, the authors concluded that the two deployments have the same

level of power consumption when aiming at the same target capacity. The authors claim that it is simpler for an operator to manage and control fewer planned microcells rather than managing hundreds of randomly deployed femtocells.

2.5.2.5 Additional approaches

Several approaches to improve the network energy efficiency have not been covered in this review as it has concentrated on the techniques which will be evaluated in this research project. Examples of non-covered techniques include, but are not limited to, traffic offloading approaches: traffic offloading to Wi-Fi access points, traffic offloading by device-to-device (D2D) communications, millimetre waves, and visible light communications. Different classes of heterogeneous networks, such as distributed antenna systems and macro-relay architectures, have also not been also covered for the same reason.

2.5.3 Radio resource management techniques

Current cellular networks have been designed to be always on; thus, a significant portion of energy is consumed during no user activity periods. An effective technique to combat this inefficiency in cellular networks is the dynamic adaptive management of network resources according to the daily variation of the traffic. This can be implemented in multiple ways including adaptive sectorisation techniques, adaptive antenna muting techniques, sleep mode techniques, and transmitted power control techniques. The adaptive sectorisation techniques have been reviewed in subsection 2.6.2.1.1.

2.5.3.1 Adaptive antenna muting

Implementing adaptive antenna muting techniques in MIMO base stations can lead to enhancing the RAN energy efficiency [96], where the base station can adapt the number of active transmit antennas according to the offered traffic load. This technique has been evaluated in [96] by varying the number of transmit antennas between 1 and 4 while the user receiver is equipped with 2 antennae. The energy efficiency was measured by area power consumption and ECR metrics. Their results have shown a significant reduction in the consumed energy when adaptive antenna muting is implemented compared with the case when all antennas are always on.

2.5.3.2 Sleep mode techniques

Sleep mode techniques consist of continuously monitoring the traffic load in the network and turning off fully or partially some elements of the network when the traffic demand is low to reduce the network energy consumption. These techniques have the advantage of no hardware

replacement being required [97]; however, performance may be compromised if no preventive solutions are adopted to avoid the trade-off between the performance and energy saving when sleep mode is implemented [98].

In LTE based networks, a fast version of sleep mode termed discontinuous transmission (DTX) can be implemented by switching off certain hardware elements of the base station whenever there is no data transmission [99-101]. The feasibility of DTX in LTE networks was discussed in [101] by transmitting only the synchronisation and broadcasting signals during six subframes per LTE frame. The authors showed a 61% of reduction in energy consumption compared to the case of no DTX. Similarly, a novel time domain sleep mode technique in LTE is proposed in [102], where the number of active subframes per frame is calculated as a function of the offered traffic load. Their results showed that up to 90% savings in the energy consumption at low traffic load.

When enabling sleep mode in homogeneous networks, different methods of implementation are cited in literature: random, load-aware, and distance aware implementation methods, for example [103]. The authors of [104] proposed switching off base stations based on a combination of their average load and the average distance to their associated users. They showed that doing so results in better energy efficiency in terms of the consumed power and bits per joule metric compared to randomly switching off the base stations. Importantly, the authors of [105] indicated that switching off more base stations will not always lead to more energy savings if the QoS level needs to remain at the same level as when no sleep mode is enabled. This is because the required extra transmit power in active base stations can outweigh any energy savings.

Introducing sleep mode in heterogeneous networks is simpler than that in the macro cell only deployments. When small cells are turned off, the active macrocells are able to maintain the required coverage [106]. The results of [107] showed that when macro-pico deployment with dynamic sleep mode is enabled in picocells, less energy is consumed than in macro only deployment.

Generally, either in homogeneous or heterogeneous deployments, two sleep mode implementation schemes have been identified: centralised and distributed schemes. The difference between them is that one base station takes the role of coordinator in central schemes and collects real-time information about the status of the whole network which allows it to control the process of on/off switching of base stations in an efficient way [108, 109]. In distributed schemes [109], no coordination between the base stations is needed. Each base station independently decides its on/off switching pattern. The authors of [97] state that “it is generally believed that centralised schemes achieve more energy savings because the central

coordinator base station has a complete picture of the network status." However, this statement ignores the overhead of coordination between the base stations and the energy consumed by the backhaul links during the coordination process.

2.5.4 Massive MIMO deployments

Massive MIMO is considered as a promising technology which has the potential to meet the high capacity requirements of the next generations of mobile networks. Base stations are equipped with a very large number of antennae, and many user terminals can be served simultaneously by the same frequency-time resources without suffering severe inter-user interference [19, 110]. As a result, high values of cell spectral efficiency are obtained. Having a very large number of antennae at the base station has the advantage of achieving high array gains, which results in improving the signal received at the user equipment and thus, better coverage is achieved. In single cell ideal massive MIMO systems, it has been shown in [20] that the base station transmit power can be reduced by a factor proportional to the number of antennae without affecting the achieved data rate if ideal channel estimation is assumed.

The authors of [111] have presented a power consumption model for the massive MIMO systems and evaluated their energy efficiency by including the circuit power consumption at a wide range of numbers of antennae at the base station when different linear precoding techniques are assumed. Their findings showed that the energy efficiency in bits per Joule is maximised at a finite number of antennae which varies according to the used precoding technique. They also showed that RF radiated power per antenna decreases with the number of antennas, with a value ranging from 10–100 mW. The authors stated that "massive MIMO can be built using low-power consumer-grade transceiver equipment at the BSs instead of conventional industry-grade high-power equipment"[111]. However, no results about the actual energy consumption versus the number of antennas and the RF transmitted power were provided, Chapter 7 in this thesis investigates the impact of increasing the number of antennas and RF transmitted power on the energy consumption of massive MIMO deployments.

Unlike the work in [111], where the PA efficiency considered to be constant, the authors of [112] investigated the impact of power amplifier efficiency variation versus the PA output power on the energy efficiency of massive MIMO systems. Their results showed that at high spectral efficiency targets, the losses in the PA due to the degradation in the PA efficiency become significant, and operating the PA at higher transmit power becomes more energy efficient than low transmit power values. The energy efficiency of massive MIMO networks during low periods is investigated in [113], where the authors formulated the problem as an optimisation problem to find the optimal transmit power, number of antennae, number of users and number of pilots which minimise the overall consumed power at a specific target area capacity value.

Their results showed that, for both MRT and ZF precoding techniques, an adaptive switching off some of the antennas at the base stations is more energy efficient than keeping the number of antennae constant.

In [114], the authors compared the spectral and energy efficiencies of massive MIMO and small cell RANs using stochastic geometry modelling tools. Their results showed that massive MIMO outperforms the small cells only when the density of users is small. In addition, a small cell network always offers better energy efficiency than massive MIMO; however, the authors only considered the RF transmit power in their analysis. The same issue of comparing the energy efficiency of massive MIMO and small cells has been also studied in [115] by assuming identical user density, antenna density, and data rate requirements. Their results showed that when the antenna density is high, massive MIMO is more energy efficient than small cells if the per-antenna circuit power in massive MIMO is less than the power consumption of each antenna in sleep mode in small cells, or if an adaptive antenna switching off is allowed in massive MIMO. If not, small cells are the more energy efficient option to deploy.

2.5.5 The utilisation of renewable energy resources.

Due to the rise in energy cost, and to reduce their carbon footprint, network operators have started seriously considering the deployment of renewable energy sources for powering their base stations. Renewable energy sources can be exploited to reduce the grid power consumption when hybrid powered base station are deployed and considered an attractive option for network operators to be deployed in areas where the access to grid power is difficult or not available. Traditionally, operators usually rely on off-grid diesel generators to power the sites which have no access to the grid; however, this leads to increasing the energy cost and causes more pollution.

A significant number of publications have appeared in recent years investigating the feasibility and sustainability of using renewable energy sources in cellular networks. For instance, the results obtained in [116] demonstrated that deploying heterogeneous networks consisting of grid powered macro base stations and hybrid grid and renewable powered small cells is beneficial for cellular network operators in terms of the cost and energy sustainability. Furthermore, the trade-off between the degree of user satisfaction in terms of coverage constraints and the percentage of renewable energy used has been studied in [117], where the authors show that more than 75% of average users can be met by only 25% of non-renewable energy in a single cell scenario. The role of renewable energy resources is expected to increase in ultra-dense small cell deployments, with many publications have investigated the benefits of deploying hybrid power small cells (on grid plus renewable energy resources) on the energy efficiency of networks. For example [118] considered an energy aware traffic offloading scheme where the

traffic is offloaded from the macro and grid powered small cells to renewable energy powered small cells which leads to significant energy savings. As this approach is not covered in the current research project, more details on the implementation, the advantages, and the challenges facing this approach are out of the scope of this thesis. the role of renewable energy resources, especially in dense small cells is proposed to be part of the future work in the final chapter of the thesis.

2.6 Summary

An overview of the evolution of cellular networks has been presented in this chapter, followed by a discussion of the issues resulting from an increase in traffic demand and the need for operators to improve the capacity of their network to meet high data rates and capacity requirements in the next generation networks. Operators best practice has also been considered in terms of improving the capacity of the existing networks and the need for further densification by the deployment of more sites which include macro and small cells.

The importance of the issue of energy consumption is presented in more detail by highlighting the need for consistency in the use of metrics to measure and review the existing power consumption models in the open literature. The final section is dedicated to reviewing the impact of the various capacity improvement approaches on the RAN energy efficiency, with especial focus on network planning and deployment-related approaches.

Before concluding this chapter, it is worthwhile mentioning that the right choice of energy efficiency metric and using an accurate base station power consumption modal are the two main pillars in the process of defining a consistent evaluation framework for the RAN throughput and energy consumption. As we will see in chapter 3, one metric is not enough to capture the full picture of energy consumption in the network because of other parameters such as traffic load, target capacity and required coverage have also an impact on the RAN energy efficiency.

Chapter 3

Joint Energy and Spectral Efficiency Evaluation Framework for Cellular Networks

3.1 Overview

The primary objective of network operators has always been to meet the data rate requirements of users whilst fulfilling radio coverage targets in terms of both population density and geographic spread, the latter often being enforced by a country's spectrum agency. The constant growth in demand for wireless internet connectivity has continued to fuel the requirement for high data rates. To meet this demand, mobile operators have traditionally sought to design their mobile network to be spectrally efficient as measured in units of bit/s/Hz.

This approach served operators well for the development of the first, second and third generation mobile networks and was largely achieved through a combination of improvements in transceiver signal processing technology and a reduction of the inter-site distance between base stations. Whilst the latter strategy leads to significant increases in spectral efficiency through greater frequency reuse, it also substantially increases the amount of cellular infrastructure installed. Given the low power efficiency of radio base stations and the need to achieve even higher data rates, operators began to regard energy consumption as a significant issue for fourth generation (4G) networks. This concern was born out of a combination of issues including operational expenditure (the cost of energy had risen significantly making electricity costs a considerable portion of the overall operational costs), and environmental factors (climate change was driving operators to adopt green policies in order to reduce their carbon footprint). A particular concern was that large portions of each operator's network were powered by costly and environmentally unfriendly diesel generators. Thus, research into 4G networks placed the design for low energy consumption on a par with spectral efficiency.

With the deployment of 4G networks, attention has turned to the standardisation of the fifth generation (5G) of radio access networks. To meet the even higher expected demand for data services, a 1000 fold increase in area capacity (bit/s/km^2) of the access network is sought. The large increase in capacity will be predominantly achieved by further reducing the average inter-site distance between base stations or access points. A mixture of approaches is envisaged,

though small cell densification and heterogeneous networks are regarded as among the most effective methods of attaining the intense frequency reuse needed to support this higher capacity. Studies of 4G networks have clearly shown that site densification using the same macrocell infrastructure, whilst enhancing capacity, results in a significant increase in total radio access network (RAN) energy consumption [34]. In order to ameliorate counter this effect, a variety of energy saving techniques have been investigated including base station sleep modes [119] and adaptive sectorisation [120]. Many of these techniques rely on scaling the energy consumption with traffic load thereby only saving energy at low traffic loads. In general, the development of such energy saving techniques has been hampered by the lack of a consistent evaluation framework for network planning purposes that accurately accounts for the energy consumption as well as the spectral efficiency of a mobile cellular (RAN).

In this chapter, we develop a new base station power consumption model and adopt a consistent evaluation framework to evaluate the energy efficiency of radio access networks. The proposed power consumption model is an update to the existing Green Radio power consumption model, where the scalability of the power consumption versus the cell traffic load and the number of base station antennas is enhanced. The degradation of the power amplifier efficiency when the base station transmits at low RF power due to the peak to average ratio PAPR is also captured in this model, a new method of modeling the cooling power consumption in the base station site is also introduced. The evaluation framework is based on three figures of merit: the throughput gain (TPG), the energy consumption gain (ECG) and the energy throughput gain (ETG). These figures of merit can be determined, respectively, from the following three metrics:

1. The throughput per unit area or area throughput efficiency ($\mathrm{bit/s/m^2}$).

2. The power per unit area or area power efficiency($\mathrm{watt/m^2}$).

3. The throughput per energy unit or bits per joule(bit/J) which often called in the literature the energy efficiency (EE) [28].

The three figures of merit provide a joint energy and spectral efficiency framework suitable for evaluating a 5G RAN. The framework is used in our research to evaluate the spectral and energy efficiency of three RAN deployments:

a. Macrocell only RANs.

b. Small cell only RANs.

c. Heterogeneous macro/small cell RANs.

The impact of backhaul power consumption on the overall RAN energy consumption is also investigated.

The remainder of this chapter is organized as follows. In section 3.2, we highlight the reasons for updating the base station power consumption model and for proposing a different energy efficiency evaluation framework. In section 3.3, the process of modelling the power consumption in LTE base stations is presented, followed by the presentations of the energy efficiency metrics and evaluation framework in section 3.4. In section 3.5, we explain the system model which will be used for this present research. The analysis of energy and spectral efficiency in macrocell only RANs is covered in section 3.6, and the two cases of small cell only deployments and heterogeneous deployments are investigated in sections 3.7 and 3.8, respectively. The impact of the backhaul power consummation is added to the analysis for all the considered study cases in section 3.9. Finally, the chapter summary is presented in section 3.10.

3.2 Motivation

A number of base station power consumption models have been developed and available in the literature, and the energy efficiency metric of (bit/J) is widely used to investigate the issue of energy efficiency in wireless networks. This begs the question of why a new base station power consumption model and different energy and throughput evaluation framework is needed. We attempt to answer this question in this section by highlighting the drawbacks of existing models, and reasons for adopting a different framework to evaluate the energy efficiency in cellular networks.

3.2.1 Base station power consumption modelling

Knowing the accurate power consumption of the RAN is a necessary step for estimating its energy efficiency. As 60% to 80% of a cellular network energy is consumed by the radio base stations (RBS) [36], accurate models of power consumption are needed for the various types of RBSs deployed in a RAN. A number of RBS power consumption models are available in the open literature. Significant generic models were developed in [59],[40],[38] and [27] based on measurements taken from specific vendor's equipment. The models provide a method of estimating the RBS total power consumption P_{site} as a function of the transmitted radio frequency (RF) power P_t . The models have high levels of commonality because they are derived from similar RBS architectures. In this chapter, an enhanced version of the Green Radio (GR) RBS parametric model is presented, which was originally developed by the Mobile Virtual Centre of Excellence (MVCE) using data supplied by a number of manufacturers and

operators [43]. The enhanced version models the non-linear relationship between the base station transmitted RF power and the PA efficiency, and accommodates base station equipped with multiple-in-multiple-out (MIMO) antenna configurations which were not included in the previous version. In addition, a straightforward method to account for the power consumption of the cooling unit as a function of the cooling equipment efficiency is introduced.

Similarly, the model differs than the EARTH power consumption model [40] in estimating the losses in the power amplifier stage, and in the cooling unit. In 2015, IMEC [27] released an advanced power consumption model to provide a prediction of the power consumption of present and future cellular base stations. Although the IMEC model supports a wide range of cellular base station types and many operating conditions, it is only available through a web interface which causes difficulty when integrating it into system level simulations. In addition, certain details regarding the power consumption of certain subsystems of the base station model are not publically available. For these reasons, the author proposed a detailed and flexible power consumption model which is easy to use in system level simulations.

3.2.2 Energy Efficiency Metrics

Several types of network level energy metrics for wireless networks have been reported in the open literature. However, there is considerable ambiguity over their use because they can lead to contradictory conclusions when used to evaluate the same RAN configuration. The first example of these energy efficiency metrics is the energy consumption ratio (ECR) with units of $(\mathrm{J/bit})$, which indicates the total energy consumed for the transmission of one information bit (notionally taken on an end-to-end basis). This category includes the energy consumption ratio ECR with units of $(\mathrm{J/bit})$ and its reciprocal (EE) with units of $\mathrm{bit/J}$ to reflect the engineering design requirement to maximise the information bits carried per joule of energy consumed. The *ECR* metric was first identified in [121] for wired networks and adopted as an energy efficiency metric in the Green Radio project [34], where $\mathrm{ECR_{RAN}}$ was defined as the ratio of total RAN energy consumption E_{RAN} to the total number of information transported bits M_{RAN} in an observation time T. Based on this definition, the ECR can be expressed as a ratio of total RAN power consumption P_{RAN} to the total RAN throughput R_{RAN} as shown in (3.1).

$$ECR_{ran} = \frac{E_{RAN}}{M_{RAN}} = \frac{E_{RAN}/_{T}}{M_{RAN}/_{T}} = \frac{P_{RAN}}{R_{RAN}}. \tag{3.1}$$

The ECR must be interpreted carefully: a low value of ECR implies high energy efficiency. If network traffic load varies, which is typically the case, then for low traffic loads the same RAN appears inefficient compared with the case of high traffic loads. This can lead to misleading

conclusions when comparing different RAN types if the offered traffic load in both scenarios is not predefined. The same applies to the energy efficiency EE measured by $(\mathrm{bit/J})$ metric. When high traffic load values are present in the network, the network appears to be very energy efficient. Conversely, the same network appears to be inefficient when the traffic load is low.

A second example of energy efficiency metrics is the area power efficiency or power per unit area with units of $\mathrm{watt/m^2}$. This metric was used during the EARTH project [40] where the network with the lowest area power efficiency consumes the least energy. However, this metric does not take into account the RAN average throughput which means that it needs to be accompanied by the ECR or EE metric to provide meaningful conclusions when comparing the energy efficiency of two RANs, or two configurations of the same RAN.

A relative energy efficiency metric named the energy consumption gain (ECG) also developed during the Green Radio project [34] and adopted in this thesis to be used jointly with throughput gain metric TPG, to provide a straightforward method for comparing the relative energy consumption of two RANs. The RAN ECG defined in (3.2) is taken as the ratio of the energy consumption $\mathrm{E_{RAN,REF}}$ of a reference or benchmark RAN to the energy consumption $\mathrm{E_{RAN,TEST}}$ of the RAN under test.

$$ECG_{ran} = \frac{E_{RAN,REF}}{E_{RAN,TEST}}. \tag{3.2}$$

The advantage of the ECG and TPG metrics is that an explicit definition of the RAN traffic load is included in the analysis for both the reference and under test RANs, thereby avoiding the ambiguity associated with the ECR and EE metrics. When the ECG is greater than unity, the RAN being tested is consuming less energy, i.e. more energy efficient than the reference RAN.

3.3 Base station power consumption model

Modelling the RBS power consumption involves a comprehensive campaign to measure and characterise the power consumption of each constituent unit over a range of operating conditions and environments. The measurements are used to construct a parametric model applicable to a wide range of RBS types. As we have already highlighted in the previous section, a number of radio base station power consumption models already exist in the literature. “These models often have a high level of commonality as they are derived from similar base station architectures” [43]. Figure 3-1 shows the basic architecture of a typical single antenna single sector base station site.

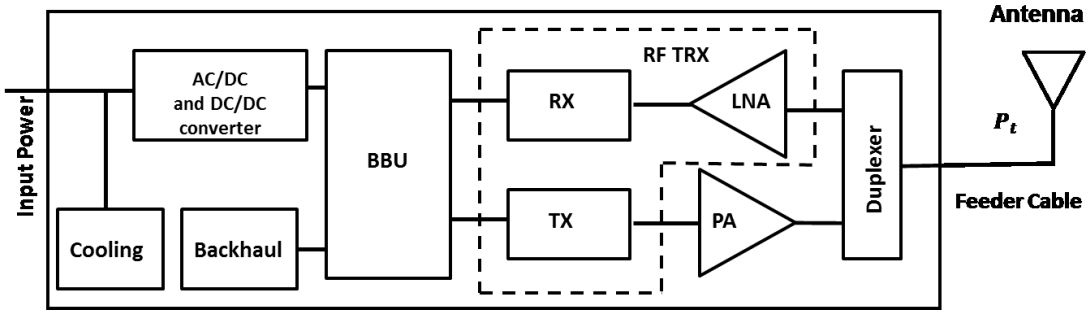

Figure 3-1: Radio base station simplified architecture

Typical RBS units include the power amplifier (PA), the RF transceiver unit, the baseband (BB) processing, the power supply unit, the cooling (air-conditioning) unit, and backhaul unit. These units can be categorized based on whether or not there is a dependency on the traffic load. The main load dependent unit in the base station is the PA, its power consumption scales with the cell average load α, which ranges from zero to unity, and indicates to the resource utilization in the base station, and to the base station transmitted power. The load independent units include the baseband processing unit, the RF transceiver, and backhaul unit. In practice, the load dependency of the power consumption of the baseband processing unit is very small compared to the total RBS power consumption, and considered to be load independent in this thesis [27]. The power consumption of the power supply and cooling units depends on their efficiencies as well as the power consumption of the other units in the RBS. Consequently, there is some dependency on the cell load for these units, which is not linear, as they continue to consume energy even at zero load.

The overall average power consumption of an RBS is modelled as the sum of the power consumption of the seven units mentioned, as expressed in (3.3).

$$P_{site} = P_{cool} + P_{bh} + P_{rect} + n_s \cdot n_t \cdot (P_{bb} + P_{trx} + P_{pa}) \,. \qquad (3.3)$$

In (3.3), the terms P_{site}, P_{cool} and P_{rect} denote the power consumption of the RBS site, the cooling unit and the backhaul, respectively and the terms P_{rect}, P_{bb}, P_{trx} and P_{pa} denote the power consumption of the power supply unit, baseband processing unit, RF transceiver circuitry, and the PA, respectively. The parameters n_s and n_t refer, respectively, to the number of sectors per RBS site, and the number of transmitting antennas per sector. The power consumption in the cooling and power supply units is calculated as a percentage of the sum power consumption of the power amplifier, RF transceiver, and baseband processing unit. The method of modelling the power consumption of each unit is fully explained in the following subsections.

3.3.1 Power amplifier

The PA is often the main power consuming unit in the base station and may account for almost 50% of its power consumption [122]. The PA's power consumption P_{pa} may be written as a function of the average transmit RF power per antenna P_t, the PA efficiency η_{pa}, and the RF feeder cable efficiency η_{feed} , as shown in (3.4).

$$P_{pa} = \frac{P_t}{\eta_{pa} \cdot \eta_{feed}} . \tag{3.4}$$

The RF feeder cable efficiency is usually characterised by its losses σ_{feed} in dBs, and must be converted from dB to a linear RF feeder efficiency. The term in P_t can be written as $P_t = \alpha \cdot P_{t,max}$ where α denotes the average cell traffic load between 0 and 1. In LTE systems, the cell load is defined as the ratio of used resource blocks to the total number of resource blocks. $P_{t,max}$ denotes the maximum transmit RF power per antenna. Multicarrier signals as found in OFDMA exhibit (PAPRs) necessitating the PA being backed-off from its saturation power level in order to operate in the linear region of its input-output transfer function, thereby avoiding excessive nonlinear distortion. Operating a PA below the on-set of saturation results in a reduced PA efficiency, which can be approximated by equation (3.5) [123].

$$\eta_{pa} = \sqrt{\frac{P_{t,pa}}{P_{sat}}} \cdot \eta_{pa,peak} = \sqrt{\frac{\alpha \cdot P_{m,pa}}{P_{sat}}} \cdot \eta_{pa,peak} . \tag{3.5}$$

In (3.5), the terms $P_{t,pa}$, P_{sat} and $\eta_{pa,peak}$ denote the PA's output power, saturation power and peak efficiency, the latter obtained when $P_{t,pa} = P_{sat}$. PA usually operates at backed off maximum average transmitted power $P_{m,pa}$ equals to P_{sat} in dBm minus the back off value BO_{dB} in decibels. In case of the PA efficiency at $P_{m,pa}$ is known and equals $\eta_{pa,m}$. equation (3.5) can be expressed as in (3.6)

$$\eta_{pa} = \sqrt{\frac{\alpha \cdot P_{m,pa}}{P_{m,pa}}} \cdot \eta_{pa,m} = \sqrt{\alpha} \cdot \eta_{pa,m} . \tag{3.6}$$

Equation (3.6) clearly illustrates the nonlinear relationship between the PA power consumption and the cell average load and demonstrates the slower decrease in power consumption with decreasing load compared to a linear model.

Figure 3-2 illustrates how is the efficiency for class D power amplifier $\eta_{pa,m}$ is degraded due to operating at backed off transmitted power $P_{m,pa}$, where the back off value in dB is calculated by (3.7).

$$BO_{dB} = P_{sat} - P_{m,pa} \ , \tag{3.7}$$

Where both P_{sat} and $P_{m,pa}$ are in dBm units. For example, when the PA peak efficiency of 75%, and back off value of 8 dB are assumed, the PA efficiency $\eta_{pa,m}$ equals 30% calculated by (3.5) when the cell average load equals 1. Note that the PA efficiency will degrade to lower values when the PA operate at output transmitted power less than $P_{m,pa}$ due to a reduction in the cell average load. The results of Figure (3-2) are generated by using class D PA with a peak efficiency of 75% which is assumed in the macro base stations in this thesis in order to have the PA operating at an efficiency of 30% without any PA efficiency improvement techniques when backed off by 8 dB. Values from 70% to 90% for class D power amplifier are reported in literature [50, the 124]. Different PA efficiency values need to be used if different PA classes are assumed.

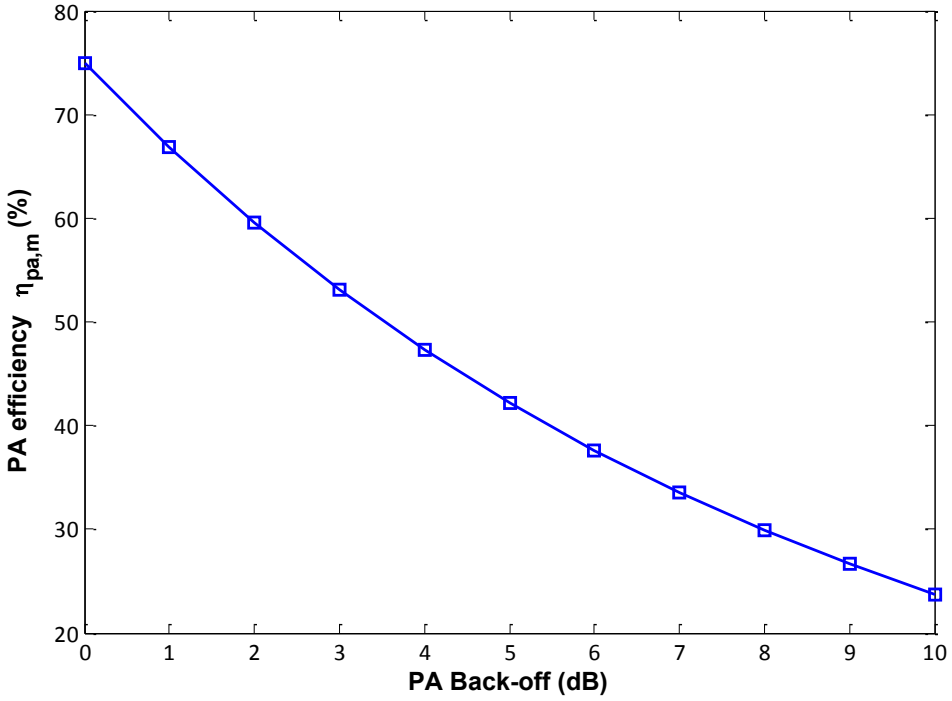

Figure 3-2: Class D PA efficiency Vs. PA back-off (dB)

3.3.2 RF transceiver and Baseband processing units

The RF transceiver, which is responsible for electrically processing the RF signals at the base station, includes electronic circuits for clock and carrier generation and distribution, up and down conversion, filtering, buffering, low noise amplification and both the analog-to-digital and digital-to-analog conversions. The per sector power consumption of an RF transceiver P_{trx} of

bandwidth B may be estimated from equation (3.8) with respect to a reference RF transceiver unit [41]. The terms in $P_{trx,ref}$ and B_{ref} denote the power consumption and bandwidth, respectively, of the reference RF transceiver when using one transmit antenna per sector.

$$P_{trx} = \frac{B}{B_{ref}} \cdot P_{trx,ref} \,. \tag{3.8}$$

The power consumption of the baseband processing unit P_{bb} is be modelled in a similar way to that of the RF transceiver, with dependencies on the number of transmit antennas, and the bandwidth, as shown in equation (3.9). The cell average load does not significantly influence the power consumption of the baseband processing unit ; therefore, P_{bb} is considered to be independent of α [41]. In (3.9), the terms in $P_{bb,ref}$ and B_{ref} denote the power consumption and bandwidth, respectively, of the reference BB unit when using one transmit antenna per sector.

$$P_{bb} = \frac{B}{B_{ref}} \cdot P_{bb,ref} \,. \tag{3.9}$$

Note that both P_{trx} and P_{bb} are the power consumption of the RF transceiver, and the baseband unit per single transmit antenna, and that they scale linearly with the ratio of the actual used bandwidth to the reference bandwidth value: i.e. doubling the bandwidth leads to doubling their power consumption.

3.3.3 Power supply and cooling units

The base station power supply unit, which consists of AC-to-DC and DC-to-DC converters, are often modelled to have conversion efficiency $\eta_{AC/DC}$ value lies between 85% to 90% [39]. A value of 85% is used in this thesis. Note that the backhaul power consumption is not included when estimating P_{rect} because part of the backhaul power consumption occurs in the backhaul aggregation node which is not located in the base station site, while the cooling unit is assumed to have its own power supply.

Site cooling is required at macrocell base station sites to maintain an appropriate temperature inside the radio base station cabinet. When estimating the power consumption of the cooling unit, an ambient temperature of 25^{o}C is usually considered. The amount of heat generated inside the cabinet is obtained by estimating the overall power which is consumed by the equipment inside the cabinet and dissipated as heat. This value of power is converted to British Thermal Units (BTU) per hour by multiplying it by the constant 3.4121. The amount of power converted to heat equals the total power consumed by the base station minus the RF transmitted power, and the losses in the feeder cable. The energy efficiency of a cooling unit is determined by its

energy efficiency rating EER which indicates that the cooling unit can remove EER BTUs per hour for each watt of electrical power consumed by the cooling equipment. Hence, the cooling unit power consumption can be estimated by (3.10). Equation (3.10) allows estimation of the power losses in the cooling unit not only as a percentage of the power consumption of the base station, but also as a function of the EER of the used cooling equipment, which was not accounted for in the previous mentioned power consumption models.

$$P_{cool} = \frac{3.4121}{EER \cdot \eta_{AC/DC}} \cdot \left(n_s \cdot n_t \cdot (P_{bb} + P_{trx} + \left(P_{pa} - \frac{P_t}{\eta_{feed}} \right) \right). \tag{3.10}$$

3.3.4 Backhaul unit

The backhaul network includes the intermediate transmission links that connect the base station sites to the core network. Different communications technologies are used in the backhaul such as optical fibre, copper wire or microwave links. The power consumption of the backhaul P_{bh} in a macro cell networks is often omitted as it represents a small amount of power compared to the total power consumption of the macro base station. However, the backhaul power consumption becomes an important part of the overall power consumption in a heterogeneous or small-cell network. The value of the ratio of the backhaul power consumption to the total RAN power consumption depends on the technology used, and on the network topology deployed. For example, [125] has estimated the power consumption of a fibre backhaul as lying in the range 8 to 17 watts. Often, a nominal value of 10 W is assumed in the open literature when using an optical fibre backhaul [126]. In contrast, when microwave links are used in the backhaul, the power consumption per link can be as high as ~93 W [127], which is considerably greater than the fibre case and will have a larger impact on the overall power consumption of the RAN. As mentioned earlier, part of the backhaul power consumption takes place in the aggregation switch. For instance, of the 10 watts, only 1-2 watts are consumed by the fibre interface module, which connects the base station to the fibre cable, while the remaining is consumed in the aggregation switch.

3.3.5 Overall base station power consumption

The overall power consumption of base station site can be estimated as the sum of the power consumption of the different base station sub-systems used earlier, as in (3.11).

$$P_{site} = P_{cool} + \frac{n_s.n_t}{\eta_{AC/DC}} \cdot \left(\frac{B}{B_{ref}} \cdot \left(P_{BB,ref} + P_{RF,ref} \right) + \frac{P_{t,max} \cdot \sqrt{(\alpha_s + \alpha_t)}}{\eta_{pa,m} \cdot \eta_{feed}} \right), \quad (3.11)$$

Where $P_{t,max}$ is the maximum RF transmit power per antenna, $\eta_{pa,max}$ is the power amplifier efficiency when operating at $P_{m,pa}$, note that $P_{m,pa} = P_{t,max}/\eta_{feed}$. The term $\eta_{AC/DC}$ refers to the efficiency of power supply unit, and η_{feed} refers to feeder cable efficiency. The cell average load α equals the sum of $\alpha_s + \alpha_t$, where α_s is the minimum average load in the cell when the traffic is zero and it consists of the signalling and control, signals. In LTE, the value of α_s depends on the bandwidth B, and number of antennas n_t, value of α_s =0.1 is used in this thesis [40] which can vary slightly with the bandwidth and number of antennas. The term α_t is used throughout the thesis to refer to the cell average traffic load.

Table 3-1 lists the parameters of the power model that have been used to estimate the total power consumption of the various base station sites used in this research. These values are obtained from [43] and [40] and can vary between different manufacturers. They also depend on the equipment manufacturing date and on the technology used. The PA efficiency $\eta_{pa,m}$ for macro base stations in Table 3-11 is calculated by (3.6) for a class D power amplifier which has peak efficiency $\eta_{pa,peak}$ equal to 75%, and back-off equal to 8 dB.

Table 3-1: The power model parameters

Parameter	Macro-cell	Micro-cell	Pico-cell
Transmit Power per Antenna ($P_{t,max}$, W)	40	6.3	0.20
Bandwidth (B_{ref}, MHz)	20	20	20
Transceiver Unit ($P_{RF,ref}$ W)	13	6.5	1.0
Processing Unit ($P_{bb,ref}$, W)	30	27	3
Fibre Backhaul (P_{bh}, W)	10	10	10
PA Efficiency ($\eta_{pa,m}$)	30%	23%	10%
Antenna Feed Cable Efficiency (η_{feed})	0.5	0.79	1
Power supply Efficiency ($\eta_{AC/DC}$)	0.85	0.85	0.85
Energy Efficiency Rating EER	11	11	11

Figure 3.3 shows the total site power consumption using the proposed power model (Enhanced Green Radio) of a 3-sector, macro-cell base station, with a single antenna per sector, and a bandwidth of 20 MHz. The total power consumption is plotted versus the cell average load α,

where a value of 0.1 is used for α_s and the the backhaul power consumption is not included in the site total power consumption, and

Equation (3.11) can be approximated as a linear function of the cell average traffic load α_t, in the form of the sum of a fixed overhead power consumption P_{oh} associated with the load independent parts of the model, and a dynamic radio-head power consumption P_{rh} associated with the load dependent parts as expressed in (3.12).

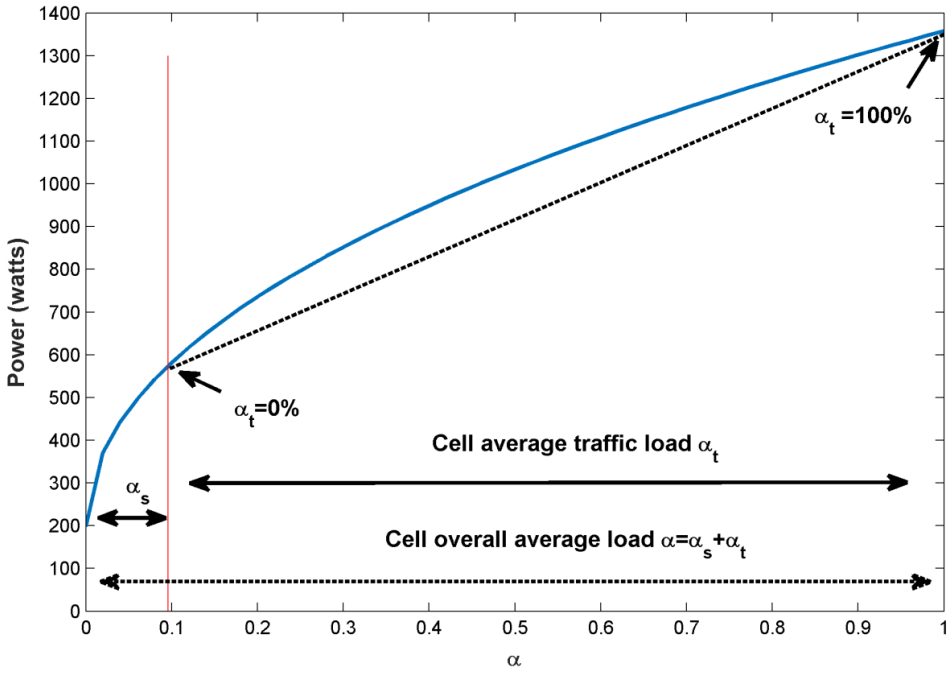

Figure 3-3: Power Consumption of 3-sectors Macro Base Station

$$P = P_{oh} + \alpha_t \cdot P_{rh}. \tag{3.12}$$

The dashed line in Figure 3-3 represents the total power consumption of a 3 sectors macro site versus α_t ,estimated by (3.12), where P_{oh} equals the radio base station power consumption at no traffic load, and P_{rh} equals the gradient $\frac{\Delta P}{\Delta \alpha_t}$ obtained from the detailed power mode in (3.11). Table 3-2 shows the obtained values of P_{oh} and P_{rh} for different types of base stations.

Table 3-2: The radio head & overhead parts of the power model

Cell Type	Macro	Micro	Pico
$P_{t,max}$	46 dBm	38 dBm	23 dBm
n_s	3	1	1
n_t	1	1	1
P_{oh}	566 W	49.20 W	5.38 W
P_{rh}	783.8 W	23.12 W	1.51 W

3.3.6 The power-load dependency of various types of base stations.

The dependency of the power consumption of base station on the cell average traffic load varies from one base station type to another. The variation of power consumption of the different sub-systems of versus the cell average traffic load is depicted in the figures (3-4) to (3-6) for macro, micro and pico base stations. It is clear that the macro base station power consumption exhibits high load dependency, while this load dependency tends to diminish in the case of picocells. Hence, reducing the macro cells load by offloading their traffic to more efficient small base stations or Wi-Fi access points is considered one of the more effective methods of reducing the overall RAN power consumption as we will see in chapter 6.

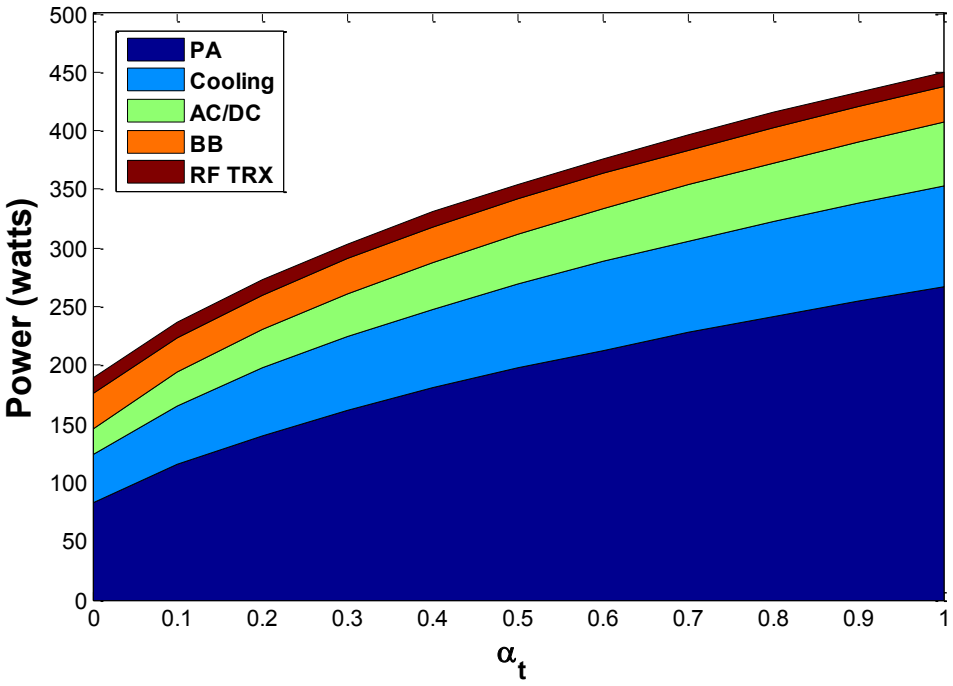

Figure 3-4: Power consumption of omnidirectional macro base station versus α_t

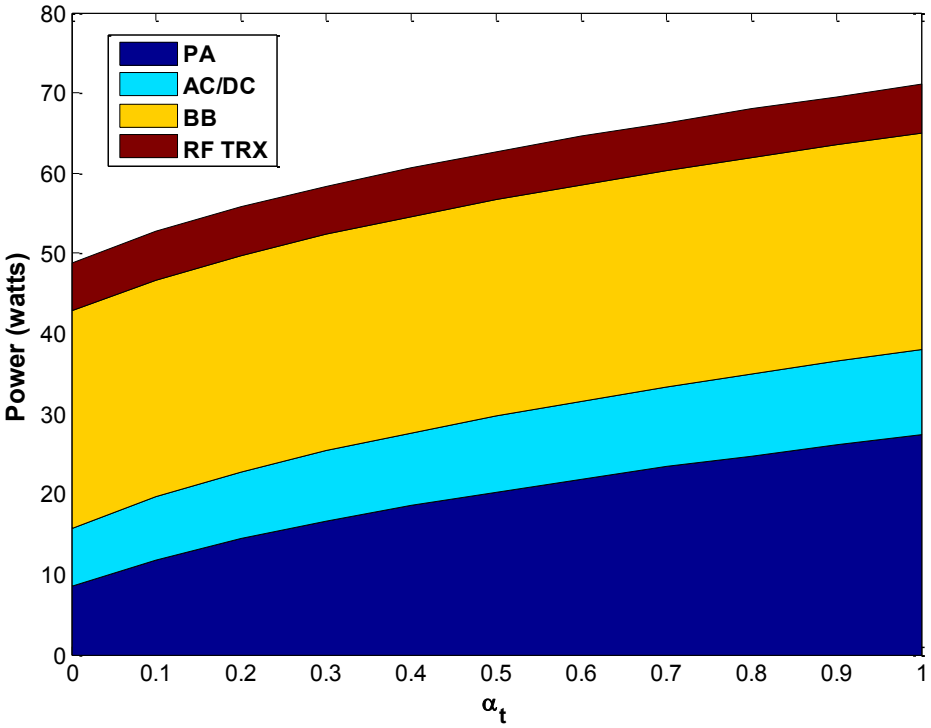

Figure 3-5: Power consumption of micro base station versus α_t

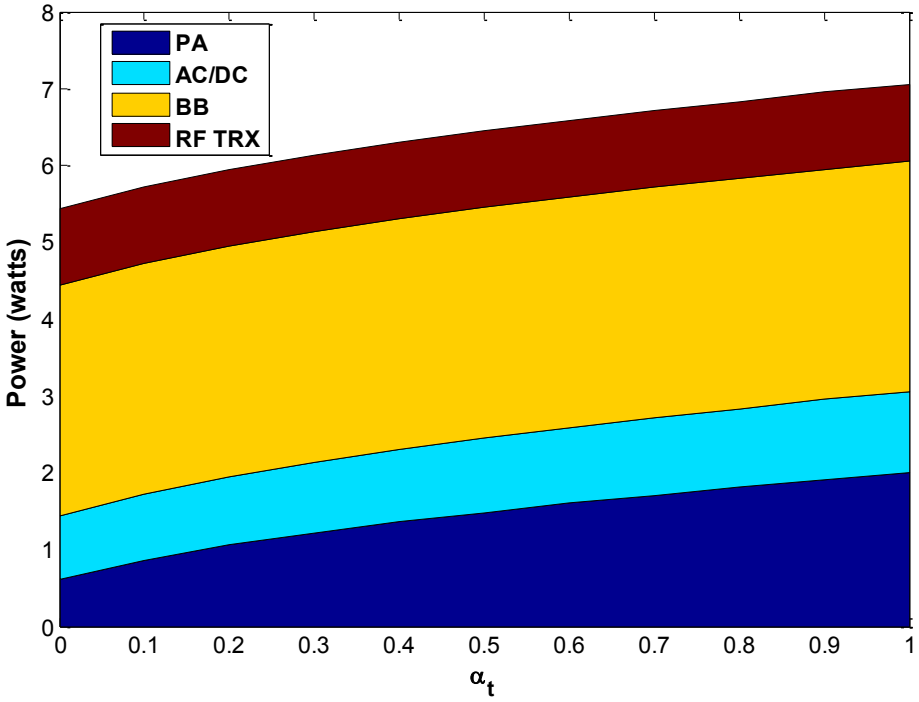

Figure 3-6: Power consumption of pico base station versus α_t

3.4 Energy efficiency metrics

As highlighted in section 3-2, the traditional energy efficiency metrics, such as the EE and ECR, exhibit an inherent ambiguity when comparing the energy consumption of two networks as it is unclear whether the improvements in the energy efficiency are attributable to true energy savings, or to an increase in the data throughput. This can lead to misleading claims when comparing the EE of two networks. Hence, to draw meaningful conclusions regarding the network energy efficiency, the throughput needs to be predefined when using the bits per joule metric.

The evaluation framework adopted in this thesis developed by O'Farrell [43] separately develops quantifiable energy and throughput efficiencies as well as a new joint figure of merit formed from the product of both. That is, the ECG is used as a relative energy measure with respect to a reference network; the throughput gain TPG is used as a relative throughput measure. Their product, ECG times TPG, forms a new, joint, relative EE and throughput figure of merit termed the energy throughput gain ETG. The advantage of this framework is that ECG can clearly indicate any gains or losses in the RAN energy consumption when comparing the energy consumption of two RANs. It can also be defined in terms of the area power densities of the two RANs, and when multiplied with the TPG yields the third figure of merit ETG which indicates the relative improvement of the EE of the evaluated network with respect to the reference network and consists of the ratio of the EEs the two RANs.

The ECG between two networks (RAN_1 and RAN_2) is given by equation (3.13) where a reference baseline network RAN_1, consisting of N_1 cells each transmitting with average power P_1, is compared to a network RAN_2, consisting of N_2 cells each transmitting with average power P_2. The total energy consumption of each RAN is denoted $\{E_i: i = 1,2\}$. Implicit in (3.13) is the condition that the observation time T (i.e. a sufficiently long period over which the assessment is made), and the RAN coverage area A have the same respective values in both RANs.

$$ECG = \frac{E_1}{E_2} = \frac{N_1 \cdot P_1 \cdot T}{N_2 \cdot P_2 \cdot T} = \frac{P_{RAN1}}{P_{RAN2}}, \tag{3.13}$$

Where P_{RAN1} and P_{RAN2} are the total consumed power in RAN_1 and RAN_2, respectively. Similarly, the TPG between two networks is given by Equation (3.14). The reference network RAN_1 transports a data volume D_1 bits during the observation time T, whereas test network RAN_2 transports a data volume D_2 bits during the same observation period.

$$TPG = \frac{D_2}{D_1} = \frac{N_2 \cdot D_2/T}{N_1 \cdot D_1/T} = \frac{N_2 \cdot R_2}{N_1 \cdot R_1} = \frac{R_{RAN2}}{R_{RAN1}}, \tag{3.14}$$

Where R_1 and R_2 represent the average cell throughput in RAN_1 and RAN_2, respectively. R_{RAN1} and R_{RAN2} are the overall average throughputs of the two RANs. Thus, an expression for the energy throughput gain ETG is obtained by taking the product of (3.13) and (3.14) to give equation (3.15). The expressions in (3.15) demonstrate the way in which the ratio of the RAN_1 and RAN_2 energy efficiencies EE_1 and EE_2 respectively, with units of bit/J, can be partitioned into an energy ratio component and a throughput ratio component. This partition of the ETG metrics allows energy savings and throughput gains to be assessed separately, in particular, to assess whether a true energy saving has been obtained or not.

$$ETG = ECG \cdot TPG = \frac{E_1}{E_2} \cdot \frac{D_2}{D_1} = \frac{{}^{D_2}/_{E_2}}{{}^{D_1}/_{E_1}} = \frac{EE_2}{EE_1}, \tag{3.15}$$

Where EE_1 and EE_2 are the bits per Joule metrics for the two RANs. When the coverage area is A, the ECG can be expressed as the ratio of the power per area metrics of the two RANs, as shown in (3.16). We also note that the ratio N_1/N_2 is approximated by the ratio A_2/A_1, where A_1 and A_2 are the cell coverage areas in RAN_1 and RAN_2, respectively. Hence, the ECG can also be expressed as the ratio of the cell power area densities of the two RANs, as in (3.16).

$$ECG = \frac{\frac{P_{RAN1}}{A}}{\frac{P_{RAN2}}{A}} = \frac{N_1 \cdot P_1}{N_2 \cdot P_2} = \frac{{}^{P_1}/_{A_1}}{{}^{P_2}/_{A_2}}. \tag{3.16}$$

By substituting $N_1/N_2 = A_2/A_1$ in (3.14), we can obtain an estimation of TPG as the ratio of the two area throughput densities of the two RANs as (3.17).

$$TPG = \frac{{}^{R_2}/_{A_2}}{{}^{R_1}/_{A_1}}. \tag{3.17}$$

Similarly, the ETG can be expressed as the ratio of the individual EEs of the two RANs as in (3.18).

$$ETG = \frac{{}^{R_2}/_{P_2}}{{}^{R_1}/_{P_1}} = \frac{{}^{P_1}/_{R_1}}{{}^{P_2}/_{R_2}}. \tag{3.18}$$

The advantage of using ECG, TPG, and ETG from equations (3.16) to (3.18), is that the cell power consumptions P_i, throughputs R_i and coverage areas A_i are readily calculable or measurable, thereby providing an accurate, straightforward means of comparing the energy consumption and throughput of two RANs. It is also worth noting that when the TPG equals unity, the ECG and ETG amount to the same measurement.

In dense deployments of small cells, the notion of cell coverage becomes less meaningful, as cell coverages may overlap, and the base station deployments tend to be random and are not characterised by their coverage areas, but by their deployment densities. The proposed framework can be expressed in terms of the average density of base stations λ with units of (cell/km^2), as shown in (3.19).

$$ECG = \frac{P_1 \cdot \lambda_1}{P_2 \cdot \lambda_2}, TPG = \frac{R_2 \cdot \lambda_2}{R_1 \cdot \lambda_1}, ETG = \frac{R_2/P_2}{R_1/P_1}, \quad (3.19)$$

Where λ_1 and λ_2 are the cell densities (cell/km^2) in the reference and the being tested deployments, P_1 and P_2 are the base station transmit power in the two RANs. R_1 and R_2 are the cell average throughput in the two RANs.

On the other hand, when a heterogeneous network deployment consisting of two tiers (macro tier plus small cells tier) is considered, a slight modification in (3.19) is needed to evaluate the energy efficiency, and throughput gain for the heterogeneous RAN with reference to a macro only RAN, as depicted in equations (3.20).

$$ECG_{Het} = \frac{P_m \cdot \lambda_m}{P_m \cdot \lambda_m + P_s \cdot \lambda_s}, TPG = \frac{R_m \cdot \lambda_m + R_s \cdot \lambda_s}{R_m \cdot \lambda_m}, ETG = \left(\frac{R_m \cdot \lambda_m + R_s \cdot \lambda_s}{P_m \cdot \lambda_m + P_s \cdot \lambda_s}\right) \cdot \frac{P_m}{R_m}, \quad (3.20)$$

Where P_m and P_s are the transmit power of the macro and small cell RBSs, λ_m and λ_s are the cell densities of the macro and small cells tiers, and R_m and R_s are the cell average throughputs of the macro and small cells, respectively.

3.5 System model for homogeneous and heterogeneous networks

In this thesis, We focus on the downlink performance and the energy consumption of homogeneous and heterogeneous networks which use LTE RBSs. Unless stated otherwise, the following general conditions are assumed in this thesis when investigating the various considered RANs.

- Homogeneous macro cells and small cells are deployed according to a 2-tier hexagonal layout and consisting of 19 sites.
- In the case of heterogeneous networks, the small cells are deployed following a random uniform distribution or following a regular pattern within the coverage of a macro cell.
- Users are deployed following random uniform distribution in the target area. In certain cases, some of the users are deployed in clusters.
- The process of user association is based on the strongest received power, i.e. users associate with the cell which offers them the highest received power. In heterogeneous networks, the

cell range expansion (CRE) is employed by adding a bias to the received power from the small cells to avoid having most of the users associated with the parent macro cell to avoid the small cells being underutilised.

- All macrocell base stations are assumed to operate in the same frequency band in homogeneous networks in this thesis. Two cases are considered for heterogeneous networks: first the case of orthogonal carrier allocation where small cells use a different frequency band than the one used by the macro cell layer to avoid the issue of inter-layer interference: second, the case of co-channel frequency allocation, where both the macro and small cells operate on the same frequency band, an inter-layer interference management scheme is used.
- The 3GPP urban macro and urban micro path loss model is used to model both the path loss and shadowing in the carried out system level simulations.
- Shannon formula is used to estimate the user data rate R_u as a function of the user signal to interference and noise $SINR_u$ and the allocated bandwidth W_u, as in (3.21).

$$R_u = W_u \cdot (\min(\log_2(1 + SINR_u), S_m) , \tag{3.21}$$

Where S_m represent the maximum achieved spectral efficiency, and its value depends on the highest modulation scheme used. The highest modulation scheme considered in this thesis is 64 QAM..

- Round Robin scheduling is used where the time-frequency resources of each cell are allocated evenly among the associated users. If no users are associated to a base station, it transmits only the synchronisation and reference signals, which represent between 5% to 10% of the full RF transmit power of the base station.
- The terms cell average load and cell resource utilisation may used interchangeably in this thesis to refer to the same notion, which is the ratio of the occupied time-frequency resources to the total available resources in the cell. They are also used to indicate the average RF transmitted power of the base station.
- In the case of a homogeneous macro cell deployment consisting of *M* macro base stations, the base stations are indicated by BS_i ($i \in \{1,2,\ldots\ldots,M\}$), and the signal to interference and noise at a user UE_k associated with BS_i is estimated by (3.22).

$$SINR_{i,k} = \frac{P_i \cdot g_{i,k}}{\sum_{j=1, j\neq i}^{M} P_j \cdot g_{i,k} + N} , \tag{3.22}$$

Where P_i is the base station transmit power, $g_{i,k}$ is the channel gain between the base station *i* and user *k*, and N is the noise level at the user UE_k.

- Similarly, in case of the co-channel heterogeneous deployment, the user $SINR$ is estimated by considering the interference of both the macro and small cells. If orthogonal channel

deployment is considered, the user $SINR$ is calculated by only considering only the interference from the same frequency base stations.

3.6 Energy and throughput efficiency analysis in a macrocell RAN

Deploying more macro sites has been and continues to be one key approach used by operators to increase the capacity of their existing RANs. In addition to the technical issues of inter-cell interference and the high cost of macro base stations together with the difficulty of finding new sites, deploying more macro sites increases the RAN energy consumption. In this section, the proposed base station power consumption model, and the energy efficiency evaluation framework presented in section 3.4 are used to investigate the TPG, ECG, and ETG of a homogeneous macrocell RAN based on LTE RBSs. A Matlab static system level simulator was developed to estimate the users' *SINR* distribution and the RAN average throughput. The network model follows a hexagonal layout, as shown in Figure 3-7, where each base station transmits the same RF power Pt, and is equipped with a single omnidirectional antenna with a gain of G_t. The single link capacities are calculated using Shannon formula. The main simulation parameters are listed in Table 3-3.

Table 3-3: Simulation Parameters

Parameter	**Value**
Frequency (MHz)	2000
Bandwidth (MHz)	20
Macro BS Antenna Gain (dBi)	15
Small-cell BS antenna Gain (dBi)	Micro/Pico-cell: 6/2
Pathloss Model & Shadowing	3GPP Uma & Umi
Traffic Model	Full Buffer
User Location distribution	Indoor Uniform
Users	200/Km^2

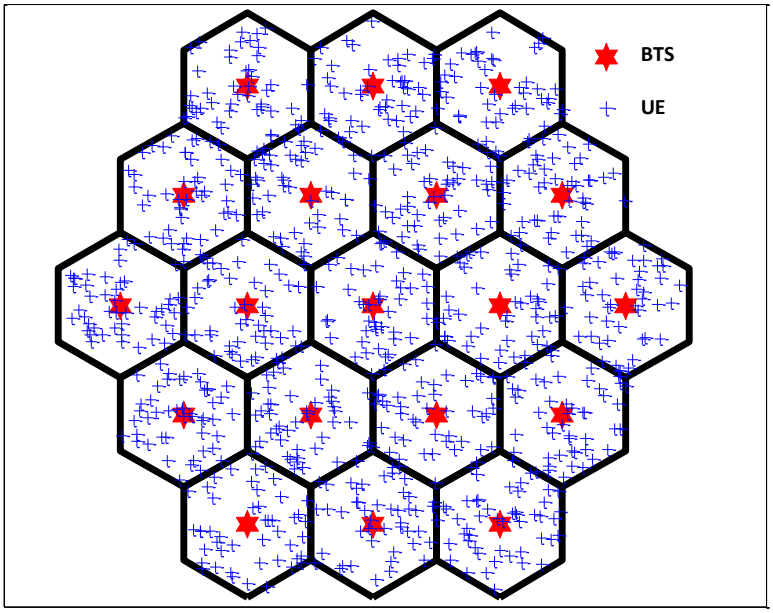

Figure 3-7: Hexagonal radio access network layout

The RAN average throughput is defined as the sum of the average data rates of the users deployed inside the target area. The users are assumed to be uniformly distributed over the target area. UE statistics are only collected from the centre cell to avoid underestimating the inter-cell interference which affects users located at the edge of the RAN area. All the users are assumed to be indoor. The average received signal at each user P_r in decibels is calculated by using the link budget analysis shown in (3.23).

$$P_r = P_t + G_t + G_r - PL - L_B \,, \tag{3.23}$$

Where P_t is the RF base station transmit power, G_t and G_r denote transmitter and receiver antenna gains, L_B denotes the building penetration loss, and PL refers to the path loss attenuation due to distance and shadowing effects between the antenna and UE. The 3GPP urban macro path loss Uma is used to model both the distance dependent and shadowing large scale fading in the simulation [128].

The user's *SINR* can be expressed as a function of the user's signal to interference ratio (*SIR*), the user's signal to noise ratio (*SNR*), and the cell average load α in the interfering cells, as shown in (3.24) where it is assumed that each cell has the same average load α.

$$SINR = \frac{1}{\frac{\alpha}{SIR} + \frac{1}{SNR}} \,. \tag{3.24}$$

As a full buffer scenario is considered in this chapter, all the base stations are assumed to transmit at full power, and the cell average load is always equal one. The value of *SIR* depends only on the position of the mobile users inside the cell, and not on the inter-site distance (ISD), nor the base stations transmit power P_t , the reason is all base stations transmit at the same power. On other hand, the user's SNR depends on the user location, the ISD, and P_t. When SNR is very high, the impact of noise becomes negligible compared to the inter-cells interference, and the network operates in an interference limited regime. Figure 3-8 shows how the user's *SINR* approaches the value of *SIR* at high *SNR* values for a cell edge user with *SIR* value of -3dB.

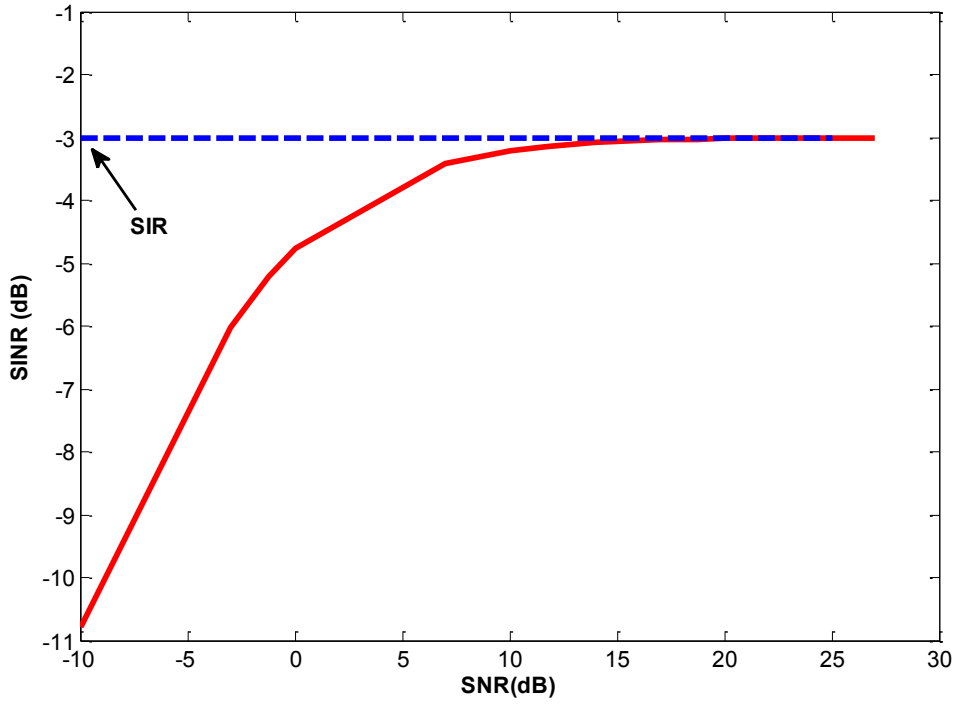

Figure 3-8: SINR vs. SNR for a cell edge use, SIR = -3 dB

3.6.1 Macrocell densification

In this subsection, the impact of increasing the density of deployed macro base stations on the RAN throughput and energy consumption is evaluated. The effect of reducing the macro site radius from 1000 to 200 m on the RAN average throughput and energy consumption is quantified by estimating the throughput gain TPG, energy consumption gain ECG, and the energy throughput gain ETG for each macrocell radius considered.

Two cases of RF transmited power are considered in our analysis: 1) When the same value of maximum transmit power $P_{t,max}$ of base the station is used regardless of the macro cell radius; 2) when the value of $P_{t,max}$ is determined as a function of the target coverage of the site, i.e. it is calculated to guarantee a minimum required *SINR* at the cell edge.

3.6.1.1 The fixed same transmit power case

The *SINR* cumulative distribution function is plotted in Figure 3-9 for various considered cell radii while the same transmit power is used for each considered cell radius. The simulation results show that reducing the cell radius while keeping the same transmit power leads to improving the *SINR* distribution before it saturates when the network becomes operating in an interference limited regime. Therefore, keeping the transmit power constant beyond this point will not lead to any benefit as the *SNR* values are already high and because all the base stations transmit at the same power and any further reduction in the ISD would lead to increasing both the received signal power and the interference, simultaneously.

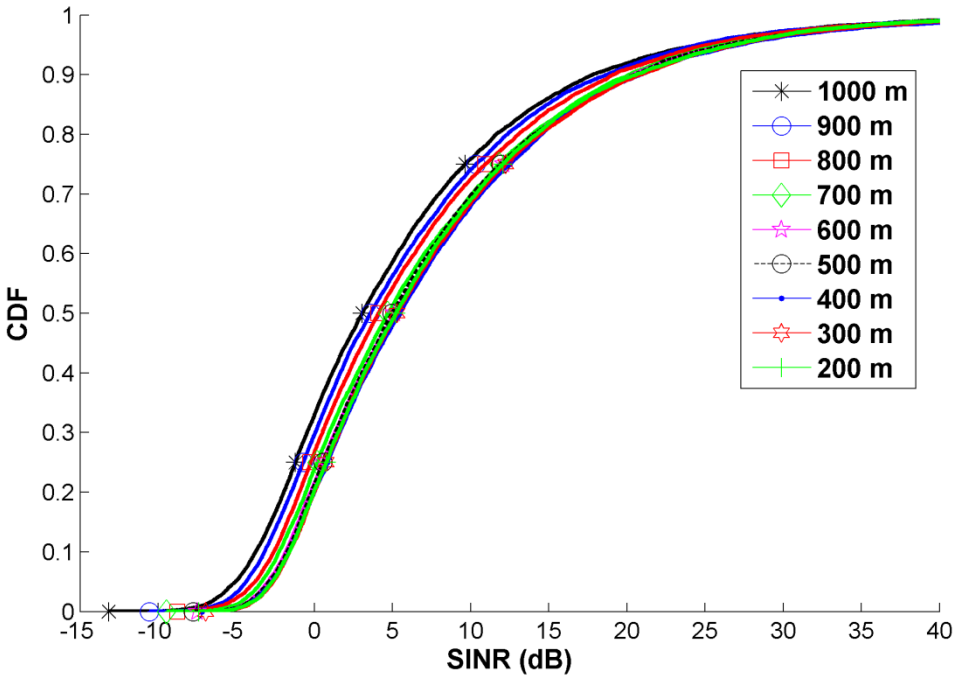

Figure 3-9: The CDF of SINR for the case of same RF transmit power in a macrocell RAN at cell radii values from 200 m to 1000 m

In terms of energy efficiency, always transmitting at the same the $P_{t,max}$ of (46 dBm) regardless of the ISD has the advantage of ensuring that the power amplifier operates at the same efficiency, 30% at 46dBm of transmit power in this case. Reducing the transmit power degrades the PA efficiency if no efficiency enhancement techniques, such as envelope tracking, are implemented [129], as shown in Figure 3-10.

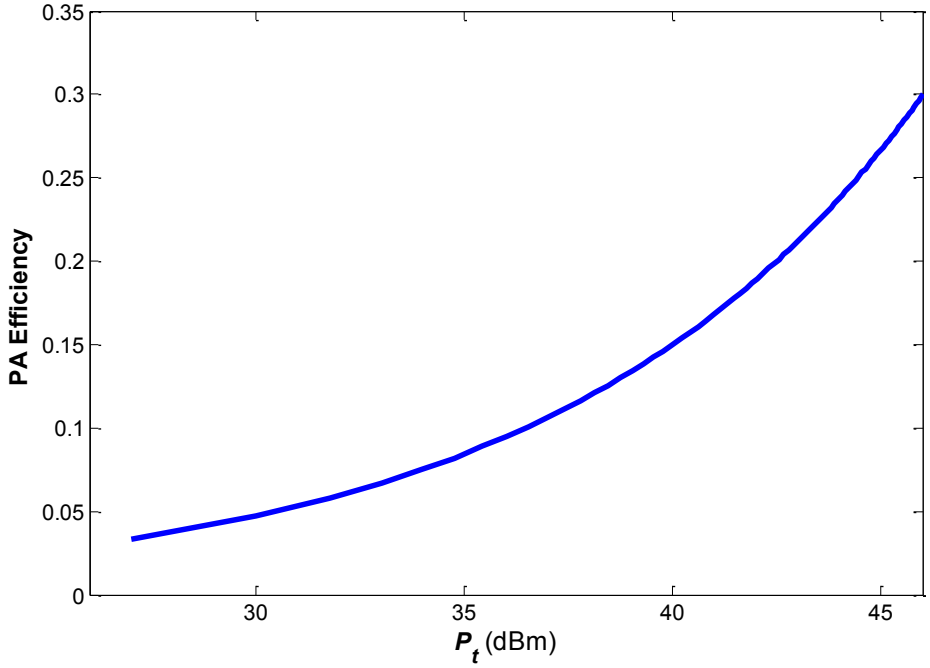

Figure 3-10: Power amplifier efficiency versus transmitted power

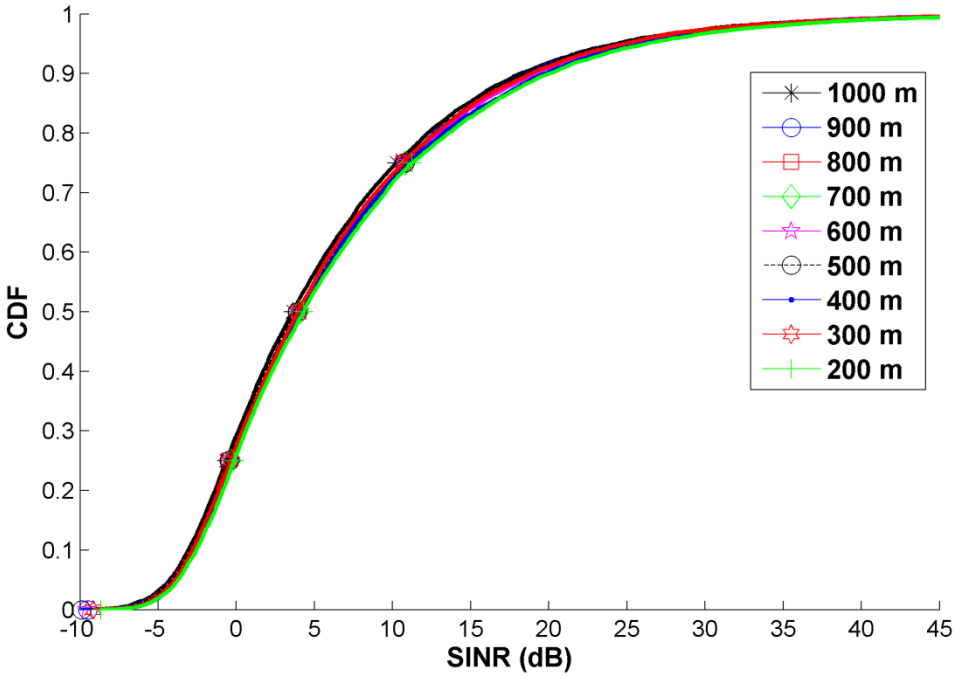

Figure 3-11: The CDF of SINR in case of variable RF Transmit power in macrocell RAN at cell radii values from 200 m to 1000 m

3.6.1.2 Variable Transmit Power case

In this subsection, an *SNR* target value of zero dB for an indoor cell edge user is assumed, this value is used by following the same approach in [90] to have an SNR of 20 dB for the outdoor

cell edge user, which is equivalent of the typical value of -3dB for the SINR of the outdoor cell edge users.

The noise level at the user equipment is calculated by (3.25). It is equal to -94 dBm for a bandwidth of 20 MHz.

$$N = 10 \cdot \log_{10}(B) + N_0 + NF \ , \tag{3.25}$$

Where B is the bandwidth, N_0 is the noise power spectral density and equals -174 dBm/Hz, and NF is the user equipment noise figure equal to 7 dB. To achieve the target *SNR* of zero dB, -94 dBm of received power P_r at the cell edge is required. The value of base station transmit power P_t is determined from (3.23) when the values of G_t, G_r, PL, and L_B are known. As -3dB is the typical value of *SIR* at the cell edge of a homogeneous macro cell RAN, the *SINR* achieved when the *SNR* equals zero is approximately -4.77 dB, calculated using (3.24).

The *SINR* CDF of users in the central cell is shown in Figure 3-11, where we see clearly that the curves of CDFs are almost overlapping and the SINR distribution is independent of the cell radii. When evaluating the RAN energy efficiency for the case of a variable transmit power P_t two sub cases are considered:

a. We keep the power amplifier efficiency constant regardless of the value of P_t and equal always to $\eta_{pa,m}$ which equals to 30% as already shown in 3.3.1. This case corresponds to the situation when different designs of power amplifiers are used for each target transmit power, which are determined by the corresponding cell radius. It may also correspond to the case when efficiency improvement techniques, such as envelope tracking, are implemented in the power amplifier.
b. We keep the same the case of the same power amplifier design for all the different transmit power values P_t. The disadvantage of this case is the degradation of the power amplifier efficiency when the base station RF transmitted power level is reduced, which leads to increasing the power consumption of the base station as shown in Figure 3-12.

Figure 3-13 shows the used P_t values for the two cases of same and variable transmitted power versus the considered cell radii. The cell density is calculated as $1/A_c$ where A_c is the cell area and has the units of cell/km^2. When calculating the throughput gain TPG, a cell radius of 1000 m is taken as the reference RAN deployment scenario. The TPG is calculated at the different cell densities by dividing the RAN area throughput of each considered cell density on the area throughput of the the reference RAN as in (3.26).

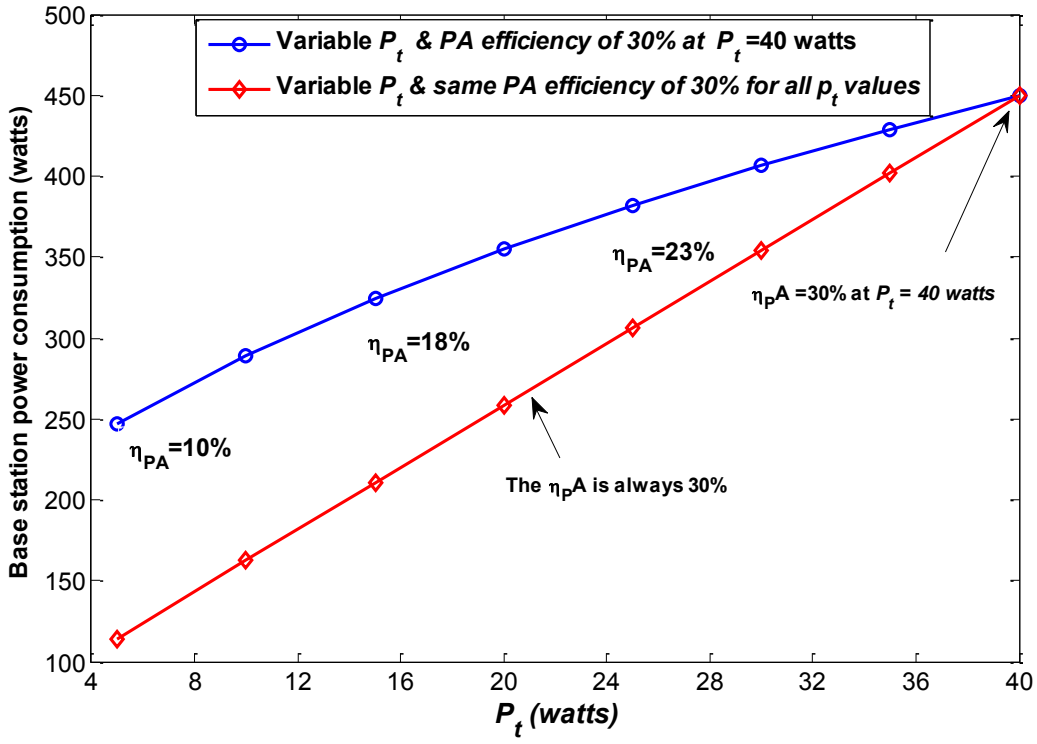

Figure 3-12: The impact of PA efficiency degradation on the power consumption of an omnidirectional macrocell base station

$$TPG_i = \frac{\lambda_i \cdot R_i}{\lambda_1 \cdot R_1}. \tag{3.26}$$

In (3.26) λ_i is the cell density of the *i*-th RAN deployment, R_i is the cell average throughput of the *i*-th RAN deployment, λ_1 is the cell density of the reference RAN deployment and R_1 is the cell average throughput of the reference RAN. Having a the same fixed transmit power P_t for all cell densities leads to a slightly higher throughput gain compared to variable transmit P_t as shown in Figure 3-14. For instance, a throughput gain of 30 for the case of fixed P_t is reached compared to 27 for case of variable P_t when the macro cell radius is reduced from 1000 m to 200 m.

Keeping P_t constant has the disadvantage of increasing the consumed power compared to the two cases of variable P_t, as shown in Figure 3-15 which plots the area power consumption versus the macro cell density. The results for the area power consumption results show the existence of an optimum density of macro cells at around 1 cell/km^2 when variable P_t, and fixed power amplifier efficiency are assumed, while a continous increase in the area power consumption versus the cell density is observed in the other two cases. The results demonstrate that the variable P_t cases always consume less power than the same P_t case, except for 1000 m cell radius because 49 dBm is used versus 46 dBm in case of using the same fixed P_t.

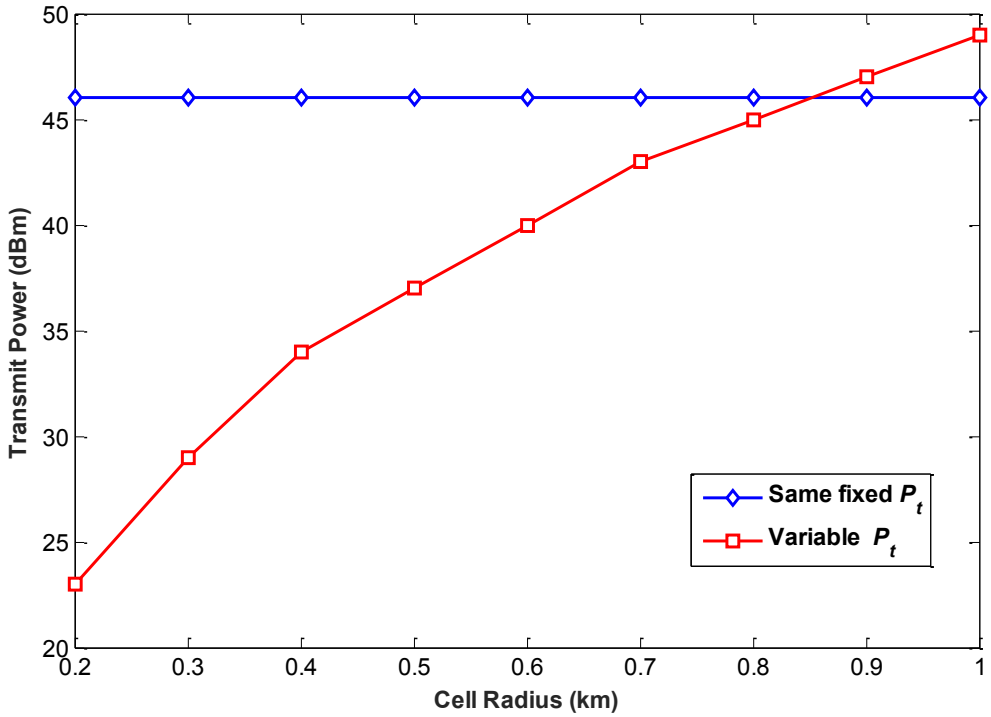

Figure 3-13: The transmit power values in the two cases of macrocell RAN.

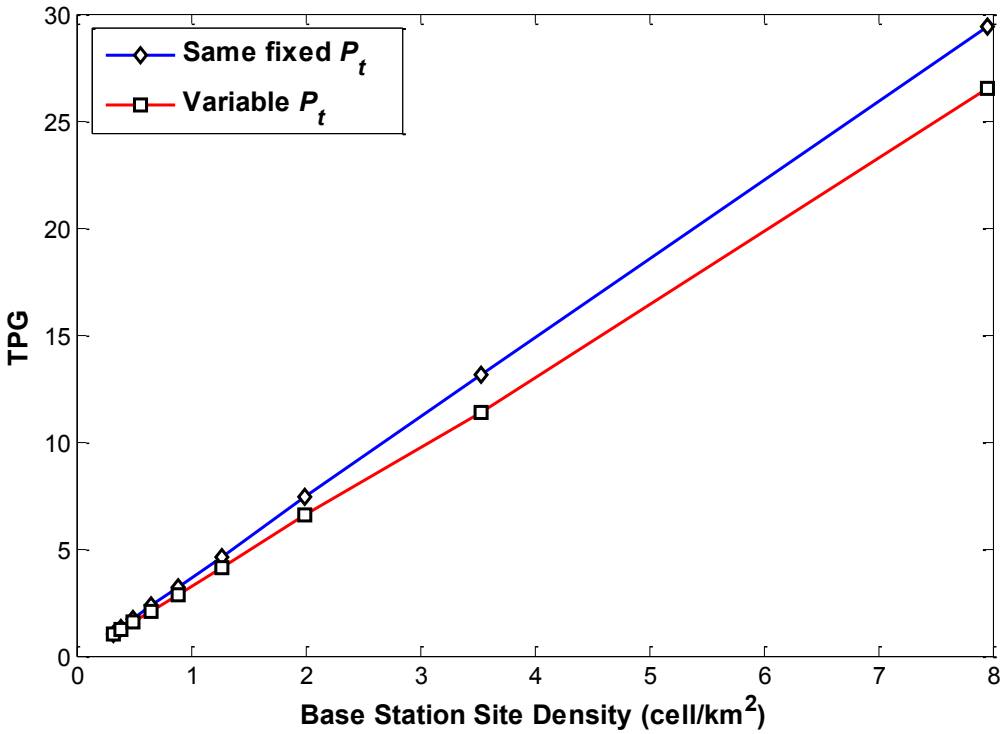

Figure 3-14: The TPG results for macrocell densification

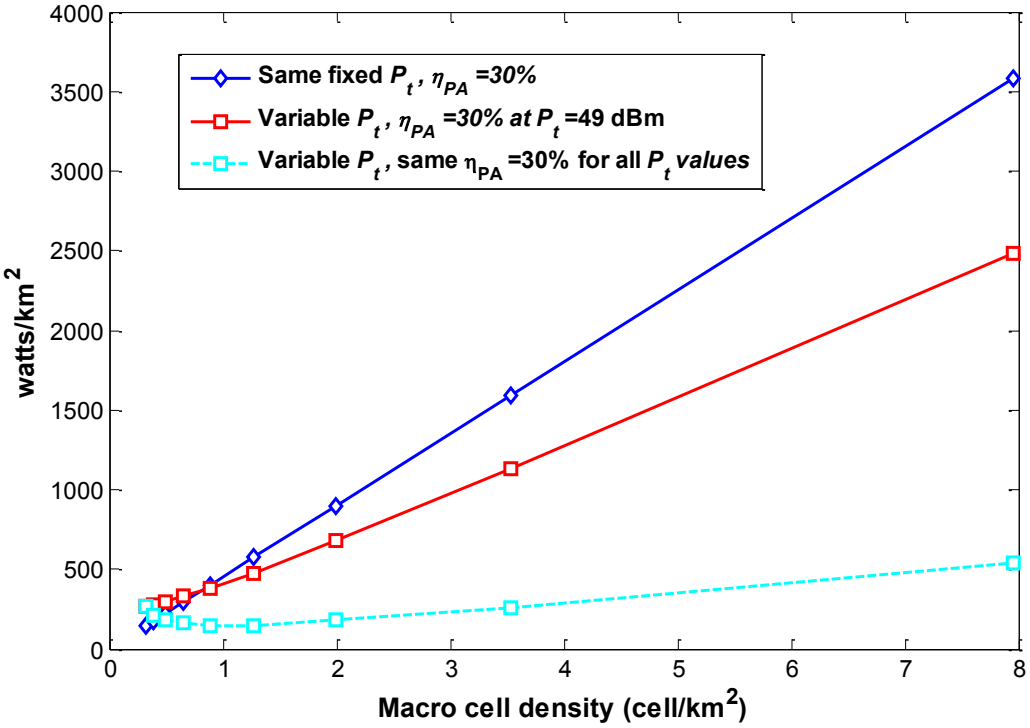

Figure 3-15: The results for area power consumption of macrocell RAN

When evaluating the RAN energy efficiency using the bit/J metric, the results show also that the variable P_t cases are more energy efficienct than the fixed P_t case. However, this metric does not show the existence of an optimum density in the case of variable P_t and same fixed power amplifier efficiency. The results also did not to show a continous increase in the RAN consumed energy versus the cell density. Therefore, using only the bit/J metric has the disadvantage of not specifying whether the improvement in EE is due to a reduction in the power consumption, or due an increase in the RAN throughput, as shown in Figure 3-16.

The RAN ECG can be calculated for different cell densities by (3.27).

$$ECG_i = \frac{\lambda_1 \cdot P_1}{\lambda_i \cdot P_i} . \qquad (3.27)$$

In (3.27), P_i refers to the macro site power consumption at transmit power P_t, and P_1 is the base station power consumption of the reference RAN at P_t of 46 dBm and at 1000 m cell radius. Figure 3-17 shows that the ECG decreases monotonically versus the macro cell density in the two cases of same P_t and variable P_t with changing power amplifier efficiency. However, in the case of variable P_t and fixing power amplifier efficiency, the ECG reaches a maximum value at site density of 1 cell/km^2 then starts to decrease at higher densities which means that the network consumes the least amount of energy at this cell density and any reduction in the cell density would lead to an increase in the RAN energy consumption. Also,

any further densification is not justified from energy consumption point of view unless more capacity is required

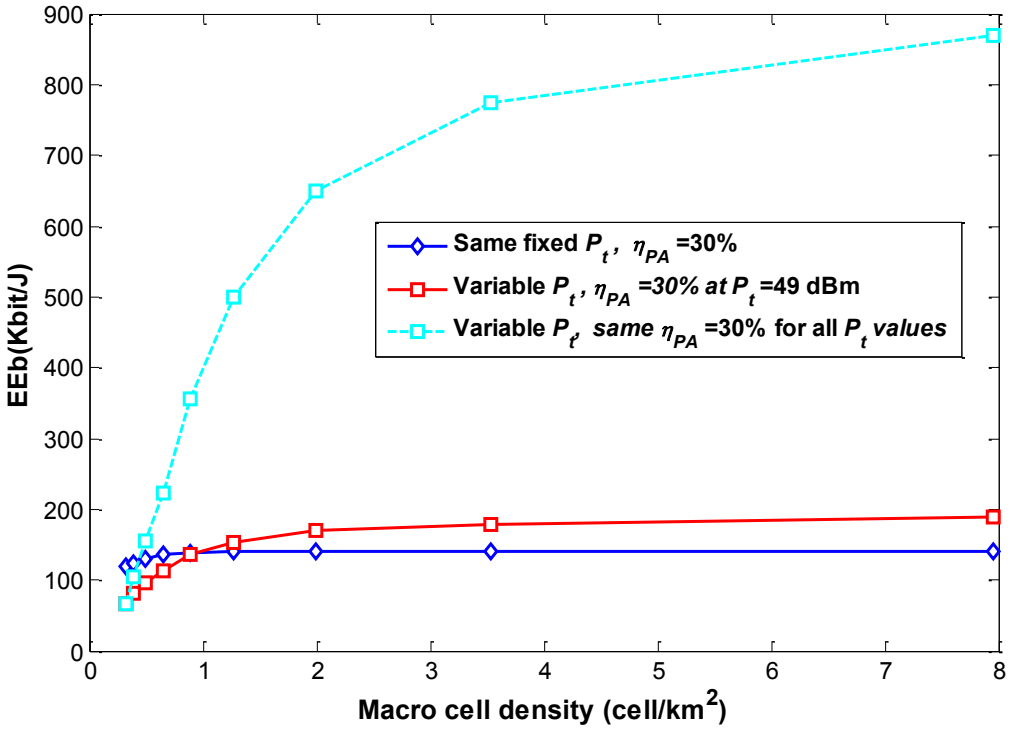

Figure 3-16: The results for EE of macrocell RAN

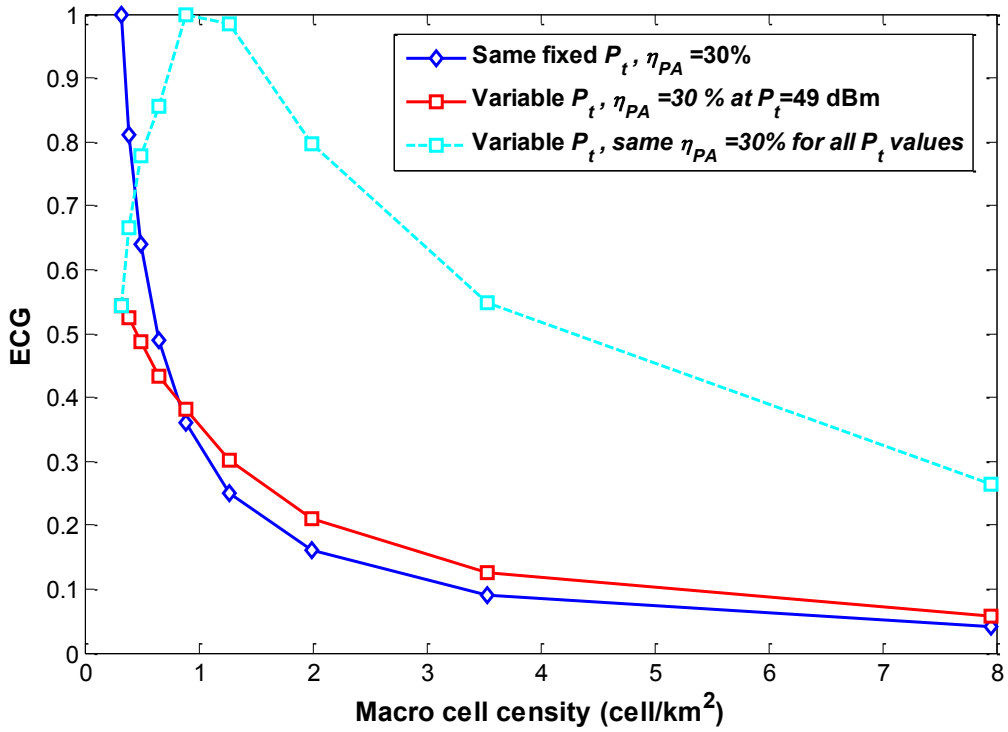

Figure 3-17: The results for ECG of macrocell RAN

The product of TPG and ECG forms the energy throughput gain ETG, which follows the same trend as the bit/J metric as shown in Figure 3-18. When comparing the considered cases of same and variable P_t, the case of variable P_t with same power amplifier efficiency of 30% achieves a maximum ECG value at density of 1 cell/km^2 , then start to decrease when the mace cell density increases. While the in two other cases, the ECG show continuous decrease versus the cell density, which is demonstrates that the relative gain is the TPG is accompanied by an increase in the RAN energy consumption. Comparing the results of ETG with ECG shows that maximizing the EE metric does not always mean minimising the energy consumption. The bit/J metric can provide insights regarding the RAN energy efficiency only when the target capacity is predefined in the two RANs under comparison, in such case, the TPG equals one, and the ECG and the bit/J metric lead to the same conclusions regarding energy consumption in the evaluated RAN.

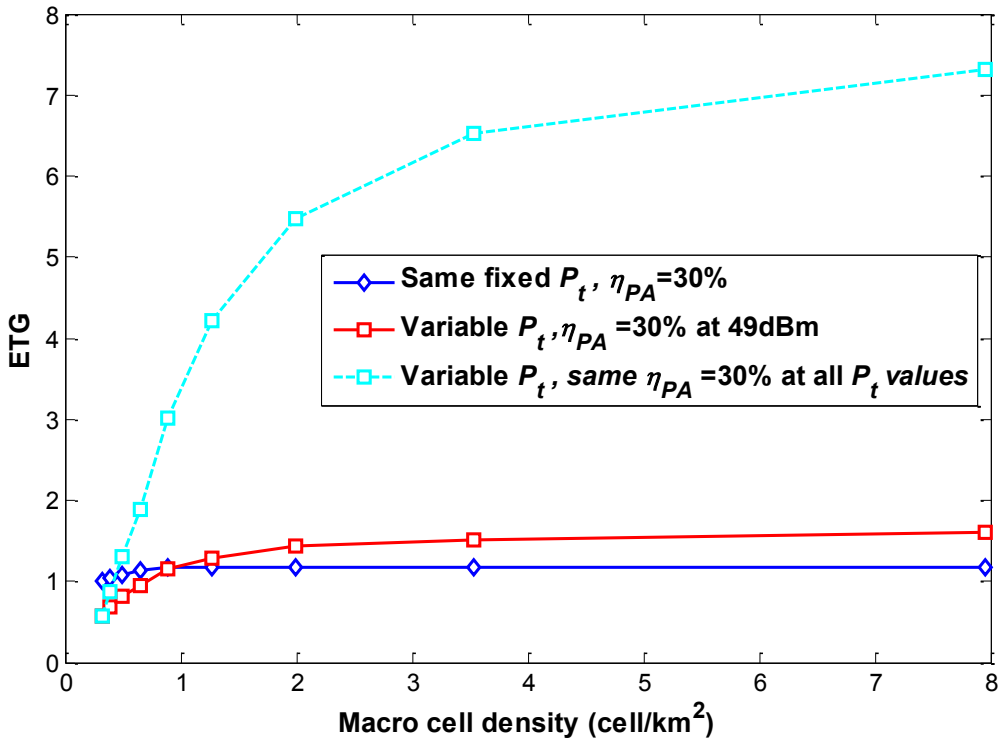

Figure 3-18: Results for the ETG of macrocell RAN

The results for energy consumption in a macro cell RANs indicate large macro cells (1000 m radius) cannot offer high area throughput density and require high transmit power to ensure the cell edge target *SINR*. On the other hand, an aggressive densification of macrocells can offer high area throughput values, but the price is a significant increase in the RAN energy consumption, even if variable transmit power and same power amplifier efficiency are assumed.

3.6.2 Energy efficiency improvement techniques in macrocell RANs

Various techniques have been proposed to enhance the average throughput and reducing the energy consumption of macro RANs. A brief overview of a number of these techniques is presented in this section. Simple scenarios are simulated to indicate the way in which energy consumption decreases when implementing these techniques.

- Reducing the energy consumption of the hardware components in the base station leads to large savings in the base station power consumption [129]. For example, improving the PA efficiency from 30 % to 60 % in the evaluated macrocell RAN improves the ECG from 0.32 to 0.62 (almost two times) at cell density of 1 cell/km^2 in the case of the same fixed P_t is assumed, as depicted in Figure 3-19.

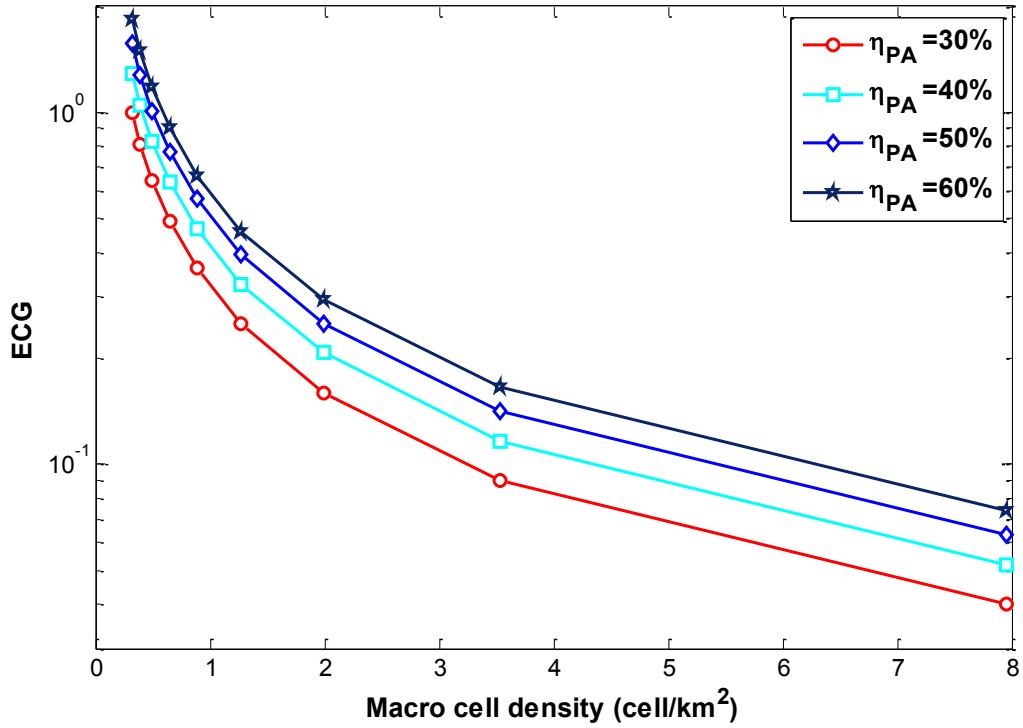

Figure 3-19: The ECG versus macrocell density at various PA efficiency values of macrocell RAN

- In distributed base station architectures, the baseband processing unit is located in the base station cabinet, while the radio equipment and power amplifier are located on the top of the mask with a fibre cable connection between the base station cabinet and the RF equipment. Such a design eliminates the feeder cable losses and the cooling requirements [51]. Figure 3-20 shows the ECG improvement of a macro cell RAN when distributed base stations are deployed compared to the centralised base station architecture. In the centralised base station architecture, all the equipment is located in

the base station cabinet, and a copper cable is used to connect the power amplifier with the antennas at the top of the mask. This design suffers from feeder cable losses (3dB), and from the need for cooling unit to remove the generated heat inside the base station cabinet.

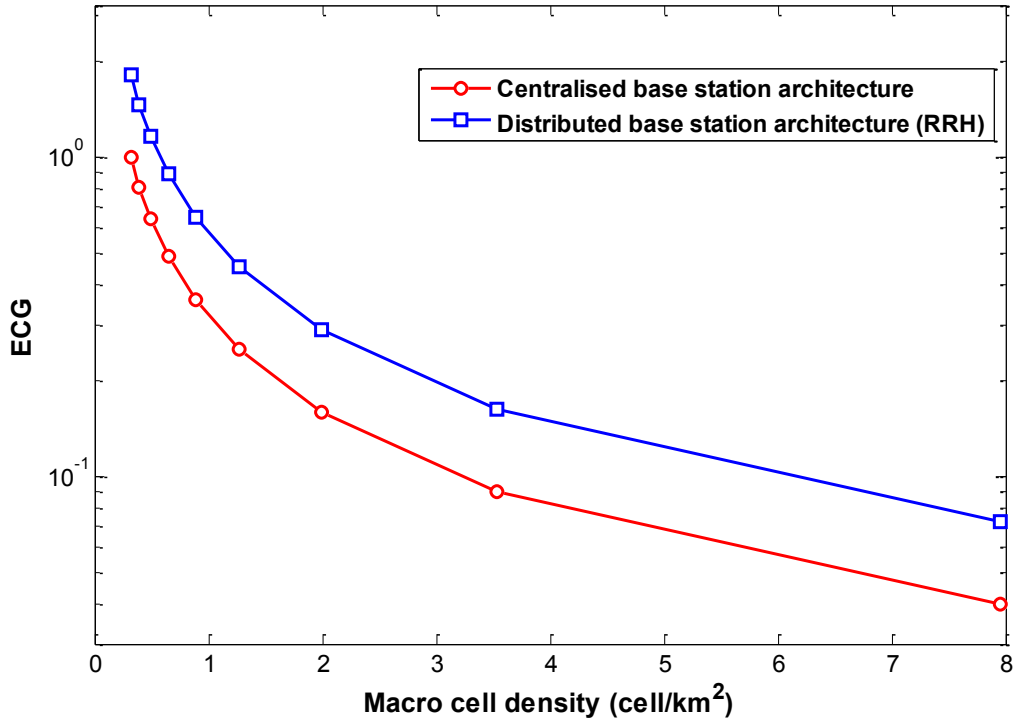

Figure 3-20: The ECG versus the macrocell density for distributed and centralised base station architecture

- Deploying high order sectorised base stations can improve the RAN average capacity by a factor equal theoretically to the number of sectors. However, the drawback of this method is the increase in power consumption of the base station site. Fortunately, the implementation of the adaptive sectorisation technique can reduce this increase in the power consumption. More details are presented in chapter 4.
- MIMO techniques can improve the RAN coverage and throughput with great efficacy. However, this involves installing more hardware in the base station in comparison with a SISO base station. Chapter 5 is dedicated to discussing the issue of energy efficiency of a MIMO enabled RANs in detail.
- More advanced techniques, such as turning off some macrocell base station components selectively during periods of low traffic [97] and the implementation of energy efficiency aware resource allocation techniques [130], can improve the RAN energy efficiency. The discontinuous transmission DTX techniques are also discussed in chapter 5.

3.7 Small cell densification

The deployment of more macrocell base stations transmitting at high power cannot continue without limit because of the rise in the energy consumption and the cost of macrocell base stations, coupled with the difficulty of finding new sites.

Given the continuous increase in demand for wireless access services, operators have considered many solutions to meet this demand. Increasing the density of network by the deployment of low power and cost-effective nodes (small cells) is one of the solutions considered to be a key enabling technique for achieving high capacities in the next generations of cellular networks. These low power nodes include various types of base stations such as microcells, picocells and femtocells. Microcells and picocells are usually deployed by the network operators, while femtocells are deployed by the end users in their private residences. The impact of the deployment of these small cells on the RAN throughput and RAN energy efficiency is evaluated in this section.

Small cells can be deployed in indoor as well as outdoor scenarios. They can be deployed as an overlay to an existing macrocell layer, or also as a standalone small cell only deployment such as in outdoor hot spot areas. Homogeneous deployments of pure micro only and pico only cell scenarios are investigated in this section. The TPG and ECG are evaluated with reference to a baseline reference macrocell RAN. The network model consists of small cells placed outdoors in a uniform hexagonal grid with different cell radii. Two cases are considered: microcells only in Case 1, and picocells only in Case 2. As with the case of macro cell deployments, in the case of same fixed transmit power, the values of 38 dBm and 28 dBm are used for the micro and picocells, respectively. In the case of variable P_t , the transmit power is calculated for every cell radius to achieve an SNR target of 0 dB at the cell edge. The values of P_t for micro and pico cells are shown in Figure 3-21. The only difference from the case of macro cell RAN is that the power amplifier efficiency is not assumed to stay fixed when changing the transmit power P_t as it is unlikely to have different power amplifier designs for each considered cell radius in small cells.

Figure 3-22 shows that increasing small cell density leads to an increase in the TPG and reduction in the ECG, which follows the same trend obtained in a macrocell RAN. However, the advantage of small cells is that higher throughput gains are achieved, and less energy is consumed when compared with the macrocell RAN, as shown in Figure 3-23. For example, deploying macrocells with a cell radius of 500 m and P_t of 46 dBm result in a TPG of 4 and ECG 0f 0.25 compared to a reference macro cell radius of 1000 m, while in the case of micro cells, the TPG reaches 21 for the same level of energy consumption. Higher values are obtained

when pico cells are considered, at the same ECG 0f 0.25, the TPG is approximately 120 in the case of same fixed P_t pico RAN, which corresponds to a 30 times improvement in the TPG compared with a macro cell RAN with 500 m radius. The results also demonstrate the advantage of varying the transmit power over using the same fixed transmit power in the two types of cells. When comparing the micro and pico cells, it is clear that, for the cell densities considered, pico cells consume less energy than micro cells to achieve the same TPG value. For example, a TPG of 100 with reference to the macro cell RAN of 1000 m radius, is achieved at an ECG of 0.077 in the case of fixed P_t micro cells and at an ECG of 0.248 in the case of fixed P_t pico cells, which is equivalent of a 3.6 times improvement in the ECG. The ECG values have been calculated with reference to the macro cell RAN with cell radius of 1000 m and fixed transmit power of 46 dBm.

When using the ETG to quantify the relative improvement in the bit/J metric for the micro and pico RANs, a continuous improvement in the ETG is observed in the two cases of pico and microcells, as shown in Figure 3-24. However, the ECG and TPG are needed in order to show whether or not this improvement is a result of a reduction in the power consumption or an increase in the RAN throughput.

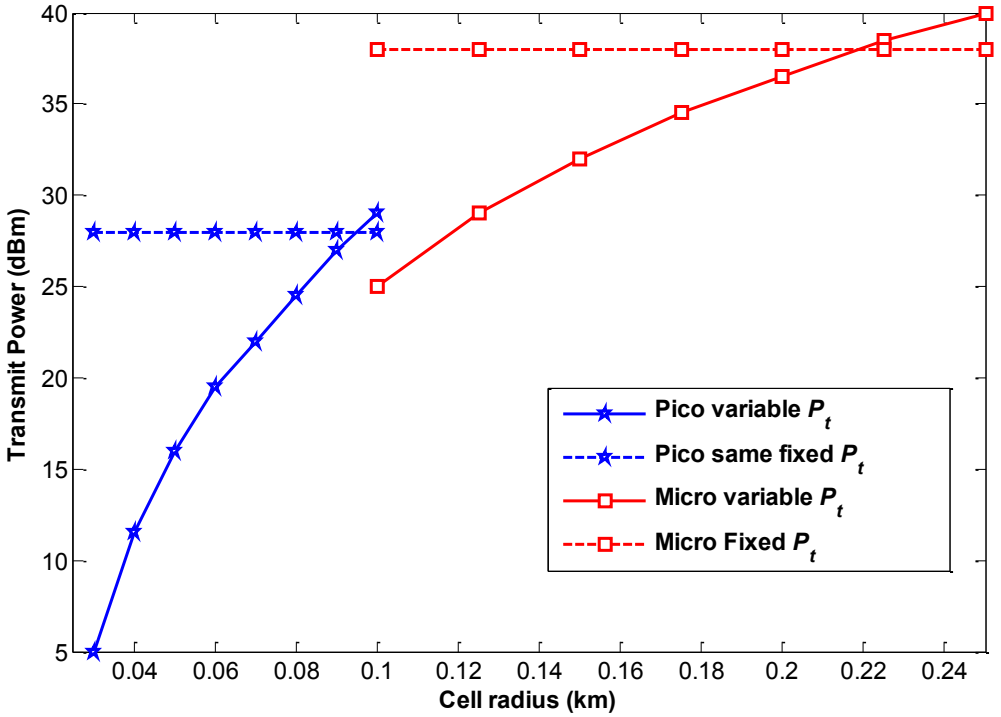

Figure 3-21: The results for RF transmit power in pico and microcell RANs

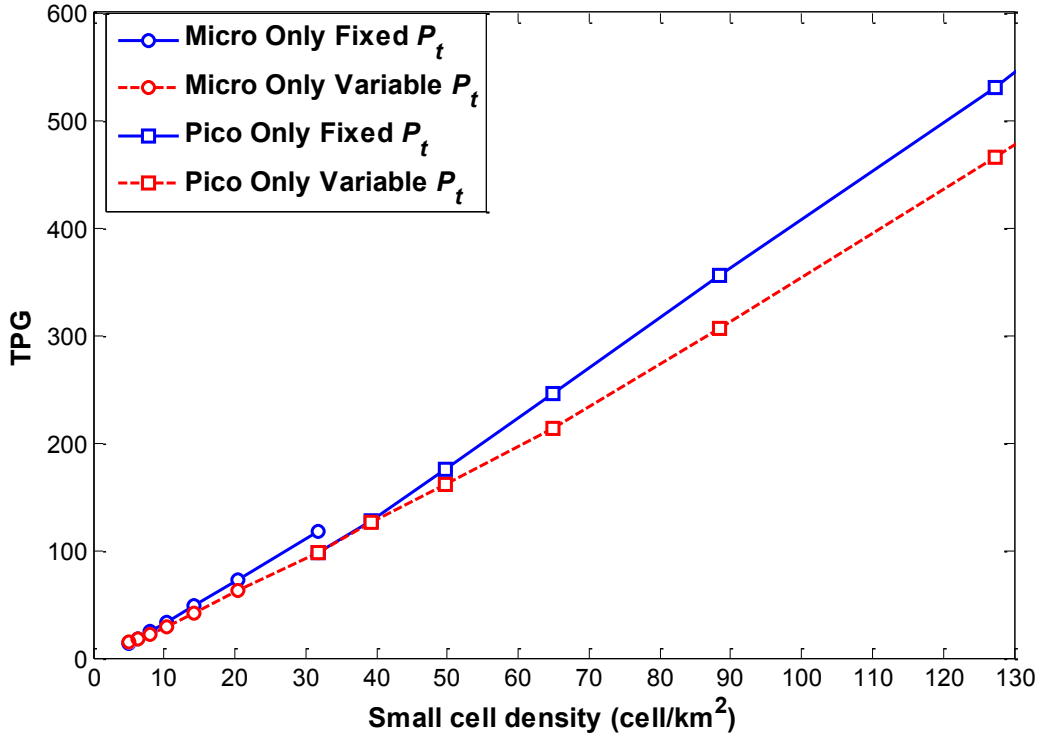

Figure 3-22: The results of TPG for small cell only deployment

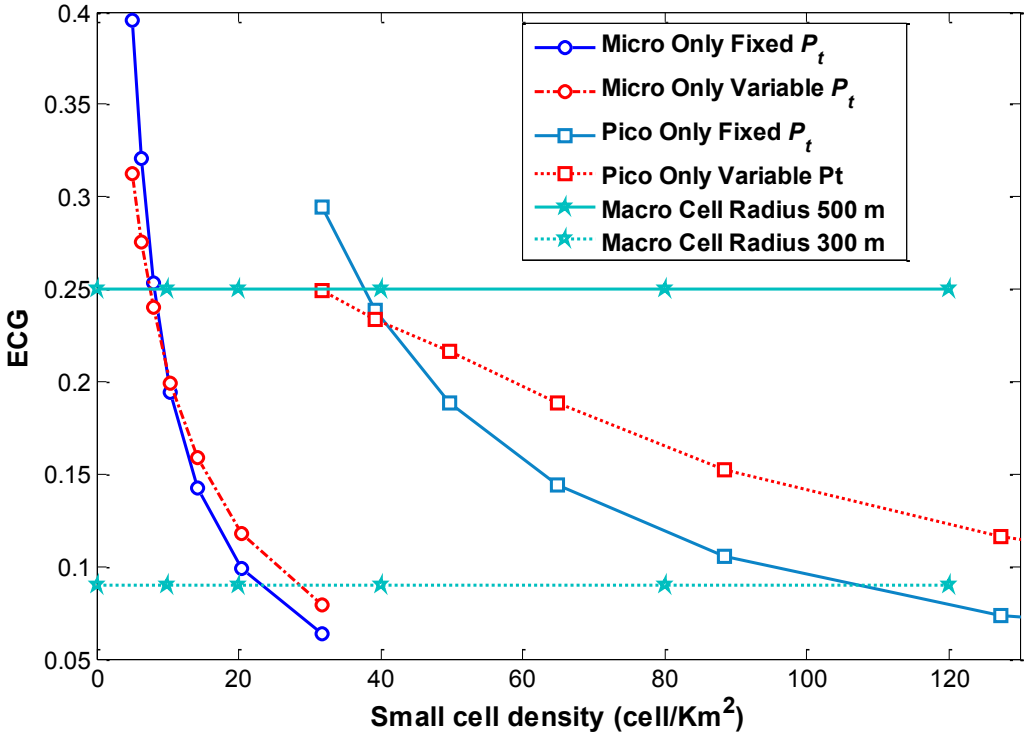

Figure 3-23: The results of ECG for small cells only deployments

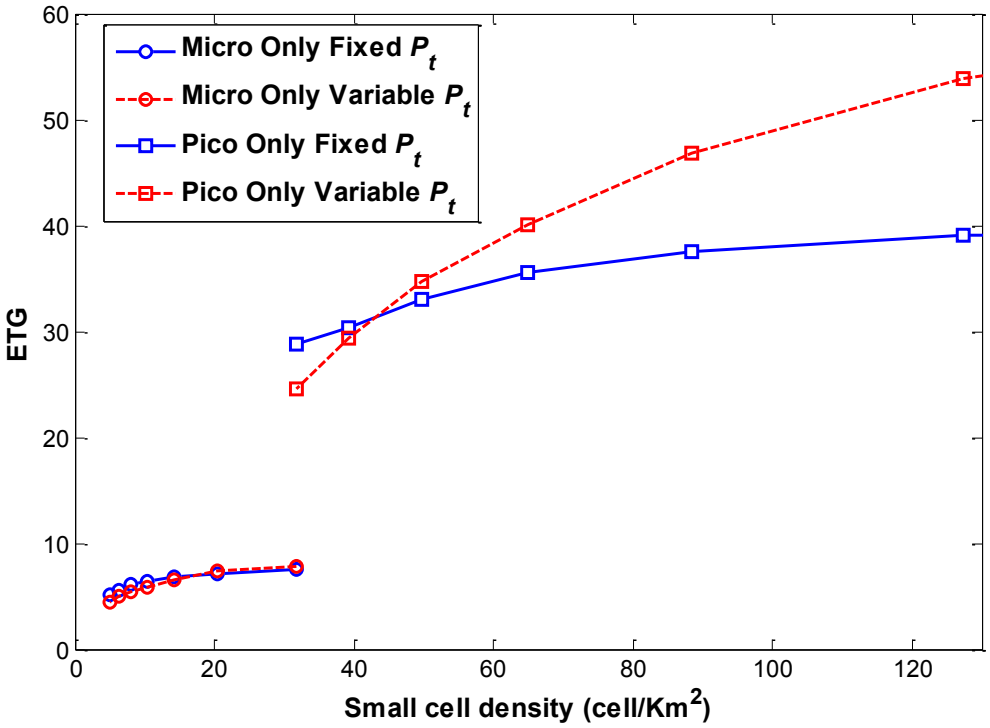

Figure 3-24: The results of ETG for of small cell only deployments

3.8 Heterogeneous Networks

As indicated earlier, a radio access network consisting of only small cells can offer higher throughput and consumes less energy than a macrocell RAN. However, due to certain challenges, such as the mobility management and backhaul requirements, these types of deployments have limited use cases such as indoor deployments, and outdoor hot spot scenarios. Small cells are usually deployed as an overlay to an existing macro layer to form a heterogeneous network. Deploying small cells can improve the RAN coverage and capacity in a flexible way. However, adding more nodes to the macrocell may lead to an increase in the RAN energy consumption. In this section, the impact of adding an overlay of small cells to a macro layer on the RAN average throughput and the RAN energy consumption is investigated.

3.8.1 Heterogeneous network layout

The network layout of heterogeneous network consists of two layers: 1) The macrocell layer, which consists of 19 omnidirectional macro sites, each of which has a coverage radius of 1 km, deployed in the form of a hexagonal grid; 2) An overlay of small cells distributed uniformly in the macro cell coverage areas, as shown in Figure 3-25. Note that the users are deployed in all macrocells, for improving the clarity of the figure, the users deployed in the noncentral cells are not shown in the figure. The deployment density of the macro RAN cell is denoted by λ_m , and

the small cell density is denoted by λ_s , R_m is the macro cell average throughput, R_s is the small cell average throughput, P_m is the macro base station power consumption and P_s is the small cell power consumption.

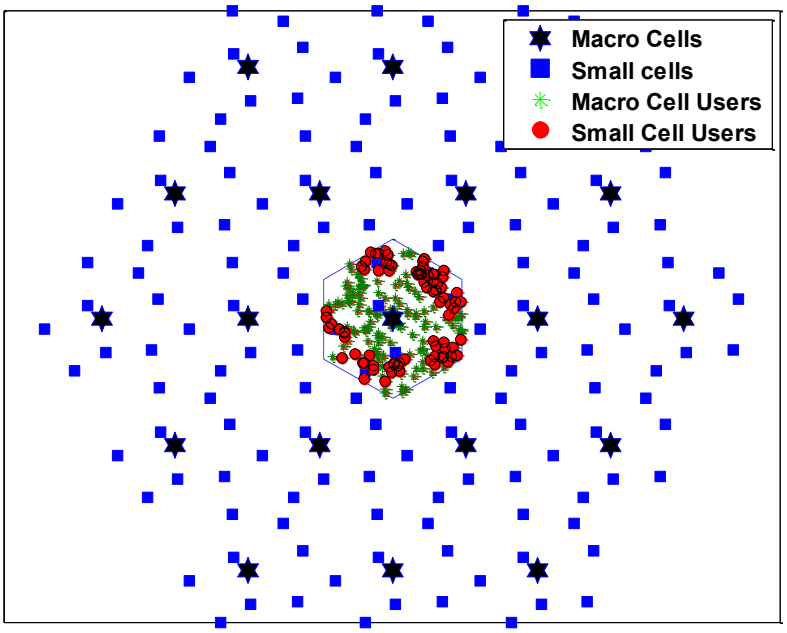

Figure 3-25: Heterogeneous network layout

3.8.2 The analysis of throughput and energy efficiency

The TPG and the ECG of the heterogeneous RAN are calculated with reference to a homogeneous macrocell RAN with density λ_m expressed by (3.28) and (3.29), respectively.

$$TPG = \frac{\lambda_m \cdot R_m + \lambda_s \cdot R_s}{\lambda_m \cdot R_m} = 1 + TPG_s \,, \tag{3.28}$$

$$ECG = \frac{\lambda_m \cdot P_m}{\lambda_m \cdot P_m + \lambda_s \cdot P_s} = \frac{ECG_s}{1 + ECG_s} \,, \tag{3.29}$$

Where $TPG_s = \frac{\lambda_s \cdot R_s}{\lambda_m \cdot R_m}$ and $ECG_s = \frac{\lambda_m \cdot P_m}{\lambda_s \cdot P_s}$, which demonstrates that the TPG of heterogeneous RAN is always better than macro only RAN, while the ECG of the heterogeneous RAN is always less that macro only RAN if full buffer traffic is assumed.

The actual cell average throughput is a function of many parameters such as user distribution, cell's average load, inter-cell interference and fading characteristics. However, in an interference limited regime, and when the same amount of bandwidth is allocated to every cell,

the average cell throughput can be considered to be the same regardless of the cell type, which means that the ECG will scale almost linearly with λ_s. Assuming an orthogonal frequency allocation to the macro and small cells eliminates the cross layer interference between the macro and small cells. The co-channel deployment case is considered in chapter 6. The allocated bandwidth B in the case of macro cell only scenario is divided between the two layers in the case of heterogeneous deployment. By assuming equal partition of the bandwidth between the macro and small cells, the heterogeneous RAN TPG can be expressed by (3.30).

$$TPG = \frac{1}{2} + \frac{\lambda_s}{2.\lambda_m}. \tag{3.30}$$

If the power consumption of a macrocell base station P_m is K times larger than the small cell power consumption P_s, the value of K is expressed as in (3.31), and the ECG in (3.29) can be rewritten as in (3.32).

$$K = \frac{P_m}{P_s}. \tag{3.31}$$

$$ECG = \frac{K.\lambda_m}{K.\lambda_m + \lambda_s}. \tag{3.32}$$

Both TPG and ECG can be calculated directly from (3.30) & (3.32) by fixing λ_m, and increasing λ_s gradually.

When pico cells with P_t =28 dBm is assumed, and an omnidirectional macro cell with P_t =46 dBm, the value of K is equal to 30 calculated using the power consumption model. Figure 3-26 shows a linear increase (green dotted line) in the TPG versus the small cell density when the macro cell density is kept constant. The ECG monotonically decreases with an increase in the small cell density, as shown in Figure 3-27. For instance, the TPG is improved 7.5 times when the pico cell density is increased from 5 to 40 cell/km^2, while the ECG is reduced from 0.6 to 0.25. Similar results of TPG are obtained by running a system level simulation for the two cases of macro/micro, and macro/pico heterogeneous deployments, as shown in Figure 3-26. The main simulation parameters are the same as those listed in Table 3-3, except that we used a fixed transmit power of 28 dBm for pico cells and 38 dBm for micro cells. Cell range expansion bias value (CRE) of 15 dB is used in case of pico cells and found to give the highest RAN throughput, the impact of CRE on the RAN performance and RAN energy consumption is investigated in chapter 6. The allocated bandwidth is 10 MHz for the macro layer, and 10 MHz for the small cells layer. At a high density of small cells, the TPG increase begins to slow due to the increase in the number of interferers, and also due to increasing the probability of having idle small cells without any associated users.

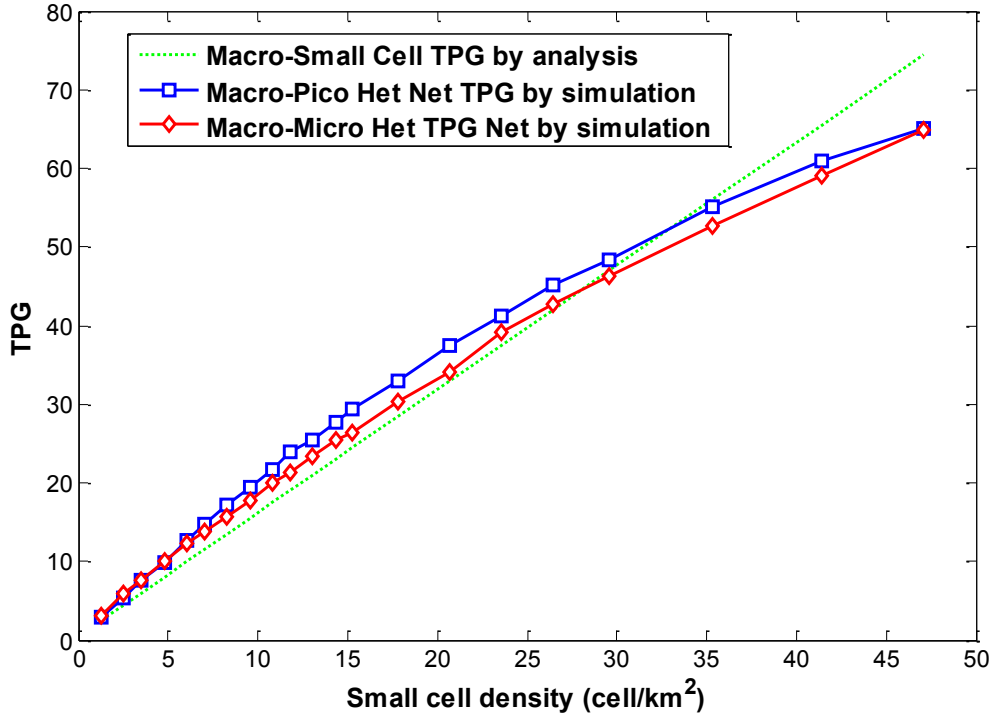

Figure 3-26: The results for TPG of Het-Net deployments

The results of Figure 3-27 show that the macro/pico deployments are far more energy efficient than the macro/micro deployments.

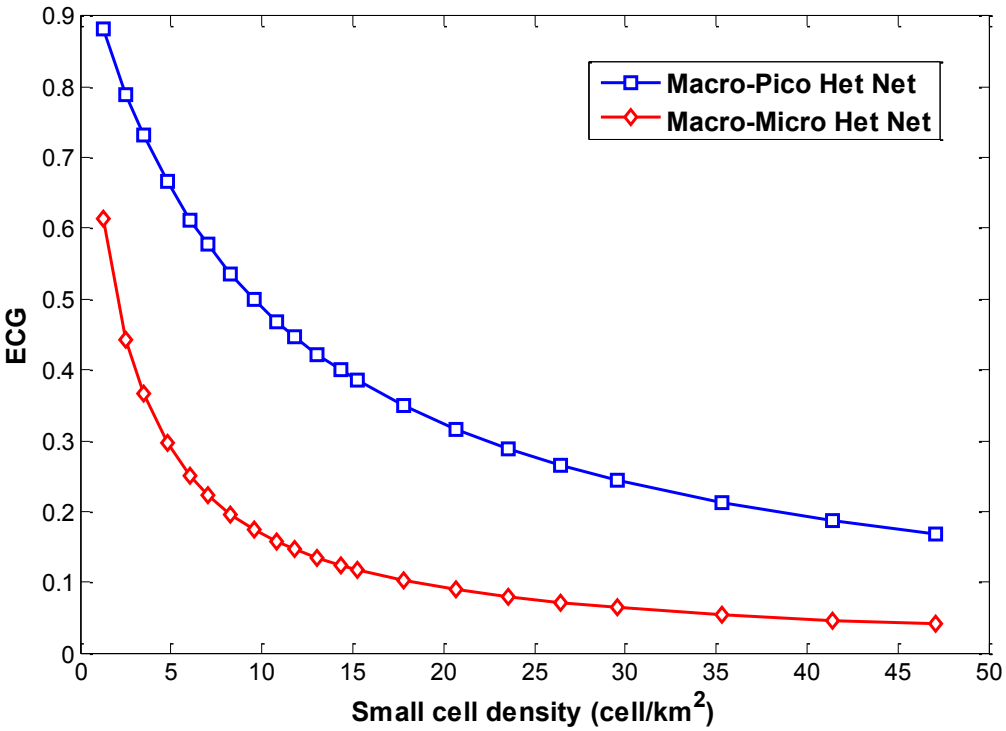

Figure 3-27: The results for ECG of Het-Net deployments

The same trend is shown in Figure 3-28 when using the ETG as a metric, the ETG of macro/pico RAN is 4 times higher than the ETG of macro/micro RAN. Importantly, the ETG starts to degrade beyond a certain density of small cells, which means that the bit/J metric of the Het-Net starts to decrease after this density. This is explained by the fact that the relative improvement in the TPG becomes less than the relative reduction in the ECG beyond this density.

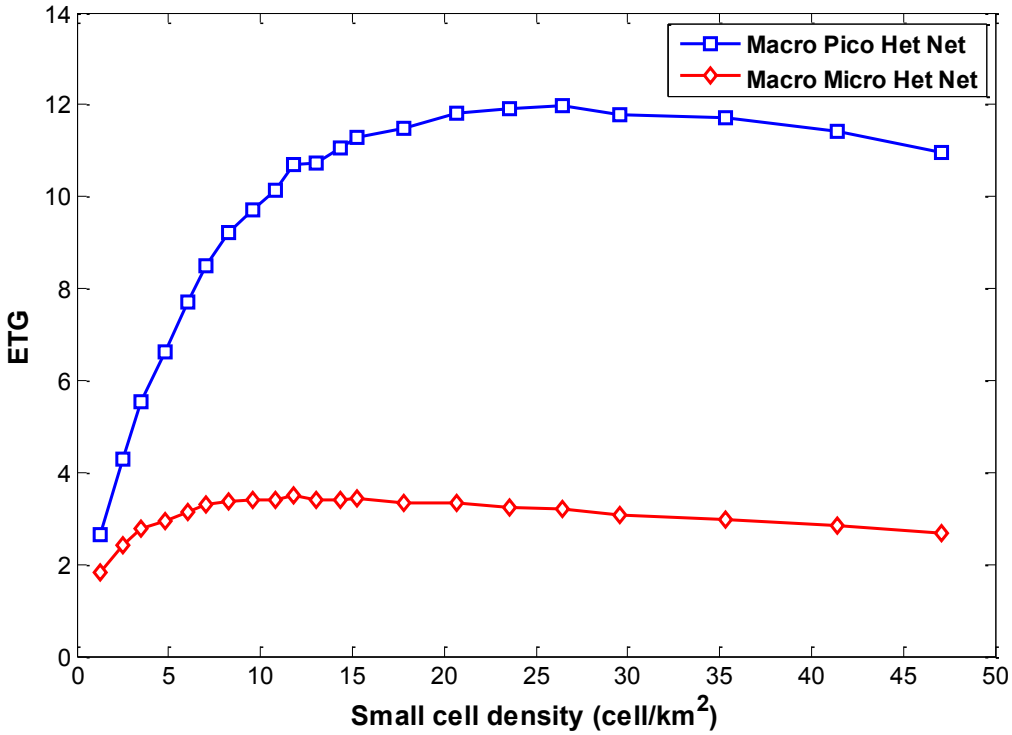

Figure 3-28: The results for ETG of Het-Net deployments

3.8.3 TPG and ECG of small cells versus HetNets and macrocell only RANs

To answer the question of which deployment type is able to achieve a specific target capacity while consuming the least amount of energy, the ECG of the investigated deployments is plotted versus the TPG as shown in Figure 3-29, where TPG can be considered here as a target improvement in the RAN throughput to achieve.

The ECG and TPG values are obtained from the results of previous sections: the TPG value is an indication of the target area throughput density. For example, TPG of 1 is equivalent to 17 $\mathrm{Mbit/s/km^2}$, which represents the achieved area throughput by a reference macro only RAN at cell radius of 1 Km. Therefore, the deployment which has the highest ECG value at a target TPG is considered the more energy efficient deployment and consumes the least amount of energy at this TPG value. The results indicate that when the TPG target is higher than 40,

picocells are always the most energy efficient deployment option, followed by the macro/pico HetNet deployment, while for TPG values less than 40, the heterogeneous macro/pico deployment is the most energy efficient deployment option.

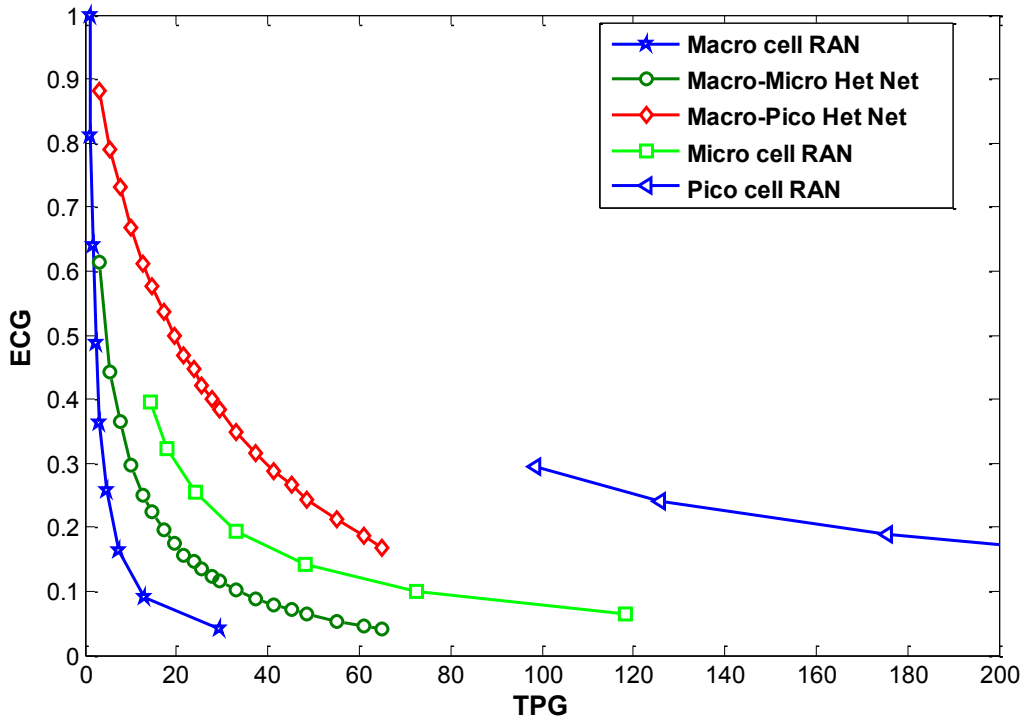

Figure 3-29: ECG versus TPG of various considered deployments

3.9 Impact of the backhaul on the RAN energy consumption

The power consumption of backhaul in macrocell RAN is often omitted because its value is relatively small compared to the power consumption of a macro base station. However, this is not true for the small cells or HetNets. The impact of the backhaul power consumption on the RAN ECG is evaluated by rewriting the ECG expressions to include the backhaul power consumption in the different deployments, as shown in (3.33).

$$ECG = \frac{\lambda_{m,ref}.(P_m+P_{bh,m})}{\lambda_m.(P_m+P_{bh,m})+\lambda_s.(P_s+P_{bh,s})}, \quad (3.33)$$

Where $\lambda_{m,ref}$ refers to the macro cell density in the reference deployment, λ_m is the density of macro cells in the deployment being tested, which is equal to zero in pure small cell only deployments, $P_{bh,m}$ refers to the backhaul power consumption of the macro base station. A fibre optic is always assumed for the macro cell backhaul in this analysis. A value of 10 watts

is often proposed in the literature for fibre backhaul power consumption per macro site [126]. $P_{bh,s}$ refers to the backhaul power consumption in small cells. P_m ad P_s denote the power consumption of macro and small cells, respectively.

Accurately modelling the backhaul power consumption requires a knowledge of the exact topology of the network and knowing the power consumption of the transmission links and aggregation nodes associated with the backhaul. Three values of backhaul power consumption are considered to model both fibre and wireless backhaul links [131]. Microwave backhaul links are an attractive option in terms of cost and installation time, but due to their high power consumption, they are unlikely to be used in small cell scenarios. The ECG is calculated for each deployment type by (3.33) at three assumed values of backhaul power consumption (10, 20& 40 watts). As fibre backhaul links are always assumed to be used in the case of macrocell RANs, the backhaul power consumption of macrocells is set to equal 10 watts while the backhaul power consumption for small cells and HetNet varied from 10 to 40 watts. Figure 3-30 illustrates how the ECG of micro and picocell only RANs degrades as the backhaul power consumption increases. For example, the ECG of a picocell only RAN degrades from 0.2 to around 0.1 at a TPG of 100 when the backhaul power consumption increases from 10 watts to 40 watts, which is equivalent to a 2 times increase in the RAN power consumption. The same trend is observed in the case of microcell RANs. When comparing the three deployment types, the results show that even if 40 watts of backhaul power consumption is assumed, the pico cell RANs still consumes the least energy for TPG values above 70 while the microcell RANs consumes the least amount of energy for TPG values from 4 to 70.

The impact of the backhaul power consumption on the ECG of HetNet is shown in Figure 3-31. The results show that although the backhaul power consumption significantly degrades the ECG of both macro/pico and macro/micro HetNets, they are still more energy efficient than the macro cell RAN. The macro/pico HetNet is the most energy efficient RAN for all the TPG values above 1.8.

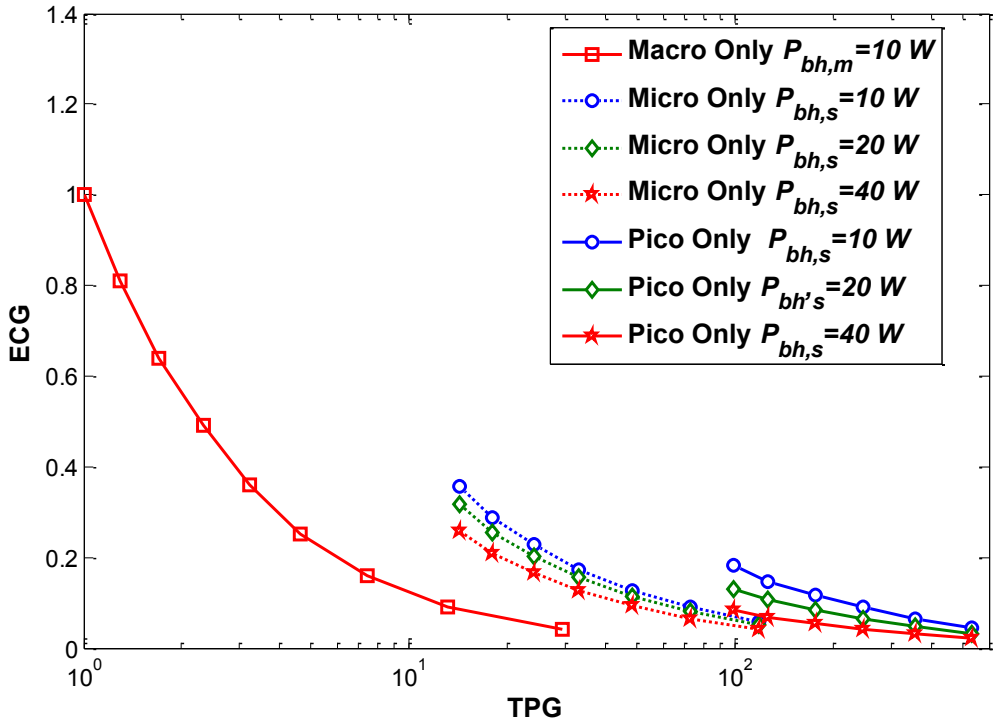

Figure 3-30: The backhaul power consumption impact on the ECG of macro and small cells deployments

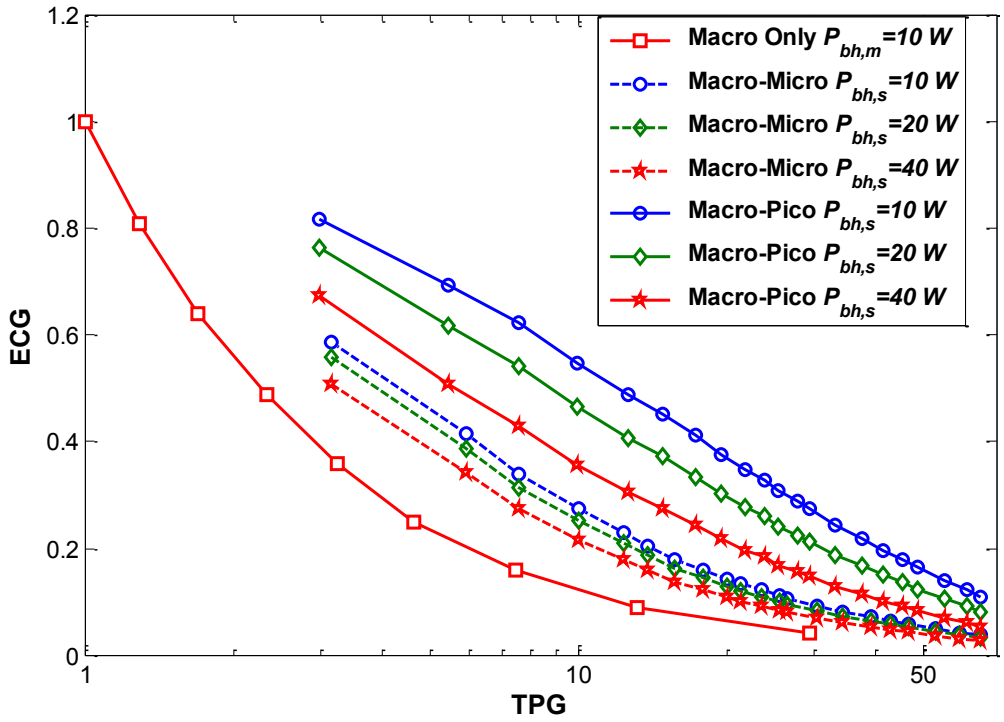

Figure 3-31: The backhaul power consumption impact on the ECG of HetNet RANs

3.10 Summary

This chapter has highlighted the motivation for proposing a different evaluation framework for the energy efficiency in cellular networks. The process of modelling the power consumption in LTE base stations has been detailed, followed by presenting the throughput and energy efficiency metrics and how they can give more insights into the energy consumption than the widely-used bit/J. The system model used in this chapter and through this thesis is also explained. To demonstrate how this framework can be used, it was applied to various case studies, including macro only, small cells, and heterogeneous deployments. For each deployment type, the TPG and ECG are calculated to avoid any misleading conclusion about the RAN energy consumption when using only the bit/J as a metric. Interestingly, the results showed that pico cell only deployments can attain up to 3 times increase in the TPG and 2.27 times increase in the ECG simultaneously when compared with macro only RANs at high target capacities. While it offers 2 times more capacity and reduces the energy consumption by 12% when compared with the macro/pico HetNet deployments. Finally, in addition to comparing the ECGs of different RAN types, the impact of backhaul power consumption on the overall RAN ECG is investigated for three backhaul power consumption levels. The results have shown that both small cell and HetNets deployments are very sensitive to the level of backhaul power consumption, but they never lose their superiority over the macro cell RAN in terms of the energy consumption when the same target throughput is required.

Chapter 4

The Energy Consumption Evaluation in Cellular Networks: High Order Sectorisation versus small cell densification

4.1 Overview

The reuse of radio spectrum through the deployment of more cells (Network densification) continues to be the key enabling technique to achieve high target capacities in the next generation of cellular networks. Therefore, the trend of base station densification in cellular networks is expected to intensify in 5G RANs. However, such growth in the number of deployed base stations will be accompanied by an increase in the total network energy consumption, which represents a major concern for network operators, both in terms of cost and environmental damage.

Network densification can be accomplished by either adding more macrocell base station sites, more sectors per site, or by deploying an overlay of small cells to form what is known as a heterogeneous network. Deploying more macro cells and adding more sectors have been the traditional methods that operators have used to expand the coverage and capacity of their existing networks. However, reducing the site to site distance within a macrocell RAN cannot continue without limit due to the technical issues of inter-cell interference, and more importantly, the cost of macrocell base stations coupled with the difficulty of finding new sites, especially in urban and dense urban areas.

In this chapter, we focus on radio access network densification by considering the deployment of more sectors per base station site (i.e. high order sectorisation) and the deployment of a second layer of small cells when needed, as two approaches for improving the RAN capacity. We investigate how the RAN energy consumption is influenced either when one, the other or both of these approaches is implemented. The objective is to find an energy efficient deployment strategy for mobile network operators seeking to deploy small cells alongside choosing the order of sectorisation in a RAN. Small cell densification is considered to be an effective method for enhancing the capacity and coverage of a 5G RAN. However, these techniques are accompanied by an increase in overall RAN energy consumption. This is because densification increases the number of deployed base stations, which adds more power consumption to the RAN. Similarly, increasing the number of sectors at the base station site amounts to increasing the number of radio frequency (RF) chains in the base station, which in

turn increases the overall power consumption by a factor approximately equal to the number of sectors used.

The energy efficiency of these two deployment approaches is evaluated. The impact of small cell densification versus high order sectorisation on the energy efficiency of a heterogeneous RAN is considered in the context of enhancing the capacity of an LTE based 5G RAN. The energy consumption of two deployment options is compared. The first option involves the densification of a 3-sector macrocell RAN by deploying an overlay of small cell base stations. The second option involves first upgrading the 3-sector sites to 6-sectors and then deploying the small cell overlay. The base station power consumption model presented in chapter 3 is used to estimate the power consumption of the radio base station. The RAN energy consumption gain ECG defined in chapter 3 is presented as the main figure of merit to quantify any gains or losses in the RAN energy efficiency. The impact of implementing an adaptive sectorisation technique on the RAN energy efficiency for the two options of three and six sector base stations is also investigated. A detailed methodology to evaluate the energy efficiency in the sectorised, and heterogeneous cellular networks is presented, followed by a RAN case study to illustrate how the RAN energy efficiency is evaluated. We also investigate the impact of applying various schemes of adaptive sectorisation on the RAN energy efficiency.

4.1.1 High order sectorisation

Present day, 4G cellular network deployments consist mainly of three sector macrocell base stations. As traffic demand grows, network operators must evolve their cellular networks to provide the required capacity. Adding more sectors to the existing macro cell sites is considered to be the most cost-effective evolution path by operators as it increases the network capacity without needing to add more base station sites to the network with new backhaul capabilities. However, due to the interference leakage between the adjacent sectors, the gain from adding more sectors does not scale up linearly with the number of sectors added to the macro cell site. Careful design of the antenna beam width is required to minimise this effect. On the other hand, a linear increase in the power consumption of macro cell sites is observed when more sectors are deployed.

To mitigate the increase in the RAN network consumption when high order sectorised base stations are deployed, many studies in the literature have proposed using adaptive sectorisation techniques to reduce the overall energy consumption by addressing the limitations of designing the RAN to meet the peak traffic demand. When the traffic intensity is low, the fixed sectorisation solution is no longer energy efficient as radio infrastructure unnecessarily remains switched on. In adaptive sectorisation, the radio base station site is reconfigured to have fewer and larger beam width sectors during periods of low traffic load. Adaptive sectorisation has also

been proposed to enhance the network throughput in unbalanced traffic scenarios by adapting the antenna pattern when an uneven traffic distribution is encountered.

4.1.2 Heterogeneous Networks

The concept behind Heterogeneous Networks (HetNets) is to overlay an existing homogenous macro network with additional smaller low power base stations. These can be micro, pico, femto base stations, or a combination thereof. Densifying the macrocell RAN by deploying small cell base stations as an overlay has the advantage of immediately targeting traffic hot spots in a cost-effective way. Several published papers have shown that HetNet deployments improve the RAN throughput by increasing the spectrum reuse factor while helping to alleviate the network energy consumption by deploying low power base stations where and when they are needed. As highlighted in chapter 3, deploying small cells as an overlay over the macro cells improves the RAN average throughput, and consumes less energy than the case of macrocell only scenarios. The disadvantage is that a large number of backhaul links are needed for the small cells. This energy saving can be increased by switching off the idle small cells during periods of low traffic volume. Moreover, the strategy of deploying heterogeneous networks is cheaper than a macrocell only upgrade path. More recently, the strategy of an ultra-dense deployment of small cells has gained significant attention and is regarded as one evolutionary path towards the achievement of the target capacities in 5G. However, deploying a large number of small cells poses several concerns regarding the energy consumption and the backhaul requirements. A reduction in the RAN RF transmitted power is observed when the density of small-cell base stations increases and when sleep mode is implemented [90]. This observation may not hold when taking the total power consumption of each base station into account as the base stations still consume some amount of energy even whilst in sleep mode status. Another important issue that arises when the deployment density of small cells increases is the significant amount of energy consumed by the backhaul links (up to 50% of the RAN total power consumption [91] and [43]), which may limit the advantages of heterogeneous networks as shown earlier in chapter 3.

4.2 Power consumption of sectorised macro base stations and small cell base station sites

The enhanced Green Radio power model is used to estimate the power consumption of sectorised macro, micro and pico base stations in this chapter. By using the parameters listed in Table 4-1.

Figure 4-1 shows clearly that the power consumption of macro cell sites scales linearly with the number of sectors. This is because each sector has a separate RF transceiver, power amplifier, and baseband processing unit. Hence, the improvement in the RAN throughput by deploying

high order sectorised sites is always accompanied by an increase in the RAN overhead power consumption.

Table 4-1: Power Model Parameters

Parameter	Macro-cell	Micro-cell	Pico-cell
Transmit Power Per Sector (W)	40	6.3	0.25
Bandwidth (MHz)	20	20	20
Transceiver Unit (W)	13	6.5	1.0
Processing Unit (W)	30	27	3
Fibre Backhaul (W)	10	10	10
PA Efficiency	30%	23%	10%
Antenna Feed Cable Loss (dB)	-3	-1	0

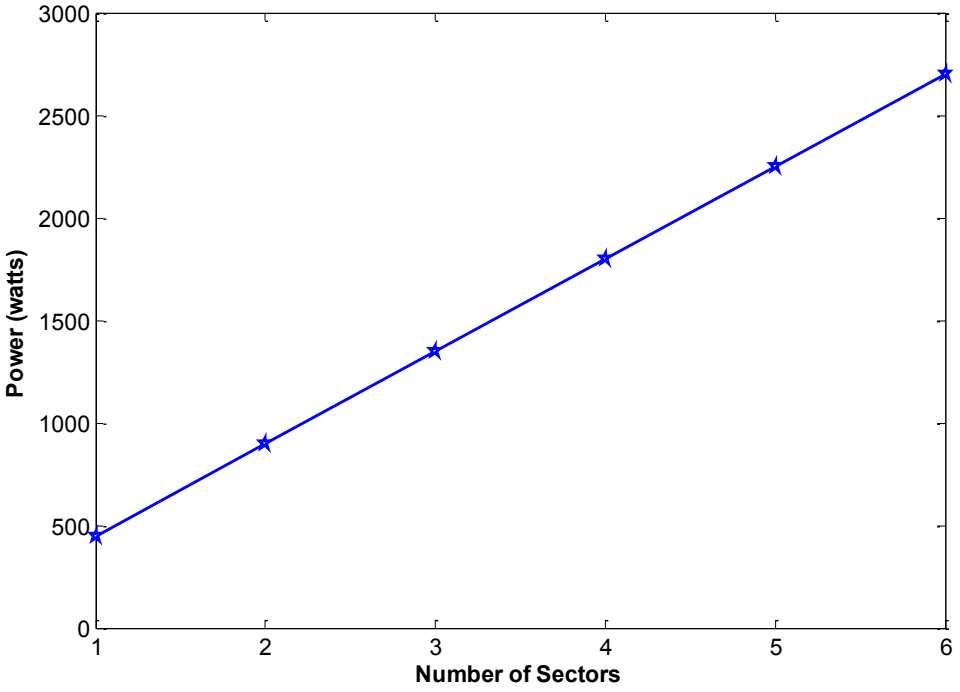

Figure 4-1: Power consumption versus sectorisation order in macro cell base station

The power consumption of micro and picocell base stations is plotted versus the cell average traffic load in Figure 4-2 and Figure 4-3, respectively. The values of power consumption of macrocell for 1 to 6 sector sites, and for micro and picocell base stations are used in the RAN energy consumption analysis throughout this chapter.

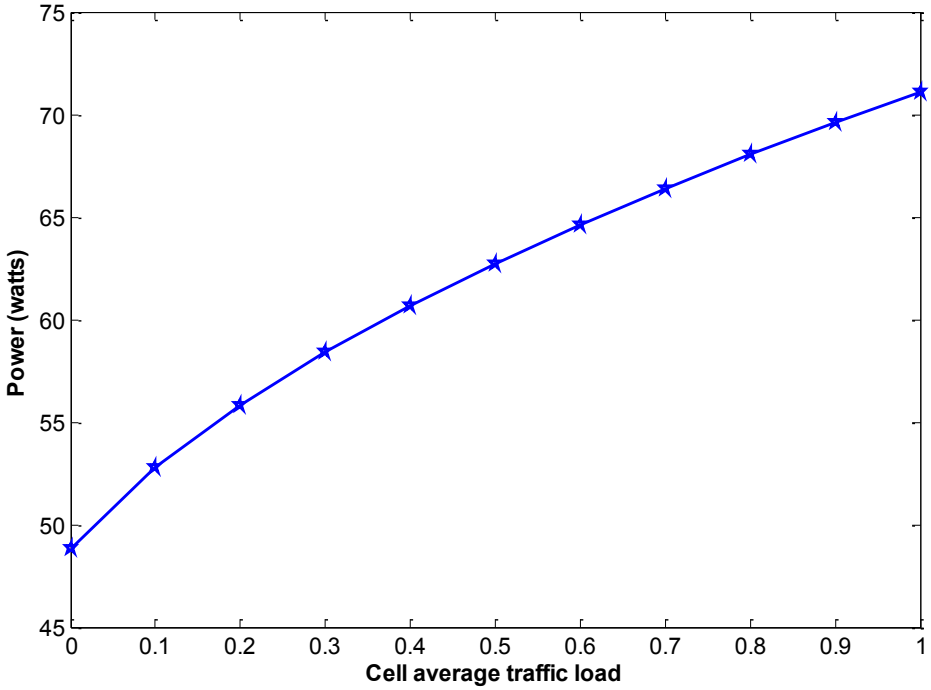

Figure 4-2: Micro cell base station power consumption versus α_t

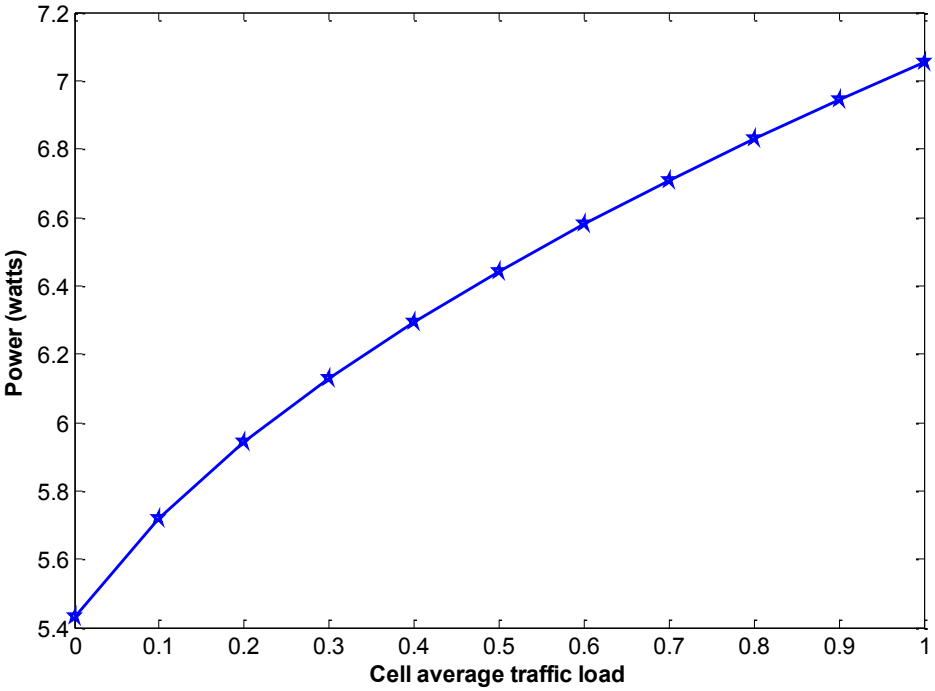

Figure 4-3: Pico cell base station power consumption versus α_t

4.3 TPG and ECG evaluation

The evaluation framework defined in chapter 3 has been applied, where the energy consumption gain ECG and throughput gain TPG are used for evaluating the RAN energy consumption and RAN throughput. The ECG between RAN_1 (which consists of a number N of 3 sector macro cell sites, and a number N_1 of small cells per macro cell site), and RAN_2 (which consists of a number N_2 of 6 sector macro sites, and a number N_2 of small cells per macro cell site) is given by equation (4-1).

$$ECG = \frac{E_1}{E_2} = \frac{(P_m + N_1 \cdot P_s) \cdot T}{(2P_m + N_2 \cdot P_s) \cdot T}, \tag{4.1}$$

Where P_m refers to the 3-sector macro site power consumption, the 6-sector macro site power consumption is $2P_m$, and T is the observation time which is sufficiently long over which the assessment is made. The RAN coverage area and the RAN offered traffic load have the same respective values in both RANs.

The cell average capacity of an omnidirectional macro cell, and of a small cell can be considered to be equal in an interference-limited scenario when no inter layer interference between the macro and small cells is assumed, and when the same allocated bandwidth is assumed for the macro and small cells. The cell average capacity of an omnidirectional cell is denoted by C in this chapter. The average capacities of 3-sector C_1 and 6-sector C_2 heterogeneous RANs expressed as a function of C and the sectorisation gain G_s for each considered sectorisation order. The TPG between the two networks RAN_1 and RAN_2 can be expressed by (4.2).

$$TPG = \frac{C_2}{C_1} = \frac{G_{s2} \cdot C + N_2 \cdot C}{G_{s1} \cdot C + N_1 \cdot C} = \frac{G_{s2} + N_2}{G_{s1} + N_1}. \tag{4.2}$$

The values of the sectorisation gain for 3-sectors (G_{s1}) and for 6-sectors (G_{s2}) should ideally equal 3 and 6 respectively. However, due to the interference leakage between adjacent sectors, the exact values of sectorisation gain need to be estimated using a system level simulation model of the 3 and 6 sectorised homogeneous RANs. The energy efficiency of the two deployments of 3-sector and 6-sector heterogeneous RANs are evaluated when the same target area capacity density (Mbit/s/km^2) is assumed, i.e. when the TPG equals one in (4.2).

4.4 Sectorisation capacity gain estimation

As highlighted in the previous section, deploying sectorised base station sites increases the RAN's capacity and, in principle, offers a capacity gain equal to the number of deployed sectors. In practice, the interference leakage between the adjacent sectors limits the capacity gain. The

sectorisation capacity gain G_s, shown in (4.3), for different sectorisation orders, needs to be known in order to evaluate the RAN TPG and the RAN's energy efficiency.

$$G_s = \frac{sectored\ site\ average\ capacity}{omni\ site\ average\ capacity}. \tag{4.3}$$

A MATLAB based static system level simulator was developed to estimate the sectorisation gain G_s for different orders of sectorisation ranging from 1 to 6. The network model considered consists of a homogeneous macrocell, multi-user RAN covering a flat, square geographic area of 3-by-3 km. The same number of macro cell sites and coverage area are assumed to be equals in all the simulations. Table 4-2 tabulates the system simulation parameters used. The mobile users are deployed uniformly in the (x, y) coordinates of the target service area. The downlink signal to noise and interference ratio *SINR* for each user is calculated by considering the interference from all the base stations in the service area. Performance data is obtained for the centre cells only in order to avoid underestimating the amount of inter-cell interference experienced by the users located at the edge of the service area. Furthermore, all the mobile users are assumed to be located indoors. The base station antennas have azimuth $A(\theta)$ and elevation $A(\varphi)$ beam pattern gains in dBi given by Equations (4.4) and (4.5) respectively, while the 3D antenna gain is approximated by (4.6) [132].

$$A(\theta) = -min\left[12\left(\frac{\theta}{\theta_{3dB}}\right)^2, A_m\right]. \tag{4.4}$$

$$A(\varphi) = -min\left[12\left(\frac{\varphi-\varphi_{tilt}}{\varphi_{3dB}}\right)^2, A_m\right]. \tag{4.5}$$

$$A_G(\theta, \varphi) = A_{GB} - \min\left[-\big(A(\theta) + A(\varphi)\big), A_m\right]. \tag{4.6}$$

The terms in $\theta_{3\mathrm{dB}}$ and $\varphi_{3\mathrm{dB}}$ denote the 3 dB beam width in the azimuth and elevation directions, respectively. A_m is the minimum antenna attenuation (a value of 25 dB was used in the model), φ_{tilt} is the boresight tilt angle, and A_{GB} is the antenna boresight gain. Using the simulation model developed, the site average capacity is estimated for each sectorisation order as the sum of average capacities of site sectors, and used to calculate the sectorisation gain by using (4.3). The RAN sectorisation gain with respect to an omnidirectional base station site is plotted in Figure 4-4 for sectorisation orders from 1 to 6.

Table 4-2: System level simulation parameters

Parameter	**Value**
Frequency (MHz)	2000
Bandwidth (MHz)	20 MHz (10 MHz for macro, 10 MHz for small cell layer)
RF Power (dBm)	Macro/Micro/Pico: 46/ 38/ 23
Macro cell radius (km)	0.5
BS antenna height (m)	Macro/small cell: 30/6
BS antenna tilt angle (degrees)	Macro/small cell: 6/0
BS antenna boresight gain (dBi)	6/3/1-sector macro cell:17.5/15/12
Small-cell omni antenna gain (dBi)	Micro/Pico-cell: 6/2
Macro BS Antenna $\theta_{3\mathrm{dB}}$ (degrees)	2/3/4/5/6-sectors 90/75/65/45/33
Macro BS Antenna $\varphi_{3\mathrm{dB}}$ (degrees)	10.5
Outdoor/Indoor wall loss (dB)	20
Cell range expansion Bias	Micro 5 dB / Pico 15 dB
Pathloss model (dB)	3GPP Uma & Umi [133]
Traffic Model	Full buffer
User location distribution	Uniform

4.5 ECG analysis in sectorised RANs

When a sectorised network is deployed, a sectorisation capacity gain is obtained as shown in Figure 4-4. However, the key penalty associated with this gain in capacity is an increase in the overall RAN power consumption. When increasing the number of sectors between RANs from $n_{\mathrm{s1}} = 1$ to $n_{\mathrm{s2}} = 6$, the RAN power consumption increases six times, and the ECG monotonically decreases with increasing number of sectors according to the ratio $ECG \propto n_{\mathrm{s1}}/n_{\mathrm{s2}}$ as plotted in Figure 4-5. When sectorisation orders higher than 6 are considered, the sectorisation gain tends to reduce due to the increase of inter-sector interference, whereas the ECG continues to reduce by the same factor.

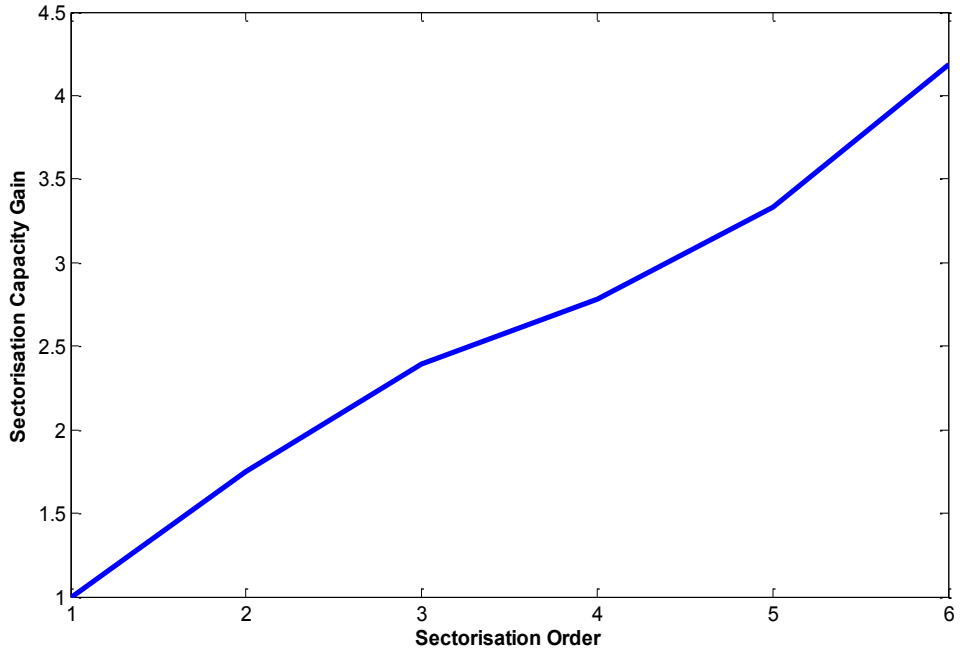

Figure 4-4: The results of sectorisation gain versus sectorisation order in macro RAN

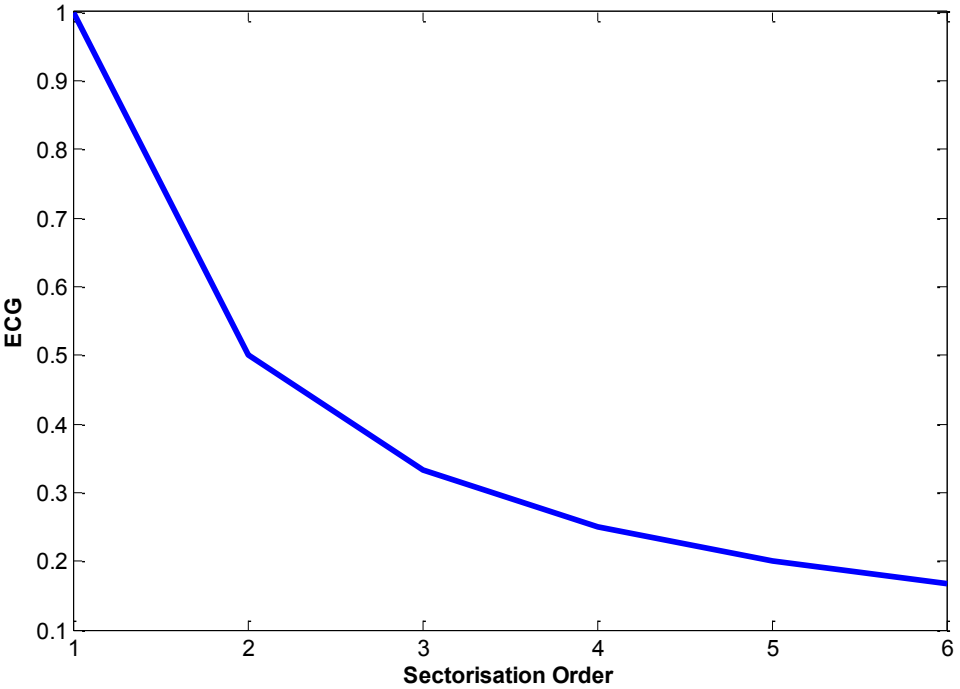

Figure 4-5: The results of ECG vs. sectorisation order in macro RAN

4.6 Adaptive sectorisation

A RAN is usually dimensioned to support a peak traffic requirement. Due to the temporal and spatial variation of the network offered traffic load, a substantial portion of the network resources is underutilised for a majority of the time, which causes unnecessary energy consumption in the network. Such a traffic characteristic suggests that the sectorisation order of a base station site should be reduced when the traffic load is low. This may be achieved by using an adaptive sectorisation technique [73], which reduces the energy consumption by adapting the number of sectors as well as the antenna beam width according to the offered traffic load. For example, as shown in Figure 4-4, a 6-sector radio base station, with a sectorisation gain of 4.2 and a sector antenna beamwidth of 33º , may be reconfigured to a 3-sector base station, with a sectorisation gain of 2.4 and a sector antenna beamwidth of 75º when the cell average load falls below the ratio $(2.4/4.2)$, and to a 1-sector base station with a unity sectorisation gain and an omnidirectional antenna when the relative load falls below $(1/4.2)$. Table 4-3 shows the various sectorisation gains and the maximum supported average traffic load values for the various sectorisation orders considered in this chapter. Note that a cell average load of 1 supported in the 6-sector case represents the peak offered traffic the RAN is designed to deliver. Once this value decreases, switching to low sectorisation orders can take place according to the results of Table 4-3.

Table 4-3: Adaptive sectorisation from 1 to 6 sectors

Sectorisation order	Sectorisation gain	Maximum supported cell average load
6	4.2	1
5	3.4	0.81
4	2.8	0.66
3	2.4	0.57
2	1.75	0.41
1	1	0.23

When switching between 1, 3, and 6 active sectors, the observation time T may be regarded as partitioned into three intervals $\{T_1, T_3$ and $T_6\}$ corresponding to the 1, 3 and 6 sector operating modes in the reconfigurable base station constrained by $\{T = T_1 + T_3 + T_6\}$. Such an adaptive sectorisation technique may be realised by the reconfigurable antenna design described in [74], whereby the number of sectors and their azimuth beam widths are controlled by a tuneable reflector. Equation (4.7) gives an expression for the ECG of an adaptive sectorisation scheme with respect to a fixed 6-sector base station. The term α_6 is the cell average load for the 6-sector case whereas α_i represents the cell average load for the i-sector case. Similarly, the term $P_{m,6}$ represents the base station site power consumption for 6-sectors, whereas $P_{m,i}$ represents the base station site power consumption for i-sectors.

$$ECG_{adaptive} = \frac{P_{m,6}(\alpha_6)\cdot T}{\sum_{i=1,3,6} P_{m,i}(\alpha_i)\cdot T_i}. \quad (4.7)$$

Automatically switching between the different sectorisation modes depends on the offered traffic value. Further energy savings may be obtained by progressively reconfiguring the number of sectors from 6 through 5, 4, 3, 2 or 1 which is called fine adaptive sectorisation in this thesis as we will see in section 4.8.2. Though more complex, this arrangement achieves a finer sectorisation resolution matching the network resources to the prevailing offered traffic load, which leads to significant power consumption savings at low average traffic values as depicted in Figure 4-6.

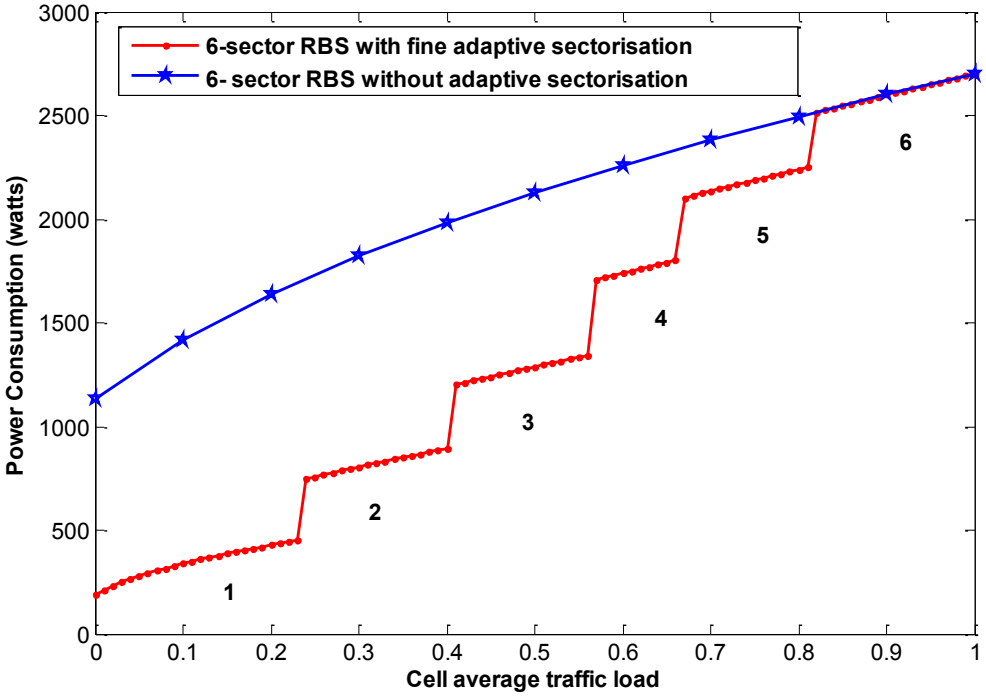

Figure 4-6: Power consumption reduction by adaptive sectorisation in 6-sector base station

4.7 Analysis of ECG in sectorised heterogeneous RANs

In this section, the ECG of two upgrade paths for a cellular RAN are compared. One is based on introducing high order sectorisation to an existing 3-sector macro layer before deploying an overlay of small cells while the other is based on adding small cell overlays to a 3-sector macro RAN. The central question considered is whether or not a RAN upgrade path involving the deployment of small cells first on the top of an existing 3-sector (the first deployment option) is more energy-efficient than upgrading to high order sectorised macro cell sites first and then deploying a small cells overlay on top of the 6-sector macro RAN (the second deployment option), when the same target area capacity density is assumed.

To evaluate the average throughput of a multi-cell multi-user heterogeneous RAN, a static system level simulator is employed as a modelling tool. In a first deployment option (Option-1), small cells are deployed as an overlay on top of a 3-sector macrocell layer. In a second deployment option (option-2), small cells are deployed as an overlay on top of a 6-sector macrocell layer. In the two deployment options, the macro layer and small cell layers are allocated two different frequency carriers to avoid the inter-layer interference. The 6-sector RAN offers a sectorisation capacity gain G_s over the 3-sector RAN (see Figure 4-4), therefore fewer small-cells are needed on the top of 6-sector macro cell layer to support the same offered traffic load. The same macro cell RAN is used as a starting point for the upgrade; hence, the difference between the two RANs is the number of deployed small-cells and the number of sectors per base station site. The small-cells deployed can be either micro or pico cells in the scenarios considered. The small-cells are deployed uniformly in a regular hexagonal layout around the 3-sector and 6-sector sites as depicted in Figure 4-7.

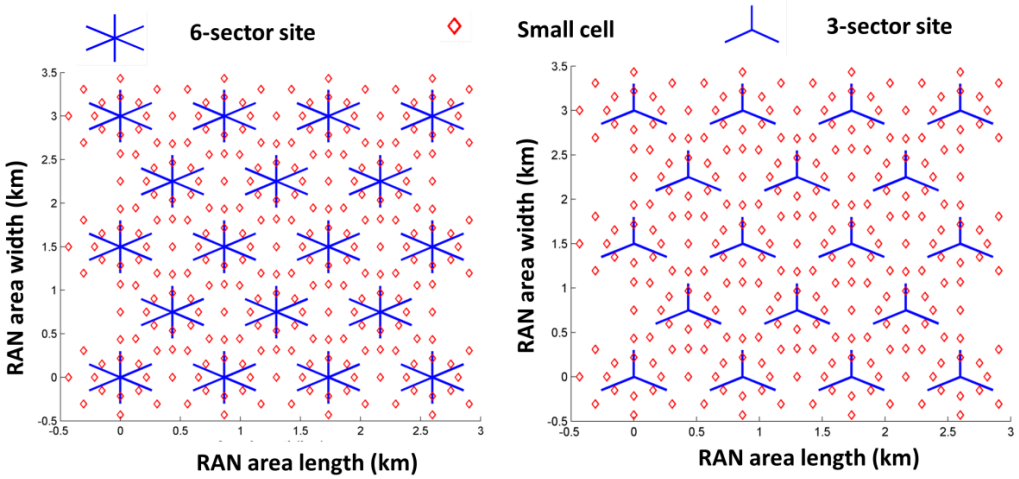

Figure 4-7: 6-sector and 3-sector RAN layouts

Denoting the first (3-sector macro-cell) and second (6-sector macro-cell) deployment options by subscripts 1 and 2, respectively, the RAN ECG can be estimated by (4-1). The terms P_m and P_s denote the average power consumption of a 3-sector macro-cell, and omnidirectional small-cell, respectively. The terms N_1 and N_2 denote the numbers of small-cells deployed per macro-cell in options-1 and 2, respectively. The power consumption for the 6-sector macro-cell sites is then expressed in terms of the consumption for the 3-sector sites as equal to $2P_m$. Typically, P_s is much smaller than P_m, and is given by $P_s = m \cdot P_m$, where $0 \leq m < 1$ and its numeric value is obtained from the ratio $P_s\ /P_m$. The value of m is obtained using the power consumption model of macro and small-cell base station described in chapter 3, which yields typical values for m of

0.0610 for micro-cells and 0.0130 for pico-cells. Substituting $P_s = m \cdot P_m$ in (4.1) allows us to write the ECG as a function of m, N_1, and N_2 as shown in (4.8).

$$ECG = \left(\frac{1+m \cdot N_1}{2+m \cdot N_2}\right). \quad (4.8)$$

Both N_1 and N_2 are estimated by running a system level simulation for the two deployment options while progressively increasing the number of deployed small-cell per base station site. The number of small-cell required to achieve a certain RAN capacity per unit area can then be interpolated. When the ECG is less than unity, the heterogeneous RAN with 3-sector macro cells is more energy efficient than the heterogeneous RAN with 6-sector macro cells. If the small cell power consumption is very low, then the value of m tends to zero, and the heterogeneous RAN ECG approaches 0.5 in the limit, which demonstrates that deployment option-1 is always more energy efficient than option-2, providing that the small cell power consumption P_s is sufficiently small. Equation (4-2) expresses the throughput gain of a 6-sector macro cell heterogeneous RAN with reference to a 3-sector macro cell heterogeneous RANs as a function in N_1, N_2, G_{s1} & G_{s2}. By setting the throughput gain TPG equal to 1 in (4-2), i.e. the same target capacity requirement in the two deployment options is assumed, the number of small cells N_1 can be written as a function of N_2 as in (4.9).

$$N_1 = G_{s2} - G_{s1} + N_2. \quad (4.9)$$

By substituting (4.9) in (4.8), The ECG can be written as a function of the number of small cells and sectorisation gain as in (4.10).

$$ECG = \left(\frac{1+m \cdot (G_{s2} - G_{s1} + N_2)}{2+m \cdot N_2}\right). \quad (4.10)$$

The values of G_{s1} and G_{s2} are already estimated and shown in Figure 4-4 and equal 2.4 and 4.2 respectively, whereas the values of m were calculated by using the base station power model, m equals 0.0130 for pico cells and 0.0610 for the micro cells when 10 watts of backhaul power consumption is assumed.

Equation (4.10) is used to calculate analytically without simulation the ECG of a 6-sector macro cell heterogeneous RAN with reference to a 3-sector macro cell heterogeneous RAN as shown in Figure 4-8 as a function of the number of small cells per 6-sector macro site N_2 for the two cases of pico and micro cell overlays. The results demonstrate that the ECG is always less than 1, i.e. deploying pico or micro cells on top of a 3-sector macro cell RAN is always more energy efficient than deploying small cells on top of 6-sector macro cell RAN. Since TPG =1, the ECG is equal to the ratio of the bit/J metrics of the two RANs (ETG) as already highlighted in chapter 3, which means using either the ECG or ETG lead to same conclusion about the RAN energy efficiency in this case.

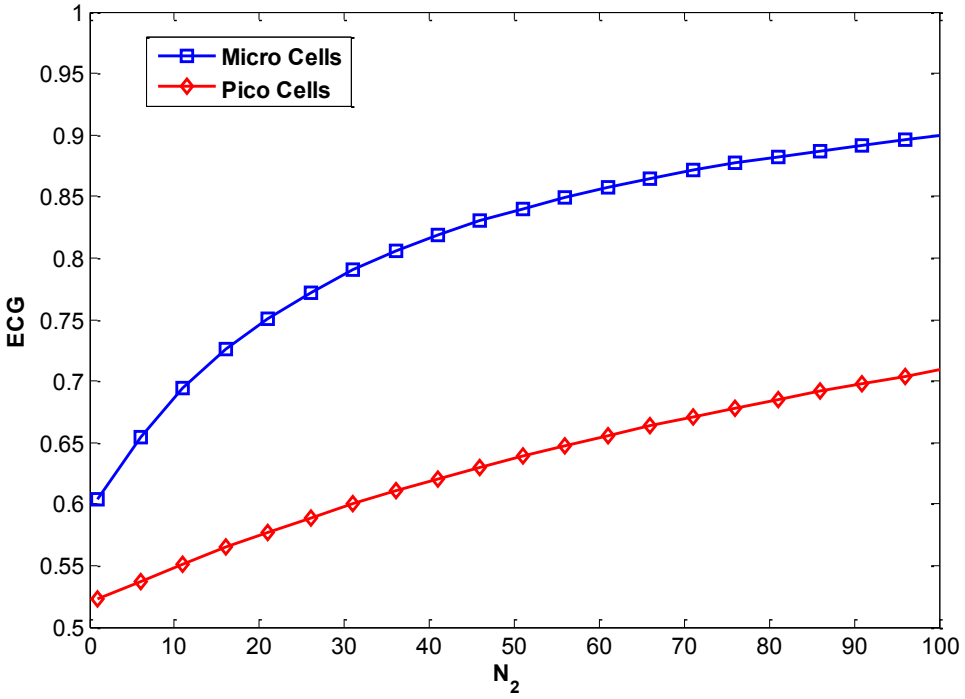

Figure 4-8: The ECG of 6 sector macro/pico & macro/micro heterogeneous RAN versus N_2

4.8 Case Study

The results for energy consumption gain of a heterogeneous network case study based on the two upgrade routes identified in the previous section are presented in this section. The ECG improvements due to implementing the adaptive sectorisation are also evaluated.

4.8.1 Small cell densification

The energy consumption of both a 3-sector macro cell heterogeneous RAN and a 6-sector macro cell heterogeneous RAN are evaluated and compared. The number of deployed small cells is estimated through a system level simulator to achieve the same area capacity density (bit/s/km^2) for the two deployment options considered.

As already mentioned, option-1 consists of a 3-sector macrocell RAN and an overlay of N_1 small-cells per macrocell, whereas option-2 consists of a 6-sector macro-cell RAN and an overlay of N_2 small cells per macro cell. The number of required small-cells in the two deployment options is estimated by running a MATLAB based static system level simulator that models the multi-cell, multi-user heterogeneous network. The simulation parameters are summarised in Table 4-2.

The ECG is calculated from (4.8) whereas the base station power consumptions are estimated using the power consumption model. The average area capacity in the units of Mbit/s/km^2 for

the two deployment options is determined using simulation, as the number of deployed small cells per macro cell is increased progressively from 0 to 21.

The number of picocells and microcells required as a function of the targeted area capacity for both deployment options are shown in Figure 4-9, a smaller number of microcells is required when compared with the number of picocells at the same target area capacity density.

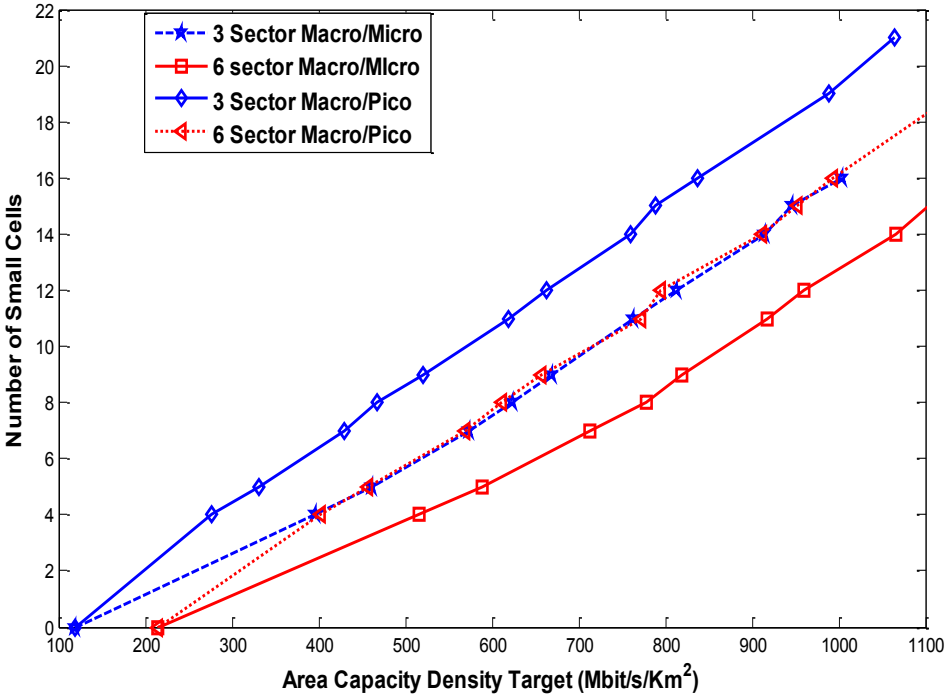

Figure 4-9: Number of required small cells versus the target area capacity density for different considered heterogeneous 3-sector and 6-sector deployments

The heterogeneous RAN ECG is calculated from (4-8) at each target area capacity density and plotted in Figure 4-10 for both the 3-sectors and 6-sectors of macro/pico cell and macro/micro cell deployments, respectively. The 3-sectors macro/pico cell deployment is used as the reference baseline deployment in (4-8), and its ECG value is always unity by definition, as shown in Figure 4-10. The results show that the ECG of a 6-sector deployments are always less than the ECG of a 3-sector deployments, and also that the ECG of a macro/micro cell deployments are always less than that of a macro/picocell deployments. Hence, the results show that deployment option-1 is always more energy efficient than deployment option-2, which agrees with the results obtained from the analysis of section 4-7. This result is only true when the power consumption of a pico or microcell is substantially less than the power consumption of a macro cell. The results also indicate that the macro/micro cell HetNet is always less energy

efficient than the macro/pico cell HetNet, regardless of the order of sectorisation used in the macro-cell site.

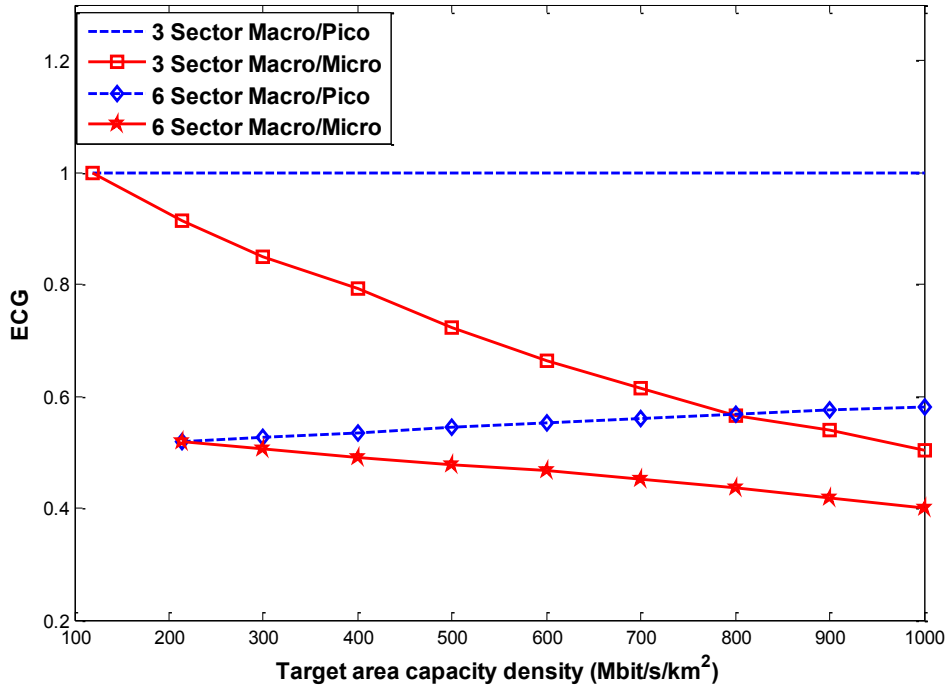

Figure 4-10: ECG versus target area capacity density by simulation

4.8.2 Adaptive sectorisation

As described in section 4.6, the ECG of a sectorised base station may be improved by implementing an adaptive sectorisation scheme, which selects the number of active sectors according to the average offered traffic load. The ECG for an adaptive 3- or 6-sector macrocell base station can be calculated from (4-7), with respect to a fixed 3-sector and 6-sector macrocell base station. Two adaptation schemes are considered for the 6-sector solutions.

1) The coarse adaptive sectorisation (CAS): the number of active sectors is switched between (6, 3 and 1) in 6-sector base station sites and between (3,1) in 3-sector base station sites.

2) The fine adaptive sectorisation (FAS): the number of active sectors is switched between (6, 5, 4, 3, 2 and 1) in 6-sector base station sites as already shown in Figure 4-6 and between (3,2 and 1) in case of 3-sector base stations sites.

For the temporal traffic profile shown in Figure 4-11 [40]. Table 4-4 gives the percentage ECG improvements of the CAS and FAS schemes over the corresponding nonadaptive schemes. The 6-sector macrocell base station benefits the most with a 33% improvement in ECG when using FAS over the non-adaptive scheme. The percentage ECG margin of improvement of the FAS

over the CAS is 12% for the traffic profile in Figure 4-11. Further improvements may be possible for other types of temporal traffic distributions or when the spatial distribution of the traffic is taken into account. The results also indicate that the 6-sector macro cell sites benefit more from adaptive sectorisation when compared to the 3-sector macro cell sites. For example, 33% versus 29% in case of FAS and 21% versus 15% in case of CAS.

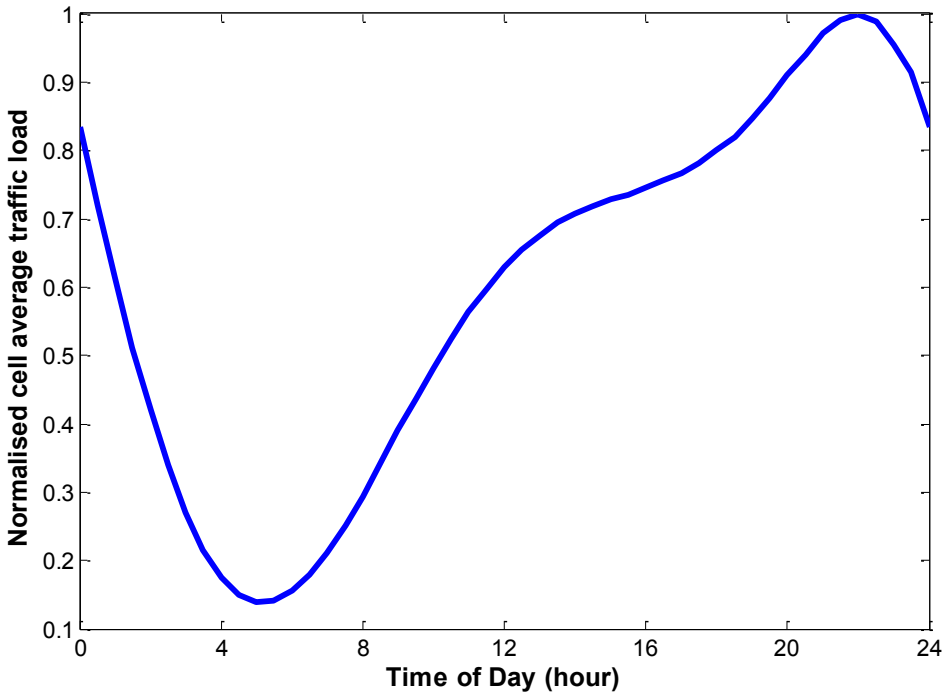

Figure 4-11: Average daily traffic profile for a European country

Table 4-4: ECG Improvements with adaptive sectorisation

	Percentage ECG Improvement	
Macro cell sectorisation	3-Sector	6-Sector
Coarse adaptive sectorisation	15 %	21 %
Fine adaptive sectorisation	29 %	33 %

The advantages of implementing the various adaptive sectorisation schemes are illustrated further in Figure 4-12 and 4-13 for the 3-sector macrocell site. The results for 6-sector macro cell site are shown in Figure 4-14 and Figure 4-15. Significant power savings are obtained during the low traffic load periods. For example, the power consumption of 6-sector macro cell site is reduced by more than 60% between 3:00 and 07:00.

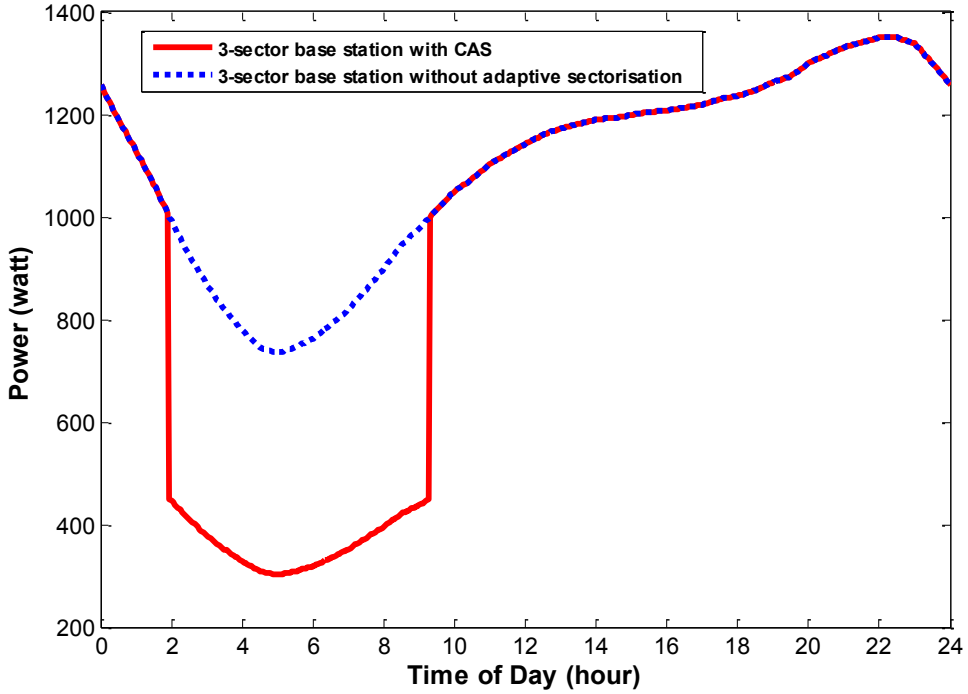

Figure 4-12: Power consumption versus time of the day comparing a 3-sector macro cell site with CAS and without adaptive sectorisation

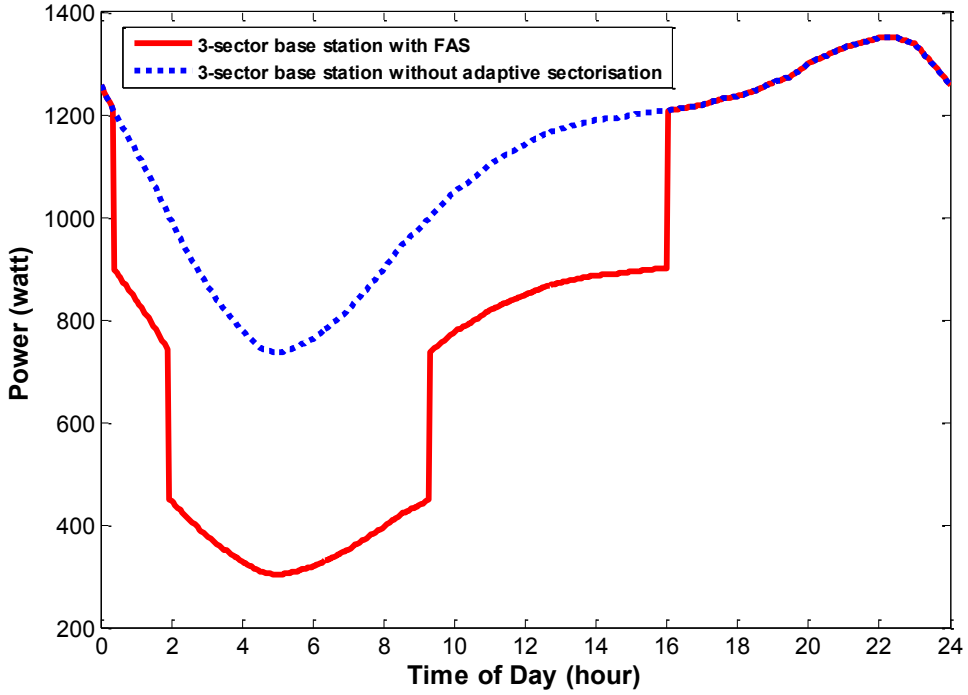

Figure 4-13: Power consumption versus time of the day comparing a 3-sector macro cell site with FAS and without adaptive sectorisation

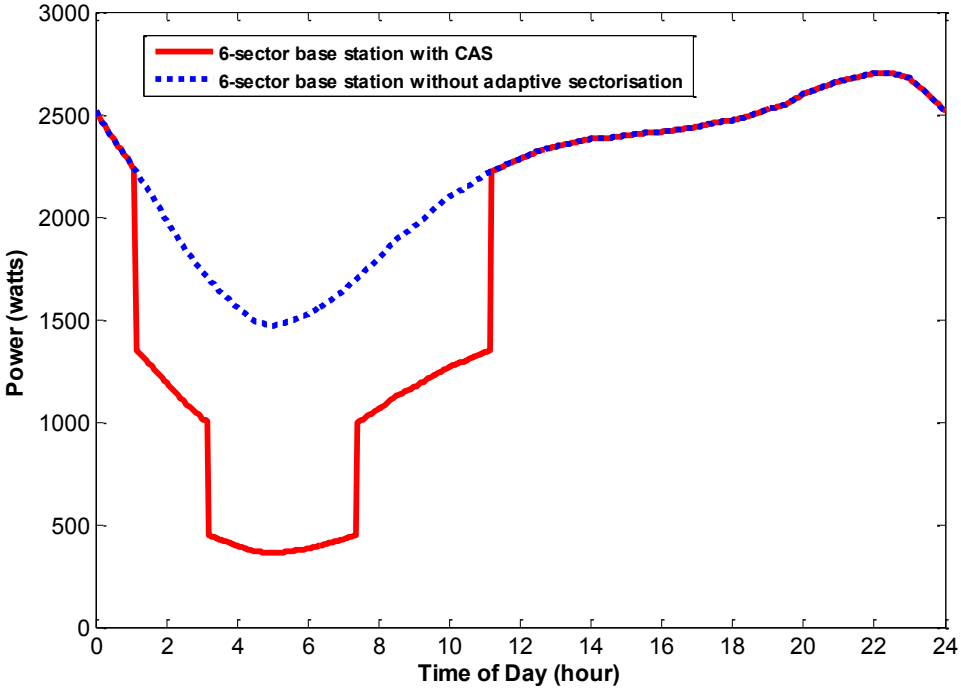

Figure 4-14: Power consumption versus time of the day comparing a 6-sector macro cell site with CAS and without adaptive sectorisation

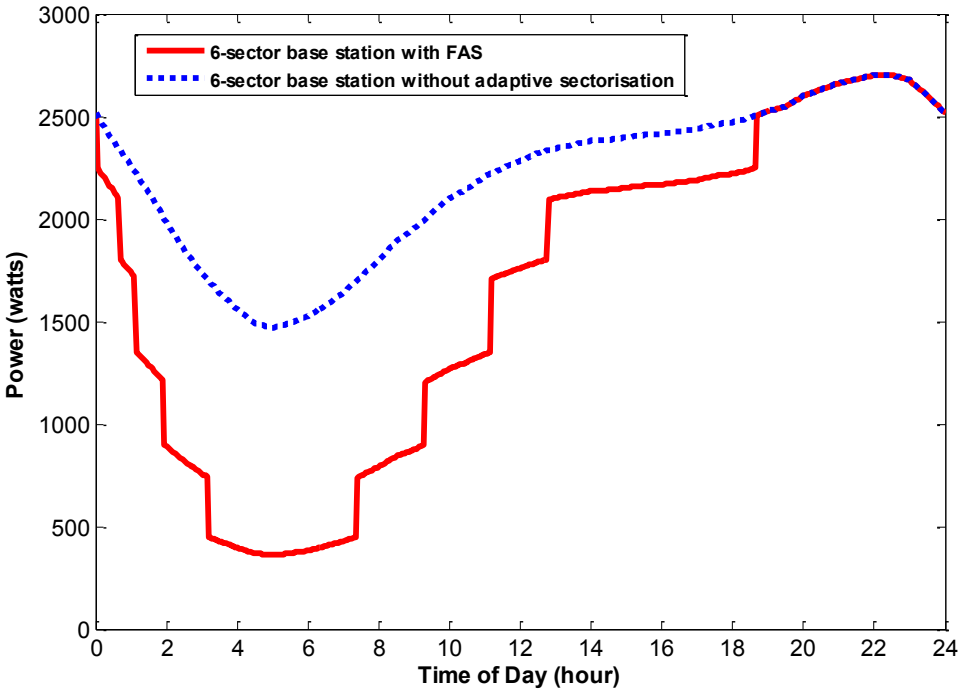

Figure 4-15: Power consumption versus time of the day comparing a 6-sector macro cell site with FAS and without adaptive sectorisation

The adaptive sectorisation techniques may be implemented in the HetNet deployments investigated in section 4.8.1 in order to improve the ECG for an adaptive 6-sector macro cell HetNet (i.e. adaptive 6-sector macro cells plus omnidirectional small cells) with reference to a fixed and an adaptive 3-sector macro-cell HetNet. To estimate the ECG for 6-sector macro cell HetNet with adaptive sectorisation with respect to a non-adaptive 3-sector macro cell HetNet, equation (4.1) is modified to take into account the daily average power consumption of the macro and small cells as shown in (4.11).

$$ECG = \frac{E_1}{E_2} = \frac{\mathrm{P_m}(\alpha)+N_1 \cdot \mathrm{P_s}(\alpha)}{\frac{2\mathrm{P_m}(\alpha)}{ECG_a}+N_2 \cdot \mathrm{P_s}(\alpha)}, \tag{4.11}$$

Where $\mathrm{P_m}(\alpha)$ denotes to the average power consumption of 3-sector macro cell site averaged over a period of one day. $\mathrm{P_s}(\alpha)$ denotes to the average power consumption of small cell site average over a period of one day. $\mathrm{ECG_a}$ denotes the energy consumption gain of a 6-sector macro cell site when one of the adaptive sectorisation techniques is implemented. The ECG versus area capacity for macro/pico heterogeneous deployments are shown in Figure 4-16. Two adaptive sectorisation schemes are implemented in 3 and 6-sector macro/pico deployments.

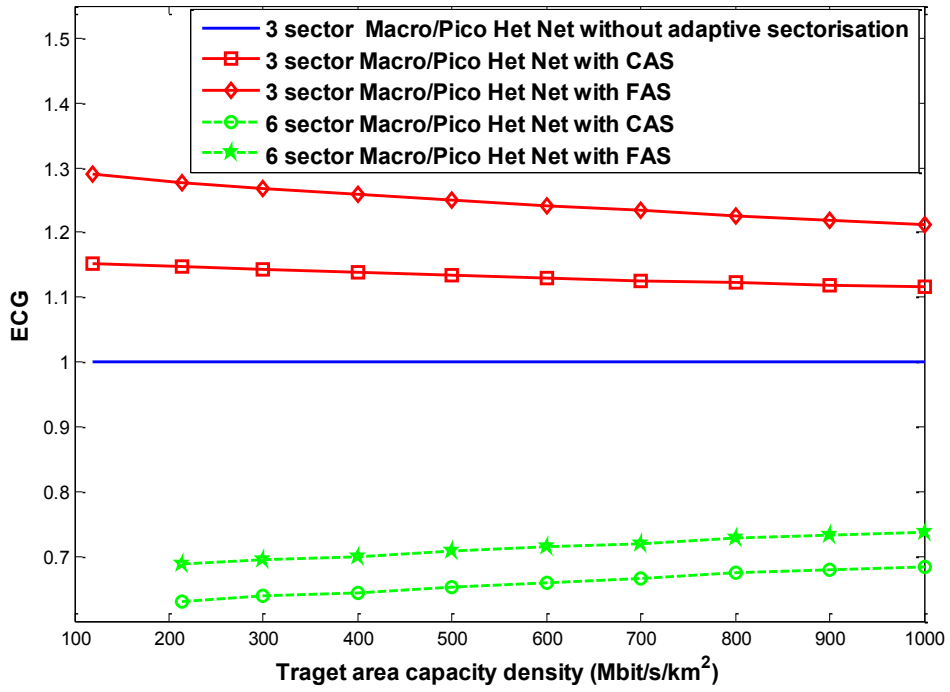

Figure 4-16: ECG versus target area capacity for sectorised macro/pico deployments when adaptive sectorisation is implemented

The results for the macro/micro HetNet are shown in Figure 4-17, the reference network being a fixed 3-sector macro/pico RAN. The ECG is plotted to compare the CAS and FAS schemes. The results show that the FAS is always more energy efficient than the CAS in all the HetNet deployments studied. Also, both adaptive schemes in macro/pico and macro/micro HetNets in the 3 and 6-sector cases are more energy efficient than the fixed sectorisation schemes as shown Figure 4-16 and Figure 4-17. The ECG of CAS and FAS schemes for a 6-sector macro/pico and 6-sector macro/micro HetNet are always less than unity, which indicates that the fixed 3-sector macro/pico heterogeneous networks are always more energy efficient than the corresponding 6-sector schemes, irrespective of which adaptive sectorisation scheme is used.

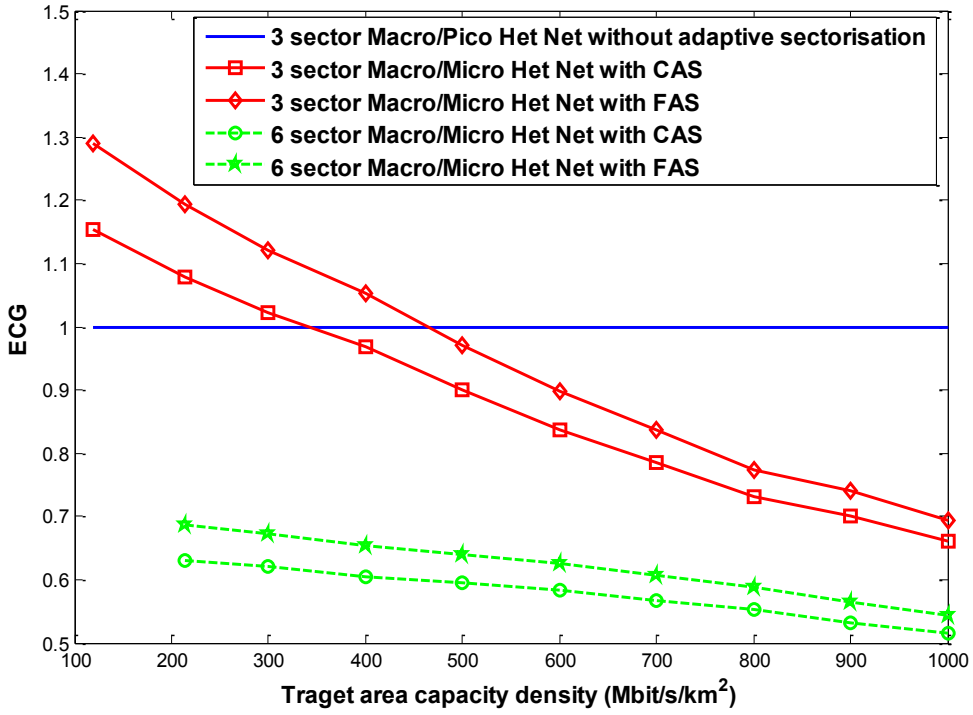

Figure 4-17: ECG versus target area capacity for sectorised macro/micro deployments when adaptive sectorisation is implemented

4.9 Summary

This chapter has addressed the issue of energy consumption in cellular networks, which arises when high order sectorisation and small cell densification are used to enhance the HetNet capacity. The aim of the chapter was to ascertain if a mobile network operator can save energy by increasing the sectorisation order before densifying with a small cell overlay or should small cell overlay be added without increasing the sectorisation order. The analysis was extended by considering adaptive sectorisation schemes to quantify how much energy is saved when sectors are switched off in low traffic conditions. The results show that the range of improvement in the energy consumption gain when using adaptive sectorisation lies between 15% to 32%. For the diurnal traffic profile considered and for all adaptive sectorisation schemes, the 3-sector macro

cell HetNet with FAS was always the most energy efficient. In conclusion, the results show that though increasing the sectorisation order to meet the capacity demands uses fewer small cells, the strategy consumes more energy than using fewer sectors with more small cells to meet the same capacity requirements. This conclusion is contra to the prevailing mobile network operators practice which deploys more sectors before adding small cells. The prevailing approach relates more to the difficulties faced by mobile network operators to find new sites for the small cells.

Chapter 5

Comparative Study of The Energy Consumption Between SISO and MIMO RANs

5.1 Overview

An unprecedented increase in the demand for mobile data access has been observed over the last decade. This increase is expected to continue, with forecasts indicating that the current traffic volume will have increased a thousand-fold by 2020 [4]. To meet the rapidly growing demand for more capacity, operators have started to deploy multiple solutions and techniques to improve the network capacity, which in turn increases the network power consumption. Multiple Input Multiple Out (MIMO) techniques have been deployed extensively in recent years to enhance either cell capacity through spatial multiplexing or cell coverage through spatial diversity without increasing the channel bandwidth or the RF transmit power. However, the circuit power consumption of a MIMO base station increases due to the need of more signal processing and RF chains when compared to a SISO base station.

As indicated earlier in chapter 2, many publications have investigated the energy efficiency of MIMO RANs in recent years. The main existing findings related to this topic can be summarised as follows:

- MIMO RANs are always more energy efficient than SISO when only analysing the RF transmit power [78] [79].
- MIMO RANs cannot deliver any power savings compared with SISO when the overhead circuit power is included in the analysis, and when only the diversity gain is exploited [77].
- Most publications have shown that there is a trade-off between the spectral efficiency and the energy efficiency when comparing the power consumption of a SISO base station with a MIMO base station. This observation is a function of the base station power model and the used energy efficiency metric [80].
- Few publications have proposed implementing the adaptive antenna muting technique; where the base station can reduce the number of transmit antennas at low traffic times to improve the energy efficiency of MIMO RANs [96].

Although a significant number of studies have investigated the issue of energy efficiency of MIMO RANs in the last fifteen years, there remains a number of issues to be addressed such as the need to use the right evaluation framework and the absence of an accurate power consumption model for MIMO base stations. Also, no publications have extended the analysis to cover the non-full buffer scenarios, nor have they investigated the impact of DTX on the MIMO base station power consumption compared to SISO.

The question of whether or not deploying MIMO base stations is more energy efficient than SISO base stations is addressed in this chapter. We attempt to answer this question by evaluating the MIMO RAN energy consumption when the overhead circuit power consumption in the base station is considered. Two cases are evaluated in this chapter as follows.

a) The case of evaluating the energy efficiency of MIMO RANs in so-called greenfield deployments, i.e. when the operator has the choice to deploy SISO or MIMO base stations. The target is to investigate whether or not a MIMO RAN can deliver the same target capacity in a more energy efficient manner than SISO. In contrast to previous publications, which use the EE metric (bit/J), we adopt the evaluation framework of chapter 3, where the consumption gain ECG is calculated for a multi-cell MIMO RAN deployment with reference to a SISO RAN when the same target capacities are assumed in the two RANs. We investigate if energy can be saved by exploiting that a smaller number of MIMO base stations than SISO base stations can deliver the same target capacity. The obtained results might also be beneficial to an operator by answering the question of whether or not upgrading the SISO base stations is more energy efficient than deploying more SISO macro sites.
b) In the second case, we examine if upgrading the SISO base stations in an existing SISO macrocell RAN to MIMO to increase the users' data rates, leads to an increase in the RAN energy consumption or not. An elastic non-full buffer traffic model is implemented in the simulator; this model allows us to evaluate the impact of the temporal variation of the offered traffic on the RAN energy consumption. The same offered traffic is assumed in the SISO and MIMO RANs. Therefore, the cell average traffic load α_t in MIMO macro cell RAN is less than that in SISO RAN. This reduction in average traffic load in MIMO RAN can be exploited to reduce the RAN energy consumption by implemeting the fast discontinuous transmission (DTX) [99-101].

Similar to the SISO deployments in the previous chapters, the downlink throughput of MIMO RAN needs to be investigated, the next section explains how the MIMO channel capacity is estimated in this chapter.

5.2 MIMO channel capacity gain

MIMO wireless systems use multiple antennas at the transmitter and the receiver, either to increase the transmission data rate via spatial multiplexing or to improve the system's reliability and coverage via transceiver diversity. When spatial multiplexing is used, MIMO offers a capacity gain when compared with SISO, with the SISO channel capacity being given by the standard Shannon formula expressed in bit/s/Hz as in (5.1).

$$C_{siso} = \log_2(1 + SNR \cdot |h|^2), \tag{5.1}$$

Where SNR represents the signal to noise ratio at the receive antenna, and h is random Gaussian variable represents the channel gain. The diversity gain is achieved when transmit or receive diversity systems are used. When multiple antennas are used at the transmitter, and a single antenna at the receiver, the system is known as multiple input single outputs (MISO); whereas the single input multiple outputs (SIMO) scheme has a single antenna at the transmitter and multiple antennas at the receiver. The capacity of both MISO and SIMO channels are given by (5.2) and (5.3), respectively [134].

$$C_{miso} = \log_2\left(1 + \frac{SNR}{N_t} \cdot \sum_{i=1}^{N_t} |h_i|^2\right), \tag{5.2}$$

$$C_{simo} = \log_2\left(1 + SNR \cdot \sum_{i=1}^{N_r} |h_i|^2\right), \tag{5.3}$$

Where N_t is the number of transmit antennas at the transmiter, N_r in the number of receive antennas at the receiver, and h_i represent the channel gain from the tranmsit antenna i to the receiving antenna in MISO, and from the transmitting antenna to the receieve antenna i in SIMO. In addition, two MIMO operating modes are considered in this chapter: 1) a spatial multiplexing MIMO mode with channel state information at the receiver (CSIR), and 2) a spatial diversity MIMO mode based on dominant eigenmode beamforming. The bit/s/Hz channel capacity of an N_t x N_r single user CSIR MIMO scheme, with N_t transmit antennas and N_r receive antennas, is given by (5.4) [16], where H is complex random channel of dimension (N_t x N_r).

$$C_{CSIR} = \log_2\left[det\left(I_{N_r} + \frac{SNR}{N_t} \cdot HH^H\right)\right]. \tag{5.4}$$

In (5.5) the CSIR MIMO channel capacity is expressed as the sum of N_t channels in terms of the eigenvalues λ_i of HH^H.

$$C_{CSIR} = \sum_{i=1}^{i=N_t} \log_2\left(1 + \frac{SNR}{N_t} \cdot \lambda_i\right). \tag{5.5}$$

For dominant eigenmode beamforming, only one information stream is transmitted and all the power is allocated to the channel which has the largest eigenvalue λ_{max}. The channel capacity in this case is given by (5.6).

$$C_{eig} = \log_2(1 + SNR \cdot \lambda_{max}). \tag{5.6}$$

Figure 5-1 shows the channel capacity versus signal to interference and noise (SINR) of the SISO and the considered MIMO schemes. The MIMO channels are modeled as unit variance Gaussian Independent, and Identical Distributed zero mean complex processes, The elements of H are complex Gaussian with zero mean and unit variance, i.e. $H_{(i,j)} \sim \mathbb{C}\mathcal{N}(0,1)$ for $i = 1,2,\ldots N_t$, $j = 1,2,\ldots N_r$.

It is clear that all considered MIMO schemes offer higher capacity gain compared to the SISO scheme. The MIMO channel capacity is used in a system level simulator to estimate the cell average capacity when MIMO is employed.

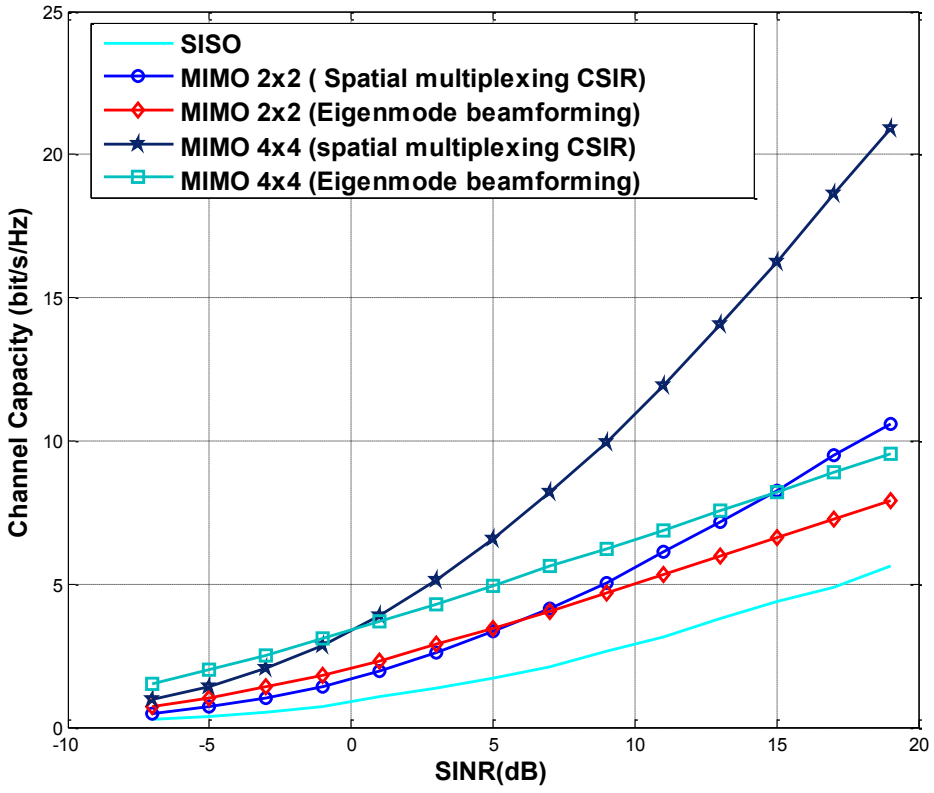

Figure 5-1: SISO and MIMO Channel Capacity

5.3 Radio base station power consumption

The accurate modeling of the power consumption of the MIMO base station is essential when evaluating the energy efficiency of MIMO networks. An increase in the power consumption of a MIMO base station is observed when compared with the SISO case. This increase is explained by the following reasons:

- Each antenna in the base station has a separate RF chain, which includes an RF transceiver and power amplifier as shown Figure 5-2 and Figure 5-3. When the same total RF transmitted power per antenna is P_t for SISO, the per-antenna RF transmit power for 2x2 MIMO is $\frac{P_t}{2}$. The MIMO gain (diversity or spatial multiplexing) is achieved without the need for extra RF power to be transmitted. If the same power amplifier efficiency for SISO at P_t, and for 2x2 MIMO at $\frac{P_t}{2}$ is assumed, the two power amplifiers in 2x2 MIMO will consume the same amount of power consumed by single power amplifier in SISO base station. However, the power consumption of the 2x2 MIMO RF transceiver (RF TRX) is double that of SISO.

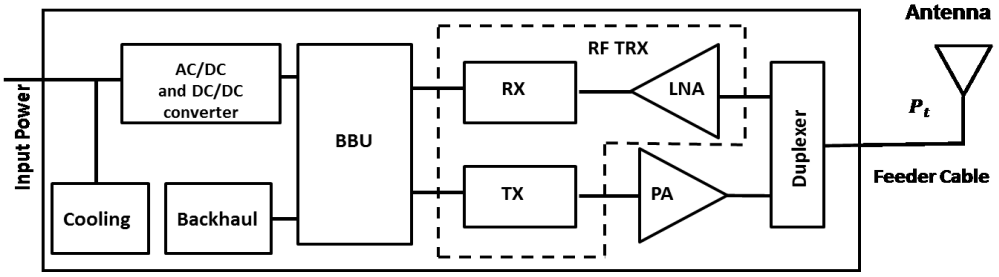

Figure 5-2: SISO base station basic architecture

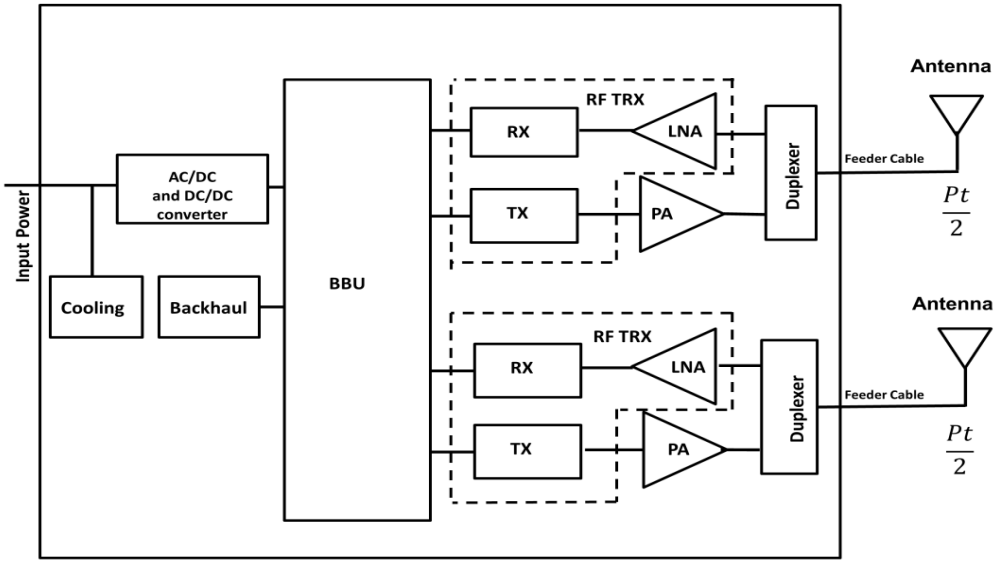

Figure 5-3: MIMO 2x2 base station basic architecture

- An increase in the baseband processing unit power consumption is observed due to more signal processing in the MIMO case. The baseband unit power consumption is usually modeled as a linear function of the number of base station antennas.
- The power losses in the power supply unit and the cooling unit are modeled as a percentage of the overall power consumption of the base station. Hence, any increase in the power consumption of the MIMO radios causes higher consumption in the power supply and cooling unit.

The overall power consumption of the base station site can be estimated as the sum of the power consumption of the base station subsystems as shown in section 3-2.
Table 5-1 and Table 5-2 list the parameters of the power consumption model used to estimate the total power consumption of the macro and picocell base stations, respectively, for the considered MIMO schemes in this chapter. These values are obtained from [40, 43].

Table 5-1: Macro cell RBS power consumption model

Parameter	**Macro 1x1**	**Macro 2x2**	**Macro 4x4**
Sectors	1	1	1
P_t/Antenna (dBm)	46	43	40
Feeder losses (dB)	3	3	3
PA efficiency	25%	25%	25%
Bandwidth (MHz)	20	20	20
Transceiver Unit ($P_{trx,ref}$, W)	13	13	13
Processing Unit ($P_{bb,ref}$, W)	30	30	30

Table 5-2: Pico cell BTS power model

Parameter	**Pico 1x 1**	**Pico 2x2**	**Pico 4x4**
P_t/Antenna (dBm)	24	21	18
Feeder losses (dB)	0	0	0
PA efficiency	10%	10%	10%
Bandwidth (MHz)	20	20	20
Transceiver Unit ($P_{trx,ref}$, W)	1	1	1
Processing Unit ($P_{bb,ref}$, W)	3	3	3

Figures 5-4 and 5-5 show the power consumption versus the cell average traffic load α of the macro and pico base station sites for 1, 2 & 4 transmit antennas. The cell average traffic load

refers to the average frequency-time resource utilisation in the cell. When $\alpha = 1$, the RF transmit power per antenna equals 40 W for a SISO macro base station and 20 W for the f 2x2 MIMO macro base station. Figure 5-4 shows the impact of adding more antennas on the macrocell base station power consumption and the large dependency of base station power consumption on α in the macro cell. Note that the point P1 refers to the power consumption at maximum traffic load, P2 is the power consumption at zero traffic load, and P3 refers to base station power consumption in DTX mode (see section 5-6.1). The value of P3 in this figure is arbitrary and shown only to demonstrate the concept.

Reducing the macro cell average traffic load can lead to a significant decrease in the site's power consumption. Similarly, when the number of antennas in a picocell base station is increased, more power consumption is observed at the same average traffic load as shown in Figure 5-5. Note that load dependency in picocell base station is very small compared with the macro case.

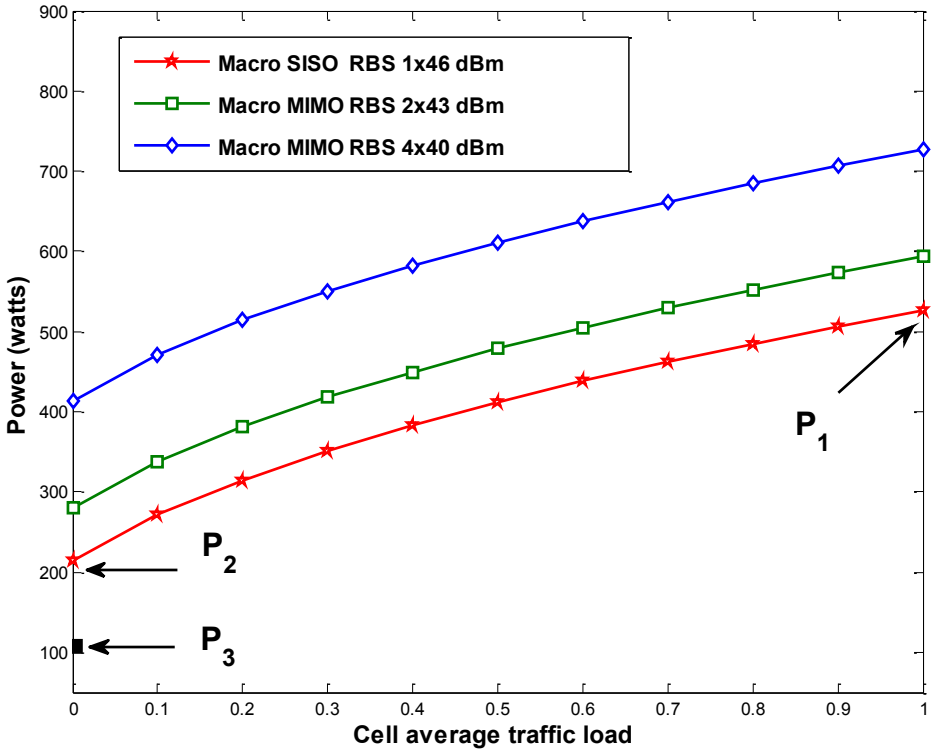

Figure 5-4: Macrocell power consumption for various MIMO schemes

Taking a SISO RAN deployment with 1 km of radius as reference deployment scenario, the ratio of the power consumption in a MIMO base station to that of a SISO , $\frac{P_{MIMO}}{P_{SISO}}$, is calculated for the macro and pico cell base stations for different numbers of transmit antennas by comparing the power model presented in chapter 3, and the Earth power consumption model [40]. The results given in Table 5-3 indicate that the relative increase in the power consumption of MIMO pico cells is larger than that of macro cells, which is explained by the fact that the

power consumption of the baseband processing and RF transceiver units scale linearly with the increase in the number of antennas. Both represent the largest power consuming units in the pico cells.

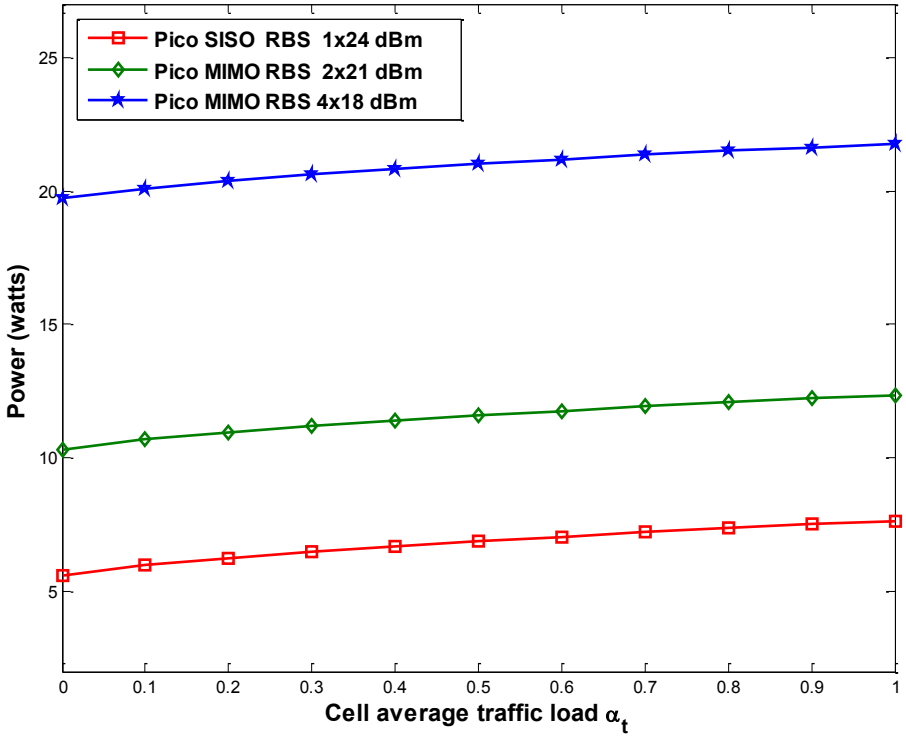

Figure 5-5: Pico cell power consumption for various MIMO schemes

Table 5-3: The increase in MIMO base station power consumption

Base Station	No of Sectors	No of	Power Consumption	$\frac{P_{MIMO}}{P_{SISO}}$ (Ch 3)	$\frac{P_{MIMO}}{P_{SISO}}$ (Earth Model)
Macro	3	1	1579	1	1
Macro	3	2	1778	1.12	1.13
Macro	3	4	2176	1.37	1.41
Macro	3	8	2971	1.88	1.97
Macro	1	1	526.4	1	1
Macro	1	2	592.7	1.12	1.13
Macro	1	4	725.3	1.37	1.41
Macro	1	8	990.4	1.88	1.97
Pico	1	1	7.66	1	1
Pico	1	2	12.36	1.61	1.5
Pico	1	4	21.77	2.84	2.58
Pico	1	8	40.60	5.29	4.69

5.4 Analysis of energy consumption in greenfield MIMO RAN deployments

When the RAN is dimensioned with cells served by MIMO base stations, a smaller number of cells are needed compared with SISO. In this regard, more detailed analysis of the energy consumption of the MIMO RAN is necessary for examining whether this strategy leads to a reduction in the RAN energy consumption or not. The RAN energy consumption is evaluated at defined target area capacities for two cases. The first case is when SISO base stations are deployed, the second case is when MIMO base stations are deployed. Since MIMO base stations can provide more capacity than SISO base stations, the number of required MIMO base stations is less than the number of SISO base stations to provide the same target capacity.

A joint analysis of the RAN average capacity and power consumption is required for the two cases of MIMO and SISO RANs, to determine the most energy-efficient option which is able to deliver the same capacity without consuming more power. The average base station power consumption P_{site} is estimated as a function of the number of antennas, and the cell average traffic load. The consumed energy in the base station site is calculated by (5.7), where T_{OH} is the observation time.

$$E = T_{OH}.P_{site} \ . \tag{5.7}$$

The RAN energy consumption is measured by the energy consumption gain (ECG). The ECG is defined as the ratio of the energy consumption E_1 of a reference RAN, here comprised of N_1 SISO base stations, to the energy consumption E_2 of a test RAN, here also comprised of N_2 MIMO base stations as shown in (5.8).

$$ECG = \frac{E_1}{E_2} = \frac{N_1.P_{SISO}.T_{OH}}{N_2.P_{MIMO}.T_{OH}}, \tag{5.8}$$

Where P_{SISO} and P_{MIMO} refer to the power consumption of SISO and MIMO base stations, respectively. An ECG value greater than one indicates that the MIMO RAN is more energy efficient than SISO. When evaluating the ECG of the two systems, the same target capacity and observation time are assumed. The RF transmitted power in SISO base station is P_t , also representing the total power which will be distributed between the MIMO transmit antennas in the case of the MIMO RAN.

The RAN average throughput gain is measured using the TPG which has already been defined in chapter 3. The TPG is written as the ratio of the MIMO RAN average capacity to the SISO RAN average capacity as in (5.9).

$$TPG = \frac{N_2.C_{MIMO}}{N_1.C_{SISO}}. \quad (5.9)$$

The MIMO cell average capacity C_{MIMO} can be expressed as function of the MIMO average capacity gain G and the SISO cell average capacity C_{SISO}, as shown in (5.10).

$$C_{MIMO} = G.C_{SISO}. \quad (5.10)$$

The value of *G* depends on which MIMO scheme is employed, the MIMO channel conditions, and the spatial distribution of users. As the same target capacity is assumed in SISO and MIMO RANs, the TPG is set to equal to unity in (5.9), and by substituting (5.10) in (5.9), we obtain a relationship between $\frac{N_2}{N_1}$ and G as shown in (5.11).

$$\frac{N_2}{N_1} = \frac{1}{G}. \quad (5.11)$$

By substituting (5.11) into (5.8), the ECG can be expressed as a function of the MIMO gain G and the ratio $\frac{P_{MIMO}}{P_{SISO}}$ as depicted in (5.12).

$$ECG = \frac{G.P_{SISO}}{P_{MIMO}}. \quad (5.12)$$

The values of $\frac{P_{MIMO}}{P_{SISO}}$ for the various base station types are provided in Table 5-3. The MIMO capacity gain G is calculated from (5.10) after estimating C_{MIMO} and C_{SISO} by system level simulation of SISO and MIMO RANs. To ensure that the MIMO RAN does not consume more energy than SISO RAN, ECG must be equal at least one, as a results, the minimum required value of G must be larger than or equal $\frac{P_{MIMO}}{P_{SISO}}$ as expressed in (5.13).

$$\mathrm{G} \geq \frac{\mathrm{P_{MIMO}}}{\mathrm{P_{SISO}}}. \quad (5.13)$$

5.4.1 MIMO gain evaluation

A Matlab static system-level simulator is developed to estimate the C_{SISO} and for SISO and C_{SISO} for SISO and various MIMO schemes condered in the chapter. A homogeneous multicell, multiuser RAN with a hexagonal cell layout is considered, where the RAN layout consists of 19 omnidirectional base stations arranged in two tiers. The performance statistics are collected from the center cell only, and user's SINR values are calculated using the interference from the two tiers of interfering cells. The RAN is simulated at different cell radii and at SISO, 2x2

MIMO, 4x4 MIMO and 8x8 MIMO schemes. The objective is to find the value of the MIMO gain G for each scheme and at each simulated cell radius. Knowing the MIMO capacity gain G is enough to determine whether the evaluated MIMO scheme is more energy efficient than a SISO scheme using (5.13), and values of $\frac{P_{MIMO}}{P_{SISO}}$ from Table 5-3. The full list of simulation parameters is shown in Table 5-4.

Table 5-4: Simulation parameters

Parameter	**Omni Macro Cell**
Frequency (MHz)	2000
Site Radius (km)	Macro 0.3 to 1
Antenna Gain (dBi)	15
UE Antenna Gain (dBi)	0
Wall Penetration loss (dB)	20
Traffic Model	Full buffer
User Distribution	Uniform
Scheduler	Round Robin
Path loss model	3GPP Uma

5.4.2 The results of MIMO gain and RAN ECG

This section presents the results of the RAN average capacities C_{SISO} , C_{MIMO} and the RAN ECG of the various considered MIMO schemes. The RAN area capacities are calculated by dividing the cell average capacity on its coverage area. Figure 5-6 shows how the RAN area capacity increases as the number of transmit antennas increases from one to eight. It also indicates that the RAN average area capacity density increases when increasing macro cell density. These results enable us to estimate the MIMO capacity gain for the 2x2, 4x4 & 8x8 MIMO schemes, as shown in Figure 5-7. Comparing the obtained values of MIMO gain G with the values of the ratio $\frac{P_{MIMO}}{P_{SISO}}$ for the omnidirectional macro sites in Table 5-3 shows that all the considered MIMO schemes can be more energy efficient than SISO schemes.

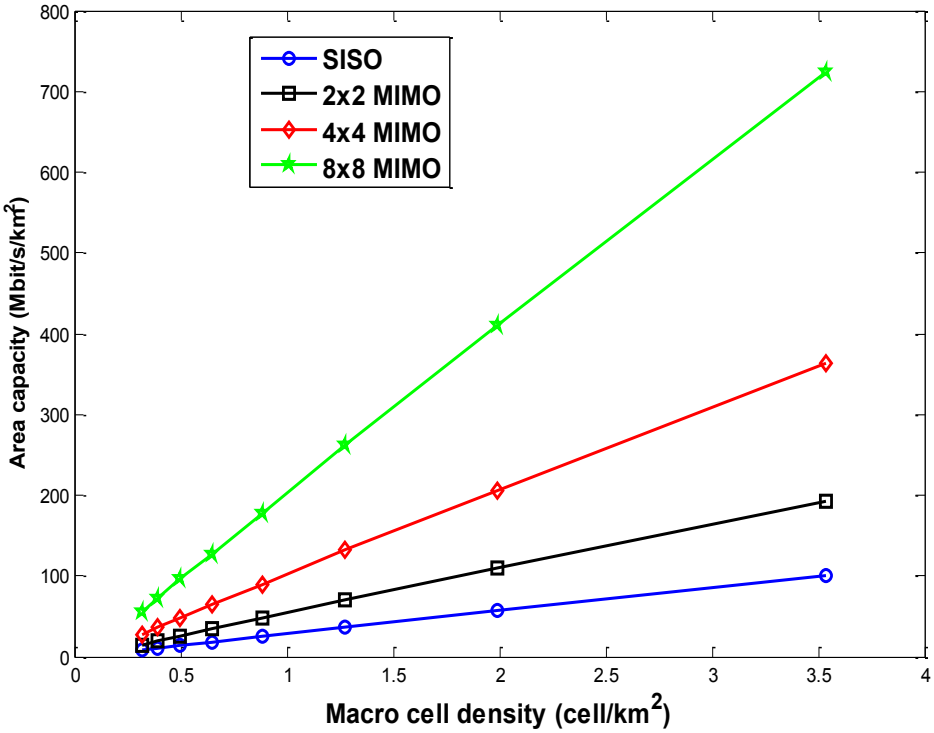

Figure 5-6: Area capacity versus the macrocell density

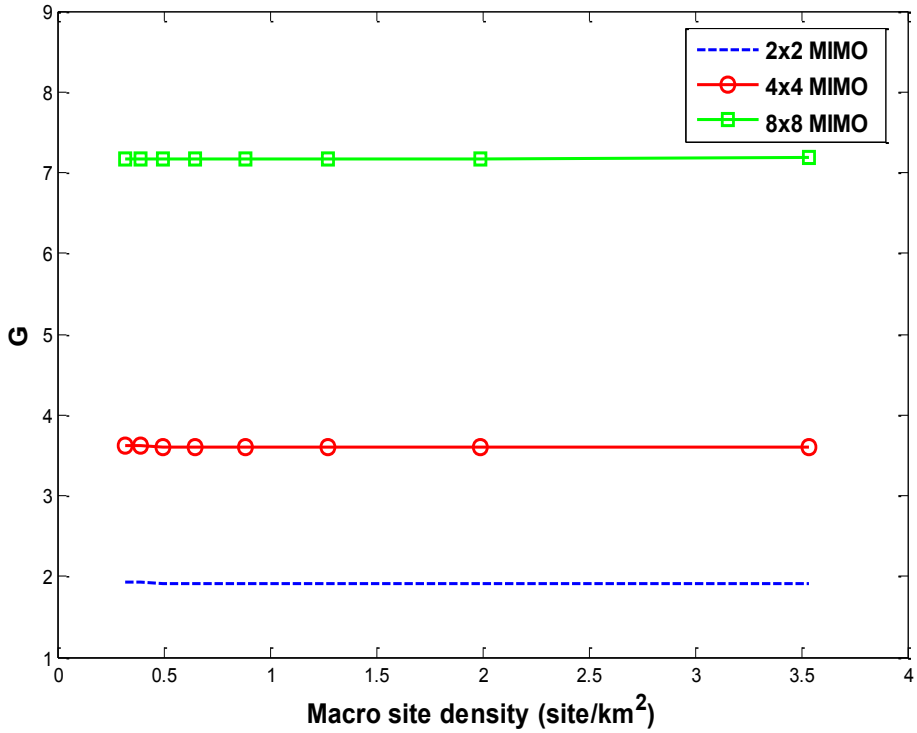

Figure 5-7: MIMO average capacity gain

The area capacity results are to calculate the number of required MIMO and SISO base stations to deliver the target area capacity. Following this, the area power consumption APC can be calculated by (5.14).

$$APC = \lambda_m . P_{RBS}, \tag{5.14}$$

Where λ_m is the macro cell density, which is obtained by dividing the number of the required base stations on the RAN area. P_{RBS} is the macro base station power consumption, which is obtained from the base station power consumption model. The APC curves for the SISO and various MIMO schemes at different target area capacity densities (from 10 Mbit/s/km^2) up to 700 Mbit/s/km^2) are shown in Figure 5-8. They clearly show that less power is consumed when higher order MIMO RANs are deployed.

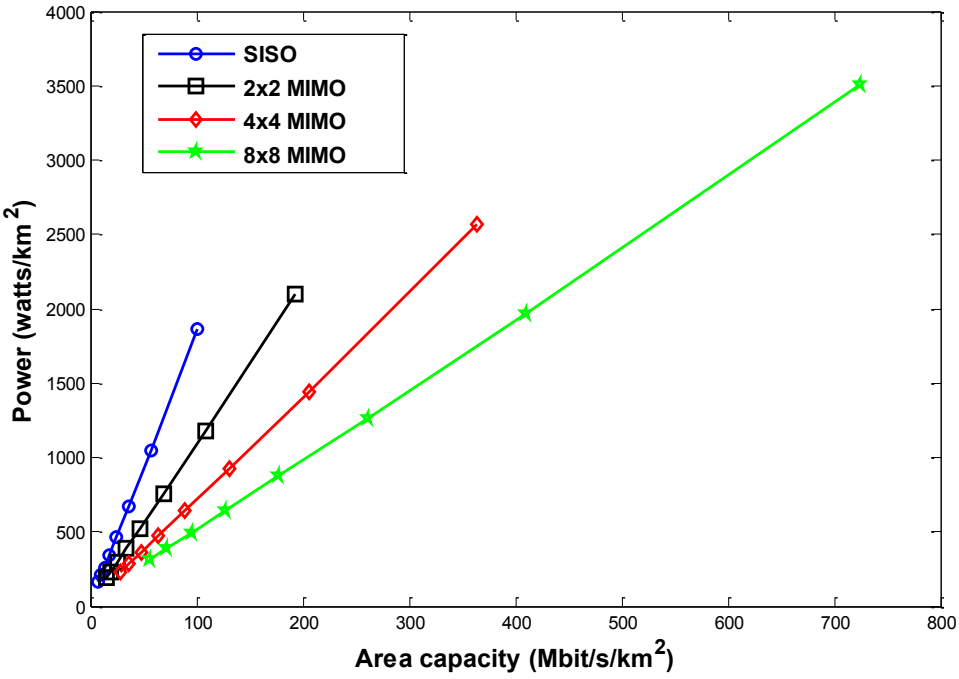

Figure 5-8: MIMO RANs' area power consumption

The ECG is also calculated for the various MIMO schemes with reference to a baseline SISO scheme with a cell radius of 1 km using (5.8). The ECG results in Figure 5-9 show that MIMO RANs can achieve better ECG than SISO at each target area capacity. On the other hand, the increase in the macrocell density leads to degradation in the RAN ECG, which corroborates the results in chapter 3. When comparing these results with the existing work, most of the existing publications [78-80] have shown that MIMO RANs are more energy efficient than SISO RANs only when the base station overhead power consumption is ignored. While the obtained results in this section shows that deploying MIMO RANs can be more energy efficient than SISO when targeting the same target area capacity density values, which agrees with the results of [82] which showed that all different MIMO schemes outperform the SISO in terms of achieving the lowest ECR when targeting the same spectral efficiency as already indicated in section 2.5.2.3.

The EE metric (bit/J) is also used to give a measure of the MIMO RAN energy efficiency. It is calculated by dividing the RAN average capacity by the RAN consumed power at each macrocell density for each MIMO scheme. Interestingly, this metric leads to the same conclusion, that MIMO RANs are more energy efficient than SISO as shown in Figure 5-10. However, it fails to show the increase in the RAN energy consumption as the macro cell density increases. All curves in Figure 5-10 indicate an improvement in the RAN energy efficiency when the density of macrocell increases, which was not the case in Figure 5-9. Therefore, using only the bit/J metric is not sufficient to explain the energy consumption and result in misleading conclusions, as explained in chapter 3.

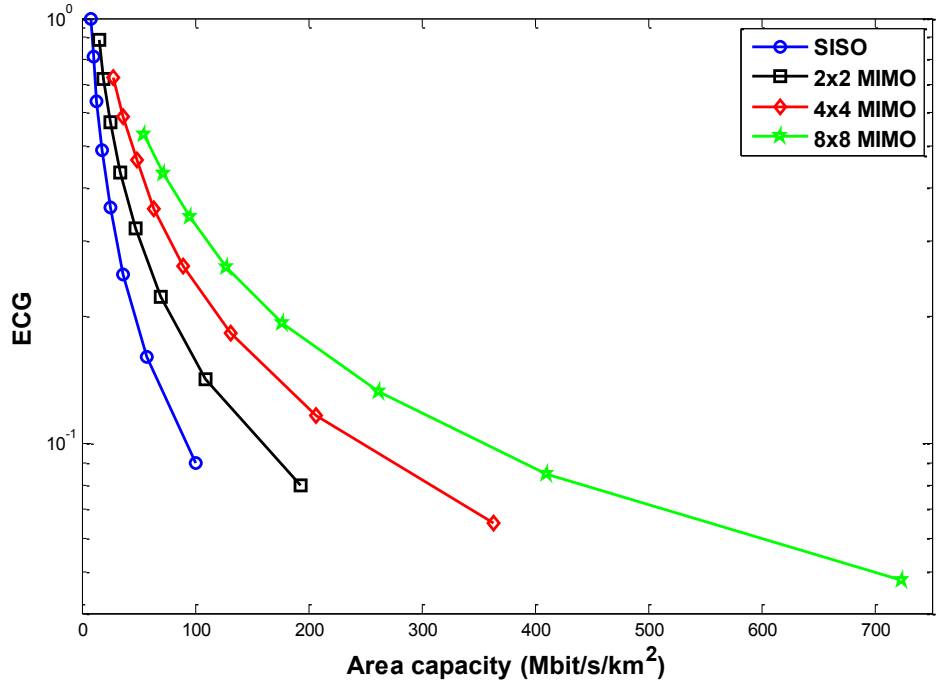

Figure 5-9: The results of the ECG for MIMO RANs

The same analysis can be applied to the case of sectorised macro base stations. The values of $\frac{P_{MIMO}}{P_{SISO}}$ for the 3-sector macro base stations are identical to the omnidirectional case. In contrast, the $\frac{P_{MIMO}}{P_{SISO}}$ values in case of pico cells are higher, which means that higher values of MIMO capacity gains are needed in pico cell MIMO RANs to make the pico MIMO RAN more energy efficient than the pico SISO RAN. For example, the case of 2x2 MIMO pico cell, a MIMO capacity gain of 1.6 is required compared to 1.12 for macro RAN.

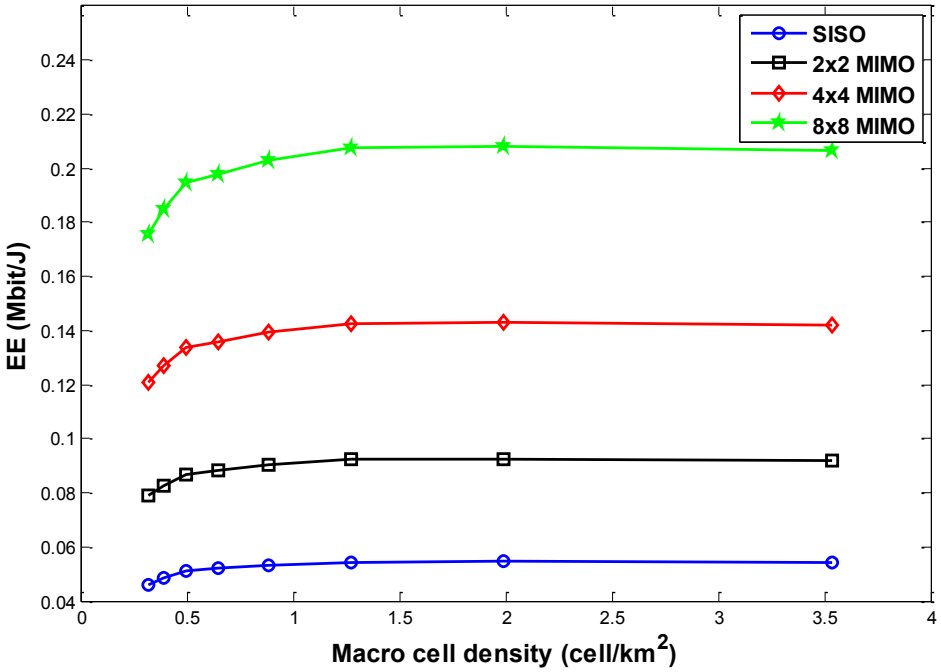

Figure 5-10: The results of bit/J for MIMO RANs

5.5 RAN energy consumption analysis when upgrading existing SISO RANs to MIMOs.

In this section, the same RAN scenario of section 5.4 is modelled but a more realistic FTP non-full buffer traffic model is used. That is, the users have a limited amount of data to send or receive. Once their data transmission is completed, the users leave the system. The users' arrival is modeled by a Poisson process, where the users are active only when they have data to download or send and stay in the system until they complete their transmission. Hence, the number of active users in the cell varies with time. To obtain accurate results, simulations are run for a protracted period of time to collect sufficient statistics from the network model. The cell average load also varies with time: its value depending on the arrival rate of user sessions, the amount of data to download, and the users' channel conditions.

5.5.1 RAN model

As an update of existing SISO RAN to MIMO is considered in this section, the number of SISO and MIMO base stations is always equal. the user arrivals are modeled as a Poisson process in time, the user locations are distributed uniformly in the target cell to reflect a wide range of SINR values comprising high SINR for the users who are close to the base station and low

SINR values for the cell edge users. A static system-level simulator is used to estimate the cell average throughput as well as the cell average traffic load for the SISO and MIMO RANs. A non-full buffer FTP traffic model with a variable arrival rate, described in 3GPP document 36.814, is adopted. MIMO user selects dynamically the MIMO mode (spatial multiplexing or diversity modes) which offer him the highest data rate. The RAN performance statistics for the same values of offered traffic are collected for SISO and various considered MIMO schemes, to be used to estimate the RAN power consumption.

5.5.2 The ECG analysis

The ECG is evaluated at various user arrival rates per cell ranging from 0.5 to 1.5 arrivals per second, whereby each user is considered to download a 2 MB file and then depart the network. The user arrival rate is an indication of the average offered traffic per cell. For example, 0.5 arrivals per second is equivalent of $0.5 \times 2 \times 8 = 8$ Mbit/s. The ECG is estimated for the various MIMO RAN types considered with reference to a SISO RAN as shown in (5.15).

$$ECG = \frac{P_{SISO}(\alpha_{SISO})}{P_{MIMO}(\alpha_{MIMO})}. \tag{5.15}$$

Note that, in contrast to the equation (5.8), the number of deployed SISO and MIMO base stations is the same in this case. α_{SISO} and α_{MIMO} refer to the average traffic load in SISO and MIMO cells, respectively. As the same offered traffic is assumed in SISO and various MIMO schemes, The TPG is always equal 1 in this case.

5.5.3 The results of ECG

The cell average traffic load values for the various SISO and MIMO schemes are estimated by running a system level simulation of each scheme. The configuration parameters are listed in Table 5-5. The cell average traffic load values versus the offered traffic are shown in Figure 5-11, the cell average traffic load are used to calculate the macrocell RAN power consumption at different cell average offered traffic values, as plotted in Figure 5-12. The ECG is calculated by (5.15) for 2x2, and 4x4 MIMO RANs with the SISO RAN as a reference. The ECG of 2x2 MIMO RAN is always greater than unity. That is, though the SISO RAN is capable of meeting the offered traffic requirement, the 2x2 MIMO RAN meets the same offered traffic requirement while expending less energy. While at MIMO orders higher than 2x2, the ECG drops below unity which means that increase in the 4x4 MIMO RAN due to installing more RF transceivers is larger than the power reduction due to the reduction in the cell average traffic load.

The trends in Figure 5-12 are attributed to the decrease in the cell average traffic load when increasing the MIMO order. While the reduced average traffic load saves energy, the increase in the number of RF chains consumes more energy. An appropriate trade-off occurs for the 2x2 MIMO RAN. Thus, from an operator's perspective, upgrading from SISO to 4x4 MIMO cannot be justified on the basis of energy consumption alone.

Our observations contradict the widely held view that adaptive MIMO antenna muting techniques always improve the RAN energy efficiency [96]. When measured by the ECG figure of merit, our results illustrate that switching from a 2x2 MIMO mode to SISO degrades the RAN energy efficiency. Additionally, the curves in Figure 5-12 show that the use of more than 2x2 MIMO at the base station leads to more energy consumption.

Table 5-5: Simulation parameters

Parameter	**Omni Macro Cell**
Frequency (MHz)	2000
Site Radius (km)	Macro 0.5 / Pico 0.1
Macro Antenna Gain (dBi)	15
Pico Antenna Gain (dBi)	2
Wall Penetration loss (dB)	20
Traffic Model	FTP (2MB file)
User Distribution	Uniform
Scheduling	Round Robin
Observation Time	100000 TTIs
Path loss model	3GPP Uma & Umi

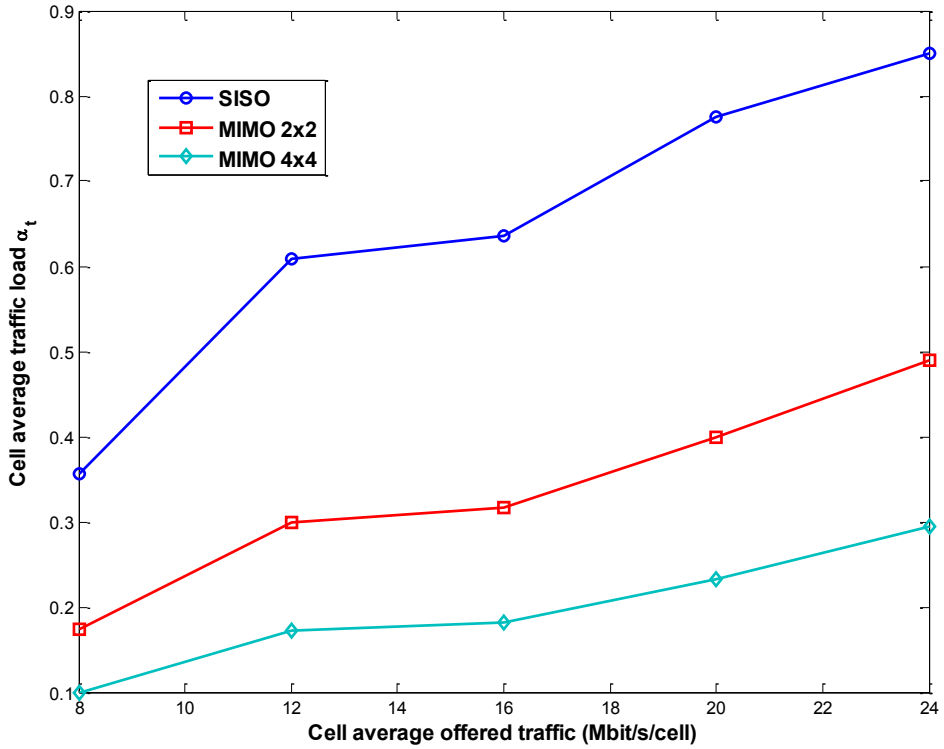

Figure 5-11: Average traffic load in SISO & MIMO RANs

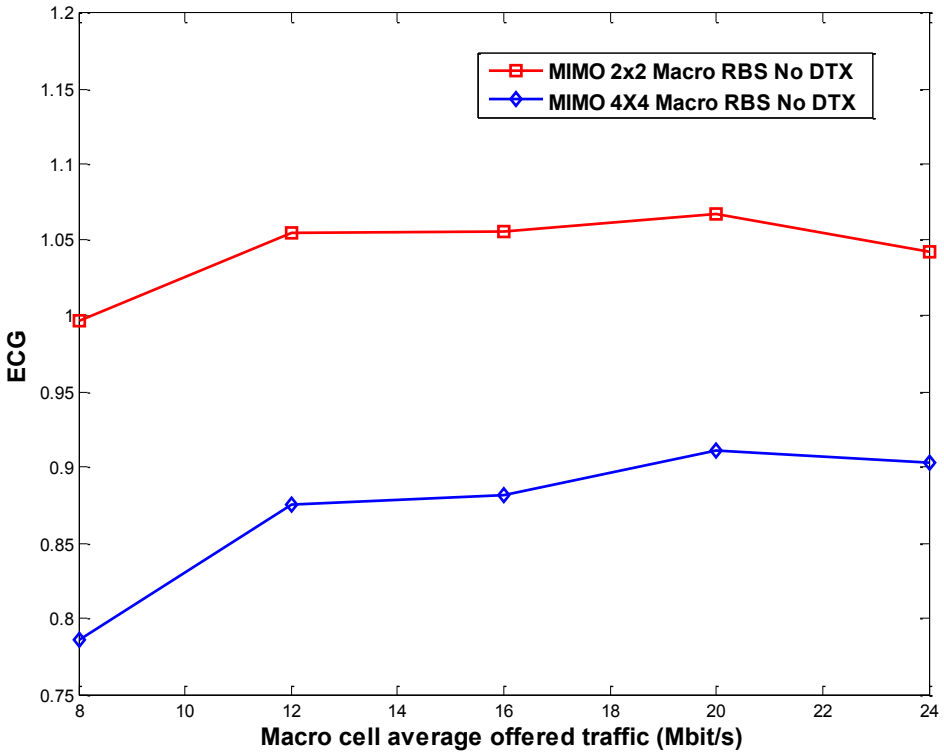

Figure 5-12: ECG of considered MIMO schemes

5.6 ECG analysis of MIMO RANs with discontinuous transmission (DTX)

As shown in the previous section, upgrading the SISO base stations to MIMO when the same level of offered traffic is assumed leads to a reduction in the cell average traffic load. This reduction in load can be exploited by switching off some or all the base station subsystems during the periods of low traffic. [15], The discontinuous transmission DTX feature, which was proposed in [101] allows for fast and short switching off some of an LTE base station components during the empty time symbols of the LTE subframe. The impact of implementing such a technique on MIMO base stations is investigated in the next section. The objective is to examine if more energy can be saved when the cell average traffic load is decreased when MIMO cells are deployed.

5.6.1 Base station power consumption with DTX

Under normal operation, an LTE base station transmits broadcasting, synchronisation and cell reference control signals, even when there is no cell data traffic. This leaves a short idle time for the implementation of the discontinuous transmission feature DTX, The LTE standard Rel-8 allows up to 6 MBSFN (Multicast and Broadcast Single Frequency Network) subframes to be transmitted per LTE frame, and each MBSFN sub-frame carries the CRS (cell-specific reference signals) signal only in the first LTE symbol [101]. Hence, one solution is to implement the DTX mechanism during the MBSFN sub-frames as more idle time is available in these subframes to implement the DTX when the average traffic load is low.

The sub-frame duration in LTE is 1 ms, which represents 10% of the frame duration, and consists of 14 LTE symbols, each of 71.4 µs duration. By considering a 30 µs sleep state transition time in the base station as indicated in [101], the remaining available idle time for DTX is $(13 \times 71.4 - 30)$ µs. A maximum of 6 sub-frames can be configured in MBSFN according to the LTE Rel-8. Therefore, the maximum percentage of idle time $\alpha_{DTX,max}$ in 6 sub-frames over one LTE frame (10 ms) is given by (5.16).

$$\alpha_{DTX,max} = \frac{6\times(1000-71.4-30)}{10000} = 0.5392 \ . \tag{5.16}$$

In (5.16), the number 6 refers to the maximum number of MBSFN subframes in LTE, 1000 is the subframe duration in µs, 10000 is the LTE frame duration in µs, 71.4 µs in each MBSFN subframe is reserved for the CRS signals, while 30 µs is sleep state transition time.

When DTX mode is enabled, the cell may be in one of three following states:

- Transmitting at full RF power, thereby consuming P_{ON} (i.e. P1 in Figure 5-4) if traffic is present in the cell.
- Transmitting only the control signals (10%) of the full RF transmit power, thereby consuming P_{OH} (i.e. P2 in Figure 5-4) when the cell has no data traffic to transmit,
- The base station is in DTX state, thereby consuming P_{DTX} (i.e. P3 in Figure 5-4), where the amount of power consumed during the DTX state P_{DTX} is a function of P_{OH} and the base station DTX factor (δ_{DTX}) as shown in (5.17).

$$P_{DTX} = \frac{P_{OH}}{\delta_{DTX}}. \tag{5.17}$$

DTX is not enabled when $\delta_{DTX} = 1$ whereas DTX is enabled when $\delta_{DTX} > 1$. The intensity of the average traffic load in the cell determines how long the cell will stay in the DTX mode. If the cell average traffic load α_t is known, then the proportion of DTX on-time in one frame α_{DTX} is estimated by (5.18).

$$\alpha_{DTX} = \min\left(\left(\left\lfloor\frac{1-\alpha_t}{0.1}\right\rfloor\right) \times 0.0899, \alpha_{DTX,max}\right). \tag{5.18}$$

The constant "0.0899" equals the ratio of maximum idle time in one sub-frame to the LTE frame duration. The term $\left\lfloor\frac{1-\alpha_{ON}}{0.1}\right\rfloor$ is equal to the number of idle sub-frames in one LTE frame, and 0.1 refers to the ratio of duration of single subframe to the frame duration. Let α_s denote the ratio of the time spent transmitting control signaling to the total time duration of an LTE frame, as expressed in (5.19).

$$\alpha_s = 1 - \alpha_t - \alpha_{DTX}. \tag{5.19}$$

If the values of δ_{DTX}, α_t, α_{DTX}, α_s, P_{DTX}, P_{OH} and P_{ON}, are known, the base station site power consumption during DTX mode can be calculated by (5.20).

$$P_{site} = \alpha_t.P_{ON} + \alpha_s.P_{OH} + \alpha_{DTX}.P_{DTX}. \tag{5.20}$$

By substituting (5.17) into (5.20), P_{site} during the DTX mode is given by (5.21).

$$P_{site} = \alpha_{ON}.P_{ON} + P_{OH}\left(\alpha_{OH} + \frac{\alpha_{DTX}}{\delta_{DTX}}\right). \tag{5.21}$$

Figure 5-13 shows the curves for P_{site} versus the cell average traffic load and is based on the macro cell base station power consumption results in Figure 5-4 (i.e. P1, P2 and P3) for an arbitrary value of $\delta_{DTX} = 4$ chosen only to demonstrate the concept. The curves show that enabling DTX gives significant power savings at low traffic loads in both SISO and MIMO systems. Similar savings are obtained for the pico cell case, as shown in Figure 5-14.

The power consumption of SISO macro cell and SISO picocell base stations are plotted in Figure 5-15 and Figure 5-16 versus wide range of δ_{DTX} values and versus cell average traffic load ranges from 0 to one. These figures clearly indicate that the larger δ_{DTX} lead to significant decrease in the base station power consumption if the cell average load is low.

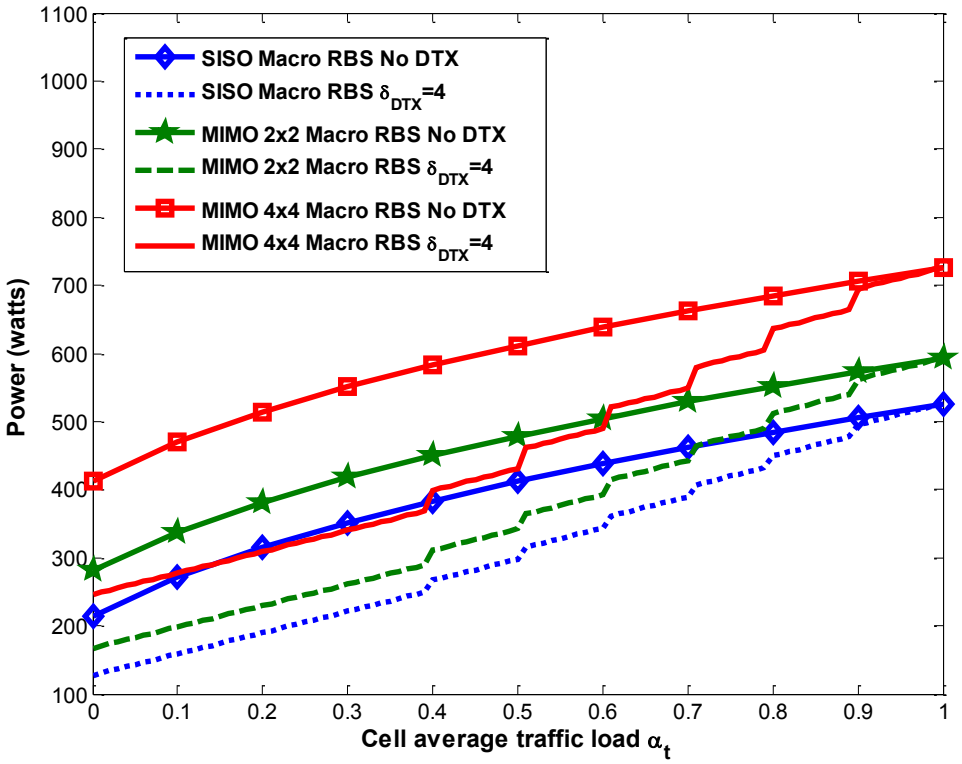

Figure 5-13: Power consumption of considered MIMO schemes with DTX in 1 sector macro base station

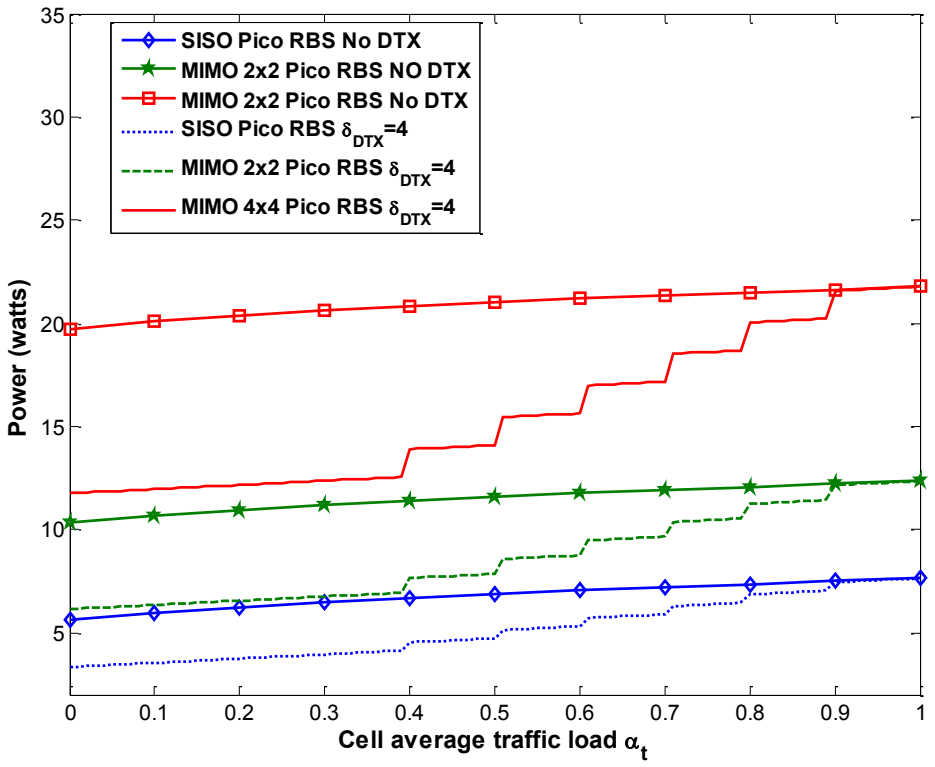

Figure 5-14: Power consumption of considered MIMO schemes with DTX in pico base station

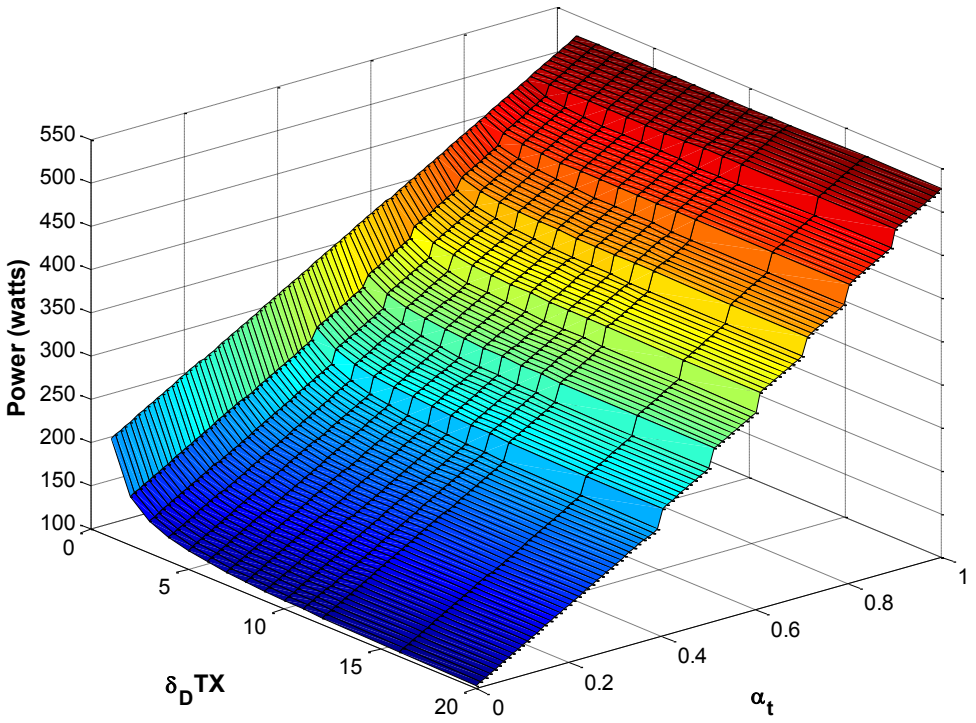

Figure 5-15: Power consumption of SISO macro base station versus the DTX factor & cell load

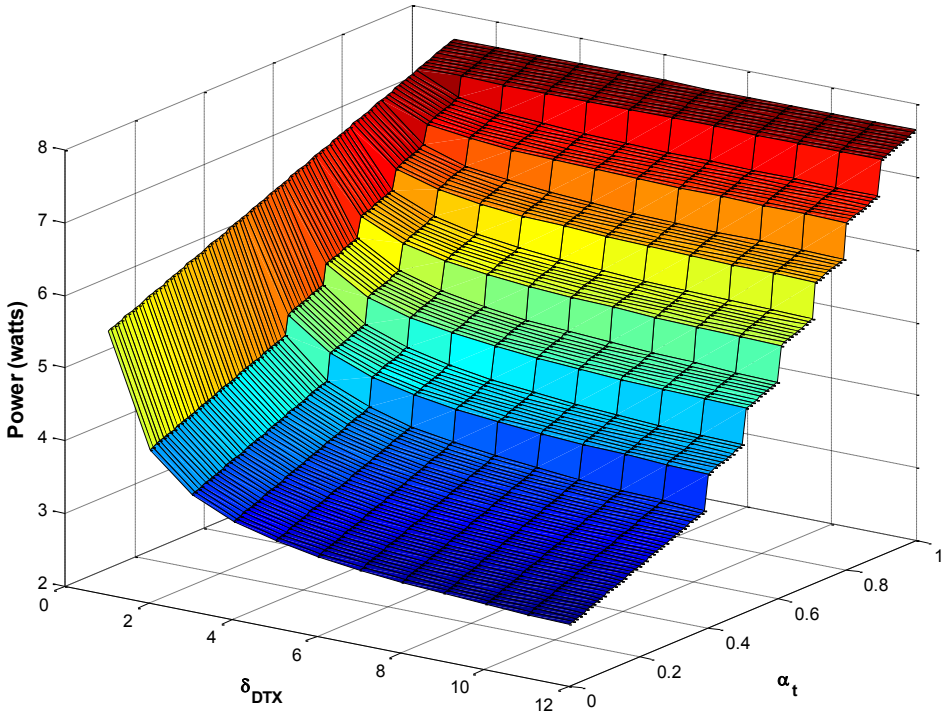

Figure 5-16: Power consumption of SISO pico base station versus the DTX factor & cell load

5.6.2 ECG of macrocell RAN with DTX enabled

When the DTX is enabled, the optimum trade-off between the cell average traffic load and the number of transmit antennas shifts to a new position. Figure 5-17 plots curves of ECG versus cell average offered traffic for the same SISO and MIMO schemes, with DTX enabled. The reference scheme is a SISO RAN with DTX disabled. The curves show that the ECG of all the MIMO schemes with DTX enabled is above one. At cell average offered traffic values below 22 Mbit/s, the 2x2 MIMO RAN achieves the highest ECG value, while at higher offered traffic values, the 4x4 MIMO RAN is the most energy efficient option when the $\delta_{DTX} = 8$. When the DTX factor δ_{DTX} increases from 4 to 8, the ECG of all considered MIMO schemes increases appreciably, while the improvement of ECG of SISO RAN is very small and vanished at high offered traffic values, which illustrates the benefits of implementing DTX in MIMO RANs.

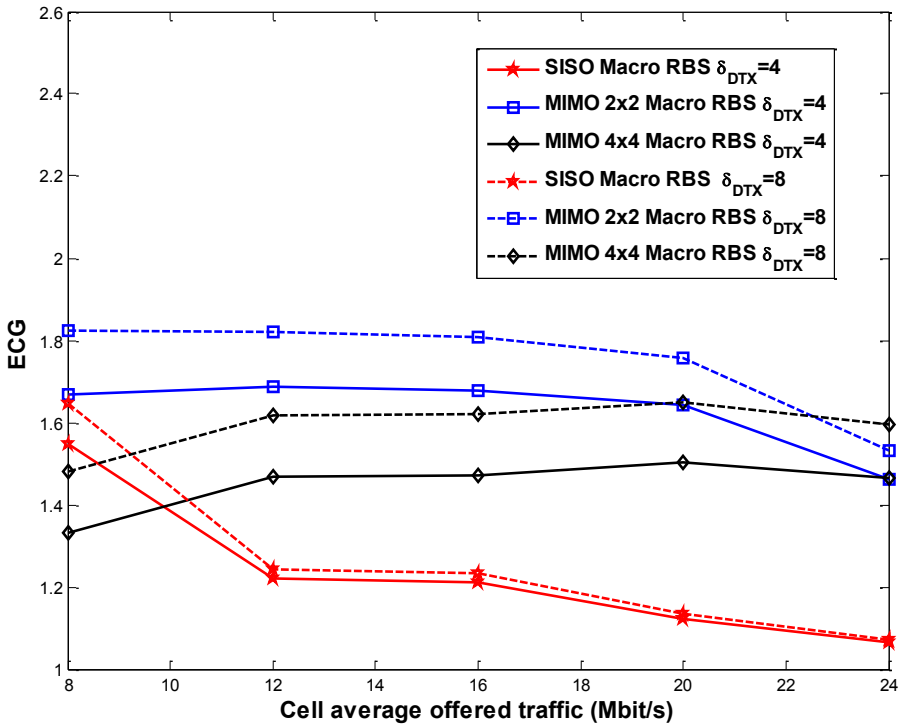

Figure 5-17: ECG of SISO and MIMO macro cell RANs with DTX enabled

5.6.3 ECG of small cell RANs with DTX enabled

We investigate the ECG of SISO and MIMO RANs when 100 m radius picocells are deployed homogeneously instead of macrocells. The remaining simulation parameters do not vary from those used in the macro cells' case. Picocell base station power consumption is used to estimated P_{ON} and P_{OH} for the pico cell base station. The reference scheme for calculating the ECG is a pico cell SISO RAN with DTX disabled. The ECG vs. cell average offered traffic is plotted in Figure 5-18 for the cases of DTX disabled and enabled. The results show that a value of $\delta_{DTX} > 8$ is needed to have the ECG of pico cell 2x2 MIMO RAN close to that of SISO at high values of offered traffic . while the ECG of the 4x4 MIMO schemes is always below unity. Also, all MIMO RAN schemes without DTX consume more energy that the SISO RAN. Additionally, the 4x4 MIMO RAN with DTX achieves almost the same ECG as the 2x2 MIMO scheme without DTX. The results are attributed to the different power consumption characteristics in pico cells compared to macro cells, whereby the larger proportion of overhead power consumption in pico cells makes their power consumption less depending on the cell average load (see Figure 5-5). Therefore, in pico cell MIMO RANs the reduction in energy consumption attributed to lower cell averge load values is very small and readily offset by the increase in the energy consumption caused by the adding additional RF chains. In DTX mode, switching off more components in the base station is required during the no traffic load periods

to achieve substantial effective energy savings which illustrated by the value of $\delta_{DTX} = 8$ in Figure 5-18 in order to have the ECG of 2x2 MIMO RAN approach the ECG level of SISO RAN at high offered traffic load values.

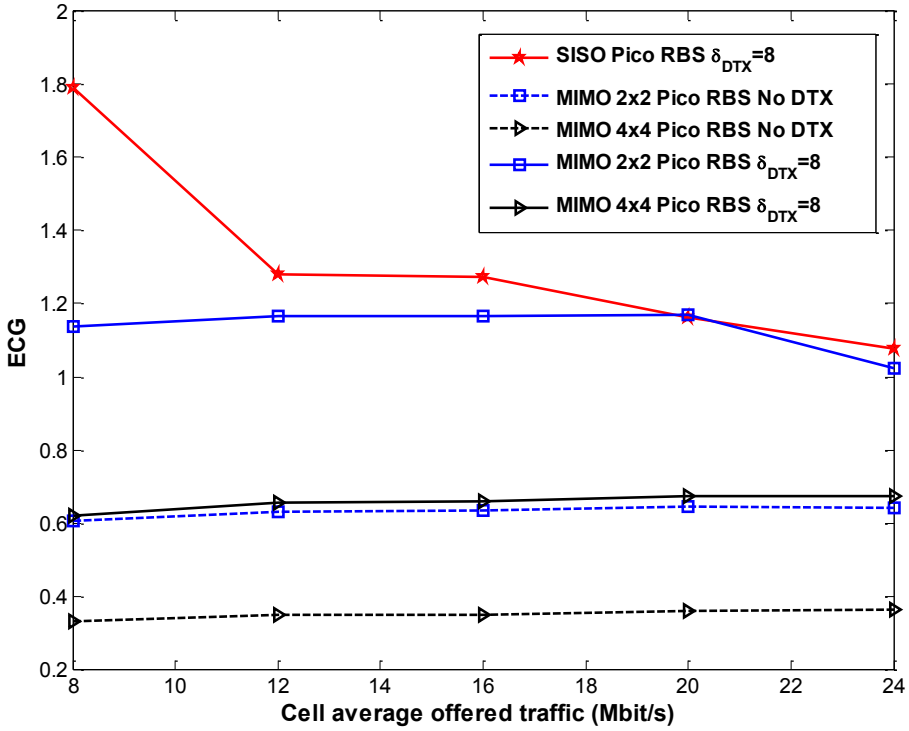

Figure 5-18: ECG of small cell SISO and MIMO RANs

5.7 Summary

An evaluation of the energy consumption of an LTE-based MIMO RANs has been presented in this chapter. The MIMO RAN ECG is evaluated with reference to a SISO RAN under the same capacity requirements. Two cases are evaluated: the first case evaluates the MIMO RAN ECG in new RAN deployment when the operator has the choice to deploy SISO or MIMO base stations. The results obtained for this case results have conclusively shown that dimensioning the RAN using MIMO base stations is more energy efficient than using SISO base stations when the same requirements of area capacity are assumed. This is due to fewer MIMO cells being required to deliver the same offered traffic. The second case evaluates MIMO macrocell RAN ECG when upgrading an existing SISO RAN to MIMO, i.e. the number of base stations is the same for SISO and MIMO deployments. Two MIMO schemes were considered in the second case: 2x2 and 4x4 MIMO. A non-full buffer traffic model was used to model the variation in cell average traffic load in order to observe the impact of the average load variation on the RAN energy consumption. Moreover, the analysis is extended by modeling of the power consumption in radio base stations when DTX is enabled.

The key findings for the second case are that for macro cells, the 2x2 MIMO RAN achieves higher ECG than SISO RAN for the same offered traffic irrespective of DTX is enabled or not. When DTX is enabled, the 4x4 MIMO RANs also become more energy efficient than SISO RAN. For pico cell RANs, the SISO RAN with DTX enabled is the most energy-efficient option. Furthermore, these results indicate that adaptive antenna muting technique should be implemented with caution in macrocell RANs, as it may lead to more energy consumption if applied on 2x2 MIMO RAN.

Finally, the main outcome of this chapter can be summarized into two points: 1) it is always more energy efficient to upgrade the existing SISO base stations to MIMO to meet the increase in demand for high area capacity requirements. 2) Even if there is no increase in the traffic demand, upgrading the existing SISO macro RANs to 2x2 MIMO improves the per users data rates, and in same time reduces the overall RAN energy consumption. On the other hand, the MIMO picocell RAN can be more energy efficient than the SISO picocell RAN only when high MIMO capacity gain is achievable.

Chapter 6

The Energy Efficiency Analysis in Heterogeneous Networks: Traffic Offloading to Small Cells and Sleep Mode Techniques

6.1 Overview

The proliferation of smart devices and the expansion of mobile services in developing societies have led to a continuous increase in the demand for wireless data services over the last decade. This trend is expected to continue over the next five years, according to Cisco visual networking index report of 2015, as already highlighted in chapter 2 [10]. The delivery of this rapid traffic growth necessitates a paradigm shift in cellular network design, whereby a progressive densification of the network using small cells is seen as one of the key enabler techniques to achieve the high target capacities in the next generation cellular networks.

The advantage of network densification with small cells is that it enhances the RAN capacity by increasing the spectrum re-user factor and reducing the distance between the user and the base station, thus improving the signal to interference and noise, and decreasing the RF power transmitted by the small cells. This can result in an increase in the RAN capacity and a reduction in the energy consumed.

However, such massive deployment of small base stations can face several challenges:

- Increasing the density of deployed small cells can lead to an increase in the total RAN energy consumption if the densification exceeds a certain limit.
- The requirements of additional backhaul links in small cell networks can outweigh any energy savings, especially if high power is required to operate the backhaul link.
- Allocating the same frequency band to the macro and small cells layers complicates the issue of interference management in the network.
- Different user association mechanisms are required to avoid having underutilised small cells, which would have a negative impact on the RAN average throughput and RAN energy consumption.

On the other hand, densifying the macrocell RAN by deploying small cell base stations as an overlay has the advantage of immediately targeting traffic hot spots in a cost-effective and energy efficient way. Moreover, the results presented in chapter 3 have already confirmed that deploying a second layer of small cells on top of existing macro sites is more energy efficient

than densifying the macro RAN with more macro sites when the same target capacity is sought. We have also concluded in chapter 4 that deploying an overlay of small cells on the top of three sector macro sites is more energy efficient than upgrading to six sector RANs before deploying the small cells.

The next step in our analysis is examining the impact of traffic offloading to small cells on the performance and energy consumption of heterogeneous RANs. Our aim is to investigate whether or not offloading a portion of macro layer traffic to small cells can lead to an energy consumption reduction. Two cases are considered in this chapter, the case of small cell deployment when a uniform user location distribution is assumed, and the case when the users are deployed in clusters around the small cells to form what is known as hotspot zones.

Most of the published work in open literature has shown that traffic offloading to small cells improves the energy efficiency when measured in bit/J due to the increase in the RAN throughput, but no energy reduction is observed in the network actual energy consumption [88]. If the same amount of offered traffic is assumed, deploying small cells decreases the average traffic load in macrocells, which in turn reduces the power consumption of macrocells. On the other hand, additional power is required to operate the base stations in small cells. The overall RAN power consumption may increase or decrease depending on whether or not the additional consumed power by the small cells is more than the power consumption reduction in the macrocells.

In addition, this chapter considers the case of the idle small cells being fully or partially switched off using sleep mode techniques [107].

The last section of the chapter investigates the throughput and energy consumption of dense heterogeneous deployments where the density of deployed small cells approaches the density of deployed users. The objective is to evaluate the TPG and ECG when the density of small cells is very high. In addition to the sleep mode, the chapter addresses the issue of interference management in heterogeneous networks by analysing the benefits of implementing the enhanced inter-cell interference coordination technique eICIC on the RAN throughput and energy consumption.

6.2 Traffic offloading to small cells

Traffic offloading to small cells has the advantage of lowering the utilisation of macrocells, which in turn leads to a reduction in the power consumption of macrocells and an improvement in the average throughput of macro users. Normally, the users are associated with the cell, which provides the strongest received signal. The user association process is described by (6.1).

$$\text{Serving cell}=\arg\ max_{m\in M}(RSRP_m)\ , \tag{6.1}$$

Where m is the cell index, M is the set of cells and RSRP is the reference signal received power. In heterogeneous networks, the transmitted power of macro cells is very high when compared to small cells; therefore, most of the users would associate with the macro cells. To avoid having underutilised small cells, the cell range expansion CRE technique is employed by adding an offset bias value to the received signals from the small cells as shown in (6.2) such that the user equipment can associate with a small cell even if it receives a stronger signal from the macro cell.

$$\text{Serving cell}=\arg\ max_{m\in M}(RSRP_m + CRE), \tag{6.2}$$

Where the value of the CRE bias lies in the range (0 20) dB and can be determined by the network as a function of traffic distribution.

6.2.1 System model for heterogeneous networks

In order to model the traffic offloading in heterogeneous networks, a system level simulation of heterogeneous RAN is developed considering different values of CRE bias to reflect various levels of offloading. Moreover, an FTP elastic traffic model is used to generate bursty time-varying traffic in the network.

6.2.2 Heterogeneous networks layout

Unlike with macro RANs, where network planning by the operators is conducted in advance to determine the locations of the macro base stations, small cells are deployed by the network operators or by end users in an unplanned or a semi-planned manner according to the spatial distribution of the expected density of traffic demand. Only macro/pico heterogeneous RANs are evaluated in this chapter. Co-channel spectrum allocation is assumed, and the same frequency band is allocated to the macro and picocells, which means inter-layer interference need to be considered.

The considered network layout consists of a hexagonal grid of macrocells and random uniform distribution of picocells, as shown in Figure 6-1. Each macro and picocell base station is equipped with a single omnidirectional antenna with a gain of G_t. The considered heterogeneous deployment consists of M macro base stations, with the base stations indicated by BS_i ($i \in \{1,2,\ldots\ldots\ldots,M\}$), and K pico cells deployed inside the macro cell coverage area. The pico cells are indicated by S_i ($i \in \{M+1, M+2, \ldots\ldots\ldots, K \cdot M\}$) . A number of users U are deployed uniformly in the target area, and the signal to interference and noise $SINR_{i,u}$ for the user u associated with BS_i is estimated by (6.3).

$$SINR_{i,u} = \frac{P_i \cdot g_{i,u}}{\sum_{j=1, j\neq i}^{M} P_j \cdot g_{j,u} + \sum_{j=M+1, j\neq i}^{(M \cdot K)} P_j \cdot g_{j,u} + N}, \quad (6.3)$$

Where P_i is the base station transmitted power, $g_{i,u}$ is the channel gain between the base station i and user u, which includes the pathloss and large scale shadowing, and N is the noise level at the user. When a base station has no associated users, only the reference and broadcasting signals are transmitted which represents around 10% of the maximum RF transmit power of the base station. If sleep mode is enabled, any idle base station stops transmitting any signals.

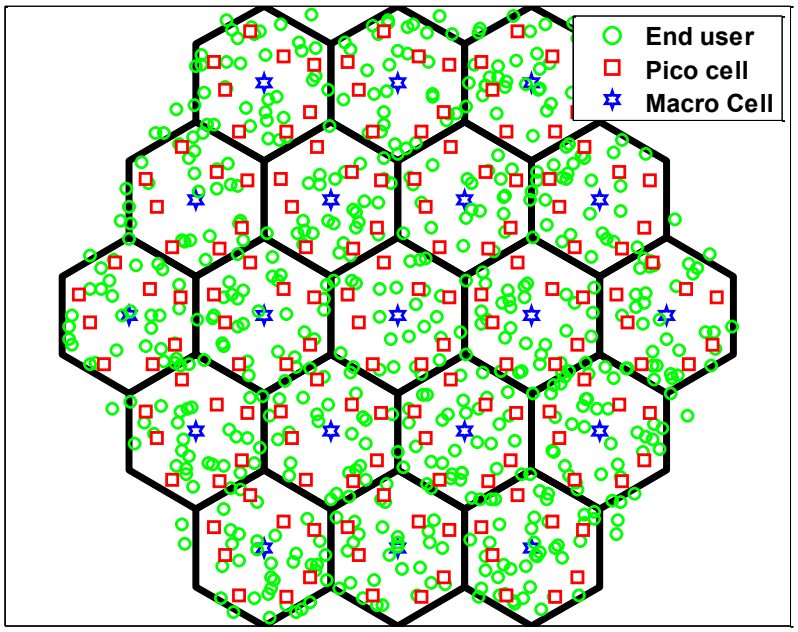

Figure 6-1: Heterogeneous network layout

Shannon formula is used to estimate the user data rate R_u as a function of the user signal to interference and noise $SINR_u$ and the allocated bandwidth W_u, as in (6.4).

$$R_u = W_u * (\min(\log_2(1 + SINR_u), S_m), \quad (6.4)$$

Where S_m represents the maximum achieved spectral efficiency. Its value depends on the highest modulation scheme used. The total RAN average throughput equals the sum of the achieved data rates of all users, as shown in (6.5).

$$\bar{R}_{RAN} = \sum_{u=1}^{U} R_u . \quad (6.5)$$

6.2.3 Traffic model

The 3GPP document 36814-900 [133] has indicated that network throughput can be evaluated using a full buffer model representing continuous traffic which models non-varying interference,

resulting in cell average load always being equal to one. While time-varying load needs to be modelled using a bursty elastic model such as FTP. Two non-full buffer FTP models are proposed in the 3GPP document: per cell traffic and per user traffic models. The per-user traffic model is adopted in this chapter as it is simpler to implement in multi-cell multi-user system level simulations. In this model, each user downloads a file with a predefined size F and reading time mean D. The reading time has an exponential distribution and refers to the time interval between two successive download requests by each user. The average offered traffic by each user is a function of D, F and file transfer time Tt, as in (6.6). The value of T_t depends on the user $SINR$ and on the bandwidth allocated to the user.

$$\bar{T} = \frac{F}{D+T_t}. \tag{6.6}$$

The average offered traffic for a single user with D equals 5 seconds with a file size of 2 MB and file transfer time ranging from 0.13 s to 10 s, as plotted in Figure 6-2 versus T_t. The 0.13 s corresponds to a bandwidth of 20 MHz allocated to a single user using the 64 QAM modulation.

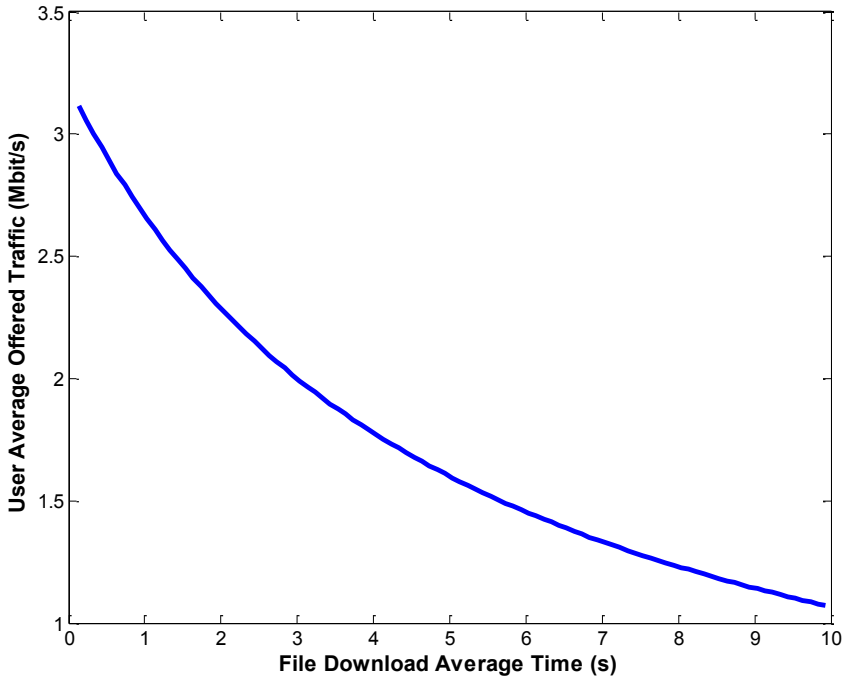

Figure 6-2: FTP traffic model

6.2.4 Throughput and power consumption analysis

The evaluation framework of chapter 3 and the proposed base station power consumption model are used to investigate the throughput and power consumption of the heterogeneous RAN described in section 6.2.1. The three figures of merit TPG, ECG and ETG are calculated for a heterogeneous RAN with reference to a macro only deployment. the cell average traffic load in

cell i is denoted by α_i in the case of a macro only RAN, and by $\hat{\alpha}_i$ in the case of a heterogeneous RAN, the throughout gain TPG of the heterogeneous RAN can be calculated by (6.7).

$$TPG = \frac{\sum_{i=1}^{K \cdot M} R_i(\hat{\alpha}_i)}{\sum_{i=1}^{M} R_i(\alpha_i)}, \tag{6.7}$$

Where $R_i(\alpha_i)$ refers to the average throughput of cell i at cell average traffic load α_i. The values $R_i(\alpha_i)$, $R_i(\hat{\alpha}_i)$, α_i and $\hat{\alpha}_i$ are obtained by running a system level simulation of a macro only and heterogeneous RAN at different pico cell densities. A TPG value higher than one means that the heterogeneous RAN delivers more data volume during the same observation period. Similarly, the energy consumption gain ECG of the heterogeneous RAN is calculated with the same reference deployment of macro only RAN, as in (6.8).

$$ECG = \frac{\sum_{i=1}^{M} P_i(\alpha_i)}{\sum_{i=1}^{K \cdot M} P_i(\hat{\alpha}_i)}, \tag{6.8}$$

Where $P_i(\hat{\alpha}_i)$ and $P_i(\alpha_i)$ are the power consumption of the base station i at the specified cell average traffic load. They are calculated using the base station power consumption model defined in chapter 3. An ECG value higher than unity is achievable only if the reduction in power consumption of macro cells is larger than the power increase due to adding more pico cells. The energy throughput gain ETG is also estimated to determine whether the traffic offloading leads to an improvement in the bit/J metric of the heterogeneous RAN with respect to the same reference macro only deployment, as in (6.9).

$$ETG = TPG \cdot ECG. \tag{6.9}$$

6.2.5 Sleep mode

Sleep mode techniques include the approaches that fully or partially switch off the base station during low traffic load periods to avoid unnecessary power consumption in the network. Sleep mode is implemented by continuously monitoring the traffic load in the network to determine when to switch off the base station. In heterogeneous deployments, small cells can be safely switched off without compromising the coverage as the macro cells are able to provide backup coverage. This section provides an investigation of the effect of implementing the sleep mode on the energy consumption of heterogeneous RANs when a bursty traffic model is used to generate the offered traffic. In our analysis, the macro base stations remain on at all times, to provide the required coverage while the pico base stations are turned off during the idle periods.

Two schemes of sleep mode are often reported in the literature - centralised and distributed sleep mode schemes [97].

- In the centralised schemes, a central server with global knowledge of the network coordinates the process of determining when to use sleep mode and selects base stations to take the role of leaders to control the process of on/off switching of the base stations. The advantage of this scheme is that small cells can be completely switched off, while the disadvantage is a coordination between the base stations is required. Therefore, the backhaul links must stay continuously on.
- In distributed sleep mode schemes, no coordination between base stations is required: each base station must decide independently when to enter sleep mode, and when to wake up. The disadvantage of this scheme is that sleeping base stations cannot be fully switched off as they need to monitor the traffic in their coverage area to decide when to wake up. On the other hand, further savings can be achieved by partially switching off the backhaul links, which represent a major energy consuming unit in small cell deployments.

A basic architecture of a pico cell base station is shown in Figure 6-2. The approximate power consumption of each unit is also indicated. If a centralised sleep mode scheme is employed, the pico cell can be completely switched off, which can save approximately 7 watts per pico cell. However, the backhaul link must stay on as the on/off process is controlled by a central base station which needs to communicate with the small cells via the backhaul links. Hence, a certain amount of power is still required to operate the fibre backhaul link even if the pico base station is in sleep mode.

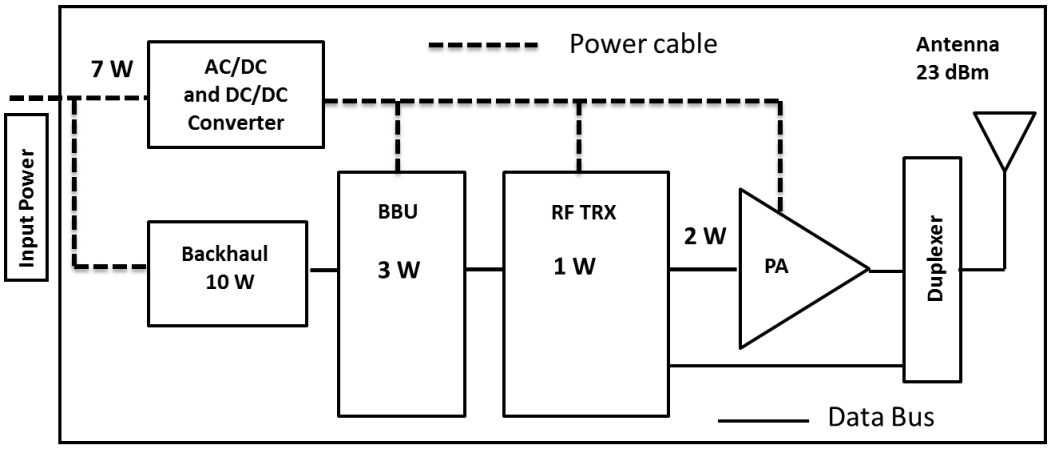

Figure 6-3: The picocell base station basic architecture

In distributed sleep mode schemes, the base station cannot be switched off completely as it must continuously monitor the traffic in its coverage area to decide when to wake up. The uplink RF transceiver is assumed to be able to perform this functionality by initiating a wake-up signal whenever it detects a signal above a certain threshold. Hence, a maximum consumed power of 1 watt is enough to operate the RF transceiver whilst in sleep mode. As no coordination between the base stations is required in this scheme, the backhaul link can also enter the sleep mode by turning off the fibre interface port at the base station, and at the aggregation node. The

aggregation node is located at the other end of the backhaul fibre link. The consumed power per base station in the aggregation node can be calculated by dividing the overall power consumption of the aggregation node by the total number of backhaul links connected to the node. For instance, the brocade 6505 switch [135] has a power consumption of 3.3 watts per port: this value can vary if a different type of aggregation nodes is used. A value of 3.5 watts is used throughout this chapter when estimating the RAN energy consumption when the sleep mode is enabled in picocells.

To evaluate the improvement in the RAN ECG when the sleep mode is enabled, equation (6.8) is modified to incorporate the sleep mode functionality. Each cell i is assumed to have a sleep mode indicator s_i which equals zero, if the pico cell average traffic load is zero and the cell is in sleeping status, otherwise it is equals one. Note that s_i is always equal to one for macro cells, as they never enter sleep mode in our analysis. The ECG when sleep mode enabled can be expressed as (6.10).

$$ECG = \frac{\sum_{i=1}^{M} P_i(\alpha_i)}{\sum_{i=1}^{K \cdot M} s_i \cdot P_i(\hat{\alpha}_i) + \sum_{i=1}^{K \cdot M} (1 - s_i) \cdot \hat{P}_i}, \quad (6.10)$$

Where $\hat{P}_i$ refers to the power consumption of base station i in sleep mode. Similarly, the backhaul power consumption must be taken into account when calculating the ECG, denoting the backhaul power consumption per base station by P_{bh} in active mode, and by $\hat{P}_{bh}$ in sleep mode. The ECG expression can be rewritten as (6.11).

$$ECG = \frac{\sum_{i=1}^{M} (P_i(\alpha_i) + P_{bh})}{\sum_{i=1}^{K \cdot M} s_i \cdot (P_i(\hat{\alpha}_i) + P_{bh}) + \sum_{i=1}^{N \cdot M} (1 - s_i) \cdot (\hat{P}_i + \hat{P}_{bh})}. \quad (6.11)$$

6.2.6 The system level simulation process

A Matlab system level simulator is developed to evaluate the TPG, ECG, ETG and the improvements in the user average throughputs compared to a reference deployment of a macro only scenario. The three mentioned metrics are evaluated at various pico cell densities as the number of deployed pico cells per one macro cell is increased from 2 to 12. The full list of parameters used in the simulation is shown in Table 6-1. Two cases are simulated: uniform user distribution and clustered user distribution. In the second case, 75% of the users are distributed in clusters around the pico cells while the remaining 25% are uniformly distributed in the target area. A value of 75% is selected only as an example of high clustering level to evaluate the effect of deploying the pico cells in hot spot zones on the RAN performance and power consumption.

The process of developing Matlab based system level simulator to evaluate the throughput and energy consumption of a heterogeneous RAN is divided into several steps. These steps are listed and briefly explained in the following subsections. Flow diagrams of the simulation process are also shown to clarify the simulation methodology further.

Table 6-1: Simulation parameters

Parameter	Value
Frequency (MHz)	2000
Bandwidth (MHz)	20
Frequency allocation	Co-channel frequency allocation
Macro transmitted power (dBm)	46
Pico transmitted power (dBm)	24
Macro BS Antenna gain (dBi)	15
Pico BS antenna gain (dBi)	6/2
Pathloss model (dB) & Shadowing	3GPP Uma & Umi
Traffic Model	FTP
File size F (MByte)	2
Mean reading time D (second)	5
Number of users	600 Indoor
Scheduling	Round Robin
Macrocells number	19
Macro cell radius (km)	0.5
Picocells per Macro K	Vary from 0 to 12
TTI interval (ms)	1
Number of simulated TTIs	40000

6.2.6.1 Deployment step

The process in this step is explained by the flow diagram in Figure 6-4. The main tasks included in this step are summarised as follows:

1) The definition of simulation parameters, such as the number of macro and picocells, bandwidth, transmit power, antenna gains, cell range expansion bias value, duration of the simulation, number of TTIs and the parameters of FTP traffic model.
2) The deployment of macro cells as a hexagonal grid and the pico cells as uniformly deployed in the target area. The users are deployed either uniformly or in clusters around the small cells.

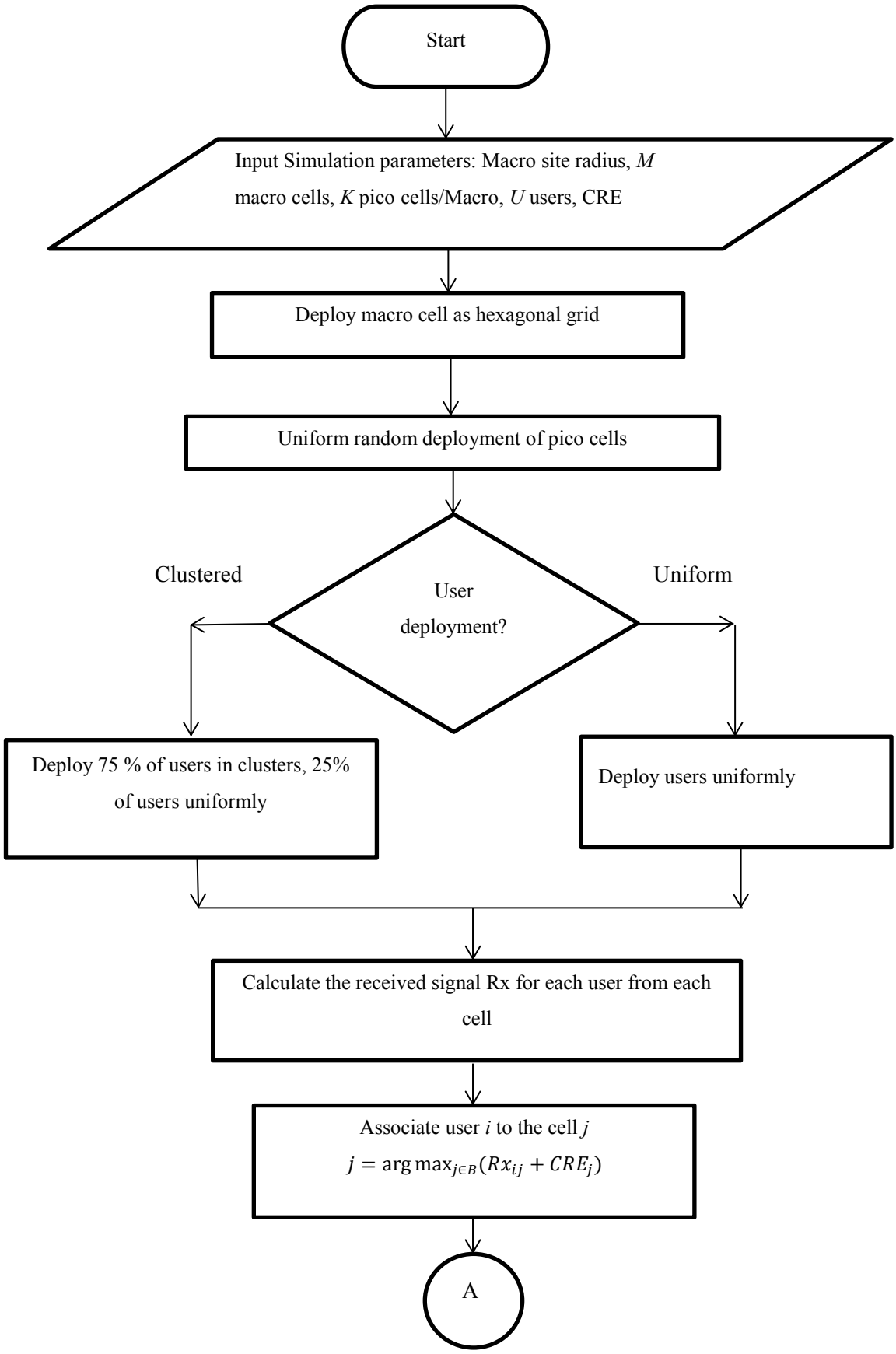

Figure 6-4: The process of the deployment step

3) The estimation of the large-scale fading matrix between each user and each deployed base station using the 3GPP Uma & Umi model, and used to calculate the received power at each user equipment from every deployed base station.
4) The association of each user equipment to the cell which provides the strongest received signal plus the CRE is carried out.

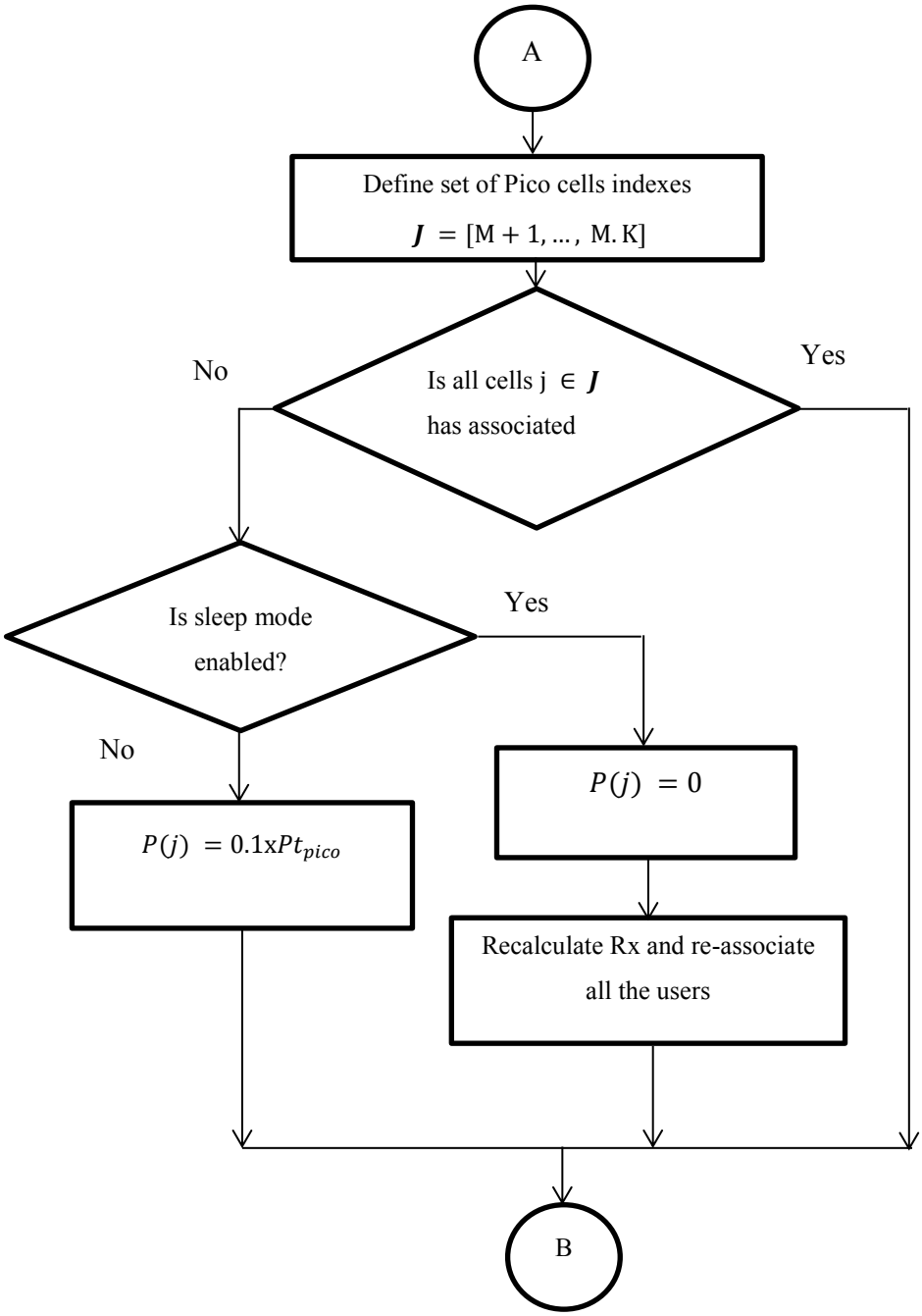

Figure 6-5: The process of switching off idle picocells

6.2.6.2 Switching off idle picocells

The flow diagram of the tasks included in this step is shown in Figure 6-5. The main tasks are listed as follows:

1) Check if any picocell has no associated users, while no sleep mode is implemented in the macrocells. The picocell base station enters sleep mode each time there no active users attached to it. Hence no degradation in the RAN throughput is observed when the sleep mode is enabled. Sleep mode can be also activated at any specified target number of active users attached to the small cells, but this would lead to a degradation in the per-user throughput.
2) If no sleep mode is enabled, reducing the transmitted power of any idle pico cell to 10% of its maximum transmit power, which corresponds to transmitting only the reference and broadcasting signals.
3) When the sleep mode is enabled, switch off any idle picocells.
4) If at least one picocell is switched off, recalculate the received power at each end user and repeat the user association process.

6.2.6.3 The generation of FTP user traffic

The users start to generate the FTP download sessions according to the employed traffic model. The details of this step are shown in Figure 6-6 and listed as follows:

1) Initiation of the users' queues and starting the simulation of the first TTI interval.
2) In each interval, find the users with non-empty queue, i.e. who have data to download.
3) If a user has an empty queue, determine whether this user will generate a new download request during the current interval by generating a random uniform number and comparing it versus the probability of the arrival of the user's new request.
4) Repeat the check for all users and update the queue status for every user in the current TTI interval.

6.2.6.4 Sleep mode and user throughput estimation.

This step includes a combination of the sleep mode implementation and user throughputs calculation, as shown in Figure 6-7. The main tasks are detailed as follows:

1) Calculation of how many active users per cell. Any picocell with no active users is switched off or its transmitted power is reduced to 10% of its full transmitted power when no sleep mode is enabled.
2) Reduction of the transmit power of any idle macro (cell has no active users) to 10% of its maximum transmitted power. This task is not shown in Figure 6-7 as it is exactly the same as with picocells, except that no sleep mode is enabled for macrocells.
3) Recalculate the received power for each user from every cell and calculate the SINR for all the users in the TTI interval z.
4) For each active user, allocate the bandwidth according to round robin scheduling algorithm and calculate the user achieved data rate.

5) Update the queue of every user by subtracting the amount of downloaded data during the current TTI interval from the previous size of the queue and continue to the next active user.

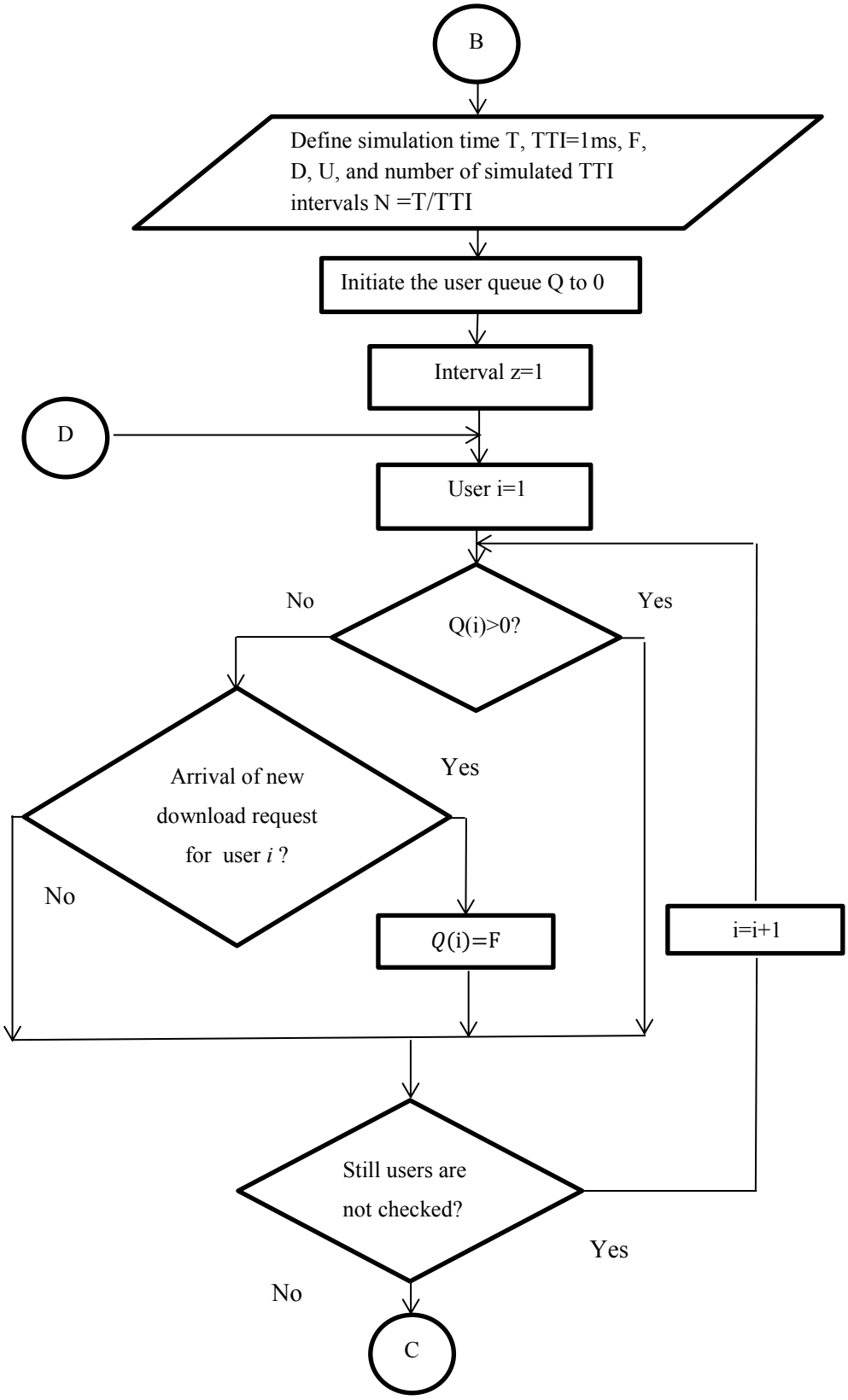

Figure 6-6: The process of the generation of FTP user traffic

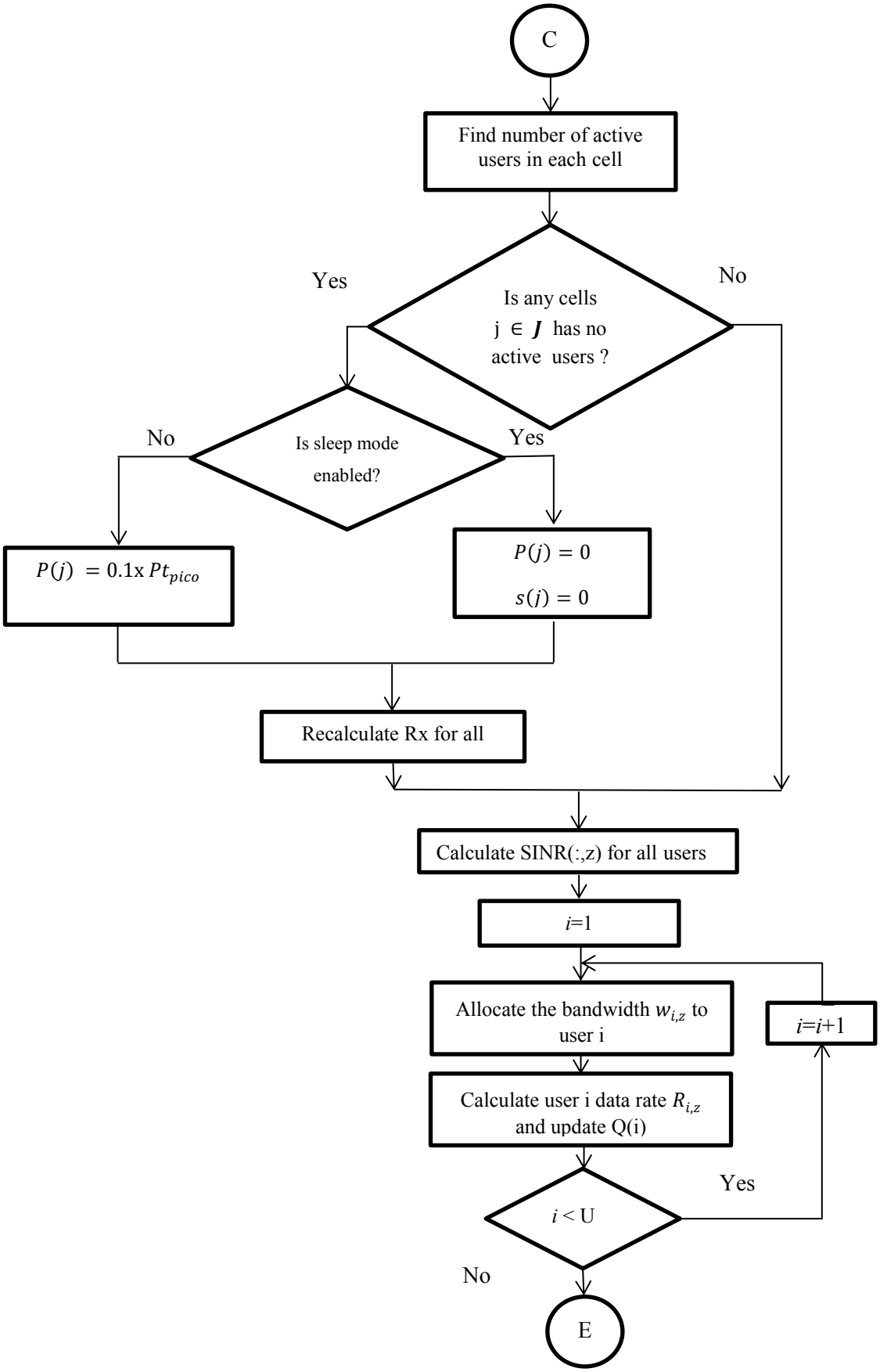

Figure 6-7: The process of the sleep mode and user's data rate calculation

6.2.6.5 Collection of results

This step includes estimating the average traffic load in every cell in the current interval, then continuing to the next TTI interval until the simulation ends. At the end of the simulation, the results of cell traffic load values and user's data rates are collected to be used in estimating the RAN average throughput in every simulated TTI interval. The results are averaged over the total number of simulated TTI intervals to be used to calculate the RAN power consumption, as illustrated in Figure 6-8.

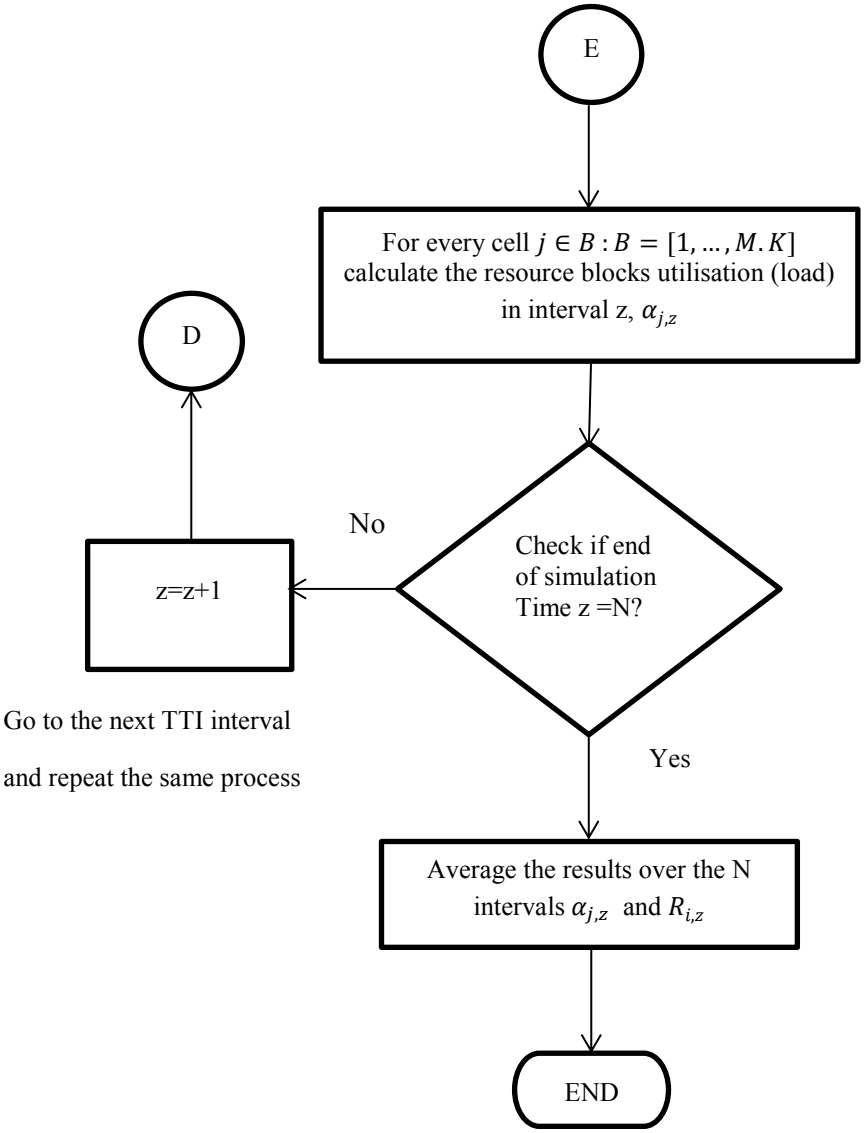

Figure 6-8: The process of collection of results

6.2.7 Throughput and Energy consumption results

The results of per user's data rates are used to estimate the RAN average throughput at the various considered pico cell densities: the cell average traffic load results are used to estimate the RAN power consumption. The throughput gain TPG and ECG are calculated for the heterogeneous RANs with reference to the macro only deployment. The ECG is calculated for two cases: when no sleep mode is enabled, and when the sleep mode is enabled in picocells. Two user deployment scenarios have been simulated: uniform user distribution and clustered user distribution. In clustered user distribution, 75% of the deployed users are assumed to be in a hot sport around the pico cell locations.

6.2.7.1 Results for uniform user deployments

Figure 6-9 shows the results of users' average throughputs when the number of deployed small cells per macro cell is increased from 2 to 12. Three CRE bias values are simulated: 10, 15 and 20 dB. Two trends are clear in the figure, the user's average data rates is improved when increasing the number of deployed picocells and increasing the CRE bias values. CRE values choice has large impact on the RAN overall throughput, and the per-user data rates, high CRE values lead to more users attached to small cells and after certain value the average per-user data rate will start to degrade, while at low CRE values, the small cells become underutilised and this leads to degrading the RAN throughput and average per-user data rate.

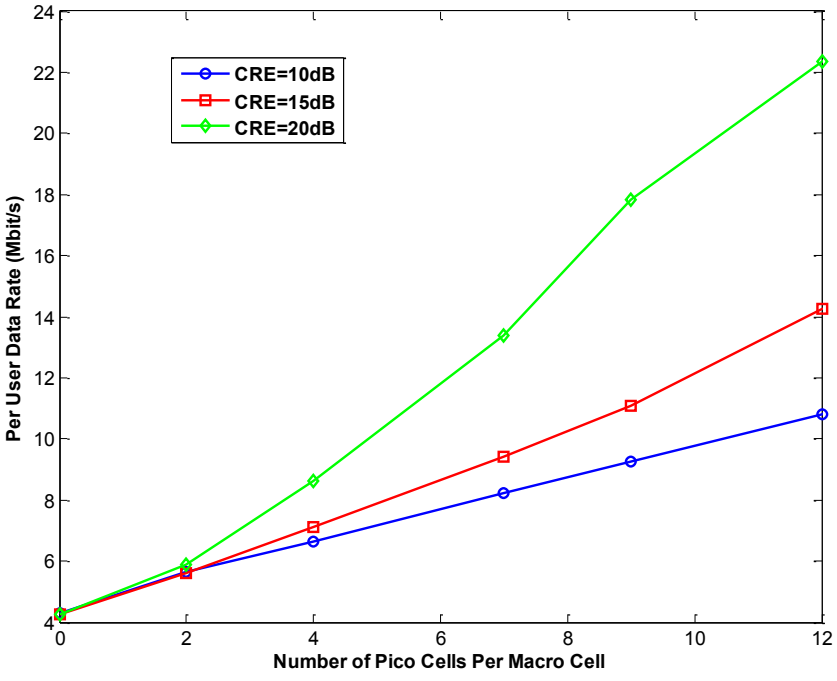

Figure 6-9: User's average data rates versus the pico cell density

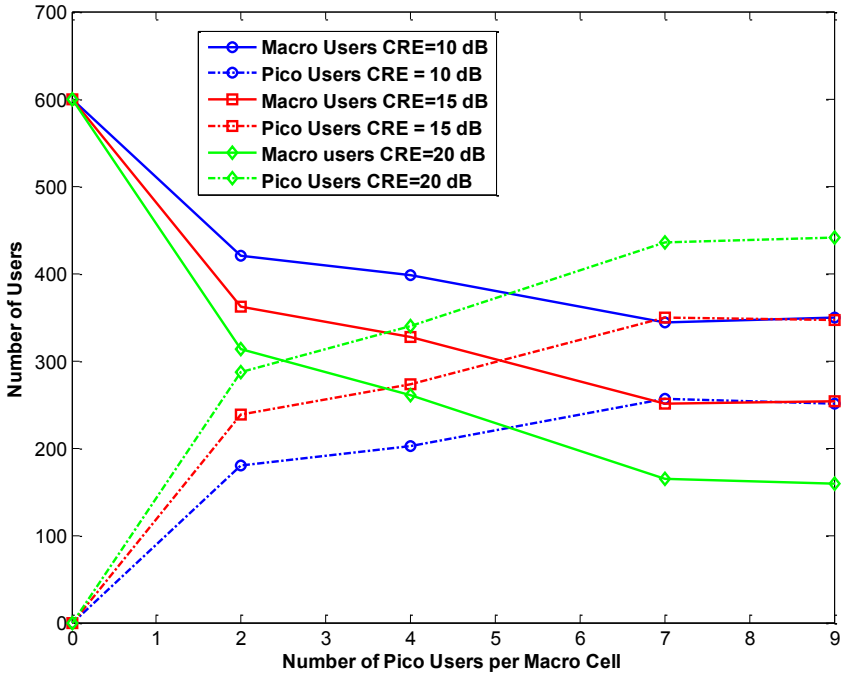

Figure 6-10: Number of macro and pico users versus the small cells density

The variation in the number of users offloaded to picocells versus the pico cell density and at different CRE values is shown in Figure 6-10. The number of users offloaded to the picocells can be increased by intensifying the pico cell density and/or by increasing the CRE bias value. For instance, the number of users associated with picocells increased four times when the pico cell density was augmented from 2 to 12 per macro cell. Similarly, when increasing the CRE from 10 dB to 20 dB, the number of pico users increased from 101 to 282 at a picocell density of 9 cells per macro cell, which can be very beneficial in terms of increasing the utilisation of picocells and improving data rates for macro users.

A. The TPG and ECG results

To quantify the possible achieved improvements in the throughput or energy consumption due to traffic offloading to picocells, we adopt the three figures of merit proposed in chapter 3: the TPG to measure any RAN throughput gains, the ECG to measure any energy consumption reduction, and the ETG to measure any relative gains in the bit/J metric with reference to the macro only deployment. Additionally, we aim to examine whether or not the ETG and ECG lead to same conclusions about the RAN energy efficiency. All these three figures of merits are evaluated with reference to the macro only scenario by using the equations (6.7) to (6.9). A clear improvement in the RAN TPG is shown in Figure 6-11 when the pico cell density is increased and when high CRE values are used. However, when evaluating the energy consumption, degradation in the ECG is observed in Figure 6-12 when more picocells are deployed. Importantly, increasing the CRE bias is detrimental to the ECG at low number of

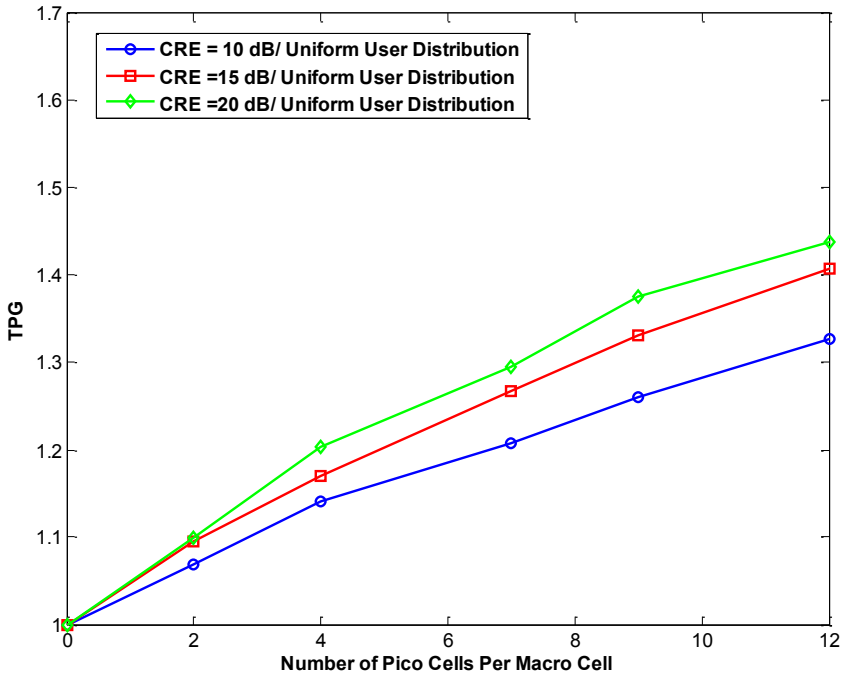

Figure 6-11: The results of TPG versus the small cell density

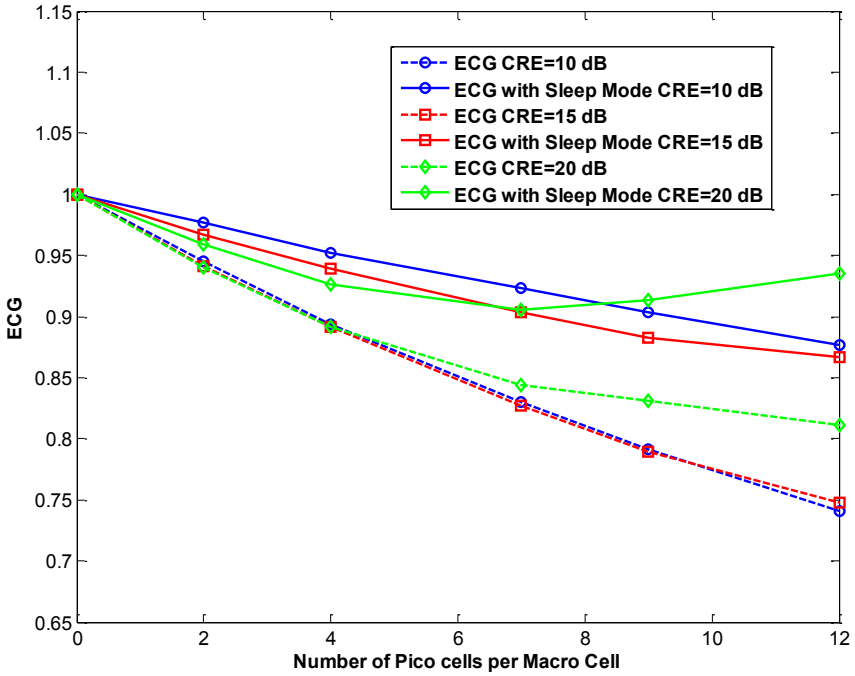

Figure 6-12: The results of ECG versus the small cell density

deployed picocells, which is due to the degradation in the throughput of cell edge pico users caused by the interference generated by the macrocells. At a high density of picocells, the number of users who share the resources of a single pico cell decreases, and they benefit from the availability of more bandwidth to each user, which means that they can finish their file download faster, leading to a reduction in the pico cells average traffic loads.

B. Sleep mode results

Enabling sleep mode in picocells can reduce the RAN energy consumption by avoiding unnecessary idle pico cells transmission when there are no active associated users. Turning off (fully or partially) any idle pico cell does not degrade the RAN coverage as the macro cells are assumed to be constantly on and able provide the required coverage. A distributed sleep mode scheme is implemented in our analysis, where an ideal on/off switching process of picocells is assumed. Hence, the obtained results here represent the potential of sleep mode rather than a realistic implementation case; in practice, certain delays are required to switch any base station on or off.

A power consumption of 1 watt used for sleeping pico base station power consumption and 3.5 watts for its backhaul link are used in this analysis. Figure 6-12 shows that the benefits of sleep mode are more visible at a high density of picocells. This is due to the probability of no active users in a certain cell is increasing when more picocells are deployed. Significant improvement in the ECG is observed when enabling the sleep mode as compared to the no sleep mode case. For example, a 12% improvement in the ECG is achieved by enabling the sleep mode at a number of 12 deployed pico cells per macro cell. Unfortunately, this improvement is not sufficient to increase the ECG above one.

Evaluating the heterogeneous RAN energy efficiency using the ETG metric may lead to different conclusions about the RAN energy consumption. For example, the results for ETG in Figure 6-13 show a continuous improvement in the bit/J metric versus the number of deployed pico cells when the CRE equals 15 and 20 dB. While an optimum density of 4 pico cells per macrocells is observed when a CRE value of 10 dB is assumed, this result does not agree with the conclusions obtained from the ECG. The ETG shows an increasing improvement in the RAN energy efficiency versus the pico cell density when the sleep mode is enabled in picocells.

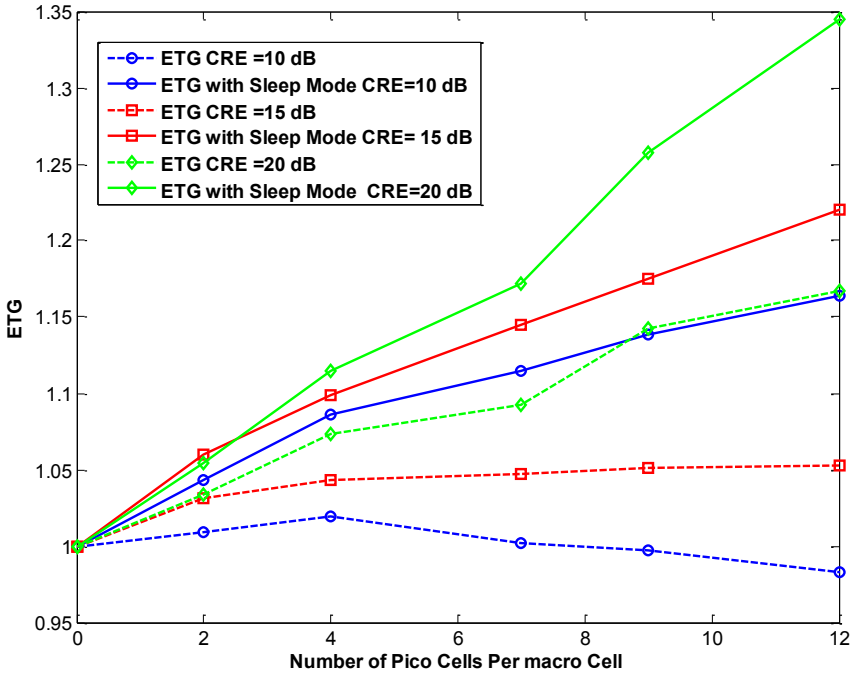

Figure 6-13: Results of RAN ETG

6.2.7.2 The results for clustered user deployments

The results of the last section have shown that uniform use deployment of small cells leads to an improvement in the user's data rates as well as in the overall RAN average throughout. However, a rise in RAN energy consumption has also been observed. In practice, small cells are often deployed in high demand locations (hot spots) to provide better coverage and less sharing of spectrum. More traffic can be offloaded to picocells in this type of deployment, which can lead to a reduction in the RAN energy consumption. In this section, the same issue of RAN throughput and energy consumption is investigated, when 75% of the users are assumed to be deployed in clusters around the pico cells while the remaining 25% are deployed uniformly in the target area. Our objective in doing this is mainly to investigate whether or not a real reduction in the RAN energy consumption is achievable. Figure 6-14 shows that more than 400 users among the total 600 deployed are associated with the pico cells at pico cell density of 7 per macro cell and at CRE value of 20 dB. This results in a more efficient utilisation of the picocells and an improvement in the user average data rate, as shown in Figure 6-15.

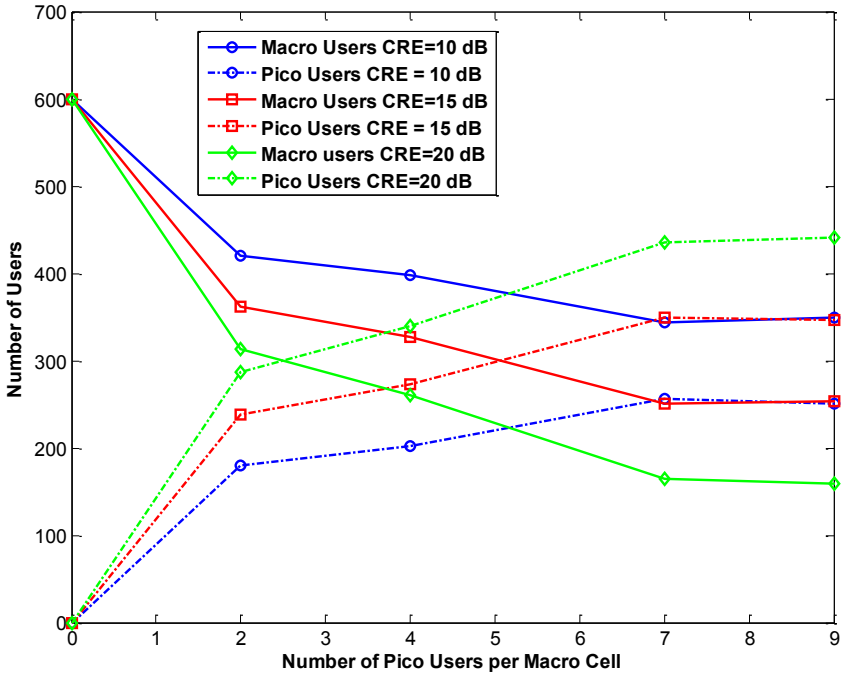

Figure 6-14: Number of macro and pico users in clustered deployments

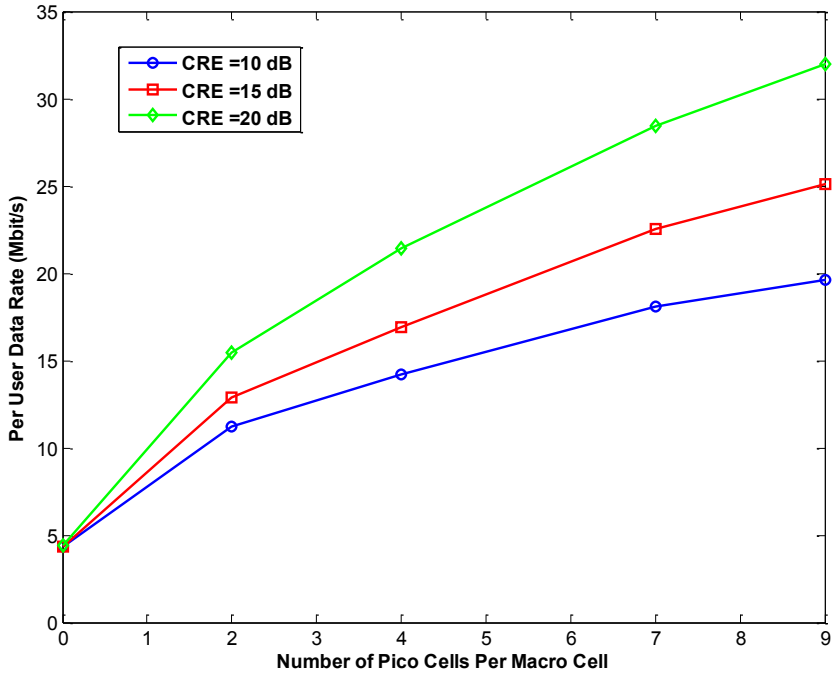

Figure 6-15: User's average data rates clustered deployments

Significant improvement in the RAN TPG is also achieved compared with the non-clustered case (see Figure 6-16). The TPG improves versus the increase in picocell density before starting to degrade slightly at picocell densities above 8. It is clear that the relationship between the TPG

and CRE value depends on the assumed pico cell density: at low pico cell densities, increasing the CRE can be detrimental to the RAN average throughput as the majority of the users associated with the pico cells suffer from high interference from the macrocell base stations. This observation disappears at high pico cell densities as the low SINR values are compensated by the availability of more bandwidth.

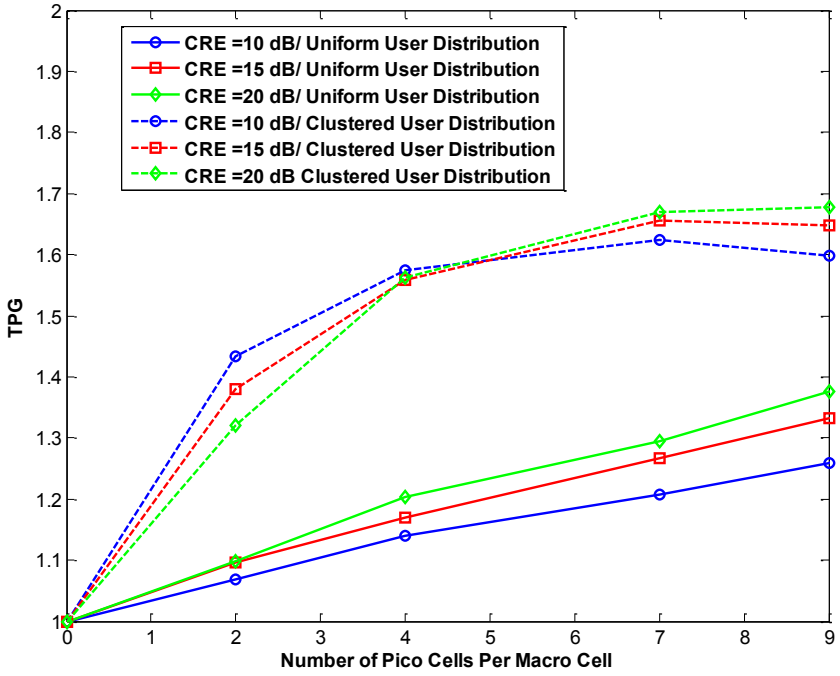

Figure 6-16: Results of TPG in clustered deployments

Interestingly, Figure 6-16 and 6-17 show that joint improvement in the TPG and ECG are achievable at CRE values of 15 and 20 dB. For instance, TPG of 1.3 and ECG of 1.2 are achieved when deploying 2 pico cells per macrocells. Thus, a 30% improvement in the RAN throughput and 20% reduction in the RAN energy consumption are obtained simultaneously. In contrast, no energy consumption reduction is observed when the CRE value is 10 dB. One must not forget that increasing the CRE value has a negative impact on the pico cell edge users; fortunately, implementing an interference mitigation technique (eICIC) can mitigate this issue, as we will show in section 6.3.

Moreover, enabling sleep mode in picocells provides further improvement in the RAN ECG. This improvement is more significant at high pico cell densities, as shown in Figure 6-17.

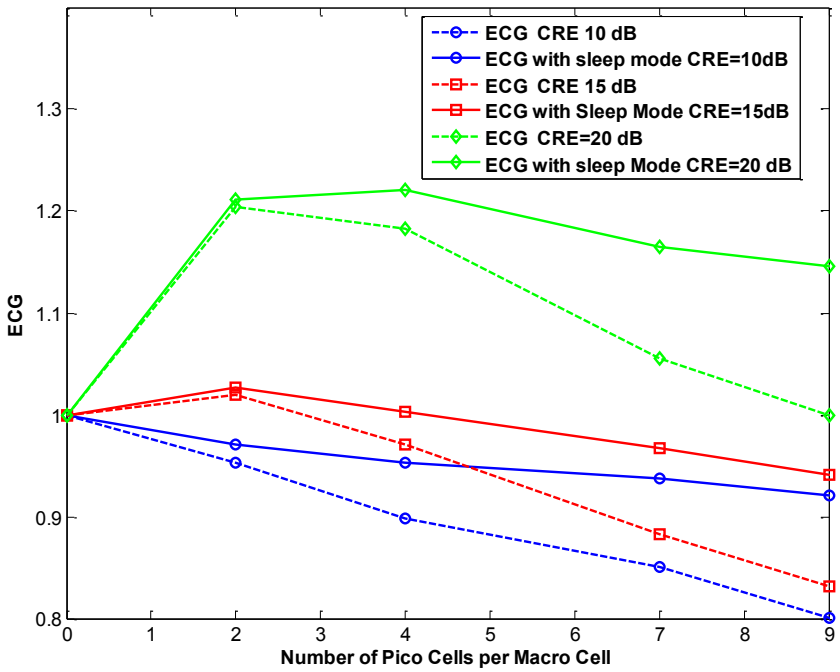

Figure 6-17: Results of ECG in clustered deployments

Finally, all the curves of the RAN ETG in Figure 6-18 are above one, meaning that the bit/J metric is improving versus the pico cell density.

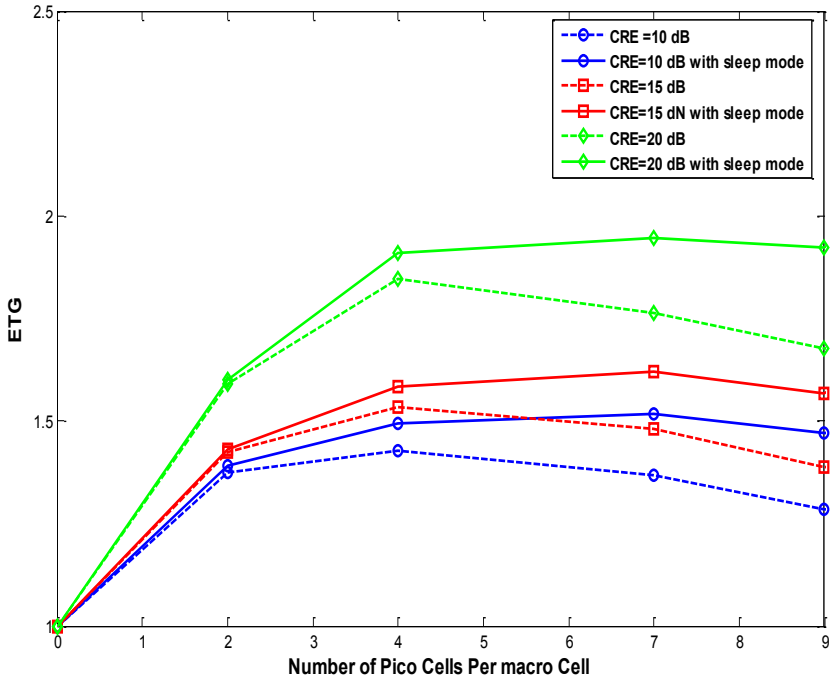

Figure 6-18: Results of ETG in clustered deployments

The results in Figure 6-18 also show the existence of an optimum pico cell density where the ETG begins to degrade beyond this point. When comparing the results of ETG with the ECG

results, we observe that both show that enabling sleep mode in picocells leads to an improvement in the RAN energy efficiency, especially at high pico cell densities. They also show the existence of an optimum pico cell density when CRE is equal to 15 and 20 dB. However, the results do not agree at CRE equals 10 dB, as the ECG is below one and degrades versus the increase of picocell density, while the ETG is always above one and shows the existence of an optimum small cells density. Hence, relying only on bit/J as an energy efficiency metric does not provide the full picture of RAN energy consumption. Thus, a combination of the three figures of merits TPG, ECG and ETG is necessary to conclusively ascertain whether the improvement in the bit/J metric is due to a real reduction in the energy consumption or not.

6.3 Dense heterogeneous deployments with eICIC and sleep mode

Current cellular networks use macro cells to provide coverage and capacity, supported by Wi-Fi access points and distributed antenna systems DAS for indoor coverage. In contrast, small cells are deployed sparsely in hotspot zones to provide more capacity where needed or to extend the macro cell coverage. Given that the evolution of the next cellular network is not driven only by the need for improving the coverage or by the growth in traffic in certain zones but also by the need for high user data rates necessary for certain content types such as high definition video streaming, dense deployment of small cells where the density of small cells can be as high as the density of active users in certain cases is required.

However, many challenges face network operators when a dense layer of small cells is deployed on the top of an existing macro layer. These challenges include but are not limited to interference management, mobility management, backhaul requirements, and the rise in energy consumption due to the large number of deployed small cells.

The focus of this section is on two of these challenges: the interference management and rise in energy consumption. Our target is to investigate how implementing an inter-layer interference management technique coupled with switching off the idle small cells can be exploited to an improvement in the RAN average throughput and a reduction in the RAN energy consumption.

6.3.1 Interference management

Interference management is a critical issue in heterogeneous networks, especially when implementing the CRE technique to allow the user equipment to associate with small cells even if they receive a stronger signal from the macrocells. The issue of interference between the macro and small cells arises when both the macro and pico tiers share the same frequency band, as the small cell edge users who are located in the CRE zone will experience high interference from the neighboring macrocell (see Figure 6-19).

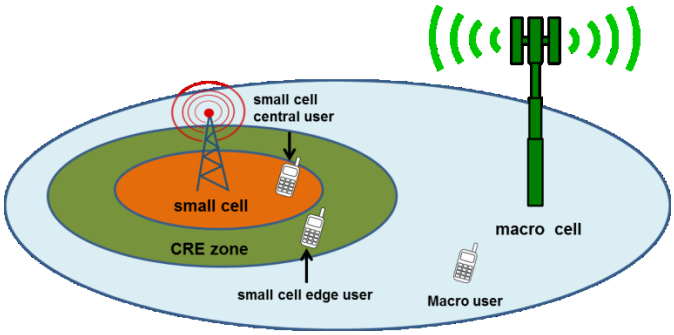

Figure 6-19: Heterogeneous RAN with CRE

An enhanced inter-cell interference coordination eICIC technique has been defined in the 3GPP LTE release 10 to allow the macro and small cells to share the same frequency band in different sub-frames. This technique uses a combination of an almost blank ABS subframe and cell expansion range expansion CRE to prevent the small cell edge users located in the CRE zone from being interfered by the macro cell signal. Different sub-frames are allocated to the two layers, and the CRE is used to expand the coverage of small cells to increase the number of users offloaded to the small cells. ABS contains only control and cell reference signals, and no data are transmitted. The macrocell transmits the ABS in a semi-static pattern and needs to inform the small cells about this pattern. Sub-frames are configured as ABS sub-frames in macro cells to allow scheduling of the small cells' edge users without being exposed to interference from the neighbor macrocell, as shown in Figure 6-20.

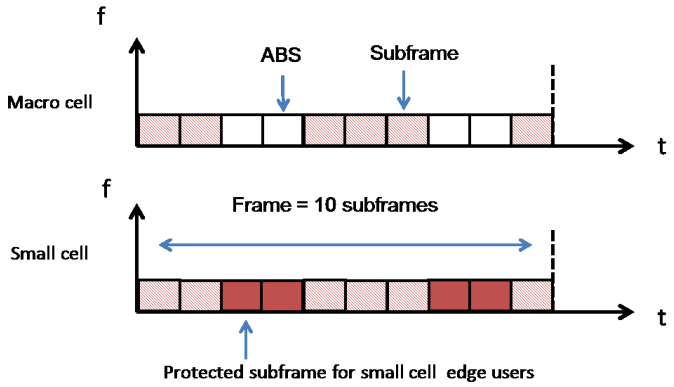

Figure 6-20: ABS format

6.3.2 System model of dense heterogeneous network

The same system model defined in section 6.2 is used here. *M* macro cells deployed in the form of an hexagonal grid, *K* pico cells per macro cells deployed uniformly, and *U* users distributed uniformly in the target area. The only difference between this and the system model defined in section 6.2 is a full buffer traffic model being used here and a time domain inter-cell interference coordination technique eICIC being implemented. The evaluated RAN corresponds to a dense heterogeneous network scenario where a small cell density of up to 50 pico cells per macro cell is considered while a fixed number of 1000 users are deployed uniformly in the

target area which corresponds to an average of 52 users per macro cell. The full list of simulation parameters are provided in Table 6-2.

Table 6-2: Simulation parameters

Parameter	Value
Frequency (MHz)	2000
Bandwidth (MHz)	20
Frequency allocation	Co-channel frequency allocation
Macro transmitted power (dBm)	46
Pico transmitted power (dBm)	24
Macro BS Antenna gain (dBi)	15
Pico BS antenna gain (dBi)	2
Pathloss model (dB) & Shadowing	3GPP Uma & Umi
Traffic Model	Full buffer
Number of users	1000 Indoor
Scheduling	Round Robin
Macrocells number	19
Macro cell radius (Km)	0.5
Picocells per Macro K	Vary from 0 to 50

6.3.3 Sleep mode

As with section 6.2.7, sleep mode is only enabled in the picocells which have no associated users. As a full buffer traffic model is used, any associated user is assumed to have always data to download. A distributed sleep mode scheme is employed, where each picocell decides independently when to enter the sleep mode and when to wake up. Hence, the backhaul links can also be partially switched off during the sleep mode period. Similar to section 6.2 A value of 1 watt is used to represent the power consumption of a sleeping picocell and 3.5 watts for its fibre backhaul link power consumption.

6.3.4 Simulation process

A Matlab system level simulation is developed to evaluate the RAN average throughput at various pico cell densities and various CRE bias values. A full buffer traffic model is employed in the simulation, and a distributed sleep mode technique is implemented in the idle picocells. The results obtained are used to calculate the TPG, ECG, and ETG of the evaluated deployments with reference to the macro only scenario. The simulation process in this section is simpler than in the case of a non-full buffer traffic model, the deployment and the on/off switching of picocells are exactly similar to those in section (6.2). Only uniform user distribution is considered here. The flow diagram of the deployment and sleep mode processes are depicted in Figure 6-21 and Figure 6-22.

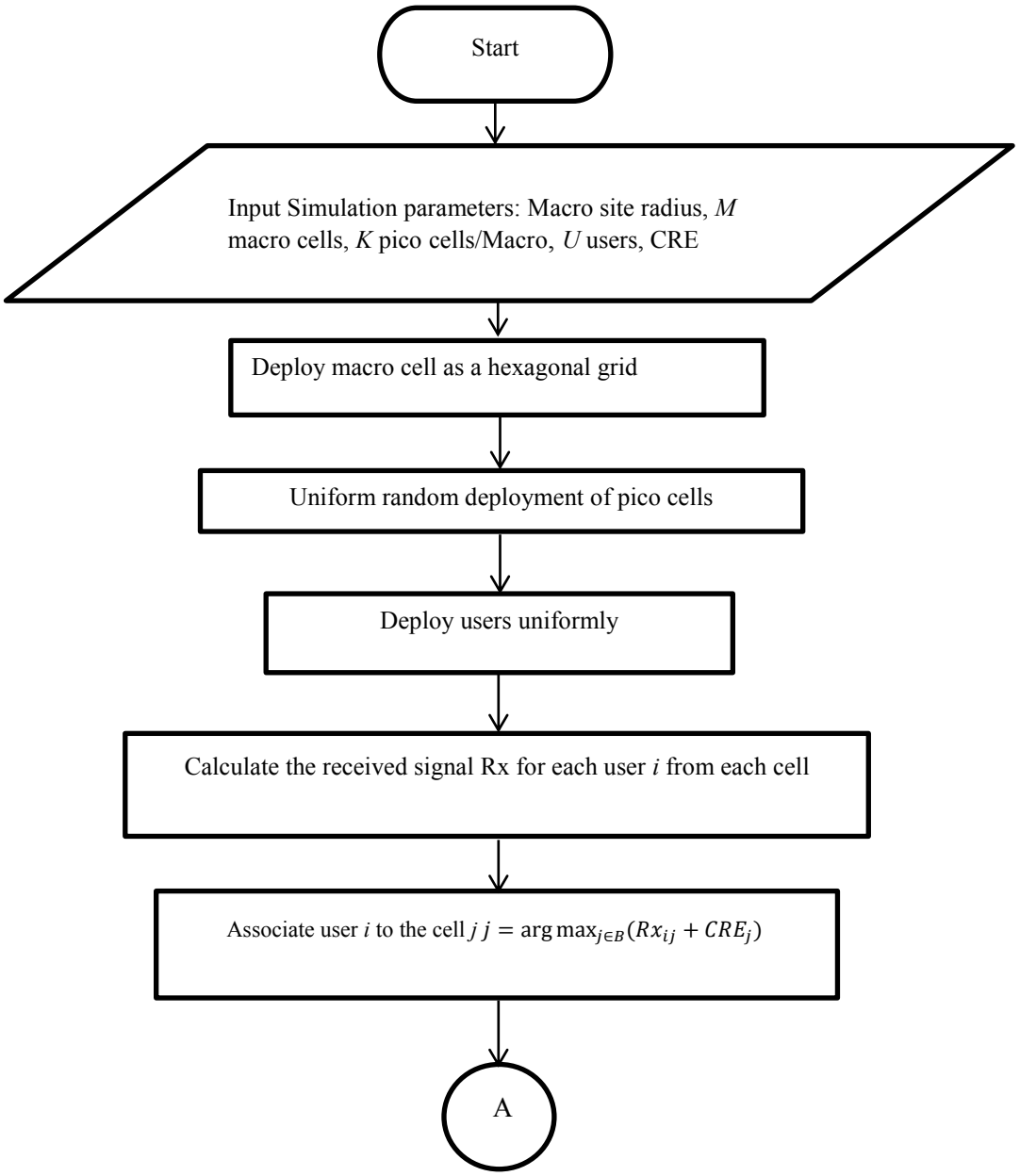

Figure 6-21: The flow diagram of deployment process

The remaining steps in the simulation process are summarised as follows:

6.3.4.1 Classification of users

In this step, the deployed users are classified to macrocells users U_m , central pico cell users U_{cp} and edge pico cell users U_{EP}. The classification between central and edge users is based on the user's SINR value: any pico user with SINR less than -3 dB is classified as an edge user. The classification is required to determine which users can be scheduled during the ABS sub-frames.

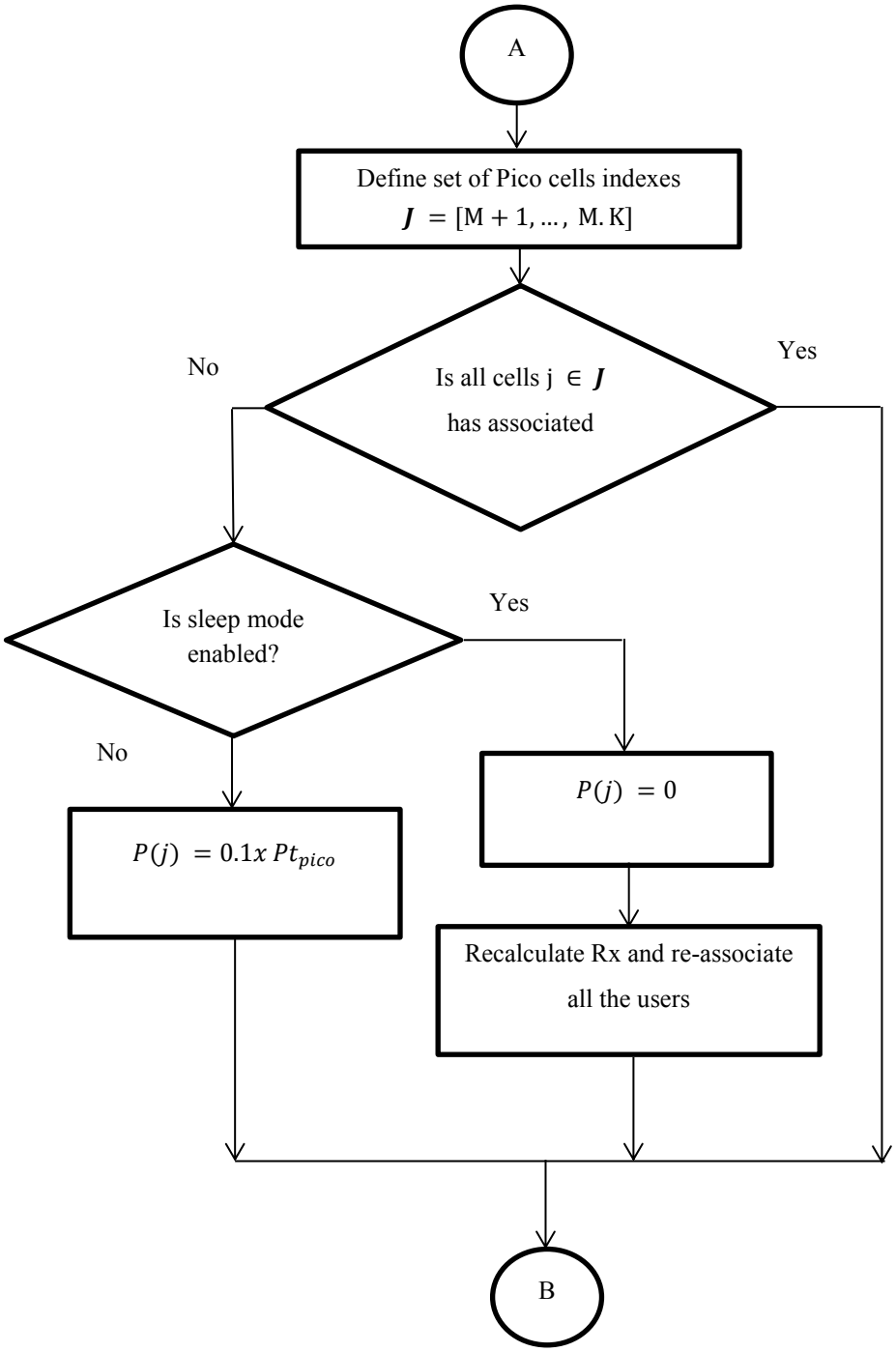

Figure 6-22: Sleep mode enabling process

6.3.4.2 Determination of ABS pattern

The determination of the ABS pattern is a semi-static process and must be updated regularly following the variation in user traffic distribution; it is updated every 40 ms in FDD LTE systems [136]. Two simple approaches are proposed to determine how many ABS sub-frames are configured in each frame. In the first approach, termed eICIC1, the number of ABS

subframes is calculated as the ratio of all pico users U_{cp} $+U_{EP}$ to the total number of deployed users U. In the second approach, termed eICIC2, the number of ABS sub-frames equals the ratio of the number of pico cell edge users U_{EP} to the total number of users U. As the number of ABS sub-frames must be an integer, the least succeeding integer of the ratio is selected, as shown in (6.12) for eICIC1 and (6.13) for eICIC2.

$$N_{ABS} = \left\lceil \frac{N_{U_{cp}} + N_{U_{EP}}}{N_U} \right\rceil, \tag{6.12}$$

$$N_{ABS} = \left\lceil \frac{N_{U_{EP}}}{N_U} \right\rceil, \tag{6.13}$$

Where $N_{U_{cp}}$, $N_{U_{EP}}$, and N_U represent the number of central pico users, the number of edge pico users, and the total number of deployed users, respectively. N_{ABS} is the number of ABS sub-frames per frame.

6.3.4.3 SINR and user data rate estimation

During the ABS sub-frame simulation, the SINR is calculated by considering the interference generated by the active pico cells only, which leads to an improvement in the SINR of the pico edge users. Depending on the adopted ABS determination approach, all the pico users in eICIC1 or only the pico edge users in eICIC2 are scheduled during the ABS. The round robin scheduling algorithm is used to allocate the spectrum resources among the scheduled users evenly. On the other hand, the macro cell users and pico cell central users are scheduled during the non ABS sub-frame simulation, and their SINR is calculated by considering the interference from all active cells. Similarly, the spectrum is allocated evenly between the scheduled users. The user data rate is calculated by using Shannon formula, as shown in the flow diagram in Figure 6-23.

6.3.5 Throughput and energy consumption analysis

The last step in the simulation is the collection of the results of users' average data rates. The results depend on whether an ABS or normal sub-frame is simulated. The final results must be averaged by taking into account the ratio between the number of ABS sub-frames and the total sub-frames per frame, as shown in (6.14).

$$\bar{R}_{user} = \frac{N_{ABS}}{N_{SF}} \cdot R_{user,ABS} + \left(1 - \frac{N_{ABS}}{N_{SF}}\right) \cdot R_{user,NSF}\ , \tag{6.14}$$

Where $\bar{R}_{user}$, $R_{u,ABS}$ and $R_{u,NSF}$ are the user average data rate, the user average data rate during the ABS and the user average data rate during normal sub-frames, respectively. N_{SF} refers to the number of sub-frames per frame.

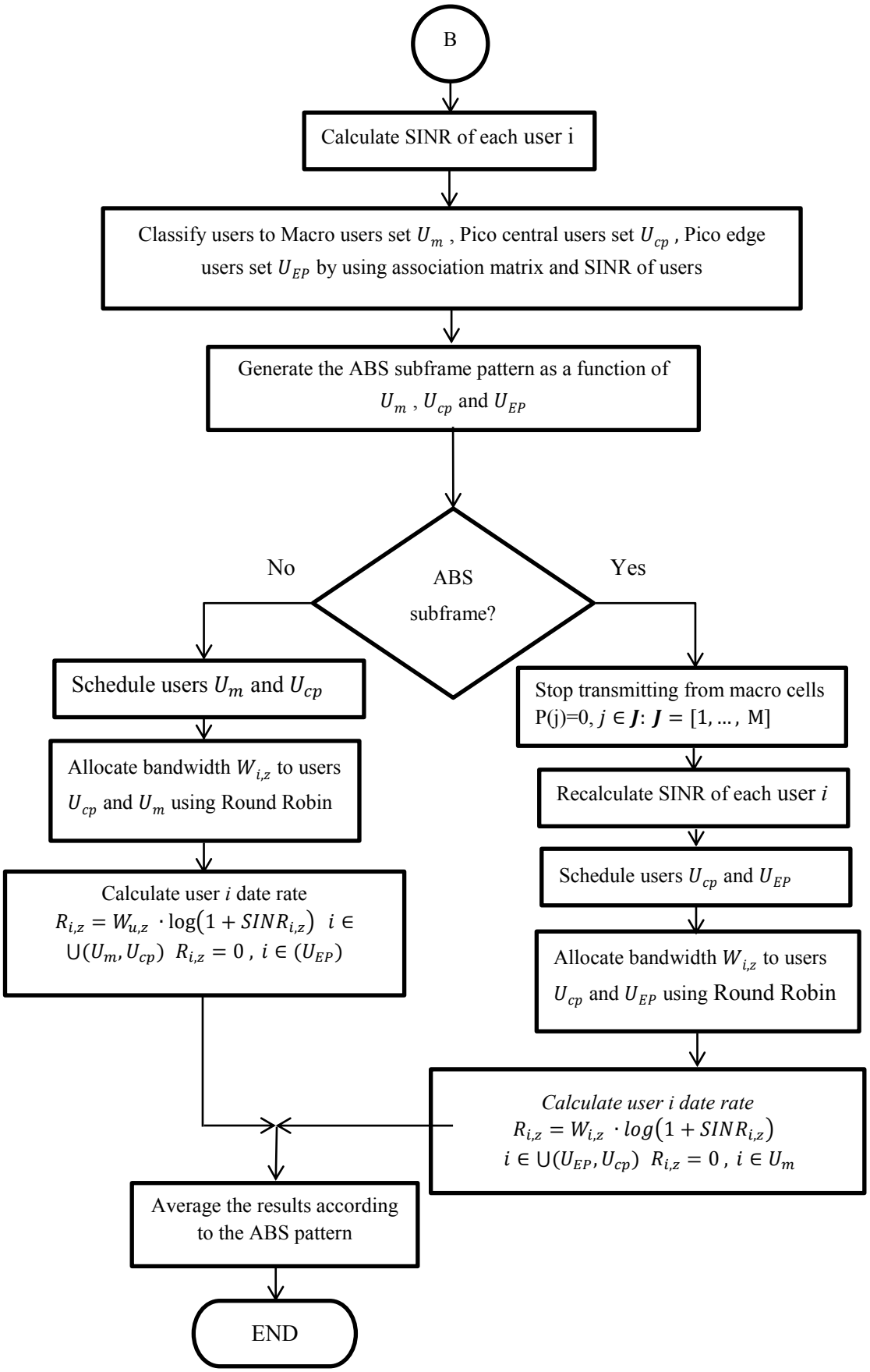

Figure 6-23: The flow diagram of eICIC simulation process

6.3.5.1 The TPG and ECG analysis

After calculating the users' average throughputs R_u , the cell average throughput R_{cell} is calculated as the sum of the throughput of users associated to the cell, as in (6.15).

$$R_{cell,i} = \sum_{u=1}^{n} \bar{R}_{user,u} \,, \tag{6.15}$$

Where *n* refers to the number of users associated with the cell. To simplify the notation, we drop the subscript cell from $R_{cell,i}$,and refer to the cell average throughput in the heterogeneous deployment by $\hat{R}_i$, and to the cell average throughput in the macro only deployment by R_i . The RAN throughput gain TPG can be calculated with reference to the macro only deployment, as in (6.16).

$$TPG = \frac{\sum_{i=1}^{K \cdot M} \hat{R}_i}{\sum_{i=1}^{M} R_i} \,. \tag{6.16}$$

Similarly, the RAN ECG is calculated using (6.17). We can see in (6.17) that the ECG is always less than one because the power consumption of any deployed picocell is always higher than zero irrespective of sleep mode is enabled or not.

$$ECG = \frac{\sum_{i=1}^{M} P_i}{\sum_{i=1}^{K \cdot M} P_i} = \frac{\sum_{i=1}^{M} P_i}{\sum_{i=1}^{M} P_i + \sum_{i=M+1}^{K \cdot M} P_i} \,. \tag{6.17}$$

As the backhaul power consumption cannot be ignored in heterogeneous networks, its power consumption is included in the ECG calculation, as shown in (6.18).

$$ECG = \frac{\sum_{i=1}^{M} (P_i + P_{bh,i})}{\sum_{i=1}^{N \cdot M} (P_i + P_{bh,i})} \,, \tag{6.18}$$

Where $P_{bh,i}$ refers the backhaul power consumption of the cell *i.* If sleep mode is enabled in pico cells, any pico cell with no associated users is deactivated. The variable s_i refers to the cell status and equals zero if the cell is in sleep mode. Hence, the ECG expression in (6.18) is extended to include the effect of sleep mode, as shown in (6.19).

$$ECG = \frac{\sum_{i=1}^{M} (P_i + P_{bh,i})}{\sum_{i=1}^{K \cdot M} s_i \cdot (P_i + P_{bh,i}) + \sum_{i=1}^{K \cdot M} (1 - s_i) \cdot (\hat{P}_i + \hat{P}_{bh.i})} \,. \tag{6.19}$$

The terms $\hat{P}_i$ and $\hat{P}_{bh.i}$ refer to the power consumption of the sleeping base station in cell *i*ts backhaul, respectively.

The implementation of the eICIC interference coordination technique does not lead only to the improvement of the throughput of picocell users, but also to a reduction in the RAN energy consumption by stopping transmission from the macro cell during the ABS sub-frames. This

reduces the power consumption of the macro cell. Note that the reference and broadcasting signals still need to be transmitted during the ABS sub-frames, which represents 10% of the base station's full transmitting power. For instance, the power consumption of an omnidirectional macro base station is decreased from 450 watts to 188 watts when the RF transmitted power is reduced from 40 to 4 watts. To evaluate how the RAN ECG can be improved from the implementation of the eICIC, the power consumption of macrocells is split into two parts: the $P_{macro,NSF}$, which refers to average power consumption of macro cells during normal sub-frames, and $P_{macro,ABS}$, which refers to the power consumption of macro cells during the ABS sub-frames. These are estimated by (6.20) and (6.21).

$$P_{macro,NSF} = \left((1 - \frac{N_{ABS}}{N_{SF}}) \cdot \sum_{i=1}^{M} s_i \cdot (P_i + P_{bh,i}) \right), \tag{6.20}$$

$$P_{macro,ABS} = \left(\frac{N_{ABS}}{N_{SF}} \cdot \sum_{i=1}^{M} s_i \cdot (P_i(\alpha_s) + P_{bh,i}) \right), \tag{6.21}$$

Where $P_i(\alpha_s)$ refers to the macro cell power consumption during the ABS subframe and α_s refers to the cell average load due to reference and broadcasting signals. Equation (6.19) is modified to incorporate the impact of eICIC on the RAN ECG, as shown in (6.22).

$$ECG = \frac{\sum_{i=1}^{M}(P_i + P_{bh,i})}{P_{macro,NSF} + P_{macro,ABS} + \sum_{i=M+1}^{K \cdot M} s_i \cdot (P_i + P_{bh,i}) + \sum_{i=M+1}^{K \cdot M}(1 - s_i) \cdot (\hat{P}_i + \hat{P}_{bh.i})}. \tag{6.22}$$

Equation (6.22) demonstrates that more improvement in the RAN ECG is obtainable by further reduction in the power consumption of a sleeping picocell $\hat{P}$ and in its backhaul power consumption $\hat{P}_{bh.i}$, or also by allowing the macro base stations to enter fast DTX mode during the ABS subframes. The benefits of implementing the DTX in macro base stations has been already investigated in chapter 5 and is not included in this chapter.

Finally, the energy throughput gain ETG is evaluated for the heterogeneous RANs to evaluate how the bit/J metric varies with the pico cell density, at different CRE values.

6.3.5.2 The TPG and ECG results

As indicated earlier, the three figures of merit TPG, ECG and ETG are calculated for the evaluated heterogeneous network, which consists of macrocells deployed in the form of hexagonal grid with a cell radius of 500 m, and an overlay of picocells with a density of

deployment varying from sparse to dense (50 pico cells per single macro cell). The range of considered values for the CRE vary between 10 dB and 20 dB to investigate the impact of changing the cell expansion range on the RAN TPG and RAN ECG. Four cases are considered in this simulation:

- No sleep mode and no eICIC
- Sleep mode and no eICIC
- Sleep mode and eICIC1
- Sleep mode and eICIC2

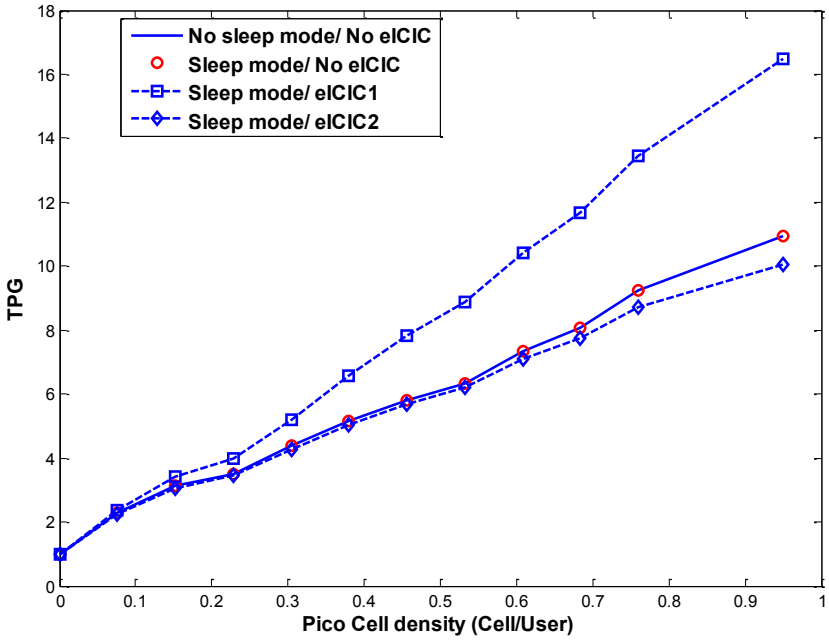

Figure 6-24: Results of RAN TPG at CRE 10dB

Figures (6.24) to (6.26) show the results for the RAN TPG at different pico cell densities and at various CRE values. The results clearly indicate that implementing sleep mode does not lead to any degradation in the RAN TPG. This is because picocells are switched off only if they have no associated users. Also, the improvement in RAN TPG due to turning off the idle pico cells is negligible because the interference generated by the macrocells dominates the interference between the picocells. By comparing the RAN TPG when eICIC1 and eICIC2 are implemented, we observe that eICIC1 provides higher TPG values. For example, eICIC1 provides a TPG value of 16 versus 10 provided by eICIC2 at a high density of deployed picocells. Unlike the eICIC1, the eICIC2 does not provide any gains to the RAN TPG at CRE of 10 dB while a very small improvement in the RAN TPG is observed at medium pico cell densities (0.3 to 0.7 cell/user) for CRE values of 15 and 20 dB, as shown in Figure 6-25 and Figure 6-26. At high

pico cell densities, the interference between the pico cells starts to increase during the ABS sub-frames, and this has a negative impact on both the edge pico users and the central pico users.

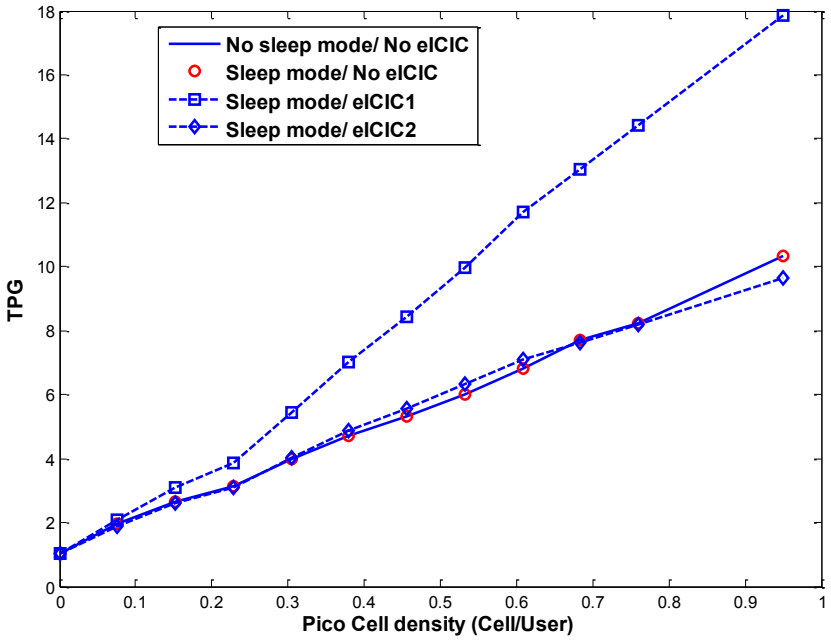

Figure 6-25: Results of RAN TPG at CRE 15dB

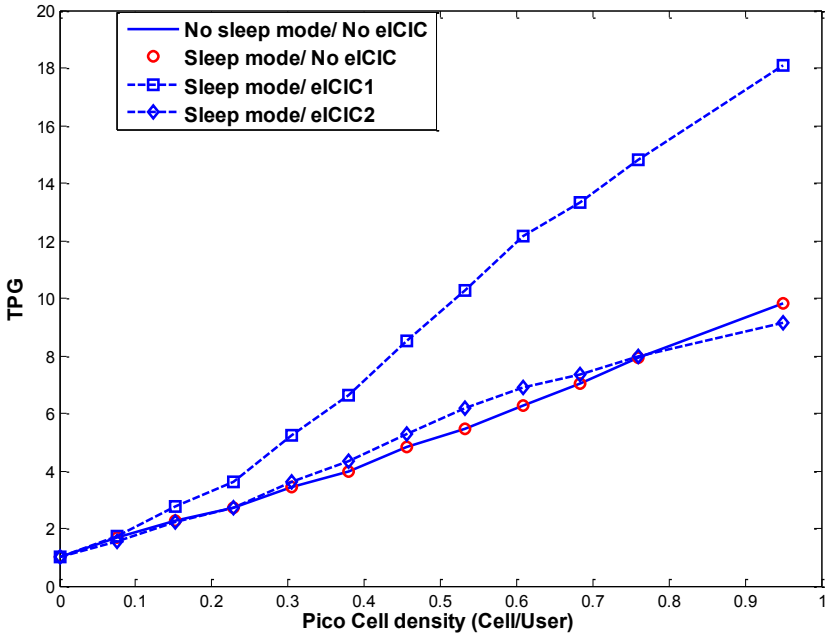

Figure 6-26: Results of RAN TPG at CRE 20dB

A comparison between the achieved TPG by eICIC1 and eICIC2 at different pico cell densities and at various CRE values is shown in Figure 6-27. The results show that eICIC1 performs better at higher CRE and at high pico densities. The inverse is observed at low pico densities as too many users share the spectrum resources of a single picocell, especially at high CRE. For

all the considered densities and considered CRE values, eICIC1 outperforms the eICIC2 as eICIC1 benefits from a higher number of ABS sub-frames, and from scheduling the central pico users in the ABS and non ABS sub-frames.

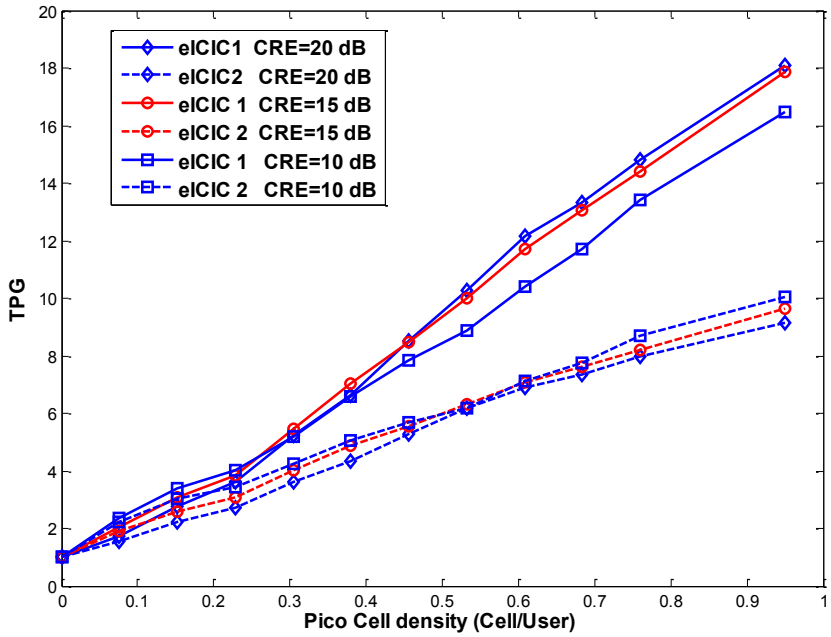

Figure 6-27: Results of TPG at various CRE values

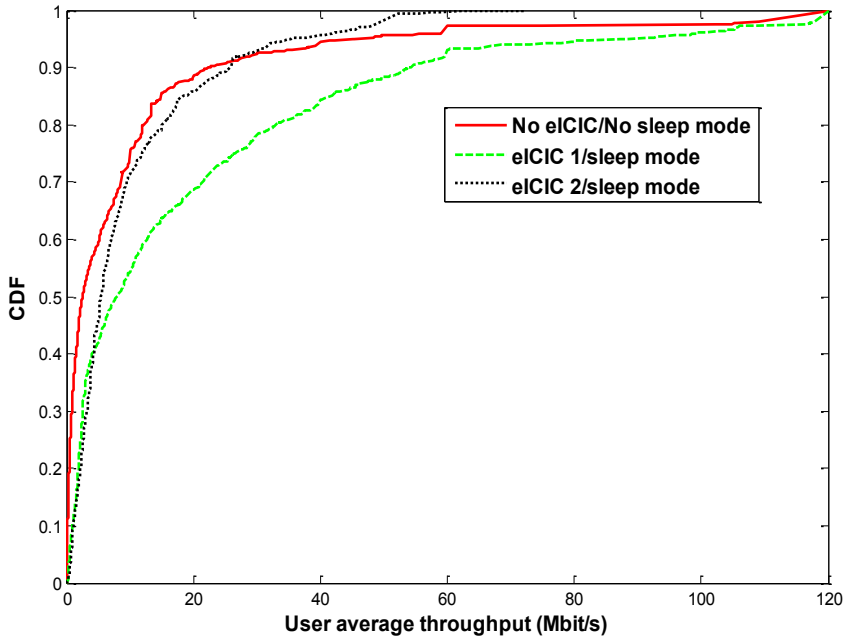

Figure 6-28: CDF of user's average throughputs

The CDF of user's average data rates is plotted in Figure 6-28 for the three cases of no sleep mode, eICIC1, and eICIC2, at CRE of 20 dB and at a picocell density of 50 pico cells per macro. We can see clearly that eICIC1 provides the highest average data rate to all deployed users apart from the cell edge users, who benefit more from eICIC2, as shown more clearly in Figure 6-29.

The reason for this is only the pico edge users are scheduled during the ABS subframes which gives them more allocated bandwidth.

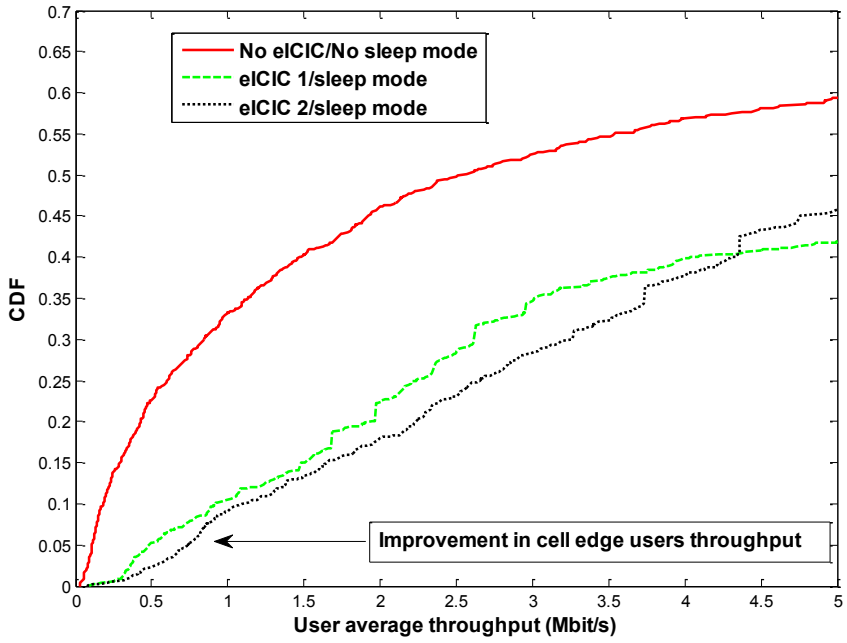

Figure 6-29: Improvement in cell edge user throughputs at CRE=20 dB and 50 pico cells per macro cell (equivalent to 0.96 cells per user)

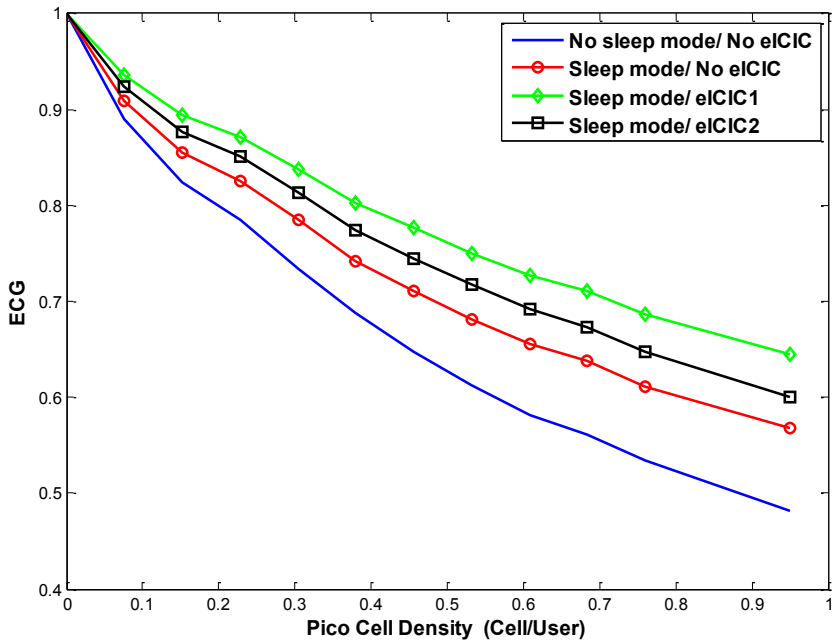

Figure 6-30: Results of ECG at CRE 10dB

A clear improvement in the RAN ECG is achieved when enabling the sleep mode in the picocells, as shown in Figure 6-30. This improvement increases with an increase in picocells density. For instance, sleep mode leads to around an 8% improvement in the ECG at a picocell

density of 0.9 cell/user while this improvement vanishes at pico cell density of 0.1 cells per user. The implementation of eICIC 1 and eICI2 provide further improvement in the ECG for all the considered pico cell densities at a CRE value of 10dB with the highest improvement being obtained by the eICIC1.

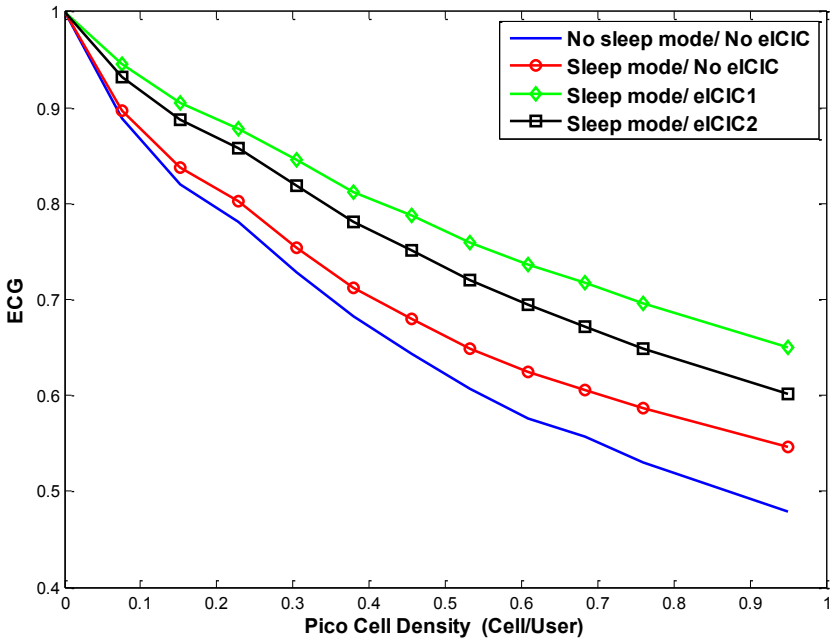

Figure 6-31: Results of RAN ECG at CRE 15dB

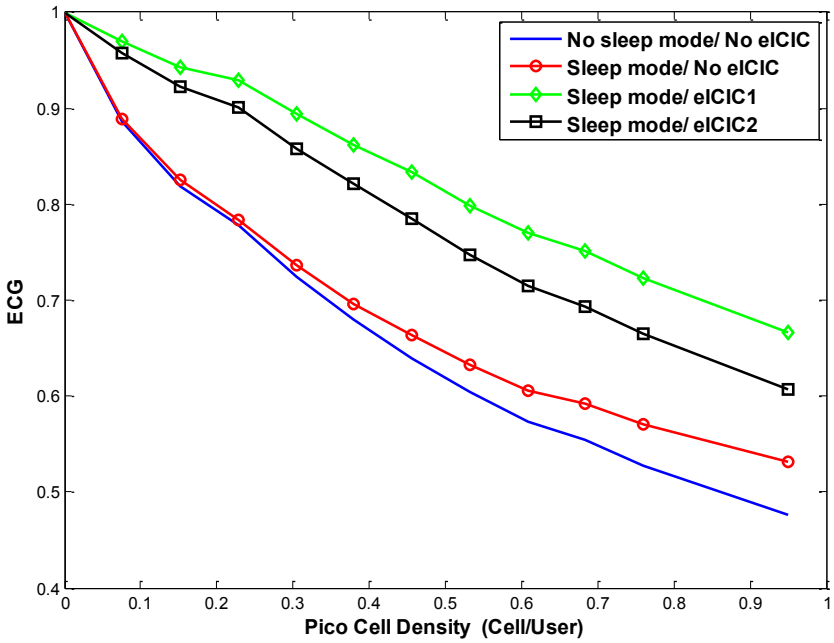

Figure 6-32: Results of RAN ECG at CRE 20dB

The same trend is observed with CRE values of 15 and 20 dB, as shown in Figure 6-31 and Figure 6-32. Enabling the sleep mode in picocells improves the RAN ECG, and further improvements are achievable with eICIC1 and eICIC2.

The influence of the choice of the CRE value on the RAN power consumption is illustrated in Figure 6-33 by comparing between the two eICIC techniques at various CRE values. The higher used CRE values lead to better ECG values regardless of which interference coordination scheme is employed. This can be explained by the fact that at higher values of CRE, more users will associate with the picocells, which results in the configuration of more ABS sub-frames per frame.

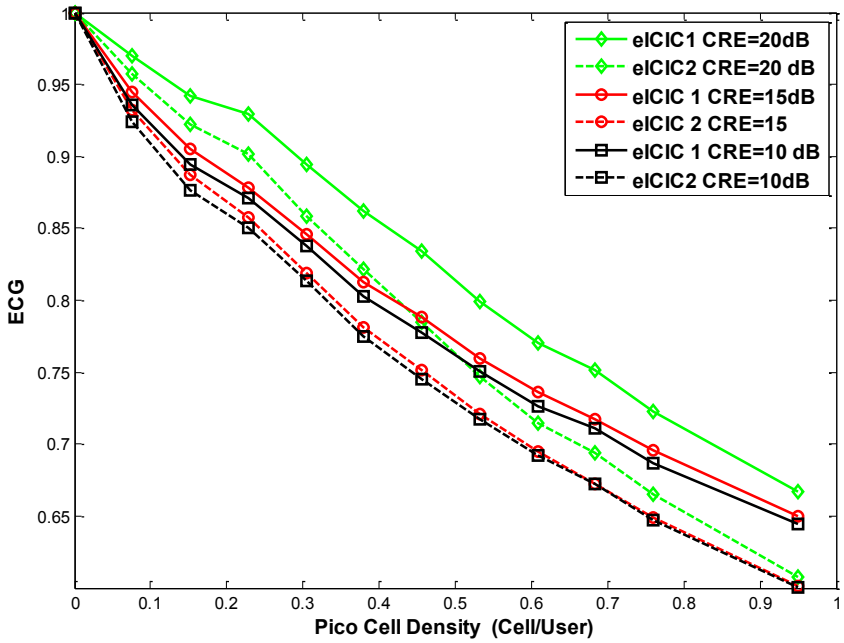

Figure 6-33: Results of RAN ECG at various CRE values

When plotting the RAN ETG versus the pico cell density at various CRE values in figures (6.34) to (6.36), the results show a continuous improvement in the bit/J metric versus the density of deployed picocells. This continuous improvement is due to the improvement in the RAN average throughput, whiles no actual reduction in the RAN power consumption is observed. The remaining observations from the ETG are similar to those obtained by ECG. The eICIC1 technique provides better ETG values than the eICIC2 while sleep mode continues to improve the ETG compared with the non-sleep mode case.

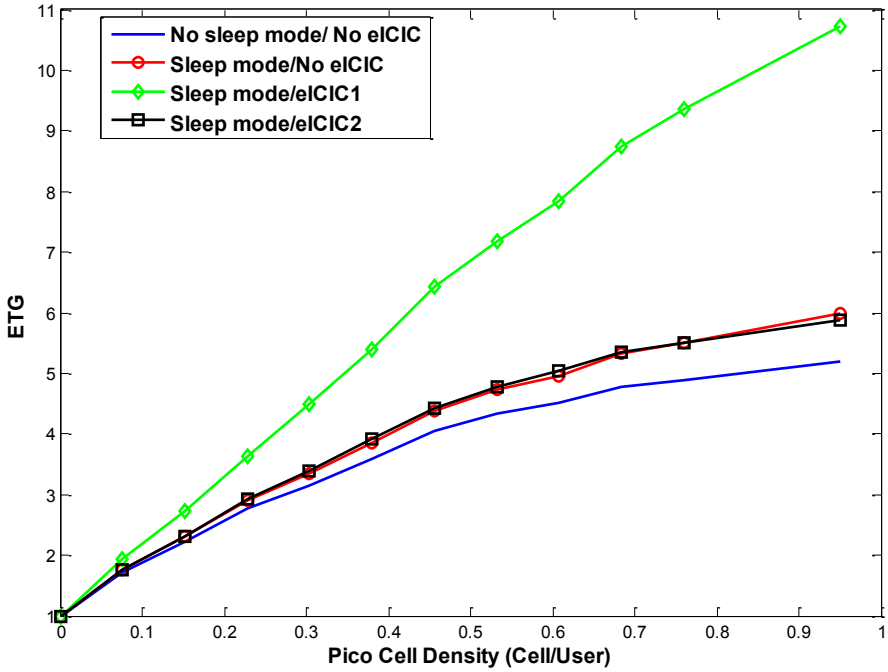

Figure 6-34: Results of RAN ETG at CRE 10dB

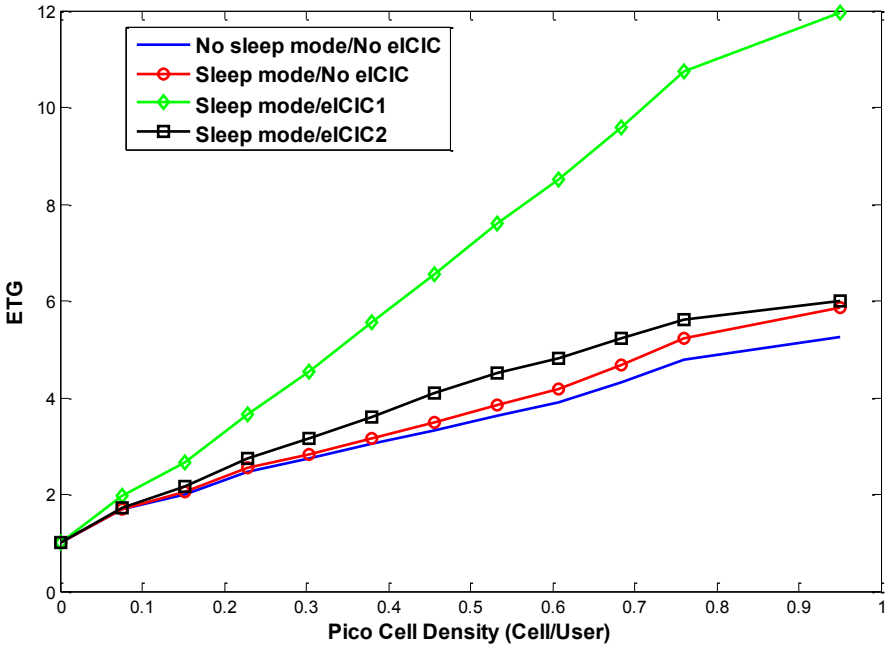

Figure 6-35: Results of RAN ETG at CRE 15dB

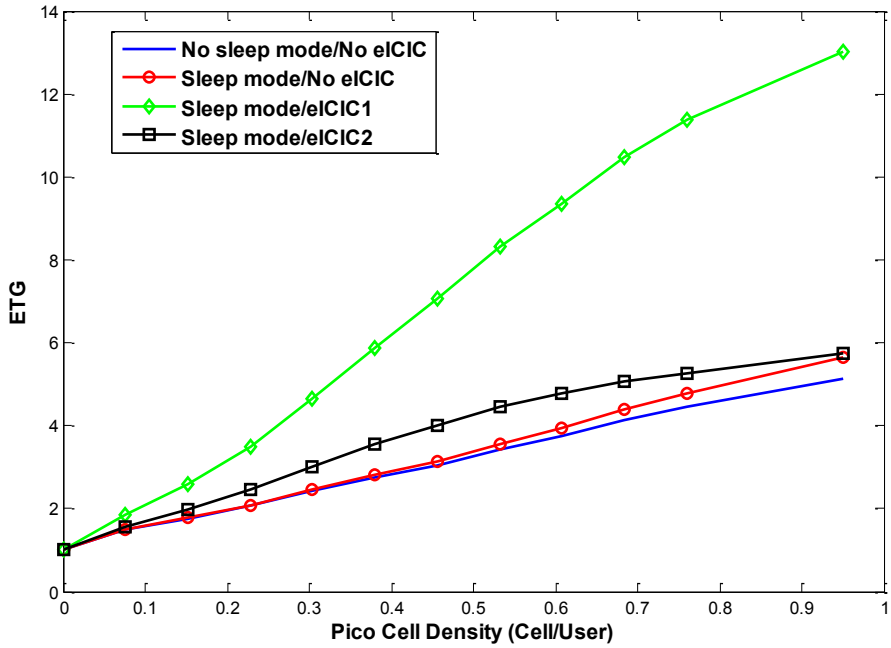

Figure 6-36: Results of RAN ETG at CRE 20dB

The variation of the ETG values for eICIC1 and eICIC2 versus the CRE used values is shown in Figure 6-37 and follows exactly the same trend as the TPG versus the CRE values which we have already seen in Figure 6-27. Higher CRE values lead to better ETG values with eICIC1 at high pico cell densities.

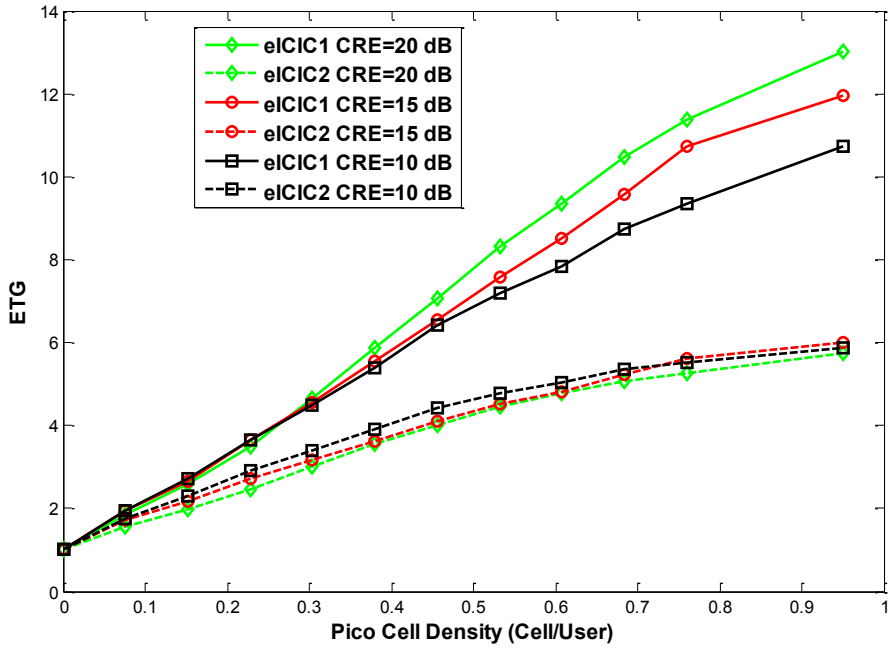

Figure 6-37: Results of RAN ETG at various CRE values

The opposite is observed in case of eICIC2: lower CRE values lead to better ETG values. The reason for this is that higher CRE values lead to an increase in the number of edge pico users, and as a consequence, the number of ABS sub-frames increases, which in turn enhances the throughput of pico edge users while degrading the throughput of the remaining deployed users.

6.4 Summary

This chapter addressed the issue of energy consumption in heterogeneous networks by considering two deployment types: sparse small cell and dense small cell deployments. In each case, the three figures of merits TPG, ECG and ETG were evaluated for the considered networks. The chapter investigated the impact of traffic offloading to small cells and the sleep mode implementation on the RAN average throughput and RAN energy consumption. A system level simulation was developed to model a heterogeneous RAN with different pico cell densities, in order to examine whether or not an improvement in the TPG and ECG is achievable by offloading the traffic to small cells. The results have shown that in case of the pico cells being deployed uniformly in the target area, the amount of reduction in the energy consumption in macrocells is less than the increase in power consumption caused by the added picocells. On the other hand, when picocells are deployed in hotspot zones, different results are obtained. A joint improvement in the RAN TPG and ECG is obtained. As expected, more improvement in the RAN ECG is obtained by implementing the sleep mode in the two cases of uniform and clustered user distribution.

The energy consumption and throughput gain of the dense heterogeneous networks have also been investigated. In addition to showing how enabling the sleep mode can lead to improvements in the RAN ECG, we have shown that the issue of interference between the macro and picocells can be dealt with in an effective way by implementing the eICIC technique. The advantages are twofold: more improvement in the RAN throughput gain and further reduction in the RAN energy consumption. One must note that when a dense layer of small cells is deployed on top macro RAN, the increase in the energy consumption is unavoidable even if sleep mode is implemented. when measuring the energy efficiency by the bit/J metric, significant improvement is observed, but this improvement is due to the increase in the RAN TPG, and not by a reduction in the energy consumption. However, when such deployment is compared with the results of chapter 3 for macro/ pico HetNet when each layer is allocated different frequency band of 10 MHz, The proposed co-channel deployment with eICIC1 and sleep mode reduces the energy consumption by a factor of 1.35 the same target capacity is sough

Chapter 7

Throughput and Energy Consumption Analysis of Massive MIMO RANs

7.1 Overview

Driven by the increase in the number of connected devices, and the need for high data rates to support applications such as video streaming and gaming online, the growing demand for wireless capacity is expected to continue over the next few years. In this context, the deployment of more traditional base stations to satisfy this increasing demand risks to lead to a huge increase in the level of the energy consumption of cellular networks. Massive MIMO has recently emerged as a promising technology to be deployed in the next generation of cellular networks [19], where a large number antennae at the base station can simultaneously serve multiple users at the same time and using the same frequency resources. Thanks to the multiplexing gain and the array gain, massive MIMO has the potential to offer huge throughput values and to reduce the energy consumption to unprecedented levels. As each user terminal is allocated the whole bandwidth in massive MIMO systems, high user data rates are also achieved.

Due to quasi-orthogonal properties of massive MIMO channels at very large numbers of antennae, they have the advantage of providing significant improvements in the cell spectral efficiency and in the energy efficiency by using linear non-complex precoding techniques such as maximum ratio transmission MRT and zero forcing ZF [20]. However, when including the circuit power consumption of the base station, a linear increase in the power consumption versus the number of antennae is observed, the reason for this increase is that each antenna has a separate RF chain which consumes a non-negligible amount of power. In addition, the rise in power consumption in the baseband processing also scales up with the number of antennae and the number of served users [111].

Several publications have investigated the issue of energy efficiency in massive MIMO networks, most of them have concentrated on identifying a relationship between the number of antennae, number of users and the energy efficiency as measured in bit/J. For example, the authors of [111, 137, 138] showed that the energy efficiency is maximised at a finite number of antennae, and this number varies according to the precoding technique used. The authors of [139] compared the performance and energy efficiency of massive MIMO networks versus typical LTE network and found that almost a 1000 times improvement in the energy efficiency is achieved compared with the LTE network. They also showed the existence of an optimum

number of users which maximises the energy efficiency of massive MIMO networks. Different results are obtained when comparing the energy efficiency of massive MIMO against small cells. In [114], the authors showed that small cell networks always offer better energy efficiency than massive MIMO when only the RF transmit power is considered; while in [115], the results showed that when the antenna density is high, massive MIMOs is more energy efficient than small cells if the per-antenna circuit power in massive MIMO is less than that of each antenna transceiver in small cells, or if an adaptive antenna switching off is allowed in massive MIMO. If not, small cells are the more energy efficient option to deploy.

More investigation on the energy consumption of massive MIMO RANs is conducted in this chapter when compared with the seminal work in [111] , the three figures of merit proposed in chapter 3 TPG, ECG and ETG are used to provide more insights on the issue of spectral and energy efficiency of massive MIMOs instead of relying only on the bits/j. Also, the massive MIMO energy consumption is evaluated and compared versus the traditional deployments of macro cells, small cell and heterogeneous networks which was not included in [111]. In addition, The process of power consumption modelling in a massive MIMO base station is explained in detail based on the existing power model in [111] which has been modified in this chapter to include the losses in the power supply, cooling unit, the impact of the degradation of power amplifier efficiency when the output power is reduced by following the same approach which was carried out in chapter 3. The massive RAN throughput evaluation is also covered in section 7.3, followed by a presentation of how the three figures of merit are calculated. The details of the used system model are explained in section 7.5 and the results are presented in the following section. The chapter is complemented by a comparison between the throughput and energy consumption in massive MIMO RANs and in the small cells and heterogeneous networks.

7.2 Power consumption modelling in massive MIMO

The massive MIMO base station power model which has been presented in [111] is adopted with some modification to be used in modelling the power consumption of a massive MIMO base station in this chapter. The overall power consumption of the base station is modelled as the sum of circuit power P_{CP} and the power consumed in the power amplifier P_{PA} as in (7.1)

$$P_{BTS} = P_{CP} + P_{PA}. \tag{7.1}$$

The circuit power consumption is composed of the sum of the power consumptions of the various components of the base station, as shown in (7.2).

$$P_{CP} = P_{FIX} + P_{TC} + P_{CE} + P_{CD} + P_{BH} + P_{LP}. \quad (7.2)$$

The terms P_{CD} and P_{BH} refer to the power consumption due to the channel coding and decoding process and to the variable backhaul power consumption; both are estimated as a function of the sum throughput delivered by the base station, and their contribution to the overall base station power consumption can be negligible. For example, their total power consumption together, according the values presented in [111] is less than one watt when the base station is delivering 1 Gbits/s of throughput. For this reason, they are not included in the power consumption estimation in this chapter. The circuit power consumption is rewritten as in (7.3).

$$P_{CP} = P_{FIX} + P_{TC} + P_{CE} + P_{LP}, \quad (7.3)$$

Where P_{FIX} refers to the fixed power required for site cooling, control and signalling, and the fixed power consumption in the baseband processing and backhaul units. The model in its original form does not include the power losses in the power supply unit $P_{AC/DC}$, and the dynamic power consumption of the cooling unit P_{COOL}. By adding these parameters and the power consumed in the power amplifier P_{PA}, the base station site power consumption can be calculated as shown in (7.4).

$$P_{site} = P_{FIX} + P_{TC} + P_{CE} + P_{LP} + P_{AC/DC} + P_{COOL} + P_{PA}. \quad (7.4)$$

The parameter P_{TC} refers to the power consumption in the RF transceiver and expressed as a function of the number of antennas at the base station, as shown in (7.5).

$$P_{TC} = M \cdot P_{BS} + P_{SYN}, \quad (7.5)$$

Where P_{BS} is the transceiver power consumption, which includes the converters, filters and mixers. The parameter M is the number of antennas, while P_{SYN} denotes the power consumption in the local oscillator, a single oscillator is assumed to be sufficient for the entire base station. It is important to highlight here that the value of P_{BS} need to be scaled with the bandwidth B [27], i.e. doubling the bandwidth would double its value, and it can be expressed as $P_{BS} = \frac{B}{B_{ref}} \cdot P_{BS,ref}$ where B_{ref} is reference bandwidth value and $P_{BS,ref}$ is the value of P_{BS} at the reference bandwidth.

The channel estimation process is carried out at the baseband processing unit in the base station. Its power consumption is approximated as a function of the number of antennae M, number of users K, coherent block size U and bandwidth B, as in (7.6) [111].

$$P_{CE} = \frac{B \cdot M \cdot K \cdot (2K-1)}{U \cdot L_{BS}} \cong \frac{2 \cdot B \cdot M \cdot K^2}{U \cdot L_{BS}} . \quad (7.6)$$

The parameter L_{BS} refers to the computation efficiency of the base station and measured in flops/watt, where flop refers to floating point operation such as one addition, subtraction, multiplication or division operation. The number of required flops for the channel estimation is obtained by finding the number of required flops for the channel estimation process for one user which is carried out by the multiplication of the received pilot (M x K) matrix with a pilot vector of length K. This multiplication requires $M \cdot (2K - 1)$ flops. This process is executed for all users K and once for per coherence block.

The parameter P_{LP} refers to the power consumption due to the process of linear processing in the baseband unit and also modelled as a function of number of antennae M, number of users K, bandwidth B, and coherent block size U. When only one pilot is allocated at each user in the uplink, and using MRT/MRC precoding and receive combining, the P_{LP} is estimated in [111] by (7.7).

$$P_{LP} = \frac{2M \cdot K \cdot B}{L_{BS}} \cdot \left(1 - \frac{K}{U}\right) + \frac{3 \cdot B \cdot M \cdot K}{U \cdot L_{BS}} , \quad (7.7)$$

Where the first term of (7.7) represents the power consumption due to the receive combining process, and the second term represents the power consumed to compute the MRT precoding matrix, which requires M multiplications, $M - 1$ summations, and one square root operation to compute $\|h\|$ for each user, then divide each element of h by $\|h\|$ for normalisation. For K users, $3 \cdot M \cdot K$ flops are needed.

The PA power consumption is modelled as a function of the PA efficiency η_{PA} and the power amplifier RF transmitted power P_t, as in (7.8).

$$P_{PA} = \frac{P_t}{\eta_{PA}} . \quad (7.8)$$

Following the same approach of chapter 3, if no efficiency improvement techniques are implemented in the power amplifier, the PA efficiency will degrade when the output power of the amplifier is reduced. For example, if the PA has an efficiency $\eta_{PA,1}$ of 30% at P_1 and its

output power is reduced to P_2, the efficiency of the power amplifier $\eta_{PA,2}$ will be degraded, as shown in (7.9).

$$\eta_{PA,2} = \eta_{PA,1} \cdot \sqrt{\frac{P_2}{P_1}}. \tag{7.9}$$

For example, at 50% output power reduction, the $\eta_{PA,2}$ degrades from 30% to 21.21%. Most of the existing work in open literature considers the efficiency of the power amplifier as staying constant when increasing the number of transmit antennas at the base station, which is correct only if the level of RF output power is kept constant regardless of the number of antennas, or if the power amplifier efficiency improvement technique is used. In massive MIMO, the RF transmitted power required to achieve a certain target capacity decreases when the number of antennas increases.

The losses in the power supply unit and in cooling unit have not been included in the original model. The power supply unit losses are included in the model by dividing the base station power consumption by the efficiency of power supply $\eta_{AC/DC}$, as shown in (7.10). The cooling unit power consumption is estimated by following the same approach as in chapter 3, section 3.3 as shown in (7.11).

$$P_{site} = \frac{P_{FIX}+P_{TC}+P_{CE}+P_{LP}+P_{PA}}{\eta_{AC/DC}}, \tag{7.10}$$

$$P_{COOL} = \frac{(P_{FIX}+P_{TC}+P_{CE}+P_{LP}+P_{PA})}{\eta_{AC/DC}} \cdot \frac{3.41}{EER}, \tag{7.11}$$

Where the EER is the energy efficiency rating of the cooling unit. The value 3.41 is used to convert the consumed power in the base station into British thermal units BTU per hour. If the RF transceiver and power amplifier are located near the antenna outside the base station cabinet, a large reduction in cooling unit power consumption is achieved, as shown in (7.12).

$$P_{COOL} = \frac{(P_{FIX}+P_{CE}+P_{LP})}{\eta_{AC/DC}} \cdot \frac{3.41}{EER}. \tag{7.12}$$

Finally, the overall massive MIMO power consumption is described as the sum of the power consumptions of all individual components of the model, as depicted in (7.13).

$$P_{site} = \frac{P_{FIX}+P_{TC}+P_{CE}+P_{LP}+P_{PA}}{\eta_{AC/DC}} + P_{COOL}. \quad (7.13)$$

The used values of the power consumption model parameters are obtained from [111], and from Table 3.1 in chapter 3. A full list of these parameters is shown in Table 7-1. Note that the used value for coherence block corresponds to a pedestrian indoor environment, where coherence bandwidth of 10 MHz and coherent time of 50 ms are assumed [17]. For different types of environments such as the outdoor vehicular case, a coherent block size of 750 channel use is used in the same reference.

Table 7-1: Massive MIMO base station power model parameters

Parameter	Value
Bandwidth B	40 MHz
Coherence block U	500000
Computational efficiency L_{BS}	12.8 Gflops/W
PA efficiency η_{PA}	30%
Fixed overhead power consumption P_{FIX}	18 W
Local oscillator power consumption P_{SYN}	2 W
Transceiver power consumption P_{BS}	1 W
Power supply efficiency $\eta_{AC/DC}$	85%
Cooling unit energy efficiency rating EER	11

Figure 7-1 shows the power consumption of a massive MIMO base station versus the number of antennae, while the RF transmitted power varies from 1 to 10 watts and the number of users is 150 users per cell. On the other hand, Figure 7-2 shows the power consumption of massive MIMO base station when the degradation in the power amplifier efficiency due to the decrease in the per power amplifier output power is taken into account. When fixing the RF output power of the base station and increasing the number of antennas, the average output power per single PA decreases, and as a result, the PA efficiency degrades.

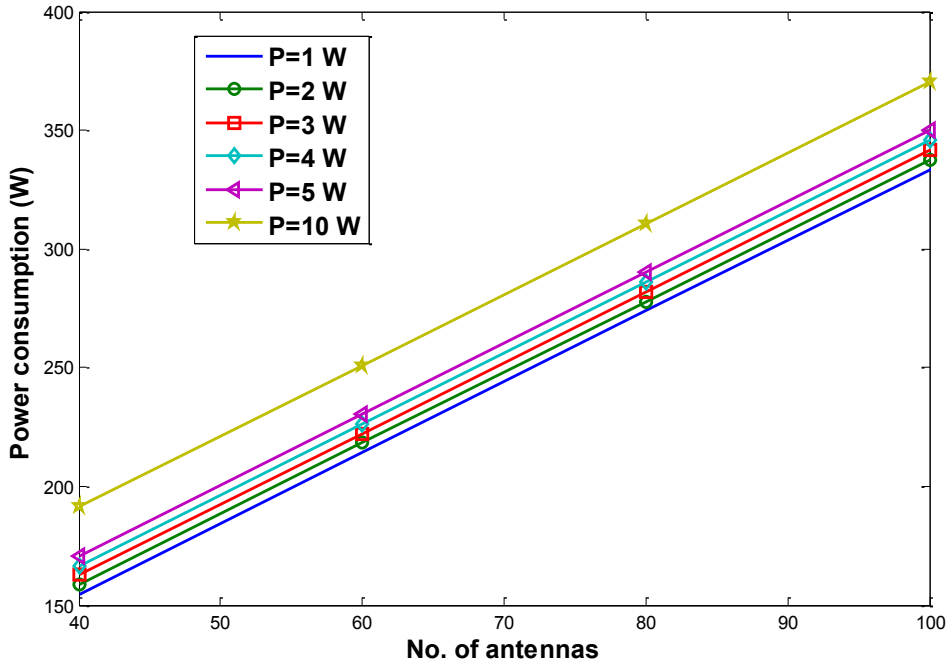

Figure 7-1: The power consumption of massive a MIMO base station at constant PA efficiency of 30% and various RF transmitted power values.

When comparing the two cases of constant and non-constant power amplifier efficiency, an increase in the power consumption of the base station with non-constant power amplifier efficiency is observed. This increase becomes more visible when increasing the number of antennae and when increasing the RF transmit power, as shown Figure 7-3 . For example, the base station power consumption increases by around 25 watts at 100 antennas and by around 50 watts at 200 antennas when 10 watts of RF transmitted power is assumed.

Moreover, the number of served users by the base station is another factor which has an impact on the base station power consumption. The reason for this is that increasing the number of users causes a rise in the power consumed by the baseband processing unit. Figure 7-4 shows how power consumption of the massive MIMO base is increasing when varying the number of served users from 10 to 150 users while keeping the number of antennas and RF transmitted power fixed.

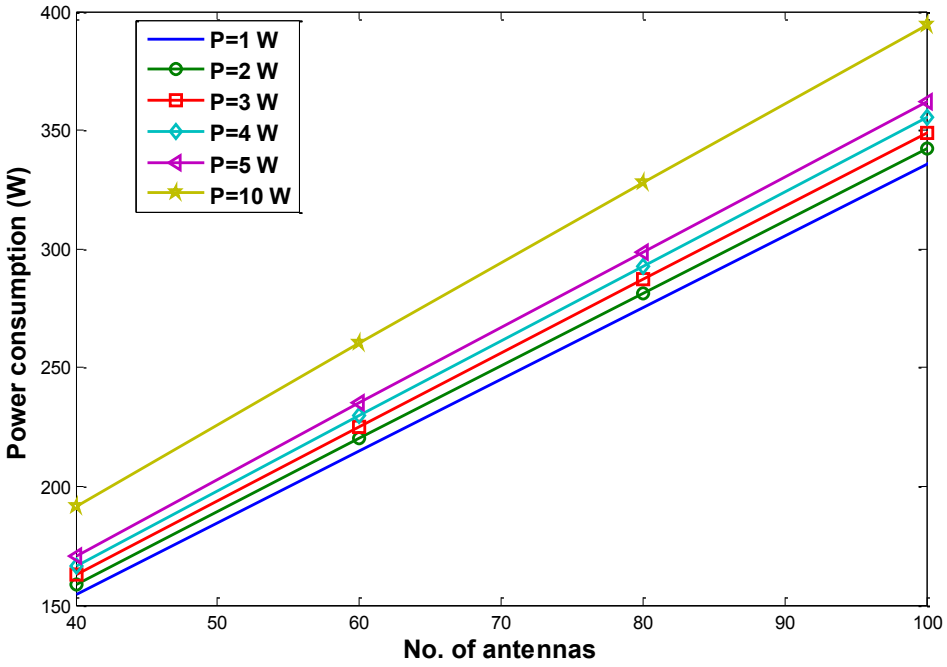

Figure 7-2: The power consumption of the massive MIMO base station at non-constant PA efficiency of 30%.

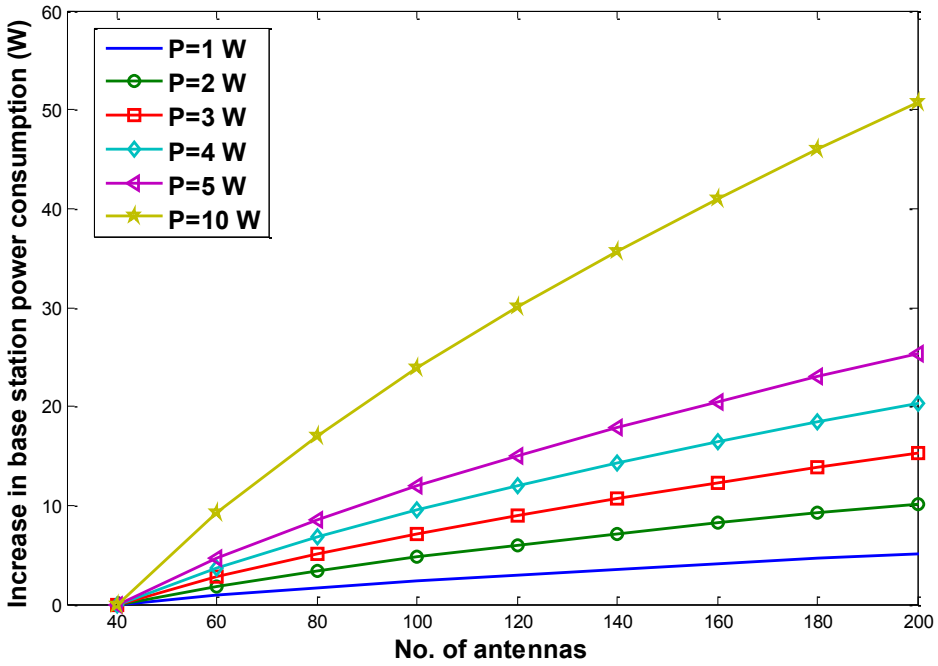

Figure 7-3: The increase of power consumption of the massive MIMO base station due to PA efficiency degradation.

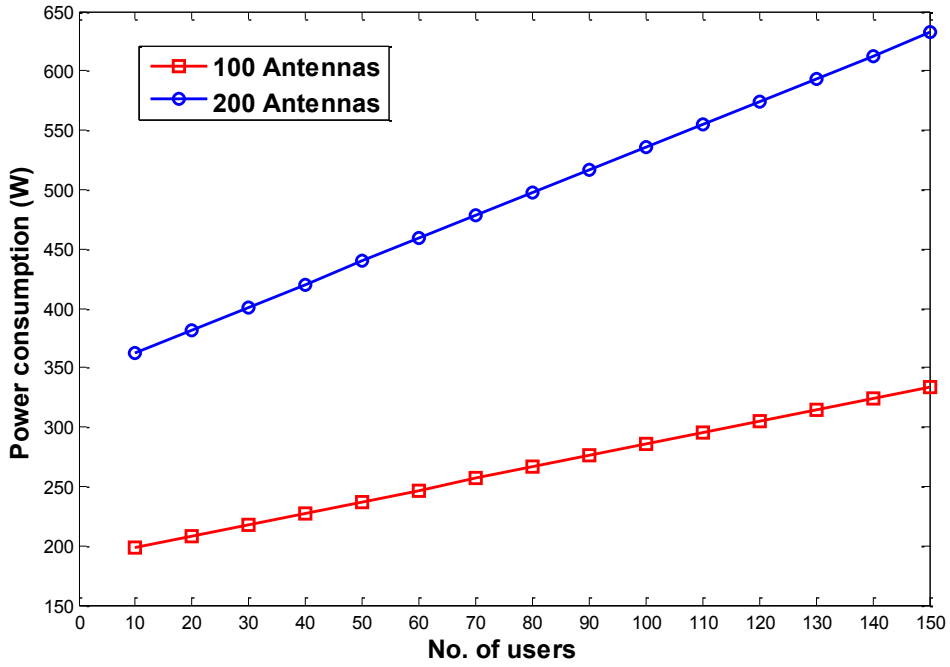

Figure 7-4: Impact of increasing the number of users on the base station power consumption when the RF transmit power is 5 watts

7.3 Throughput analysis in massive MIMO RANs

The downlink performance of a massive MIMO network is considered in this chapter, where the network consists of L cells, each equipped with M antennas, and serves K single antenna users. The channel between the ith base station and kth user in the lth cell is denoted by $\boldsymbol{h}_{l,k}^{i} = \left[h_{l,k,1}^{i} \quad \cdots \quad h_{l,k,M}^{i}\right]^{\boldsymbol{T}}$ where $\boldsymbol{T}$ refers to vector transpose. Each realisation of the channel between user k in cell l and base station i is modelled as uncorrelated Rayleigh fading $h_{l,k}^{i} \sim \mathbb{C}\mathcal{N}(0,1)$ where $h_{l,k}^{i} \in \mathbb{C}^{M}$. When considering large scale fading $\beta_{l,k}^{i}$, the channel gain is expressed as $g_{l,k}^{i} = \sqrt{\beta_{l,k}^{i}} \cdot h_{l,k}^{i}$ where $\beta_{l,k}^{i}$ refers to the large scale fading between user k in cell l and the base station in cell i.

The lth base station transmits a vector of signals $\boldsymbol{S}_l$ to their K associated users, as expressed by (7.14).

$$\boldsymbol{S}_l = \sum_{k=1}^{K} \sqrt{\rho_{l,k}} \cdot \boldsymbol{W}_{l,t} x_{l,k} \,, \tag{7.14}$$

Where $x_{l,k}$ is the data symbol sent to the user k in cell l and has unit transmit power, $\rho_{l,k}$ is the allocated transmit power to user k in cell l, and $\boldsymbol{W}_{l,k} \in \mathbb{C}^M$ is the linear precoding vector to user k for $k = 1, \ldots, K$.

The user k in cell l receives the signal $y_{l,k}$, which consists of a combination of the desired signal and the interference which composed of the intra cell interference caused by the signals sent by the serving cell to the other users in the same cell, and the inter cell interference caused by signals sent by other cells to their own users is depicted by (7.15).

$$y_{l,k} = \sum_{i=1}^{L} \left(\boldsymbol{h}_{l,k}^{i}\right)^{H} \cdot \boldsymbol{S}_i + n_{l,k}\,, \tag{7.15}$$

Where $n_{l,k} \sim \mathbb{C}\mathcal{N}(0, \sigma_n^2)$ is the additive white noise at the user equipment which has a variance of σ_n^2.

The kth user average throughput can be calculated by (7.16) when time division duplex TDD is employed as the duplexing mode, and one uplink pilot signal per user is allocated to estimate the uplink channel. The division of B by 2 refers to an equal time partition of the channel between the uplink and downlink.

$$R_{l,k} = \frac{B}{2}\left(1 - \frac{K}{U}\right) \cdot \log_2\left(1 + SINR_{l,k}\right). \tag{7.16}$$

The signal to noise and interference at user k is expressed by (7.17), where the nominator refers to the desired signal, and the denominator refers to the sum of interference and noise. The interference consists of the sum of all the signals received by the user k from all the cells minus the desired signal [18].

$$SINR_{l,k} = \frac{\rho_{l,k}\left|\left(\boldsymbol{g}_{l,k}^{l}\right)^{H} \cdot \boldsymbol{W}_{l,k}\right|^2}{\sum_{i=1}^{L}\sum_{t=1}^{K}\rho_{i,t}\left|\left(\boldsymbol{g}_{l,k}^{i}\right)^{H} \cdot \boldsymbol{W}_{i,t}\right|^2 - \rho_{l,k}\left|\left(\boldsymbol{g}_{l,k}^{l}\right)^{H} \cdot \boldsymbol{W}_{l,k}\right|^2 + n_{l,k}}\,. \tag{7.17}$$

The parameter $\rho_{l,k}$ refers to the value of average transmit power allocated to the user k in cell l. It has significant impact on the user achieved throughput, and its value can be optimised to achieve certain performance targets. For example, it can be optimised to maximise the overall cell average throughput or to maximise the fairness between the users. An equal power distribution between the active users in the cells is adopted in this chapter. Finally the overall cell average throughput R_l is calculated as the sum of all users' throughputs, as in (7.18).

$$R_l = \sum_{k=1}^{K} R_{l,k} \ . \tag{7.18}$$

7.4 Throughput and energy efficiency of massive MIMO RANs

The evaluation of the throughput and energy consumption of a massive MIMO network is carried out by adopting the same evaluation framework presented in chapter 3. The massive MIMO base station is calculated by the power consumption model described in section 7.2. The three figures of merit TPG, ECG , and ETG of massive MIMO RAN will be estimated with reference to the same baseline macro only RAN which has been used in chapter 3 section 3.6. Using the same reference of macro only RAN deployment allows us to compare the performance and energy consumption of massive MIMO versus the small cells and heterogeneous network deployments by using the results obtained in chapter 3 without running the system level simulations of these deployments again.

When the same coverage area is assumed, the throughput gain is calculated as the ratio of the massive MIMO RAN average throughput and the macro RAN average throughput, as in (7.19).

$$TPG = \frac{L_{massive} \cdot R_{massive}}{L_{macro} \cdot R_{macro}} \ . \tag{7.19}$$

The values of $R_{massive}$ and R_{macro} refer to the average throughputs of a massive MIMO cell and macro cell obtained through running a system level simulation of the two networks. The parameter $L_{massive}$ refers to the number of massive MIMO deployed cells while L_{macro} is the number of deployed macro cells. The same number of deployed users is considered in the two cases of massive MIMO and macro RANs. The number of antennas at the massive MIMO base station varies between 40 to 200, while the transmitted RF power is varied from one watt to 10 watts, in order to investigate the impact of the number of antennas and RF transmitted power on the RAN throughput and RAN energy consumption.

Similarly, when the same observation time is assumed, the energy consumption gain ECG is calculated as the ratio of the power consumption in macro RAN to the power consumption in massive MIMO RAN, as shown in (7.20). The value of power consumption for the macro base station is estimated by the power consumption model presented in chapter 3 section 3.3.

$$ECG = \frac{L_{macro} \cdot P_{macro}}{L_{massive} \cdot P_{massive}} \ . \tag{7.20}$$

Note that the ECG decreases when increasing the density of deployed massive MIMO cells. Conversely, the TPG improves when the massive MIMO cell density is increased.

Another figure of merit to consider is the energy throughput gain ETG, which indicates the relative improvement in the bit/J metric when massive MIMO is deployed compared to the reference macro deployment. It can be simply calculated by the product of the TPG and ECG, as shown in (7.21).

$$ETG = TPG \cdot ECG \ . \tag{7.21}$$

7.5 The system model for massive MIMO RANs

A multi-cell massive MIMO network consisting of L cells is considered in this chapter, where each cell contains a single base station equipped by M antennas and serves K users such that $M >> K >> 1$. Each user terminal is equipped with a single antenna. The system operates in TTD mode where uplink pilots are used to estimate the uplink channel. Due to the channel reciprocity, both the uplink and downlink channels are equal.

A Matlab system level simulation is developed to evaluate the user's average throughputs, and the overall RAN average downlink throughput when a fixed number of users in the target area is assumed and when varying the number of antennas and the value of the base station RF transmit power. Massive MIMO cells are deployed according to two-tier hexagonal layout, as shown in Figure 7-5. All users are assumed to be indoors and uniformly deployed throughout the target area. The users' association is based on the strongest received power. In others words, users associate with the cell which provides the highest received power.

The main simulation parameters are listed in Table 7-2, The users' statistics are collected from the central cell only to avoid underestimating the inter-cell interference impact for the users located at the edge of the target area.

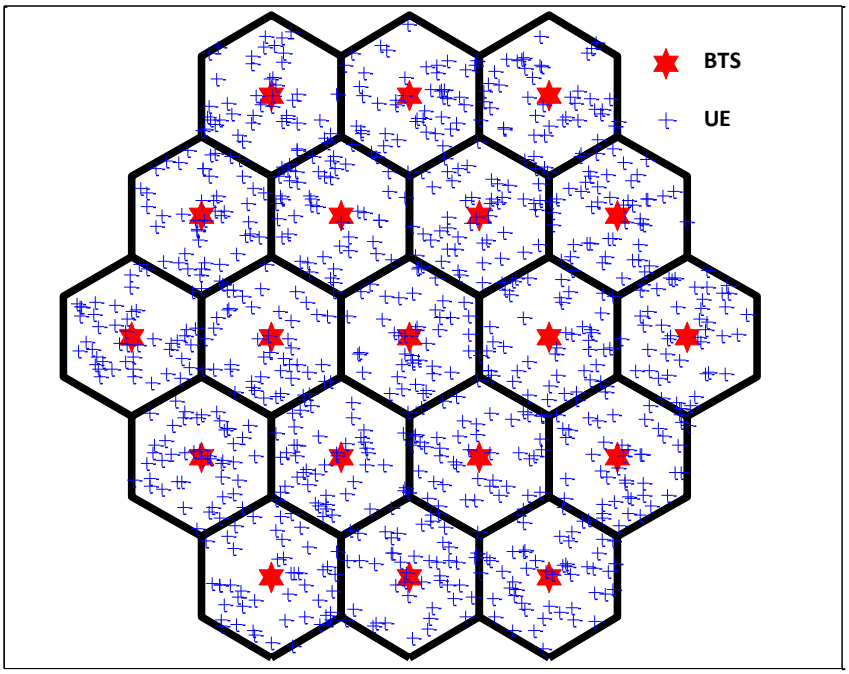

Figure 7-5: Network Layout

The first step in the simulation is deployment of the base stations and users in the target area. This is followed by calculating the distance between every single user and every base station. The 3GPP urban macro pathloss Uma is used to estimate the large scale fading $\beta_{l,k}^{i}$, which consists of distance dependent pathloss, and the attention due to the shadowing between the user k in cell l and the base station in cell i. The small scale fading channel response $h_{l,k}^{i}$ is generated by a Rayleigh distribution $h_{l,k}^{i} \sim \mathbb{C}\mathcal{N}(0,1) \in \mathbb{C}^{M}$ and used to generate the channel gain $g_{l,k}^{i}$, which is obtained by $g_{l,k}^{i} = \sqrt{\beta_{l,k}^{i}} \cdot h_{l,k}^{i}$ and implemented in (7.17) to obtain the signal to interference and noise ratio of each user's equipment.

The following assumptions are made in the analysis of the performance of massive MIMO RANs:

- Due to the availability of large coherent block size in indoor pedestrian environments [17], pilot reuse factor V is used and perfect channel estimation is assumed.
- Equal power distribution among the active users in each cell.
- MRT linear precoding technique is considered in this chapter, where the precoding normalised maximum ratio transmission MRT matrix is calculated as $\boldsymbol{W}_{l,k}^{MRT} = \frac{\boldsymbol{g}_{l,k}^{l}}{\|\boldsymbol{g}_{l,k}^{l}\|}$. It is substituted in (7.17) to estimate the SINR values of all deployed users.

The kth user's data rate in cell l is calculated by (7.22).

$$R_{l,k} = \frac{B}{2}\left(1 - \frac{V \cdot K}{U}\right) \cdot \log_2\left(1 + SINR_{l,k}\right), \tag{7.22}$$

Where V denotes the pilot reuse factor and the overall cell average throughput can be calculated as the sum of the throughput of all users deployed in the cell, as shown in (7.18).

Table 7-2: The simulation parameters

Parameter	Macro RAN	Massive MIMO RAN
Frequency (MHz)	2000	2000
Duplex mode	FDD	TDD
Bandwidth (MHz)	20	40 (download time fraction 50%)
Cell radius (Km)	1	0.5
Macro BS Antenna gain (dBi)	15	0
UE Antenna gain	0	0
Pathloss model (dB) & Shadowing	3GPP Uma	3GPP Uma
Traffic Model	Full buffer	Full buffer
User location distribution	Uniform	Uniform
Users	200 per Km^2	200 per Km^2
RF transmit Power	40 watts	1,2,3,4,5,10 watts
Number of antennas at base station	1	40-200
Precoding	NA	MRT
Pilot reuse factor	NA	3
Coherent block size (channel uses)	NA	500000 (Indoor environment)

The obtained results of cell average throughput and massive MIMO base station power consumption are used to estimate the TPG and ECG of the massive MIMO RAN with reference to the baseline macro only RAN deployment, which is also simulated using the parameters listed in Table 7-2.

7.6 The throughput and energy consumption results

The performance of a massive MIMO RAN with a cell radius of 500 metres is simulated when varying the number of antennas at the base station, and the value of RF transmitted power varies from 1 watts to 10 watts. The results show an increase in the cell average throughput when increasing the number of antennas and the RF transmitted power, as shown in Figure 7-6.

7.6.1 The results of TPG and ECG

When estimating the TPG of massive MIMO RAN by (7.19), the value of the ratio $\frac{L_{massive}}{L_{macro}}$ depends on the cell radius of two deployments considered. The results for the throughput gain follows the same trend of cell average throughput, the TPG increases with the number of antennas and with the transmitted RF power, as shown in Figure 7-7.

Figure 7-1 has already shown that the power consumption of the massive MIMO base station augments when increasing the number of antennas and the RF transmitted power. As a result, a drop in the value of the ECG of massive MIMO RAN is observed when increasing the number of antennae and increasing the transmitted power as depicted in Figure 7-8. Due to the overlapping of adjacent curves in Figure 7-8, the results for only four values of RF transmitted power are shown in the figure. The results of ECG indicate that from an energy consumption point of view, using fewer numbers of antennae and smaller transmitted RF power values is more beneficial for the network operators if the target capacity can be achieved.

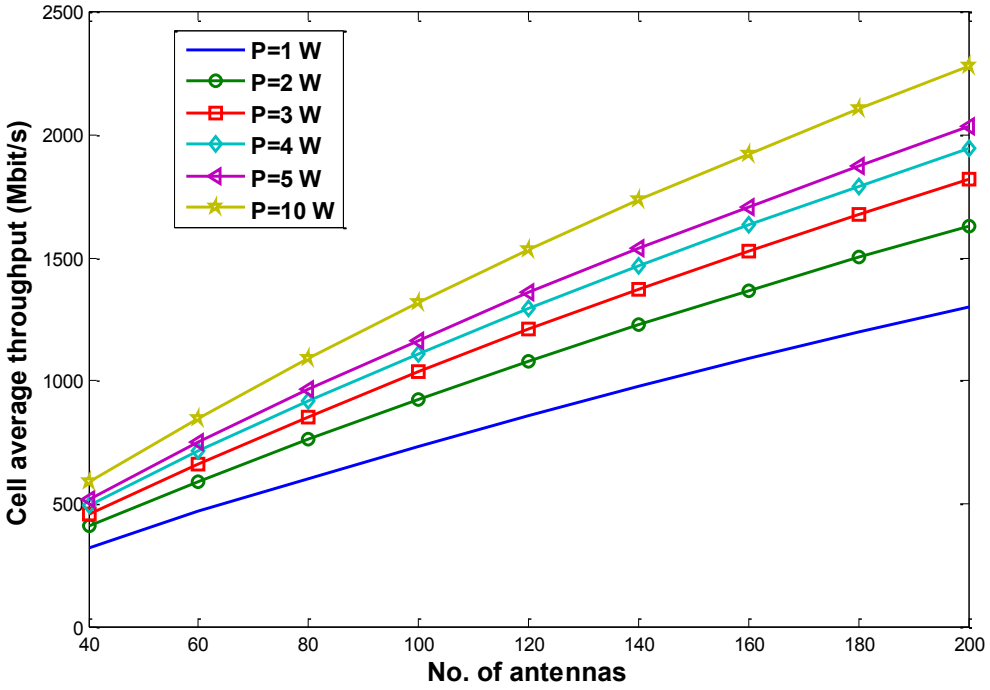

Figure 7-6: Massive MIMO cell average throughput with MRT precoding

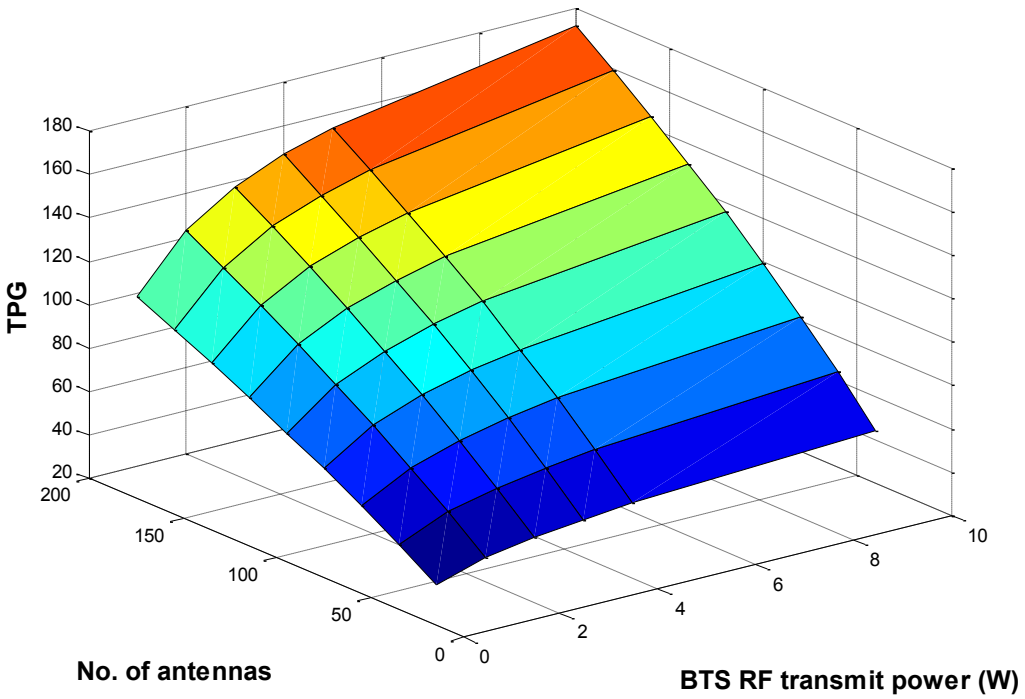

Figure 7-7: The TPG of massive MIMO RAN.

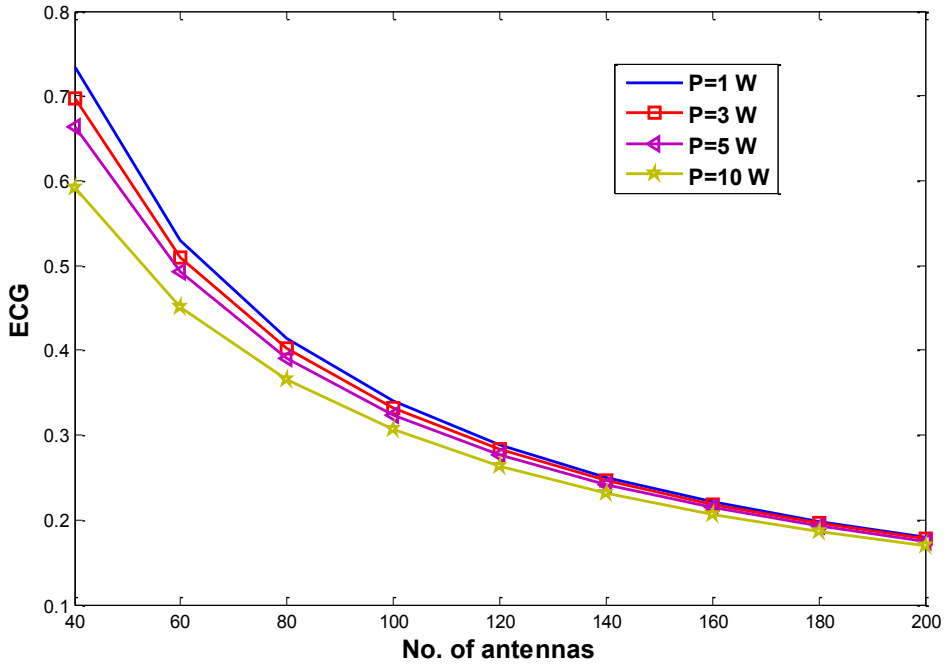

Figure 7-8: The ECG of massive MIMO RAN when the PA efficiency is constant

7.6.2 The throughput and energy consumption gain results

The energy efficiency (EE measured by the bit/J metric) of massive MIMO RAN can be calculated by (7.23) at various numbers of antennae and at different transmit power values.

$$EE = \frac{R_{massive}}{P_{massive}}. \tag{7.23}$$

The results of EE show the existence of an optimum number of antennas at the base station which maximises the EE of massive MIMO RAN, as shown in Figure 7-9. This number varies with the RF transmitted power of the base station. However, there is no such optimum number when adopting the ECG as an indicator of energy consumption in the network. This observation demonstrates once more that maximising the EE measured by bit/J does not always lead to a reduction in the network energy consumption because the absolute energy consumption exhibits a continuous increase versus the number of antennas at the base station. Hence, the EE improvement is due to an increase in the RAN throughput until it reaches its maximum level, beyond this, the relative increase in the energy consumption becomes higher than the relative increase in the throughput.

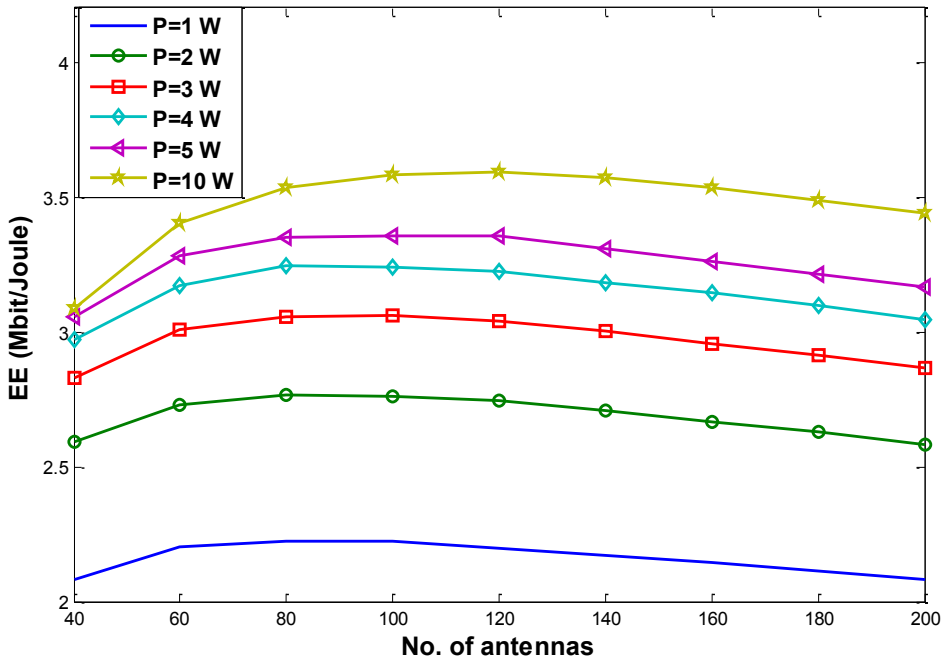

Figure 7-9: The results for the energy efficiency (EE) of massive MIMO RAN

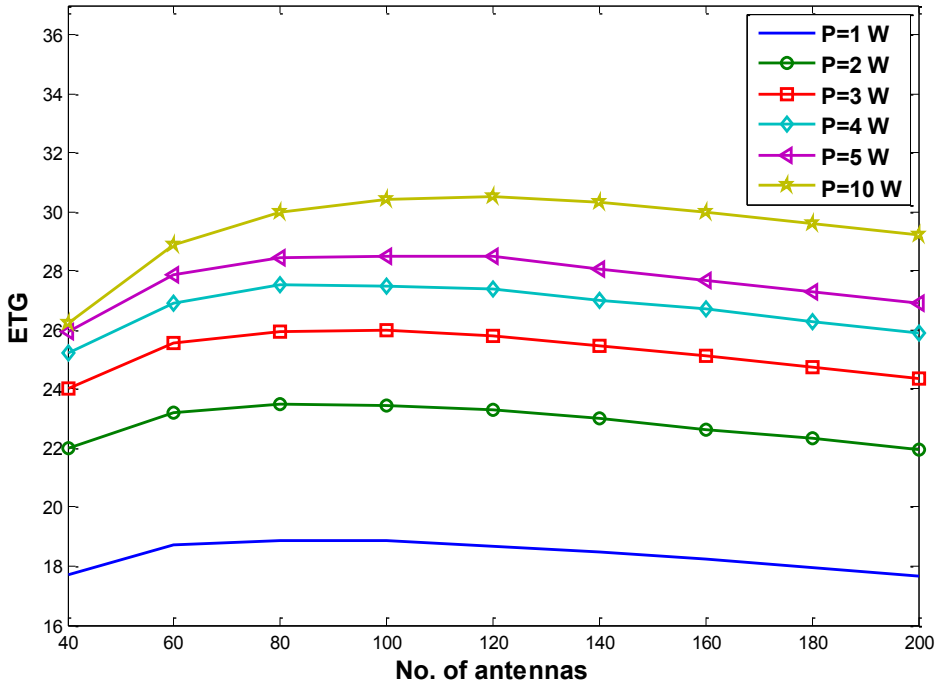

Figure 7-10: The results of the ETG of massive MIMO RAN

The same trend can be captured by estimating the energy throughput gain ETG, which reaches a maximum point at a number of antennas exactly equal to the number of antennas which yields the maximum bit/J value. The results of ETG are interpreted as a relative improvement in the EE of massive MIMO with reference of the EE of baseline macro only RAN. A maximum ETG value of 30 times improvement in the EE of massive MIMO occurs at a number of antennas laying between 100 and 120, as shown in Figure 7-10.

7.6.3 The TPG versus ECG results

As indicated previously, the TPG is calculated with reference to a baseline network deployment, where the achievable capacity of the baseline network is already known or must be evaluated. Hence, the TPG can be regarded as a target improvement to attain by the RAN capacity. From an energy consumption perspective, the objective of any cellular network operator can be expressed as achieving a certain TPG target with the highest possible ECG value. Therefore, combining the TPG and ECG results allows us to obtain one figure which serves as a guideline to determine which network deployment is able to achieve a certain throughput gain with the lowest possible level of energy consumption. For example, Figure 7-11 shows that a TPG value of 60 can be achieved with an ECG value of 0.5, which means an only twofold increase in the energy consumption is needed to achieve a 60 times increase in the RAN throughput in comparison with the macro only deployment (which by assumption has unity TPG and ECG values). Such representation of the results seems to be more important to network operators rather than only having the value of the bit/J metric, which does not indicate whether

the improvement is achieved due to an increase in throughput or due a reduction of network energy consumption.

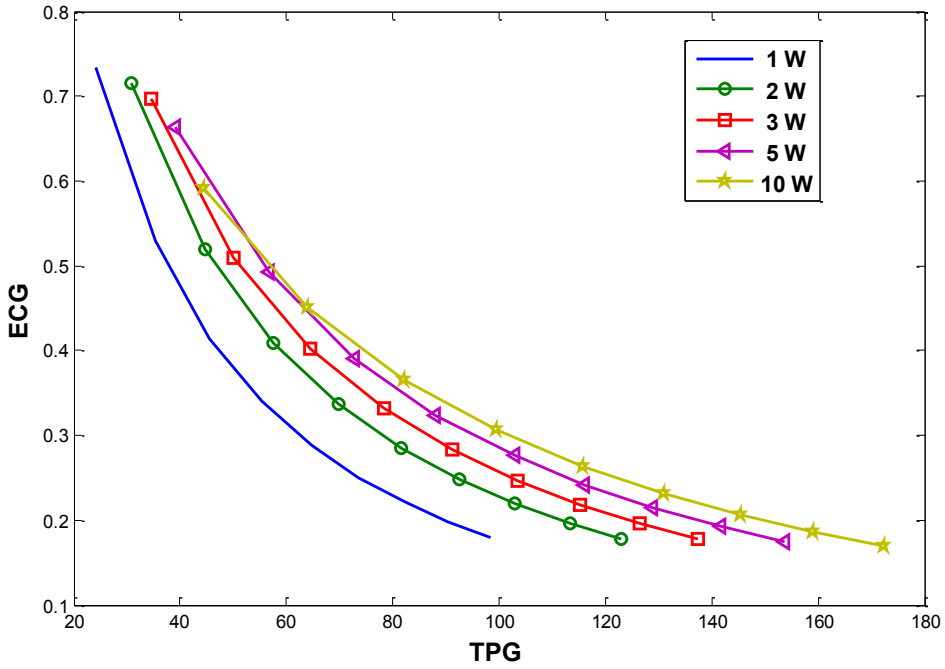

Figure 7-11: The TPG-ECG results for Massive MIMO RAN at a cell radius of 500 metres

7.7 Massive MIMO versus small cells and HetNets

As important network deployment options which are expected to play a crucial role in the next generation of cellular networks, the performance, and energy consumption of massive MIMO RANs, small cells and heterogeneous network are compared against each other. The macro only RAN with a cell radius of 1000 m was already used as a reference baseline deployment when estimating the TPG and ECG for the small cells and heterogeneous deployment in chapter 3. It was also used as a reference in this chapter to evaluate the TPG versus ECG of massive MIMO RAN. Hence, the TPG – ECG results for these three deployment options can be plotted on the same figure to facilitate comparing them against each other. The TPG – ECG results for small cell and massive MIMO are shown in Figure 7-12, where we can see that massive MIMO outperforms the micro only deployment and achieves the same ECG of the pico cell only deployment.

Similarly, Figure 7-13 compares the massive MIMO and the macro-micro and macro-pico heterogeneous deployments. When defining a target TPG value to be achieved by massive MIMO or by heterogeneous networks, the massive MIMO deployments can achieve this target with higher ECG values than the other two deployments of heterogeneous networks, which

demonstrates the potential of massive MIMO to provide superior savings in energy consumption when compared against the heterogeneous network.

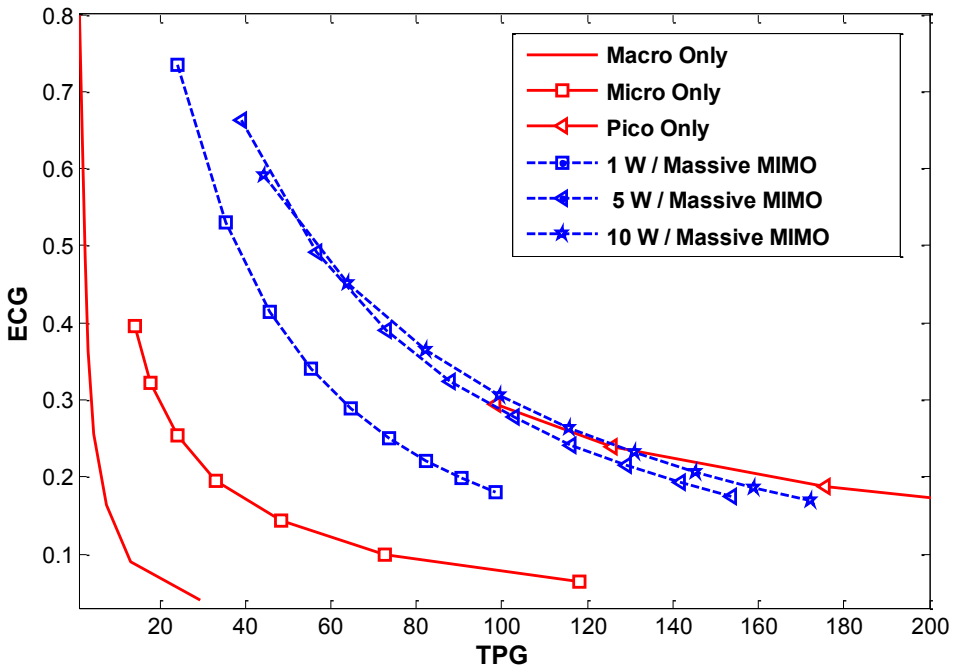

Figure 7-12: The TPG versus ECG comparison in massive MIMO and small cell deployments

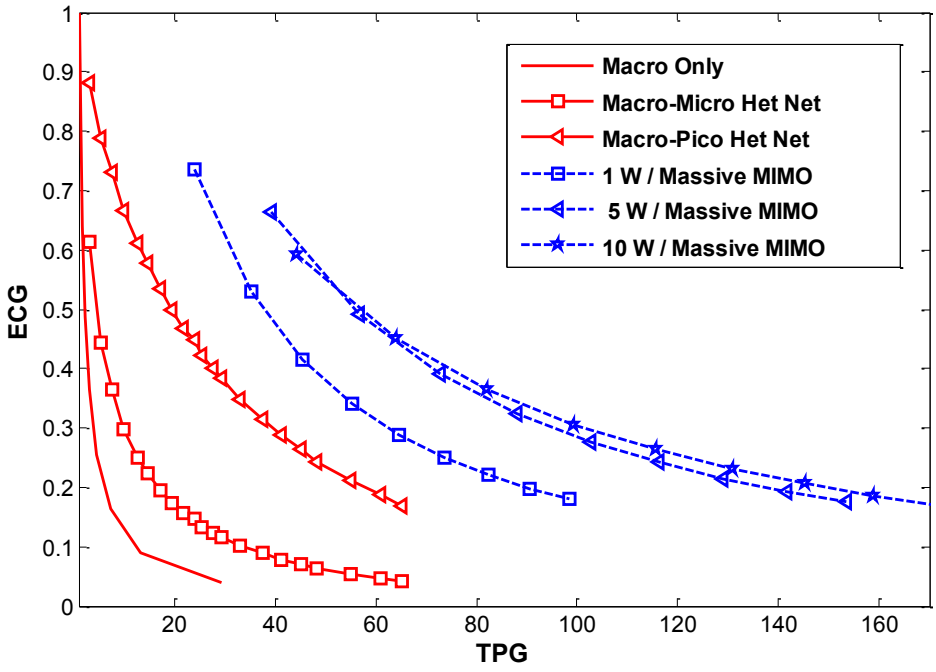

Figure 7-13: The TPG versus ECG comparison in massive MIMO and Het-Net deployments

When a backhaul power consumption of 10 watts to represent the fibre backhaul power consumption is added to the ECG analysis for each deployed base station regardless of its type,

the massive MIMO deployment becomes the most energy efficient of all the evaluated deployments, as shown in Figure 7-14. For example, massive MIMOs are able to achieve a TPG of 100 with an ECG value of around 0.3, while the pico only RAN achieve the same TPG at an ECG value of 0.18. This indicates that massive MIMO RANs consume 1.6x less energy than the pico only RANs whilst achieving a 100 times improvement in the RAN throughput with reference to a macro only reference deployment.

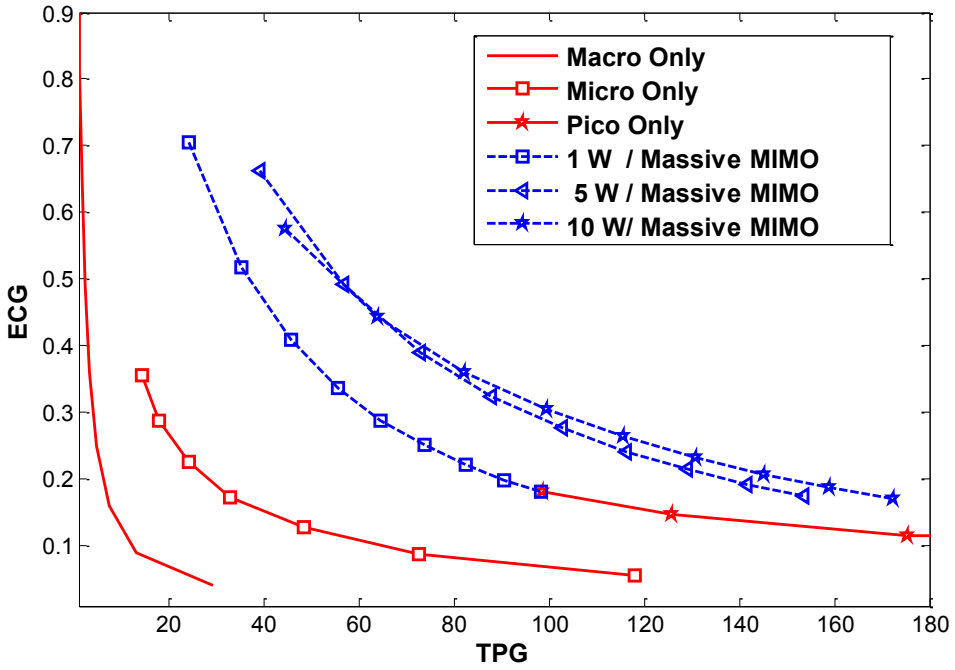

Figure 7-14: The TPG-ECG comparison between massive MIMO and small cell deployments with backhaul power consumption of 10 watts per cell considered

7.8 Summary

This chapter has investigated the issue of energy consumption in massive MIMO networks when linear MRT precoding is assumed. It began with a brief overview of massive MIMOs and the issue of the linear increase in the massive MIMO base station power consumption versus the number of antennas. The process of modelling the power consumption in massive MIMO was also detailed, and a modification to an existing power consumption model was proposed. An evaluation of the throughput and energy consumption of massive MIMO RAN was carried out with reference to a baseline deployment of macro only RAN to show the potential of such type of technology over the traditional cellular network deployments. Our findings agreed with the

existing results regarding the existence of an optimum number of antennae to maximise the massive MIMO energy efficiency measured in bit/J. However, when considering the absolute energy consumption through the ECG, the optimum number of antennas becomes the least number of antennas able to deliver the required capacity.

The chapter also included a comparison between the massive MIMO, small cells and heterogeneous networks in terms of which deployment can achieve a target TPG at the highest ECG value. The results showed the superiority of massive MIMO against the other considered deployments. However, these results are obtained by assuming pedestrian indoor environments where a very large coherence interval is used and perfect channel estimation process. Different environments which have small coherence intervals may lead to degradation in the achieved throughput due to the issue of pilot contamination between the interfering cells which in addition to the complexity of building a base station with large number of antennas are considered are the main challenging factors to overcome in massive MIMOs. On the other hand, small cells also have several drawbacks including the mobility management issue for mobile users and the huge increase in the number of backhaul links to serve the deployed small cells with represent extra cost and can lead to a significant increase in the energy consumed by these links when compared against the massive MIMO RANs.

Chapter 8

Conclusions and Future Work

8.1 Conclusions

Network operators recently realised that the traditional approach of deploying more macro cells cannot cope with the continuous growth in mobile data traffic, and if no actions are taken, the energy demand to run the networks, which are able to support such traffic volumes risks, to become unmanageable. Due to this fact, an economically sustainable capacity growth strategy needs to be adopted by the network operators when evolving their existing networks. the network energy consumption must be considered as an important key performance indicator during the phases of network planning and deployment.

In this regard, this thesis was started with the aim of providing a set of general guidelines and recommendations on what evolution path to follow by network operators to support such rapid growth in mobile data traffic and reduce the energy consumption of their networks.

Throughout the thesis, comprehensive studies of different cellular network deployments, and various algorithms have been evaluated and compared against each other by the method of system-level simulations to determine the best deployment options which are able to deliver the required capacity at a minimum level of energy consumption.

After providing an introduction to the thesis aim, objectives, motivations and listing the thesis contributions in chapter 1, a background about the evolution of cellular networks and a discussion on the need for upgrading the existing networks to meet the expected growth in traffic was presented. The enabling techniques for improving the network capacity were also covered followed by highlighting the importance of the issue of energy consumption in cellular networks. The importance of adopting a joint evaluation framework to be used throughout the thesis for evaluating fairly the throughput, energy consumption and energy efficiency in different RAN deployments is also highlighted. In addition, chapter 2 points out the need for an accurate modelling of the base station power consumption. A review of several existing base station power consumption models in the literature is presented in order to identify any limitation in the existing models. The chapter ended by a detailed review of the various energy consumption reduction approaches in cellular networks, with more focus was on the network planning and deployment-related approaches. The objective was to illustrate that the lack of a unified evaluation framework can lead to different results and even contradictory results when evaluating the same network using different methods.

The process of modelling the power consumption of a base station has been described in detail in chapter 3, and a new scalable base station power consumption model was proposed. Unlike

most of the existing models, the degradation of the power amplifier efficiency due to operating at a backed off value from the saturation power is captured by the model. Also, novel method for estimating the cooling unit power consumption is implemented.

A joint evaluation framework for the spectral and energy efficiency in cellular networks is adopted in chapter 3, where the throughput gain TPG, energy consumption gain ECG, and energy throughput gain ETG are presented as three figures of merit used to evaluate the relative improvements in throughput, energy consumption and energy efficiency with reference to a baseline reference deployment. The advantage of such a framework is that the inherent ambiguity of using the bit/J EE metric is avoided by clearly indicating whether the improvement in the energy efficiency was due to increasing the TPG, ECG or both.

The adopted framework is able to quantify the relative improvements in the energy efficiency EE by the ETG which is formed by the product of ECG and TPG, where ECG indicates clearly if a reduction in the energy consumption is obtained or not, while TPG refers to a throughout gain with reference to a baseline deployment. By adopting such a framework, the concept of an energy efficient network is not limited to maximising the bit/J metric only, but includes maximising the ECG to achieve a certain TPG target, i.e. reducing the energy consumption is one of the main focuses of network operators during any network upgrade or deployment process. Unlike the traditional bit/J metric, this framework is valid when comparing the energy consumption of two idle networks through the use of ECG, which was not possible by the bit/J or ECR, as the throughput equals zero in any idle network.

An extensive analysis of the energy consumption in a macro cell RANs was carried out to show that scaling down the macro base station average transmitted power, and fixing the power amplifier efficiency outperforms the cases of keeping the same average transmitted power of the base station regardless of the cell radius, and the case of using the same power amplifier design for wide range of power amplifier output average transmitted. The analysis also considered the microcell only RANs, picocell only RANs, macro-micro heterogeneous RANs, and macro-pico heterogeneous RANs. The results obtained have shown that pico cell only deployments consume the least amount of energy when compared with the other deployments to achieve the same target capacity, while the macro-pico heterogeneous deployments come in the second place behind the pico cell only. When the impact of the backhaul power consumption was included in the analysis, the results have shown that the energy consumption of small cells and heterogeneous networks increases significantly compared with the macrocell RANs. However, they continue to consume the least amount of energy in comparison with the macrocell only RANs when the same target capacity is required.

The issue of evaluating the energy consumption in cellular networks when high order sectorisation and small cell densification are used to enhance the RAN capacity was investigated in chapter 4, by comparing the energy consumption of 3- and 6-sector macrocell

heterogeneous RANs. The aim was to ascertain if network operators can obtain greater energy savings by increasing the sectorisation order before densifying with a small cell overlay, or should an overlay of small cells be added without increasing the sectorisation order. The results showed that densifying 3-sector macro RANs consumes less energy than upgrading to 6-sector macro RANs before deploying the small cells. These results hold true in the two cases of deploying micro and picocells. The analysis is extended by implementing various schemes of adaptive sectorisation, and evaluating the possible energy savings when the same daily traffic profile is considered in the various schemes. The observed improvements in the ECG of macro RANs depend on which scheme was implemented. For example, 15% increase in the ECG is obtained when implementing coarse adaptive sectorisation in 3-sector macrocells, whereas 32% increase is obtained for the fine adaptive sectorisation in 6-sector cells. Although increasing the sectorisation order to meet the capacity demands uses fewer small cells, this strategy consumes more energy than using fewer sectors with more small cells to meet the same capacity requirements. This conclusion is contra to the prevailing network operators' practice of deploying more sectors before adding small cells. The operators' practice arises from the difficulties of finding new sites to deploy small cells, and due to the need for backhaul links to connect the small cells with the core network.

Evaluating the energy consumption in MIMO RANs was another important issue investigated in the thesis, to examine whether or not deploying MIMO base stations leads to reduced energy consumption when compared against deploying SISO base stations if the same target capacity is sought. The same evaluation framework of chapter 3 is used to evaluate the energy consumption of various MIMO schemes with reference to SISO ones. The analysis is carried out for the case of new deployments where the operators have the choice to decide whether to deploy SISO or MIMO base stations. The results showed that fewer MIMO than SISO cells were required to achieve the same capacity requirement. As a result, the approach of dimensioning the RAN using MIMO base stations consumes less energy than using SISO base stations.

The same issue is investigated in the case of upgrading the SISO base stations in an existing RAN to MIMO base stations in order to improve the users' data rates, whilst the overall offered traffic stay at the same level. A Non full buffer traffic model is implemented to model the variation in the a average traffic load to find if the reduction in the load-dependent power consumption of a MIMO base station, due to the decrease in the cell average traffic load, can offset the increase in the power consumption of the same MIMO base station due to the added extra RF transceivers. The results of this analysis showed that deploying 2x2 MIMO base stations seems to consume the least amount of energy compared with SISO, 4x4 and 8X8 MIMO schemes. If DTX is enabled, and MIMO schemes benefit more from implementing the DTX, and upgrading to a 4x4 MIMO scheme becomes more energy efficient than keeping SISO

base stations. On the other hand, MIMO base stations in small cell deployments consume more energy than SISO ones regardless of whether the DTX is enabled or not.

Comprehensive analysis of the energy efficiency in heterogeneous networks was carried out in chapter 6, where traffic offloading to small cells, and sleep mode techniques were implemented. The objective was to investigate whether the amount of reduction in the power consumption in macrocells due to traffic offloading is larger than the increase in power consumption due to deploying more small cells or not. A bursty FTP traffic model and distributed sleep mode scheme in small cells were implemented in the simulation to quantify the possible energy savings due to such implementation. Various small cell densities and different cell range expansion values (CRE) were simulated, the users and small cells are assumed to be uniformly distributed. The results showed that even if the energy efficiency in terms of bit/J is improved, the energy consumption gain decreases which indicates to a rise in the RAN energy consumption. This increase in RAN energy consumption seems to be unavoidable in the case of a uniform user distribution. However, it can be slowed down by implementing sleep mode in small cells. Interestingly, when the small cells are deployed in the centre of clusters of users, joint improvement in the throughput and a reduction in the energy consumption is observed at CRE values higher than 15 dB.

The potential of dense heterogeneous network deployments in terms of the achieved throughput gain and energy consumption is also investigated at different small cell densities and different CRE values. The results have shown that the achieved throughput gain through such deployment is always accompanied by an increase in the network energy consumption. To mitigate this effect, a joint deployment of distributed sleep mode in small cells, and inter-cell interference coordination technique eICIC in macrocells were implemented. Although these techniques cannot prevent an increase in the network energy consumption due to deploying a high density of small cells, their implementation leads to increasing the RAN TPG and decreasing the RAN energy consumption compared with the case of no sleep mode and no eICIC.

The thesis ended by considering the throughput and energy consumption in massive MIMO deployments as a promising candidate expected to be deployed in the next generations of the cellular networks. After modifying an existing massive MIMO base station power consumption model, the same evaluation framework of chapter 3 is adopted to quantify the throughput and energy consumption of a TDD massive MIMO network with reference to a traditional macro only deployment when maximum ratio transmission (MRT) precoding and perfect channel estimation are assumed in massive MIMOs. Significant savings in the energy consumption is observed when energy consumption of massive MIMOs is compared to that of macrocell RANs when achieving the same target TPG. The energy consumption of massive MIMO is also compared versus small cells, and heterogeneous networks to show the superiority of massive

MIMOs versus all other considered deployments by achieving the highest ECG at the same target TPG. Massive MIMOs and pico only deployments consume nearly the same level of energy to achieve the same target TPG if backhaul is not considered. When backhaul power consumption is included, massive MIMOs outperforms picocells and consume the least amount of energy among all the evaluated deployments.

Finally, a set of guidelines and recommendation presented below summarise the main findings of the thesis which can be helpful for network operators and regarded as a part of an evolution path to follow by network operators, when evolving their networks.

- Macrocell densification represents the worst deployment option to consider in terms of the energy consumption. However, the throughput of the existing macro RANs can be improved by adding more sectors, while the increase in energy consumption is reduced by implementing an adaptive sectorisation scheme. Users' data rates can be improved without increasing the energy consumption by upgrading SISO macro cells to 2x2 MIMOs, or to 4x4 MIMOs if DTX is enabled. In addition, the average maximum transmitted power of a macrocell base station must be scaled down when reducing the inter-site distance, and the degradation in the power amplifier efficiency due to operating at lower output power must be avoided through custom design of the PA to ensure the operation at the same PA efficiency regardless of the cell radius, or through the use of PA efficiency improvement techniques.
- Although each network evolution is very case-specific, the following deployments are listed in order according to which ones consume the least amount of energy to achieve the same target capacity. Also, some results obtained during the research are indicated in front of each item of the list.
    1. Massive MIMOs: A reduction by a factor of 1.6 in the energy consumption is achieved by massive MIMOs when compared with picocell only at the same target capacity, and when the backhaul power consumption is included in the analysis.
    2. Picocells only: Pico cell only deployments attain up to 3 times increase in the throughput and 2.27 times reduction in the energy consumed when compared with macro only RANs at high target capacities, they also offer 2 times more throughput and reduces the energy consumption by 10% when compared with the macro/pico HetNet deployments.
    3. Macro/pico heterogeneous networks: Orthogonal channel HetNet deployment can reduce the energy consumption by a factor of 7 when compared with macro only RANs at not very high target capacities.

4. Microcells only: an energy reduction factor of 4.34 is obtained by micro only deployments when compared with macro only RANs at the same target capacity.
5. Macro/micro heterogeneous networks. A reduction factor of 2.45 in the energy consumption is achievable when compared with macro only RANs at the same target capacity.
6. Macro only deployments.

Certain deployment types such as pico only and micro only can be deployed only in specific environments such as dense urban area, stadiums and indoor deployments. Also, when low target capacities are required, pico only and micro only deployments risk becoming lightly loaded, which make the heterogeneous network deployments more suitable, as any lightly loaded small cell in heterogeneous network can be put in sleep mode without any negative impact on the network coverage which is provided by the macrocell layer.

8.2 Future work

1. Modelling of the backhaul power consumption is required to evaluate its impact on the network energy consumption; the backhaul power consumption in this thesis is often modelled by fixed amount of 10 watts per base station to represent the power consumption of fibre a backhaul link. However, the exact value can vary according to the technology used, and the network topology deployed. Modelling the power consumption when millimetre wave links or microwave links are used can be an interesting extension to the current research in the thesis. Also investigating the impact of cell average traffic load on the power consumption of backhaul links needs to be considered, especially in dense small cell deployments where the variation in the cell load is expected to be large.
2. The development of semi a distributed sleep mode scheme, where the decision of switching off the small cell is taken in a distributed manner independently by the base station itself while switching it back on, needs some coordination with a centralised unit which has global knowledge of the network status. This approach can decrease the number of wake up operations of small cells and must use new air interface functionality, not the backhaul links when coordinating with the neighbor cells to avoid having the backhaul on all the time.
3. As the power consumption of picocells continues to decrease (below 8 watts in this thesis), this power can be supplied fully or partially by renewable energy resources when available. One logic extension to this thesis can be an evaluation of dense heterogeneous network where renewable energy resources are used to supply power to

picocells in combination with a sleep mode strategy which considers the type of power supply (electric grid or renewable energy) when deciding to switch off the base station.

4. The analysis of energy efficiency of massive MIMOs needs to be extended to cover more precoding techniques, different environments where the duration of the coherent interval is small, and when channel estimation errors are considered to examine whether massive MIMO can keep its superiority or not in terms of the achieved throughput and the energy consumption versus the other deployment options. Considering the case of a non-full buffer traffic model is also required to investigate how the energy consumption is impacted during the periods of very low traffic demand, where an implementation of an adaptive antenna muting scheme may be needed to deal with such a scenario.

References

[1] H. T. A. Holma. (2011). *LTE for UMTS evolution to LTE-Advanced*.

[2] C. Cox, *An introduction to LTE : LTE, LTE-advanced, SAE, and 4G mobile communications*. Hoboken, NJ: John Wiley & Sons, 2012.

[3] A. Ericsson, "Ericsson mobility report: On the pulse of the Networked Society," *Ericsson, Sweden, Tech. Rep. EAB-14,* vol. 61078, 2016.

[4] E. Dahlman, G. Mildh, S. Parkvall, J. Peisa, J. Sachs, and Y. Selen, "5G radio access," *ERICSSON REVIEW,* 2014.

[5] B. Bangerter, S. Talwar, R. Arefi, and K. Stewart, "Networks and devices for the 5G era," *IEEE Communications Magazine,* vol. 52, pp. 90-96, 2014.

[6] C. Forster, I. Dickie, G. Maile, H. Smith, and M. Crisp, "Understanding the environmental impact of communication systems," *Ofcom final report,* 2009.

[7] L. Zhao, G. Zhao, and T. O'Farrell, "Efficiency metrics for wireless communications," in *2013 IEEE 24th Annual International Symposium on Personal, Indoor, and Mobile Radio Communications (PIMRC)*, 2013, pp. 2825-2829.

[8] H. Holma, A. Toskala, and J. Reunanen, *LTE Small Cell Optimization: 3GPP Evolution to Release 13*: John Wiley & Sons, 2016.

[9] 3GPP, "3rd Generation Partnership Project (2017) 3GPP – Releases. ," 2017.

[10] Cisco Visual Networking, "Global Mobile Data Traffic Forecast Update 2014–2019. White Paper c11-520862," *Available on http://www. cisco. com/c/en/us/solutions/collateral/serviceprovider/visual-networking-index-vni/white_paper_c11-520862. html,* 2015.

[11] Arraycomm.com. (2015, 17 December). *Cooper's Law*. Available: http://www.arraycomm.com/technology/coopers-law/

[12] P. A. J, G. D. A, N. R. U, and B. H, "An overview of MIMO communications - a key to gigabit wireless," *Proceedings of the IEEE,* vol. 92, pp. 198-218, 2004.

[13] E. G. Larsson, O. Edfors, F. Tufvesson, and T. L. Marzetta, "Massive MIMO for next generation wireless systems," *IEEE Communications Magazine,* vol. 52, pp. 186-195, 2014.

[14] T. S. Rappaport, S. Sun, R. Mayzus, H. Zhao, Y. Azar, K. Wang, *et al.*, "Millimeter Wave Mobile Communications for 5G Cellular: It Will Work!," *IEEE Access,* vol. 1, pp. 335-349, 2013.

[15] R. Singh, T. O'Farrell, and J. P. R. David, "An Enhanced Color Shift Keying Modulation Scheme for High-Speed Wireless Visible Light Communications," *Journal of Lightwave Technology,* vol. 32, pp. 2582-2592, 2014.

[16] B. Clerckx and C. Oestges, *MIMO wireless networks: Channels, techniques and standards for multi-antenna, multi-user and multi-cell systems*: Academic Press, 2013.

[17] T. L. Marzetta, E. G. Larsson, H. Yang, and H. Q. Ngo, *Fundamentals of Massive MIMO*: Cambridge University Press, 2016.

[18] T. Van Chien and E. Björnson, "Massive MIMO Communications," in *5G Mobile Communications*, W. Xiang, K. Zheng, and X. S. Shen, Eds., ed: Springer, 2017.

[19] T. L. Marzetta, "Noncooperative Cellular Wireless with Unlimited Numbers of Base Station Antennas," *IEEE Transactions on Wireless Communications,* vol. 9, pp. 3590-3600, 2010.

[20] H. Q. Ngo, E. G. Larsson, and T. L. Marzetta, "Energy and Spectral Efficiency of Very Large Multiuser MIMO Systems," *IEEE Transactions on Communications,* vol. 61, pp. 1436-1449, 2013.

[21] C. V. N. I. Cisco, "Global mobile data traffic forecast update, 2016–2021," *white paper,* 2017.

[22] Y. Li, M. Sheng, C. Yang, and X. Wang, "Energy Efficiency and Spectral Efficiency Tradeoff in Interference-Limited Wireless Networks," *IEEE Communications Letters,* vol. 17, pp. 1924-1927, 2013.
[23] R K Bhatnagar and P. K. Panigrahi, "Energy Efficiency, Clean Power as Engine for Sustainable Growth," ed, 2013.
[24] J. Thompson and C. Khirallah, "Overview of Green Radio research outcomes," in *Communications in China Workshops (ICCC), 2012 1st IEEE International Conference on*, 2012, pp. 69-73.
[25] K. Hongseok, C. Chan-Byoung, G. de Veciana, and R. W. Heath, "A cross-layer approach to energy efficiency for adaptive MIMO systems exploiting spare capacity," *Wireless Communications, IEEE Transactions on,* vol. 8, pp. 4264-4275, 2009.
[26] *GreenTouch*. Available: http://www.greentouch.org/
[27] B. Debaillie, C. Desset, and F. Louagie, "A Flexible and Future-Proof Power Model for Cellular Base Stations," in *Vehicular Technology Conference (VTC Spring), 2015 IEEE 81st*, 2015, pp. 1-7.
[28] C. Tao, K. Haesik, and Y. Yang, "Energy efficiency metrics for green wireless communications," in *Wireless Communications and Signal Processing (WCSP), 2010 International Conference on*, 2010, pp. 1-6.
[29] ITU, "Requirement related to technical performance for IMT-advanced radio interfaces," 2008.
[30] ITU, "Draft new Report ITU-R M.[IMT-2020.TECH PERF REQ] - Minimum requirements related to technical performance for IMT-2020 radio interface(s)," 2017.
[31] ETSI, "Enviromental Engineering (EE); Measurement method for energy efficiency of wireless access network equipment," ETSI2013.
[32] A. J. Fehske, F. Richter, and G. P. Fettweis, "Energy Efficiency Improvements through Micro Sites in Cellular Mobile Radio Networks," in *GLOBECOM Workshops, 2009 IEEE*, 2009, pp. 1-5.
[33] E. B. V. K. F. G. P. Hossain, Ed., *Green radio communication networks*. Cambridge, UK; N.Y.: Cambridge University Press, 2012, p.^pp. Pages.
[34] G. Weisi and T. O'Farrell, "Green cellular network: Deployment solutions, sensitivity and tradeoffs," in *Wireless Advanced (WiAd), 2011*, 2011, pp. 42-47.
[35] "Nokia Siemens Networks, "ETSI RRS05-024"," 2011.
[36] D. Lister, "An operator's view on green radio," *Keynote Speech, GreenComm,* 2009.
[37] O. Arnold, F. Richter, G. Fettweis, and O. Blume, "Power consumption modeling of different base station types in heterogeneous cellular networks," in *Future Network and Mobile Summit, 2010*, 2010, pp. 1-8.
[38] M. Deruyck, W. Joseph, and L. Martens, "Power consumption model for macrocell and microcell base stations," *Transactions on Emerging Telecommunications Technologies,* pp. n/a-n/a, 2012.
[39] C. Desset, B. Debaillie, V. Giannini, A. Fehske, G. Auer, H. Holtkamp*, et al.*, "Flexible power modeling of LTE base stations," in *Wireless Communications and Networking Conference (WCNC), 2012 IEEE*, 2012, pp. 2858-2862.
[40] G. Auer, V. Giannini, C. Desset, I. Godor, P. Skillermark, M. Olsson*, et al.*, "How much energy is needed to run a wireless network?," *Wireless Communications, IEEE,* vol. 18, pp. 40-49, 2011.
[41] H. Holtkamp, G. Auer, V. Giannini, and H. Haas, "A Parameterized Base Station Power Model," *Communications Letters, IEEE,* vol. 17, pp. 2033-2035, 2013.
[42] M. a. K. Ali Imran, E, "Energy efficiency analysis of the reference systems, areas of improvements and target breakdown," Earth Project2010.
[43] T. O'Farrell and S. Fletcher, "Green Communication Concepts, Energy Metrics and Throughput Efficiency for Wireless Systems," in *Green Communications: Principles, Concepts and Practice*, ed, 2015, pp. 19-42.
[44] MobileVCE. Available: http://www.mobilevce.com
[45] H. Claussen, L. T. Ho, and F. Pivit, "Leveraging advances in mobile broadband technology to improve environmental sustainability," *Telecommunications Journal of Australia,* vol. 59, 2010.

[46] W. H. Doherty, "A New High Efficiency Power Amplifier for Modulated Waves," *Proceedings of the Institute of Radio Engineers,* vol. 24, pp. 1163-1182, 1936.
[47] B. Kim, J. Kim, I. Kim, and J. Cha, "The Doherty power amplifier," *IEEE Microwave Magazine,* vol. 7, pp. 42-50, 2006.
[48] J. Kim, J. Son, S. Jee, S. Kim, and B. Kim, "Optimization of Envelope Tracking Power Amplifier for Base-Station Applications," *IEEE Transactions on Microwave Theory and Techniques,* vol. 61, pp. 1620-1627, 2013.
[49] S. N. Ali and T. Johnson, "A new high efficiency RF switch-mode power amplifier architecture for pulse encoded signals," in *Wireless and Microwave Technology Conference (WAMICON), 2012 IEEE 13th Annual*, 2012, pp. 1-6.
[50] S. A. El-Hamamsy, "Design of high-efficiency RF Class-D power amplifier," *IEEE Transactions on Power Electronics,* vol. 9, pp. 297-308, 1994.
[51] C. H. Tang, C. E. Wu, C. W. Lin, and C. Y. Liao, "Network energy efficiency for deployment architectures with base station site model," in *Communications in China Workshops (ICCC), 2012 1st IEEE International Conference on*, 2012, pp. 85-90.
[52] A. Conte, "Energy-Efficient Base Stations," in *Green Communications*, ed: John Wiley & Sons, Ltd, 2015, pp. 73-96.
[53] Y. Lin, L. Shao, Z. Zhu, Q. Wang, and R. K. Sabhikhi, "Wireless network cloud: Architecture and system requirements," *IBM Journal of Research and Development,* vol. 54, pp. 4:1-4:12, 2010.
[54] L. Chen, H. Jin, H. Li, J. B. Seo, Q. Guo, and V. Leung, "An Energy Efficient Implementation of C-RAN in HetNet," in *2014 IEEE 80th Vehicular Technology Conference (VTC2014-Fall)*, 2014, pp. 1-5.
[55] D. Sabella, A. d. Domenico, E. Katranaras, M. A. Imran, M. d. Girolamo, U. Salim*, et al.*, "Energy Efficiency Benefits of RAN-as-a-Service Concept for a Cloud-Based 5G Mobile Network Infrastructure," *IEEE Access,* vol. 2, pp. 1586-1597, 2014.
[56] M. S. Alouini and A. J. Goldsmith, "Area spectral efficiency of cellular mobile radio systems," *Vehicular Technology, IEEE Transactions on,* vol. 48, pp. 1047-1066, 1999.
[57] B. Badic, T. O'Farrrell, P. Loskot, and J. He, "Energy efficient radio access architectures for green radio: large versus small cell size deployment," in *Vehicular Technology Conference Fall (VTC 2009-Fall), 2009 IEEE 70th*, 2009, pp. 1-5.
[58] T. A. Le and M. R. Nakhai, "Possible power-saving gains by dividing a cell into tiers of smaller cells," *Electronics Letters,* vol. 46, pp. 1163-1165, 2010.
[59] C. Yan, Z. Shunqing, and X. Shugong, "Characterizing Energy Efficiency and Deployment Efficiency Relations for Green Architecture Design," in *Communications Workshops (ICC), 2010 IEEE International Conference on*, 2010, pp. 1-5.
[60] H. Leem, S. Y. Baek, and D. K. Sung, "The Effects of Cell Size on Energy Saving, System Capacity, and Per-Energy Capacity," in *2010 IEEE Wireless Communication and Networking Conference*, 2010, pp. 1-6.
[61] F. Richter, A. J. Fehske, and G. P. Fettweis, "Energy Efficiency Aspects of Base Station Deployment Strategies for Cellular Networks," in *Vehicular Technology Conference Fall (VTC 2009-Fall), 2009 IEEE 70th*, 2009, pp. 1-5.
[62] F. Richter, A. J. Fehske, P. Marsch, and G. P. Fettweis, "Traffic Demand and Energy Efficiency in Heterogeneous Cellular Mobile Radio Networks," in *Vehicular Technology Conference (VTC 2010-Spring), 2010 IEEE 71st*, 2010, pp. 1-6.
[63] M. Ericson, "Total Network Base Station Energy Cost vs. Deployment," in *Vehicular Technology Conference (VTC Spring), 2011 IEEE 73rd*, 2011, pp. 1-5.
[64] D. Zeller, M. Olsson, O. Blume, A. Fehske, D. Ferling, W. Tomaselli*, et al.*, "Sustainable Wireless Broadband Access to the Future Internet - The EARTH Project," in *The Future Internet: Future Internet Assembly 2013: Validated Results and New Horizons*, A. Galis and A. Gavras, Eds., ed Berlin, Heidelberg: Springer Berlin Heidelberg, 2013, pp. 249-271.
[65] S. Tombaz, A. Vastberg, and J. Zander, "Energy- and cost-efficient ultra-high-capacity wireless access," *Wireless Communications, IEEE,* vol. 18, pp. 18-24, 2011.

[66] K. Jean-Marc, C. Marceau, and G. Philippe, "A fluid model for performance analysis in cellular networks," *EURASIP Journal on Wireless Communications and Networking,* vol. 2010, 2010.

[67] H. Huang, O. Alrabadi, J. Daly, D. Samardzija, C. Tran, R. Valenzuela*, et al.*, "Increasing throughput in cellular networks with higher-order sectorization," in *Signals, Systems and Computers (ASILOMAR), 2010 Conference Record of the Forty Fourth Asilomar Conference on*, 2010, pp. 630-635.

[68] R. Joyce, D. Morris, S. Brown, D. Vyas, and L. Zhang, "Higher Order Horizontal Sectorisation Gains for 6, 9, 12 and 15 Sectored Cell Sites in a 3GPP/HSPA+ Network," 2015.

[69] I. Riedel and G. Fettweis, "Increasing throughput and fairness in the downlink of cellular systems with N-fold sectorization," in *GLOBECOM Workshops (GC Wkshps), 2011 IEEE*, 2011, pp. 167-172.

[70] R. Maslennikov, A. Trushanin, O. Testov, M. Vechkanov, A. Antipova, T. A. Thomas*, et al.*, "Azimuth and elevation sectorization for the stadium environment," in *Global Communications Conference (GLOBECOM), 2013 IEEE*, 2013, pp. 3971-3976.

[71] F. Athley, M. N. Johansson, and A. Nilsson, "Increased Sectorization: Horizontal or Vertical?," in *Vehicular Technology Conference (VTC Fall), 2013 IEEE 78th*, 2013, pp. 1-5.

[72] L. G. Hevizi and I. Godor, "Power savings in mobile networks by dynamic base station sectorization," in *Personal Indoor and Mobile Radio Communications (PIMRC), 2011 IEEE 22nd International Symposium on*, 2011, pp. 2415-2417.

[73] Q. Yinan, M. A. Imran, and R. Tafazolli, "Energy-aware adaptive sectorisation in LTE systems," in *Personal Indoor and Mobile Radio Communications (PIMRC), 2011 IEEE 22nd International Symposium on*, 2011, pp. 2402-2406.

[74] W. Guo, J. M. Rigelsford, L. Ford, and T. O'Farrell, "Dynamic basestation antenna design for low energy networks," *Progress In Electromagnetics Research C,* vol. 31, pp. 153-168, 2012.

[75] M. F. Hossain, K. S. Munasinghe, and A. Jamalipour, "Energy-Aware Dynamic Sectorization of Base Stations in Multi-Cell OFDMA Networks," *Wireless Communications Letters, IEEE,* vol. 2, pp. 587-590, 2013.

[76] D. Zhang and L. Cuthbert, "Dynamic sectorisation based on genetic algorithms for OFDMA networks," 2011.

[77] S. Cui, A. J. Goldsmith, and A. Bahai, "Energy-efficiency of MIMO and cooperative MIMO techniques in sensor networks," *Selected Areas in Communications, IEEE Journal on,* vol. 22, pp. 1089-1098, 2004.

[78] C. Turyagyenda, T. O. Farrell, J. He, and P. Loskot, "SFBC MIMO Energy Efficiency Improvements of Common Packet Schedulers for the Long Term Evolution Downlink," in *Vehicular Technology Conference (VTC Spring), 2011 IEEE 73rd*, 2011, pp. 1-5.

[79] O. Adigun and C. Politis, "Energy efficiency analysis for MIMO transmission schemes in LTE," in *Computer Aided Modeling and Design of Communication Links and Networks (CAMAD), 2011 IEEE 16th International Workshop on*, 2011, pp. 77-81.

[80] F. D. Cardoso, R. Torrea-Duran, C. Desset, and L. M. Correia, "MIMO strategies for energy efficient transmission in LTE pico-cell environments," in *Software, Telecommunications and Computer Networks (SoftCOM), 2012 20th International Conference on*, 2012, pp. 1-5.

[81] F. Heliot, M. A. Imran, and R. Tafazolli, "On the energy efficiency gain of MIMO communication under various power consumption models," in *Future Network & Mobile Summit (FutureNetw), 2011*, 2011, pp. 1-9.

[82] M. T. Kakitani, G. Brante, R. D. Souza, and M. A. Imran, "Downlink Energy Efficiency Analysis of Some Multiple Antenna Systems," in *2013 IEEE 77th Vehicular Technology Conference (VTC Spring)*, 2013, pp. 1-5.

[83] R. Bendlin, V. Chandrasekhar, R. Chen, A. Ekpenyong, and E. Onggosanusi, "From homogeneous to heterogeneous networks: A 3GPP long term evolution rel. 8/9 case study," in *Information Sciences and Systems (CISS), 2011 45th Annual Conference on*, 2011, pp. 1-5.

[84] F. Richter and G. Fettweis, "Cellular Mobile Network Densification Utilizing Micro Base Stations," in *Communications (ICC), 2010 IEEE International Conference on*, 2010, pp. 1-6.

[85] S. Tombaz, M. Usman, and J. Zander, "Energy efficiency improvements through heterogeneous networks in diverse traffic distribution scenarios," in *Communications and Networking in China (CHINACOM), 2011 6th International ICST Conference on*, 2011, pp. 708-713.

[86] T. Q. S. Quek, W. C. Cheung, and M. Kountouris, "Energy Efficiency Analysis of Two-Tier Heterogeneous Networks," in *Wireless Conference 2011 - Sustainable Wireless Technologies (European Wireless), 11th European*, 2011, pp. 1-5.

[87] L. Saker, G. Micallef, S.-E. Elayoubi, and H. O. Scheck, "Impact of picocells on the capacity and energy efficiency of mobile networks," *annals of telecommunications-annales des télécommunications,* vol. 67, pp. 133-146, 2012.

[88] H. Klessig, M. Gunze, and G. Fettweis, "Energy efficiency gains through data offloading in heterogeneous small cell networks," in *Communication Systems (ICCS), 2014 IEEE International Conference on*, 2014, pp. 117-121.

[89] G. Micallef, P. Mogensen, H. O. Scheck, and E. Lang, "Energy Efficient Evolution of Mobile Networks: Macro-Only Upgrades vs. a Joint-Pico Deployment Strategy," in *Vehicular Technology Conference (VTC Spring), 2011 IEEE 73rd*, 2011, pp. 1-5.

[90] D. López-Pérez, M. Ding, H. Claussen, and A. H. Jafari, "Towards 1 Gbps/UE in cellular systems: Understanding ultra-dense small cell deployments," *IEEE Communications Surveys & Tutorials,* vol. 17, pp. 2078-2101.

[91] S. Tombaz, P. Monti, F. Farias, M. Fiorani, L. Wosinska, and J. Zander, "Is backhaul becoming a bottleneck for green wireless access networks?," in *2014 IEEE International Conference on Communications (ICC)*, 2014, pp. 4029-4035.

[92] Z. Kan, W. Yuyu, W. Wenbo, M. Dohler, and W. Jianquan, "Energy-efficient wireless in-home: the need for interference-controlled femtocells," *Wireless Communications, IEEE,* vol. 18, pp. 36-44, 2011.

[93] C. Fengming and F. Zhong, "The tradeoff between energy efficiency and system performance of femtocell deployment," in *Wireless Communication Systems (ISWCS), 2010 7th International Symposium on*, 2010, pp. 315-319.

[94] L. M. del Apio, E. Mino, L. Cucala, O. Moreno, I. Berberana, and E. Torrecilla, "Energy Efficiency and Performance in mobile networks deployments with femtocells," in *Personal Indoor and Mobile Radio Communications (PIMRC), 2011 IEEE 22nd International Symposium on*, 2011, pp. 107-111.

[95] K. Dufková, J.-Y. Le Boudec, M. Popović, M. Bjelica, R. Khalili, and L. Kencl, "Energy consumption comparison between macro-micro and public femto deployment in a plausible LTE network," in *Proceedings of the 2nd International Conference on Energy-Efficient Computing and Networking*, 2011, pp. 67-76.

[96] P. Skillermark and P. Frenger, "Enhancing Energy Efficiency in LTE with Antenna Muting," in *Vehicular Technology Conference (VTC Spring), 2012 IEEE 75th*, 2012, pp. 1-5.

[97] J. Wu, Y. Zhang, M. Zukerman, and E. K. N. Yung, "Energy-Efficient Base-Stations Sleep-Mode Techniques in Green Cellular Networks: A Survey," *IEEE Communications Surveys & Tutorials,* vol. 17, pp. 803-826, 2015.

[98] H. Tabassum, U. Siddique, E. Hossain, and M. J. Hossain, "Downlink Performance of Cellular Systems With Base Station Sleeping, User Association, and Scheduling," *IEEE Transactions on Wireless Communications,* vol. 13, pp. 5752-5767, 2014.

[99] S. Tombaz, S. w. Han, K. W. Sung, and J. Zander, "Energy Efficient Network Deployment With Cell DTX," *IEEE Communications Letters,* vol. 18, pp. 977-980, 2014.

[100] J. F. Cheng, H. Koorapaty, P. Frenger, D. Larsson, and S. Falahati, "Energy Efficiency Performance of LTE Dynamic Base Station Downlink DTX Operation," in *2014 IEEE 79th Vehicular Technology Conference (VTC Spring)*, 2014, pp. 1-5.

[101] P. Frenger, P. Moberg, J. Malmodin, Y. Jading, and I. Godor, "Reducing Energy Consumption in LTE with Cell DTX," in *Vehicular Technology Conference (VTC Spring), 2011 IEEE 73rd*, 2011, pp. 1-5.

[102] R. Wang, J. S. Thompson, and H. Haas, "A novel time-domain sleep mode design for energy-efficient LTE," in *2010 4th International Symposium on Communications, Control and Signal Processing (ISCCSP)*, 2010, pp. 1-4.

[103] F. Han, S. Zhao, L. Zhang, and J. Wu, "Survey of Strategies for Switching Off Base Stations in Heterogeneous Networks for Greener 5G Systems," *IEEE Access,* vol. 4, pp. 4959-4973, 2016.

[104] A. Bousia, A. Antonopoulos, L. Alonso, and C. Verikoukis, ""Green" distance-aware base station sleeping algorithm in LTE-Advanced," in *2012 IEEE International Conference on Communications (ICC)*, 2012, pp. 1347-1351.

[105] F. Han, Z. Safar, W. S. Lin, Y. Chen, and K. J. R. Liu, "Energy-efficient cellular network operation via base station cooperation," in *2012 IEEE International Conference on Communications (ICC)*, 2012, pp. 4374-4378.

[106] P. Dini, M. Miozzo, N. Bui, and N. Baldo, "A Model to Analyze the Energy Savings of Base Station Sleep Mode in LTE HetNets," in *2013 IEEE International Conference on Green Computing and Communications and IEEE Internet of Things and IEEE Cyber, Physical and Social Computing*, 2013, pp. 1375-1380.

[107] I. Ashraf, F. Boccardi, and L. Ho, "SLEEP mode techniques for small cell deployments," *Communications Magazine, IEEE,* vol. 49, pp. 72-79, 2011.

[108] W. Li, W. Zheng, Y. Xie, and X. Wen, "Clustering based power saving algorithm for self-organized sleep mode in femtocell networks," in *The 15th International Symposium on Wireless Personal Multimedia Communications*, 2012, pp. 379-383.

[109] K. Samdanis, D. Kutscher, and M. Brunner, "Self-organized energy efficient cellular networks," in *21st Annual IEEE International Symposium on Personal, Indoor and Mobile Radio Communications*, 2010, pp. 1665-1670.

[110] T. L. Marzetta, "Massive MIMO: An Introduction," *Bell Labs Technical Journal,* vol. 20, pp. 11-22, 2015.

[111] E. Björnson, L. Sanguinetti, J. Hoydis, and M. Debbah, "Optimal Design of Energy-Efficient Multi-User MIMO Systems: Is Massive MIMO the Answer?," *IEEE Transactions on Wireless Communications,* vol. 14, pp. 3059-3075, 2015.

[112] Y. Guo, J. Tang, G. Wu, and S. Li, "Power allocation for massive MIMO: Impact of power amplifier efficiency," in *2015 IEEE/CIC International Conference on Communications in China (ICCC)*, 2015, pp. 1-6.

[113] H. V. Cheng, D. Persson, E. Björnson, and E. G. Larsson, "Massive MIMO at night: On the operation of massive MIMO in low traffic scenarios," in *2015 IEEE International Conference on Communications (ICC)*, 2015, pp. 1697-1702.

[114] H. D. Nguyen and S. Sun, "Massive MIMO versus small-cell systems: Spectral and energy efficiency comparison," in *2016 IEEE International Conference on Communications (ICC)*, 2016, pp. 1-6.

[115] L. Wenjia, H. Shengqian, Y. Chenyang, and S. Chengjun, "Massive MIMO or small cell network: Who is more energy efficient?," in *2013 IEEE Wireless Communications and Networking Conference Workshops (WCNCW)*, 2013, pp. 24-29.

[116] G. Piro, M. Miozzo, G. Forte, N. Baldo, L. A. Grieco, G. Boggia*, et al.*, "HetNets Powered by Renewable Energy Sources: Sustainable Next-Generation Cellular Networks," *IEEE Internet Computing,* vol. 17, pp. 32-39, 2013.

[117] M. Carreno and L. Nuaymi, "Renewable Energy Use in Cellular Networks," in *2013 IEEE 77th Vehicular Technology Conference (VTC Spring)*, 2013, pp. 1-6.

[118] E. Yaacoub, "RESCUE: Renewable Energy Small Cells for Utility Enhancement in Green LTE HetNets," *IEEE Systems Journal,* vol. PP, pp. 1-10, 2015.

[119] G. Weisi and T. O'Farrell, "Dynamic Cell Expansion with Self-Organizing Cooperation," *Selected Areas in Communications, IEEE Journal on,* vol. 31, pp. 851-860, 2013.

[120] A. Arbi and T. O'Farrell, "Energy efficiency in 5G access networks: Small cell densification and high order sectorisation," in *Communication Workshop (ICCW), 2015 IEEE International Conference on*, 2015, pp. 2806-2811.
[121] E. C. R. Initiative, "Energy Efficiency for Network Equipment: Two Steps Beyond Greenwashing," *White Paper, August,* vol. 10, 2008.
[122] M. S. Obaidat, A. Anpalagan, and I. Woungang, *Handbook of Green Information and Communication Systems*: Access Online via Elsevier, 2012.
[123] D. Persson, T. Eriksson, and E. G. Larsson, "Amplifier-Aware Multiple-Input Multiple-Output Power Allocation," *Communications Letters, IEEE,* vol. 17, pp. 1112-1115, 2013.
[124] M. A. Rojas-Gonzalez and E. Sanchez-Sinencio, "Low-Power High-Efficiency Class D Audio Power Amplifiers," *IEEE Journal of Solid-State Circuits,* vol. 44, pp. 3272-3284, 2009.
[125] B. Skubic, E. I. De Betou, T. Ayhan, and S. Dahlfort, "Energy-efficient next-generation optical access networks," *Communications Magazine, IEEE,* vol. 50, pp. 122-127, 2012.
[126] O. Blume, A. Ambrosy, M. Wilhelm, and U. Barth, "Energy Efficiency of LTE networks under traffic loads of 2020," in *Wireless Communication Systems (ISWCS 2013), Proceedings of the Tenth International Symposium on*, 2013, pp. 1-5.
[127] P. Monti, S. Tombaz, L. Wosinska, and J. Zander, "Mobile backhaul in heterogeneous network deployments: Technology options and power consumption," in *Transparent Optical Networks (ICTON), 2012 14th International Conference on*, 2012, pp. 1-7.
[128] "Technical Specification Group Radio Access Network; Evolved Universal Terrestrial Radio Access (E-UTRA); Further advancements for E-UTRA physical layer aspects (Release 9)," 2010.
[129] M. A. Hossain and R. Jäntti, "Impact of efficient power amplifiers in wireless access," in *Online Conference on Green Communications (GreenCom), 2011 IEEE*, 2011, pp. 36-40.
[130] C. Han and S. Armour, "Energy efficient radio resource management strategies for green radio," *IET Communications,* vol. 5, pp. 2629-2639, 2011.
[131] M. Paolini, L. Hiley, F. Rayal, and S. Fili, "Small-cell backhaul: Industry trends and market overview."
[132] F. Khan, *LTE for 4G mobile broadband: air interface technologies and performance*: Cambridge University Press, 2009.
[133] "3GPP TR 36.814 V9.0.0 (2010-03)," ed.
[134] G. J. Foschini and M. J. Gans, "On limits of wireless communications in a fading environment when using multiple antennas," *Wireless personal communications,* vol. 6, pp. 311-335, 1998.
[135] Brocade. (10/03/2017). *Brocade 6505 Data Sheet*. Available: www.brocade.com
[136] J. Li, X. Wu, and R. Laroia, *OFDMA mobile broadband communications: A systems approach*: Cambridge University Press, 2013.
[137] E. Björnson, M. Kountouris, and M. Debbah, "Massive MIMO and small cells: Improving energy efficiency by optimal soft-cell coordination," in *ICT 2013*, 2013, pp. 1-5.
[138] D. Ha, K. Lee, and J. Kang, "Energy efficiency analysis with circuit power consumption in massive MIMO systems," in *2013 IEEE 24th Annual International Symposium on Personal, Indoor, and Mobile Radio Communications (PIMRC)*, 2013, pp. 938-942.
[139] H. Yang and T. L. Marzetta, "Total energy efficiency of cellular large scale antenna system multiple access mobile networks," in *Online Conference on Green Communications (GreenCom), 2013 IEEE*, 2013, pp. 27-32.